The Sensory Biology of the Red Fox

—

Hearing, Vision, Magnetoreception

INAUGURALDISSERTATION

zur

Erlangung des Doktorgrades

Dr. rer. nat.

der Fakultät für

Biologie

an der

Universität Duisburg-Essen

vorgelegt von

Erich Pascal Malkemper

aus Hemer

August 2014

Die der vorliegenden Arbeit zugrunde liegenden Experimente wurden in der Abteilung Allgemeine Zoologie der Universität Duisburg-Essen durchgeführt.

1. Gutachter: Prof. Dr. Hynek Burda

2. Gutachter: Prof. Dr. Leo Peichl

3. Gutachter: Prof. Dr. Helmut A. Oelschläger

Vorsitzender des Prüfungsausschusses: Prof. Dr. Dr. Herbert de Groot

Tag der mündlichen Prüfung: 20.11.2014

Life makes sense.

Content

Zusammenfassung

In dieser Studie werden die Sinnessysteme des Rotfuchses behandelt, im Speziellen der Hörsinn, der visuelle Sinn sowie der Magnetsinn. Im ersten Kapitel präsentiere ich ein Verhaltensaudiogramm dreier Rotfüchse. Der Hörbereich des Rotfuchses umfasst 9,84 Oktaven und erstreckt sich von 51 Hz bis 48 kHz. Die absolute Sensitivität (-15 dB SPL bei 4 kHz) ist außergewöhnlich und übertrifft sogar jene der Katze. Ergänzend beschreibe ich die Morphologie des auditorischen Systems des Rotfuchses. Die Beschreibung umfasst die funktionell relevanten Parameter des Außen-, Mittel- und Innenohrs, wie z. B. Abmessungen und Gewichte der Gehörknöchelchen, Flächen der akustischen Membranen, Haarzelldichten sowie die Feinmorphologie der Cochlea. Anschließend zeige ich, dass sich die Sensitivität des auditorischen Systems gut in der Morphologie widerspiegelt und es nur aufgrund der morphologischen Parameter möglich ist, eine recht genaue Vorhersage des Audiogramms zu erstellen.

Im zweiten Kapitel stelle ich morphologische Aspekte des visuellen Systems des Rotfuchses vor. Mithilfe von Nissl-Färbungen und Immunhistochemie kartiere ich die retinalen Ganglienzellen und Fotorezeptoren für kurz- (S) und langwelliges (M/L) Licht auf der Retina des Fuchses. Auf dieser Basis berechne ich die Sehschärfe auf 6,3 Zyklen/Grad und die Schalllokalisierungsfähigkeit auf 3-4 Grad, beides innerhalb der Bandbreite anderer Karnivoren liegend. Selbiges gilt für die Verteilung der Zapfen, wobei die M/L-Zapfen einen zentroperipher abfallenden Dichtegradienten aufweisen und die S-Zapfen entlang eines dorsoventralen Gradienten an Dichte zunehmen.

Das dritte Kapitel behandelt den Magnetsinn. Für Rotfüchse wurde ein Magnetsinn postuliert, welcher ihnen womöglich bei der Jagd auf Kleinnager zunutze sein könnte. Da der Fuchs beim Jagen hauptsächlich akustische Reize benutzt, wurde ein Einfluss magnetischer Felder auf den Hörsinn hypothetisiert. Aufgrund dessen habe ich die Hörschwelle von Rotfüchsen unter verschiedenen magnetischen Bedingungen getestet, jedoch keinen Hinweis auf einen Einfluss gefunden, weshalb die Hypothese als widerlegt gelten kann. Allerdings konnte ich histologische Befunde sammeln, die für eine Alternativhypothese sprechen, die ein visuell-magnetisches System, analog wie es bei Vögeln vermutet wird, zur Annahme hat: Beim Rotfuchs, nicht jedoch bei Na-

gern, befindet sich das potentielle Magnetsensormolekül der Vögel, Cryptochrom 1, in den S-Zapfen der Retina.

Im abschließenden Teil des letzten Kapitels präsentiere ich die Ergebnisse von Nestbauexperimenten mit Waldmäusen, welche das Vorhandensein eines Magnetsinnes bei diesen Tieren demonstrieren. Weiterhin scheint dieser Magnetsinn durch sehr schwache Radiofrequenzfelder beeinflussbar zu sein – ein Charakteristikum des Radikalpaar-Mechanismus der Magnetwahrnehmung. Dies ist der erste starke Hinweis für das Vorkommen eines derartigen Systems bei einem Säugetier.

Summary

This study deals with the sensory systems of the red fox, more specifically with audition, vision, and magnetoreception. In the first chapter, I present the behavioural audiograms of three red fox specimens obtained by psychoacoustic procedures. The hearing range of the red fox covers 9.84 octaves ranging from 51 Hz to 48 kHz. The absolute sensitivity (-15 dB SPL at 4 kHz) of the red fox auditory sense is extraordinary, even exceeding that of the domestic cat. Complementary, I describe in detail the morphology of the red fox auditory system, including functionally relevant parameters of the outer, middle and inner ear, such as ossicle measurements and weight, acoustic membrane areas, sensory hair cell densities, and cochlear fine morphology. Subsequently, I demonstrate that the hearing sensitivity of the red fox is well reflected in the measurements and can be predicted with good accuracy on the morphological basis alone.

The second chapter is a treatise of some morphological aspects of the visual system of the red fox. By means of Nissl staining and immunohistochemistry, I map the distribution of retinal ganglion cells and short (S) as well as long (M/L) wavelength photoreceptors over the fox retina. Based on the retinal ganglion cell maps the visual acuity of the red fox is assumedly 6.3 cycles/degree and the sound localization ability within the range of 3-4 degrees, thus, within the range of other carnivores. The same holds true for the cone distribution, with a centroperipheral decreasing gradient of M/L cones and a dorsoventral increasing density of S cones.

The third chapter deals with the sense of magnetoreception. Foxes have been postulated to be magnetosensitive as that might help them during capture of small rodents. As prey capture is mainly auditorily guided, one hypothesis states an influence of magnetic fields on hearing sensitivity. Therefore, I determine the auditory sensitivity of red foxes in different magnetic fields and show that no influence I detectable, making the hypothesis unlikely. However, I show histological evidence in support of an alternative hypothesis which assumes a visual-magnetic system aiding prey capture, similar to the magnetosensitive system in birds: Red foxes, but not rodents, possess the potential magnetosensor of birds, cryptochrome 1 in the S cones of their retina.

As an additional part of this chapter I present the results of nest building experiments with wood mice that demonstrates the existence of a magnetic sense and furthermore suggests sensitivity to very weak radiofrequency fields, characteristic for a radical-pair based system of magnetoreception. This is the first strong evidence for such a system in mammals.

General introduction

This thesis intends to extend the knowledge about the sensory biology of the red fox (*Vulpes vulpes*). As such it is a multimodal and multidisciplinary approach and will be divided into three main chapters, each dedicated to a single sensory modality:

1. Audition
2. Vision
3. Magnetoreception

The third chapter will also elucidate experiments on the magnetic sense of the main prey of the red fox, i.e. small rodents.

The red fox

The red fox (*Vulpes vulpes*) is the carnivore with the largest natural distribution: It inhabits nearly all parts of Europe and Asia, large parts of North America and Australia as well as the northern parts of Africa (Larivière & Pasitschniak-Arts, 1996). Being a small member of the family Canidae, with a body size ranging between 3 and 14 kg, it is, however, the largest species of the genus *Vulpes* (Nowak, 1999). Due to its large geographical range the red fox has played a significant role in human-nature interactions for a long time, which is reflected by numerous representations in children's books, human tales, and mythology (already in the bible, cf. http://en.wikipedia.org/wiki/Foxes_in_popular_culture for a comprehensive overview).

In the past, peaking in the 20th century, the red fox was highly persecuted in many European and North American regions in order to stop the distribution of rabies and parasites and to obtain its valuable fur. Nowadays, as fur demands have decreased and rabies vaccination has proven to be much more effective than culling, the red fox has reached regionally variable abundances of 0.025-30 foxes per km² (IUCN/SSC Canid Specialist Group, 2004). In food rich urban habitats the densities can become even higher, leading to closer contact between foxes and humans and decreasing fear of humans. Despite a general acceptance of foxes by the public, the increasing proximity implies new sources of friction within the human-fox relationship (Harris & Smith, 1987; König, 2008). The nearly omnipresence of the red fox inspired many scientific endeavours, but research mainly focussed on applicable aspects of red fox spatial ecology (e.g. Janko et al.,

2012), population biology (e.g. Storm et al., 1976), and epidemiology (e.g. Anderson et al., 1981). Therefore, despite of its general popularity and its proverbial keen senses, it is astonishing how little we actually know about the sensory biology of the red fox.

Red fox sensory ecology

As a mostly crepuscular and nocturnal hunter (Tembrock et al., 1957), the red fox can be expected to bear special adaptations of its sensory organs (Dusenbery, 1992; Stevens, 2013). Österholm (1964) performed a study of the hierarchical use of the senses the red fox employs during prey capture in twilight and darkness. He found acoustic stimuli to be generally most effective under both conditions while olfactory cues were important only for point-blank foraging (max. 2 m distance) and visual stimuli only during daytime activities, which, however, rather rarely occurs. Using organ size as a proxy of sensory function, Nummela et al. (2013) elegantly confirmed this sensory hierarchy in the red fox, reflected by its place within a three-dimensional sensory space based on a comparative dataset of more than 100 mammalian species.

Even though the red fox opportunistically feeds on fruit, carrion (especially in winter), and whatever animal it can catch and kill (even young seals; Andriashek & Spencer, 1989), the major proportion of the typical red fox diet consists of small rodents such as mice and voles (Hockman & Chapman, 1983; Sidorovich et al., 2006). Characteristically, the fox attacks rodents from a distance by taking a large leap, the so called mousing jump, through which it pins the unsuspecting prey to the ground with its forepaws even when it is hidden under deep snow (Nowak, 1999). During the approach, the fox slowly tilts its head, bringing its ears on different elevations above the ground, which improves distances estimation. The jump is a sensory master stroke, correction of direction and distance is nearly impossible once in air, so that accurate localization of the prey prior to jumping is crucial. Hence, red foxes can be predicted to have extraordinary sound localization abilities. However, still nothing is known about the basic auditory properties of the red fox such as the fundamental absolute hearing sensitivity, rendering it difficult to estimate the validity of the few published experiments on red fox auditory behaviours. For example, in two studies on sound localization (Österholm, 1964; Isley & Gysel, 1975) the presented sound intensity was identical at all frequencies used, leaving it unclear whether the observed frequency-dependence of sound localization reflected a real property of the sound localization circuits or simply a consequence of different perception of the tones by the foxes. The bottom line is that we cannot accu-

rately describe the sensory ecology of the red fox or any other species when we lack knowledge about the fundamental morphology and functional properties of its sensory organs. Even though we know a great deal about the behaviour of the red fox, we need these fundamentals to interpret it accordingly.

Aim of the thesis

As exemplified above, it is necessary to study the basic properties of the underlying organs, in order to make sense of the function of animal sensory systems. This thesis describes basic but detailed morphological properties of the organs of hearing and vision in the red fox. Furthermore, psychoacoustic experiments were conducted to fill the knowledge gap of the red fox audiogram and strengthen the interface between form and function of sensory systems. Finally, first experiments on the speculated magnetic senses of red foxes were intended to lead the way towards further research in this spectacular new field of mammalian sensory biology. Olfaction and somatosensation were not addressed in this study. Altogether, this thesis lays a solid foundation for future complex studies on red fox sensory ecology and associated behaviours.

1. AUDITION

1.1   Introduction

1.1.1 Why study hearing in red foxes?

For red foxes, the sense of hearing is of highest importance for survival, warranting the assumption that it is particularly well developed. So far, the only data about hearing sensitivity in red foxes stem from a comparative study in which cochlear microphonic potentials were used to estimate the hearing sensitivity in several carnivores (Peterson et al., 1969). According to these measurements the red fox has a comparatively low absolute sensitivity ("inefficient mode of sound reception", Peterson et al. 1969), a finding which stands in direct contradiction to the previously stated assumption and numerous anecdotal reports (e.g. Lloyd, 1980; Henry, 1996; Labhardt, 1996). Peterson et al. (1969) themselves already admitted that cochlear microphonics might not be sensitive enough to allow for interspecies comparisons of absolute hearing sensitivity, a suggestion that was later confirmed by a meta-analytical comparison between cochlear microphonics and behavioural hearing data of 16 different mammal species (Raslear, 1974) and a detailed study on the relation between behavioural and single-unit/compound potential recording detection thresholds in chinchillas and gerbils (Dallos et al., 1978). Consequently, there is still a great lack of knowledge about the absolute auditory sensitivity of the red fox. The first chapter of this thesis specifically addresses this need and presents a red fox behavioural audiogram that can serve as a basis for further assessment of behaviours related to the sense of hearing in the red fox.

Comparative studies have shown that exact anatomical data of ear structures allow relatively accurate predictions about the hearing capabilities of mammals (Echteler et al., 1994; Hemilä et al., 1995). However, anatomical data of the red fox ear were also missing so far. The second part of the first chapter presents morphological data on the outer, middle and inner ear of the red fox and relates it to the determined properties of the behavioural red fox audiogram to further increase our knowledge about the relationship between morphology and function in mammalian hearing organs.

1.1.2 Measuring auditory sensitivity

Psychoacoustics is the simplest means to accurately understand the properties of animal auditory perception, taking into account the various stages of signal processing from the primary receptors to the higher order cognitive centres (Long, 1994; Heffner & Heffner, 2014). A fundamental property of a sensory system is the minimum energy level needed to detect an adequate stimulus. For the auditory system this translates into the audiogram, a characterisation of the distribution of perceived auditory frequencies and the minimum detection intensities at each frequency. In contrast to studies in humans, establishing an accurate behavioural audiogram in animals is tedious and time consuming. Within the framework of operant conditioning, animals must be trained to report the presence or absence of the stimulus in order to receive a reward or to avoid an electric shock (Heffner & Heffner, 1995). The chosen method mainly depends on the species to be investigated (Fay, 1992). Standardization of methodologies and techniques have over the years yielded comparable results providing a reliable and comprehensive database of vertebrate audiograms (cf. Fay, 1988). However, despite of the relatively long history of animal psychoacoustics, still only 1.2 % of all mammalian species have been adequately tested for auditory sensitivity today (Heffner et al., 2014).

1.1.3 Hearing in mammals

When mammals split up from their ancestors in the Upper Triassic, strong competition with then predominating Archosaurs is believed to have forced early mammals to become nocturnal (Kermack & Kermack, 1984). As their senses adapted to the new niche, mammals became as what can, still today, be considered hearing specialists within the animal kingdom (Jerison, 1973). Apart from several owls (Van Dijk, 1972; Dyson et al., 1998), some highly specialized fish (Mann et al., 1997; Mann et al., 2001) and amphibians (Feng et al., 2006), mammals are the only vertebrates that are universally able to acoustically perceive frequencies higher than 10 kHz (Fay, 1988; Dooling et al., 2000). The functional significance of the extension of the hearing spectrum into the higher frequency range has been explained by the need to localize sound sources by means of spectral-difference cues (Masterton et al., 1969; Heffner & Heffner, 2008a). Briefly, the availability of cues for the localization of sound in space is dependent on the relation between the wavelength of a sound and the head size of an animal. As early mammals had small heads, the need to accurately localize sound forced them to extend their hearing range to the

higher frequencies (Masterton et al., 1969). On the morphological side, the key to high frequency perception seems to have been the development of a three-ossicular transmission chain in the middle ear of mammals (Rosowski, 1992) and the coiling of the cochlea (Stebbins, 1980). In some mammals, bats and odontocetes, this development led to extreme upper hearing limits above 100 kHz (Au, 2000; Koay et al., 2003). On the other extreme, subterranean rodents secondarily shifted their hearing range back to lower frequencies, as the localization of sounds is not essential within their one-dimensional underground environment and low frequencies are better suited for communication within their tunnel systems (reviewed in Begall et al., 2007).

Another trait of the mammalian auditory system that is more pronounced than in other animals is the high interspecies diversity. No other animal group shows such large differences regarding the frequency of best sensitivity and the bandwidth of hearing (Fay, 1988). This makes studying the sense of hearing in mammalian species so particularly interesting.

1.1.4 Hearing in carnivores

The domestic cat (*Felis catus*) is definitely the most intensely studied mammal in auditory research and consequently its auditory system is also the best-known carnivore system so far (e.g. Heffner & Heffner, 1988a and references therein). The cat is special in that it is the mammal with the largest hearing range known so far (spanning 10.5 octaves at 60 dB SPL, Heffner & Heffner, 1985b) which is even more remarkable, given the observation that domestication is often accompanied by functional reductions of auditory (and other sensory) organs (e.g. Fleischer, 1973; Burda, 1985a). Besides the cat, absolute auditory sensitivity has been adequately reported only for four other terrestrial carnivore species: the raccoon (Wollack, 1965), the dog (Heffner, 1983), the least weasel (Heffner & Heffner, 1985a), and the ferret (Kelly et al., 1986). In addition, some audiograms of pinnipeds are available (Mohl, 1968; Moore & Schusterman, 1987; Wolski et al., 2003; Mulsow et al., 2011). A common characteristic of carnivore audiograms is a high sensitivity and a higher upper frequency limit (mostly defined as the frequency where the animals hear a pure tone at 60 dB SPL) than those found in other medium-sized mammals, e.g. ungulates (Heffner & Heffner, 1992a). Furthermore, carnivores have been shown to possess fairly good sound localization (5-12°; Heffner & Heffner, 1992c) and frequency discrimination abilities (Fay, 1974).

1.1.5 Anatomy and function of the mammalian ear

Three functionally complementary systems compose the auditory organ of mammals: the external ear, the middle ear, and the inner ear, more specifically the auditory partition of it, the cochlea (Møller, 2013). Each of these structures serves its own specific function: the external, middle and inner ear collect and amplify, transform, and transduce acoustic pressure waves into electric signals of the nervous system, respectively (Kandel et al., 2013). While the general *bauplan* is essential for the function and a common theme among mammals, considerable morphological and physiological differences between the ears of different species testify the ecological adaptations that sensory organs undergo during evolution (e.g. Doran, 1879; Keen & Grobbelaar, 1941; Fleischer, 1973; Hemilä et al., 1995; Nummela, 1995; Coleman & Ross, 2004; Nummela & Sánchez-Villagra, 2006; Vater & Kössl, 2011). In the following, I will mainly describe features of the human ear, but additional mammalian examples will be given, and within certain limits the descriptions can be generalized to other mammals. Whenever relevant deviations occur in other mammals, I will shortly elaborate on them.

OUTER AND MIDDLE EAR

The external or outer ear consists of the auricle (pinna) and the ear canal (meatus). Analogous to a parabola antenna, the external ear collects acoustic stimuli and focusses them onto the middle ear. Except for the external auditory meatus (but aided by the head and torso of the animal) the external ear bears a certain directionality that leads to a modification of acoustic stimuli depending on the angle of incidence, therefore allowing directional hearing. Intensity modifications mainly serve the identification of horizontal azimuth (Harrison & Downey, 1970), while spectral modifications allow for distinctions of elevation and distance (reviewed in Butler, 1975; Heffner & Heffner, 1992b). In addition, the external ear significantly amplifies sound intensity by up to 20 dB, as assessed in humans, cats and rabbits (Wiener et al., 1966; Fattu, 1969; Shaw, 1974). The most medial part of the external ear, the ear canal, is terminated by the tympanic membrane.

The middle ear is an air filled pouch, the tympanic cavity (cavum tympani), that contains a series of functionally interconnected membranes and three small bones (malleus, incus, stapes), that couple the incoming sound stimulus to the inner ear (Figure 1.1-1). In many mammals the tympanic cavity is ventrally extended and protrudes from the skull base as an oval shaped knob, then called bulla tympanica (Keen & Grobbelaar, 1941). The most lateral part of the middle ear is the

tympanic membrane, a thin cone-shaped membrane stretched within a bony tympanic ring at the medial end of the ear canal. The mammalian tympanic membrane consists of two components, a thinner and stiffer pars tensa and a loose pars flaccida, the size of which is highly variable between different species (Kohllöffel, 1984; Vrettakos et al., 1988). The function of the pars flaccida is still subject of ongoing discussions, but it probably influences low frequency sensitivity and ensures static pressure consistency on both sides of the tympanic membrane (Hellström & Stenfors, 1983; Kohllöffel, 1984; Rosowski, 2010; Rosowski, 2013). The pars tensa is the first station of the middle ear acoustic transduction chain and is directly coupled to the first of the three bones of the ossicular chain within the mammalian middle ear: the malleus.

The malleus, the largest of the three ossicles, adheres to the centre of the pars tensa (umbo) of the tympanic membrane via a long handle, the manubrium; the contact surface of this attachment differs between species: some show only local adherence while in others the whole manubrium is attached to the tympanic membrane along its entire length (Rosowski, 2010). The opposite end of the malleus, the head (caput), features a saddle-shaped surface which serves as a facet joint to the incus, the next ossicle in the chain (a flexible joint is the case in most species; in many rodents, however, the two bones are partly or completely fused; Fleischer, 1973). The region between manubrium and caput of the malleus is called the neck (collum). Two processes emerge from the malleus at the junction between the neck and the handle: a larger lateral process connected to the tympanic membrane and a shorter anterior process connected to the wall of the tympanic cavity by the anterior mallear ligament. The musculus tensor tympani inserts at the basal region of the manubrium and pulls it inwards when contracted. It is innervated by the motor branch of the trigeminal nerve (Møller, 2013).

The incus has approximately the shape of an anvil with a saddle, the incudomallear joint, positioned on the face. The longer of the two arms, crus longum, is oriented nearly vertically downwards but describes a sharp turn at its end and medially terminates in a small oval plate, the processus lenticularis, which, as part of the incudostapedial joint, connects the incus to the stapes. The shorter process of the incus, crus breve, is thicker than the crus longum and serves as an attachment for the posterior ligament of the middle ear, that fixes the incus within a small depression of the epitympanum, the fossa incudis.

The stapes is by far the smallest and most fragile of the three ossicles and bears close resemblance to a stirrup. The top (head and neck) of the stapes forms the medial part of the incudosta-

pedial joint, while its base forms an oval plate (footplate) resting in the oval window of the inner ear where it is fixed by an annular ligament (ligamentum anulare stapedium). Anterior and posterior limbs (crura) connect the footplate to the head. In many species, the neck of the stapes is connected to the wall of the tympanic cavity by means of a small muscle, the stapedius muscle, which inserts at a tendon in the stapedial neck region. Innervated by the VIIth cranial nerve (facial nerve; Blevins, 1964), contraction of the stapedius muscle leads to a sideward displacement of the stapedial head perpendicular to its normal piston-like motion during sound transduction. This stapedial reflex significantly reduces the transmission efficiency and serves to protect the inner ear from damage through overstimulation at high sound intensities (Wever & Lawrence, 1954; Galambos & Rupert, 1959; Pang & Peake, 1986). However, at certain frequencies and working in a synchronized fashion, the two middle ear muscles can also create a small gain of up to 5.5 dB at 2.5 kHz in the guinea pig (Nuttall, 1974; Rosowski, 2013).

The main purpose of the middle ear components is to overcome the impedance mismatch between the air-filled middle ear and the fluid-filled cochlea (Rosowski, 1994; Møller, 2013; Rosowski, 2013). This mismatch is caused by the low compressibility of the inner ear fluids and bone compared to the compressibility of air, and as a consequence, without a coupling solution, 99.9 % of the sound energy would be reflected at the oval window before reaching the inner ear, corresponding to a loss of sound pressure of 40 dB (Zwislocki, 1975; Møller, 2013). The middle ear matches the impedance by transforming the low pressure, large oscillations amplitude waves arriving at the tympanic membrane into small amplitude, large pressure waves by the time they arrive at the oval window (Zwislocki, 1975). The pressure gain achieved by the acoustic transforming mechanism is frequency dependent and reaches a maximum of about 25 dB in humans and 20-40 dB in animals (Nedzelnitsky, 1980; Kurokawa & Goode, 1995; Puria et al., 1997; Olson, 1998; Aibara et al., 2001).

The gain can be seen as the sum of two main components: a mechanical lever advantage and a hydraulic advantage (von Helmholtz, 1868; Wever & Lawrence, 1954; Dallos, 1973). The mechanical lever results from the fact that the malleus and incus rotate around a common axis where the lever arm of the malleus is longer than the lever arm of the incus, leading to a mechanical advantage that creates a small theoretical 1.3 fold (2.2 dB) gain in humans (mean of 36 mammalian species: 7.6 dB; Hemilä et al., 1995). A larger gain is achieved by the hydraulic advantage resulting from the difference between the area of the tympanic membrane and the area of the oval win-

dow. In humans, this area ratio is 20:1, leading to a theoretical amplification of additional 26 dB (mean of 36 mammalian species: 29 dB; Hemilä et al., 1995). Helmholtz (1863) originally proposed a third amplifying mechanism operating at the tympanic membrane: the buckling movement resulting from the conical suspension of the tympanic membrane could act as a catenary lever, yielding approximately 6 dB gain in humans. The results of extensive studies by Wever and Lawrence (1954) and Békésy and Wever (1960) initially did not corroborate the tympanic catenary lever, but more recent measurements and models of sound-induced tympanic membrane surface motions are in line with the catenary lever mechanism (Tonndorf & Khanna, 1970, 1972; Khanna & Tonndorf, 1972; Funnell et al., 1987; Fay et al., 2006). Taking the catenary lever into account, all means of amplification yield a total theoretical human middle ear gain of 34 dB. This value is lower than expected for an ideal transformer (40 dB) and much larger than what was actually measured in mammalian middle ears. The difference between the theoretical and actually measured gain can be explained by losses through ossicular elasticity (Funnell et al., 1992; Decraemer et al., 1995), flexion in the ossicular joints (Guinan & Peake, 1967; Willi et al., 2002; Funnell et al., 2005), complicated irregular translational and rotational motions of malleus and incus at high frequencies (Decraemer & Khanna, 2004), and alterations in the stiffness and effective area of the tympanic membrane (Fay et al., 2006; Rosowski, 2010), all of which are frequency dependent factors that are hard to take into account in simple models. It is evident that the middle ear does not act as an ideal transformer (Rosowski, 1991) but it is efficient enough to transfer information about biologically relevant acoustic signals to the inner ear.
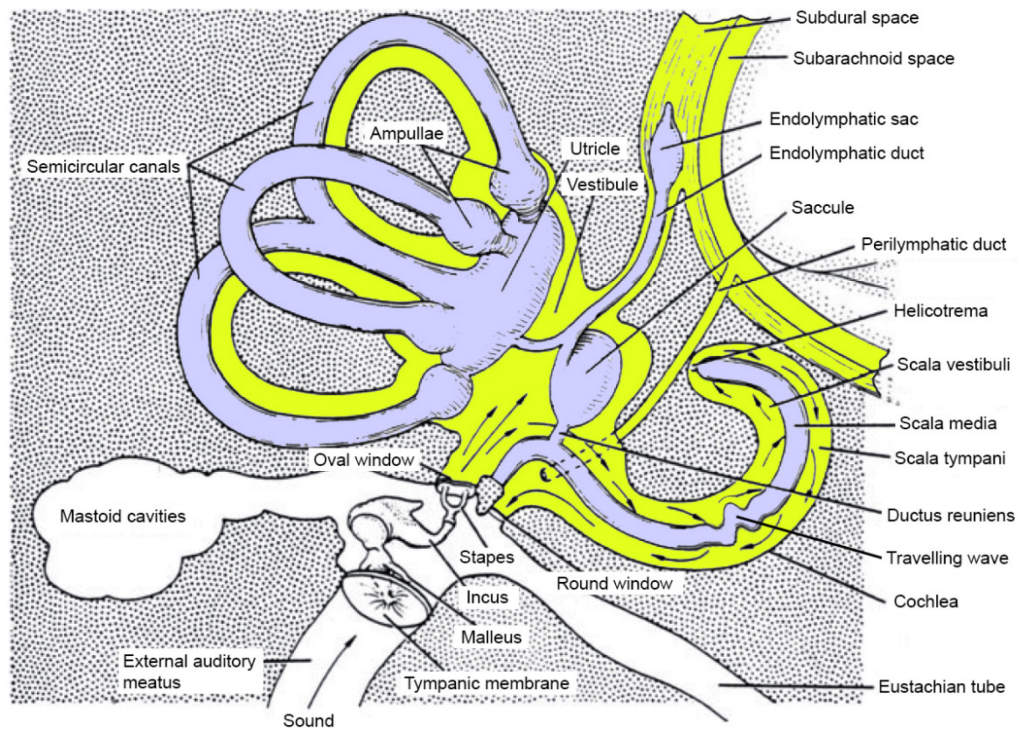
Figure 1.1-1 Schematic representation of the mammalian ear. Air filled compartments of the outer and middle ear are shown in white, perilymph filled and endolymph filled areas of the inner ear are shown in light green, and light purple, respectively. A travelling wave resulting from the pivotal stapes motion is schematized in the middle of the cochlear partition. See main text for explanations in the functions of the different compartments. Modified from Echteler et al. (1994).

INNER EAR

The mammalian cochlea is located within a helical tube in the temporal bone. This bony laby-rinth describes a species-specific number of 1.5 to 4.5 turns with cochleae of humans and cats having 2.75 and 3 turns, respectively (West, 1985; Echteler et al., 1994; Ketten, 2000). Along its entire length the cochlea contains three membranous compartments or scalae (membranous laby-rinth): the upper scala vestibuli, the lower scala tympani, and the scala media (cochlear duct) in between. The scala tympani is topographically (but not physiologically, see below) separated from the scala media by the basilar membrane (BM) and a part of the bony labyrinth, the osseous spiral lamina. The scala vestibuli is separated from the scala media by the thin, two-layered Reissner's membrane. A small aperture at the tip of the cochlea, the helicotrema, connects the scala vestibuli with the scala tympani and allows for the exchange of fluids. The inner ear of mammals not only consists of the auditory system (the cochlea) but also of the vestibular apparatus (vestibule and semicircular canals). Scalae media and vestibuli both protrude into the vestibular portion, while the scala tympani ends at a membrane-covered opening in the otic capsule, the round window,

facing the air filled middle ear. As already mentioned above, the oval window, holds the footplate of the stapes and faces the basal scala vestibuli (overview in Figure 1.1-1).

The auditory receptors are located in the organ of Corti, a characteristic accumulation of several specialized cell types sitting on top of the BM (Figure 1.1-2). They consist of two different types of hair cells, which derive their name from characteristic assemblies of stereocilia on their apical surface. The hair cells spiral along the cochlear duct, always with a single row of inner hair cells (IHC) and typically with three to four rows of outer hair cells (OHC, more rows in some mole-rat species; Bruns et al., 1988). The length of the BM and the number of IHCs and OHCs vary considerably across species, with reported BM lengths from 2.9 mm to 71 mm and total hair cell numbers from 10,000 to 30,000 (Burda et al., 1988; Ketten, 2000).

The IHCs and OHCs are divided by the tunnel of Corti which is lined by slender outer and inner pillar cells. Deiters' cells are sitting below the hair cells and keep those in place much like an egg cup is holding an egg. Other important supporting cells include the tall Hensen's cells and smaller Claudius cells which sit on the BM on the external side of the OHCs. An acellular membranous sheet, the tectorial membrane, crucial for cochlear function, covers the organ of Corti. The longest stereocilia of the OHCs are embedded in the tectorial membrane while the stereocilia of the IHCs are not in direct contact with it. The organ of Corti is bounded by membranous structures that suspend the BM: the limbus sitting on the bony spiral lamina on the medial side of the helix and the spiral lamina which lines the lateral wall of the bony labyrinth. On the inside of the spiral lamina a stripe of highly vascularized tissue, the stria vascularis, helps to maintain the ionic fluid composition within the scala media. The scala media contains endolymph, a high potassium, low sodium fluid very similar to intracellular liquid, while the scalae vestibuli and tympani contain perilymph, which is high in sodium and low in potassium. Additionally, the potential of the endolymph is highly positive compared to the perilymph (Schmidt & Fernandez, 1963). The functional consequences of this physiological difference are important for the transduction process at the sensory hair cells as will be explained below.

The cochlea is a resonating pressure difference detector (Wever & Lawrence, 1950; Voss et al., 1996). During sound stimulation, the stapes pushes into the oval window in a piston-like manner. The motion induces sinusoidal pressure changes within the scala vestibuli. As the diameter of the helicotrema is too small to act as a shunt between both perilymphatic scalae, the pressure changes create travelling waves on the BM. The thickness of the BM increases from the apex to

the base while the width decreases, resulting in a maximal stiffness at the base (Vater & Kössl, 2011). Due to the constantly changing stiffness along the cochlear duct the amplitude of the travelling wave reaches a maximum at the positions of its frequency dependent resonance: high frequencies are represented at the stiff base, low frequencies in the flexible apex region of the cochlea (Ehret, 1978). This principle of a place-specific frequency analysis was originally proposed by von Helmholtz (1863), but it was von Békésy (1960) who delivered substantial experimental evidence for the tonotopic organization of the cochlea and the travelling wave theory which still stands today.

The bending of the BM creates a shearing motion between the tectorial membrane and the organ of Corti that directly depolarizes the OHCs by opening cation channels at the stereocilia, giving way for an inflow of potassium ions (Davis, 1958). The channel opening is mediated by tip links which are stretched between the stereocilia and the rapid potassium inflow is the consequence of the high potassium concentration and positive endochochlear potential of the scala media (Dallos, 1992). Only the apical part of a cochlear hair cell is bathed within the endolymph, the rest of the cell is surrounded by perilymph. The resulting transmembrane potential is the driving force of the potassium inflow and depolarization of the hair cell after stereocilia bending (Ehret & Göpfert, 2013). The depolarization leads to calcium influx at the base of the hair cell, which triggers the release of the neurotransmitter glutamate that excites downstream bipolar cells of the cochlear ganglion. Repolarization of the hair cells is acquired through release of potassium, which is returned into the endolymph via a series of gap-junction-coupled supporting cells and, ultimately, the stria vascularis (Kikuchi et al., 2000). The excitation of the OHC does not mediate information about the perception of an acoustic stimulus to higher auditory centres but starts a feedback loop that leads to an active change in the length of the excited OHCs. The transformation is mediated by the motorprotein prestin and can change the length of the cylindrical OHCs by up to 5 %, leading to a considerable reinforcement of the travelling wave (Dallos, 1992; Zheng et al., 2000; Liberman et al., 2002). A loss of this amplification mechanism through OHC loss goes along with a significant reduction of auditory sensitivity (Dallos & Harris, 1978). The shearing between the BM and the tectorial membrane not only excites the OHCs but also creates a fluid drag that opens cation channels and depolarizes the IHCs, the actual auditory receptor cells. In contrast to the OHCs, the IHCs are predominantly afferently innervated by fibres of the cochlear nerve. The synapses between the IHCs and the afferent nerve fibres are glutama-

tergic (Bobbin, 1979; Ehrenberger & Felix, 1991). The afferent nerve fibres exit the cochlear duct through windows in the bony walls, the habenula perforata, and reach the cell somata of the bipolar auditory neurons that are located in Rosenthal's canal, which follows the spiral course of the cochlear partition. Further centrally, they form the cochlear nerve within the bony modiolus and transmit information to the cochlear nucleus in the brainstem, the first relay station of the brain auditory processing circuits. For more details on cochlear innervation see Spoendlin (1985) and Møller (2013). For excellent reviews on the functional anatomy of the mammalian cochlea, see Echteler et al. (1994) and Slepecky (1996).
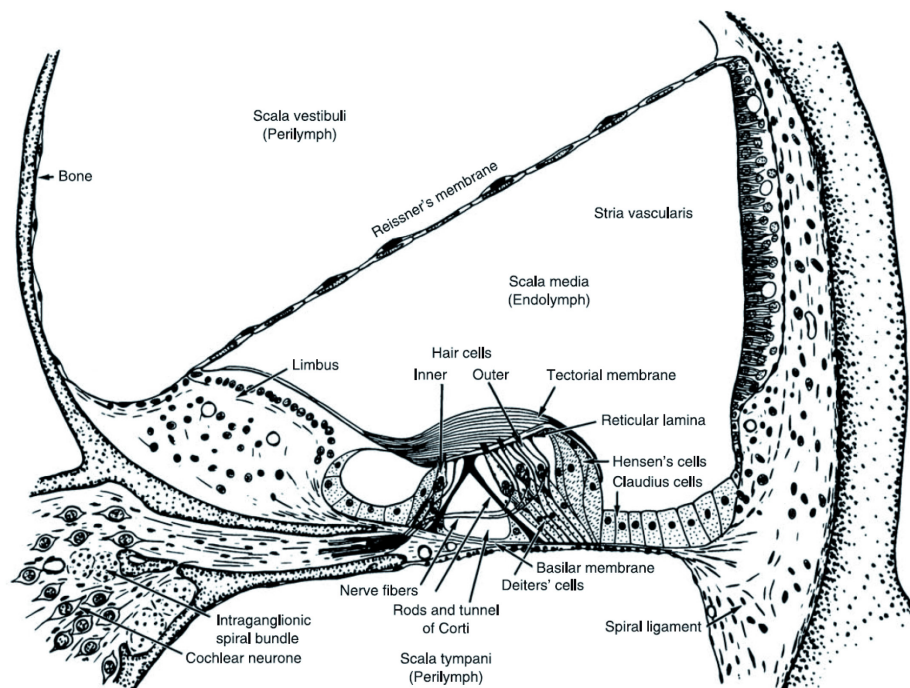
Figure 1.1-2 Section through one half-turn of the mammalian cochlea revealing details about the fine structure of the organ of Corti (adapted from Møller, 2006). Refer to the main text for the function of the specific parts of the auditory organ.

1.1.6 Comparative functional morphology of auditory structures

The sensory equipment of every species was shaped by evolution to perfectly fulfil the demands imposed by the inhabited ecological niche (Dusenbery, 1992; Stevens, 2013). This selection balances the trade-offs among different sensory modalities (Nummela et al., 2013) and fine-tunes each sense for its specific purpose. Especially in the mechanical auditory system, but also in the other senses, morphology reflects function and this supposition can been exploited to make cer-

tain predictions about the hearing capabilities of inaccessible or even extinct species on the basis of anatomical data alone (e.g. Rosowski & Graybeal, 1991).

From the functional description of the outer and middle ear given above, one might suppose that it is relatively easy to straightforwardly predict the auditory sensitivity of a mammal species by simply calculating the total impedance transformation efficiency, which is quickly done by summing up the gain of each component (lever arm ratio, area ratio, possibly tympanic membrane lever advantage). Following this simple logic, the efficiency of every mammalian middle ear might be expressed in a single number, the impedance transformer ratio (ITR) which is the acoustic impedance at the oval window divided by the acoustic impedance at the tympanic membrane:

$$\frac{Z_{TM}}{Z_C} = \frac{A_{OW}}{A_{TM}} \left(\frac{l_I}{l_M}\right)^2 \quad \text{(Dallos, 1973)}$$

where Z_{TM} is the impedance at the tympanic membrane, Z_C the impedance at the cochlea, A_{OW} the area of the oval window, A_{TM} the area of the tympanic membrane, l_I the incus lever arm, and l_M the malleus lever arm. Thus, using four simple morphological parameters, ITR and very similar ratios (e.g. the pressure transformer ratio, the product of lever and area ratio) have been used to estimate and compare the auditory capacities of a variety of animal species (Wever & Lawrence, 1954; Coleman & Ross, 2004; Coleman & Colbert, 2010).

However, as already stated above, the middle ear does not act as an ideal impedance matching device and thus these "ideal/lossless transformer ratios" (Dallos, 1973) oversimplify the biological situation and might lead to inaccurate conclusions in species comparisons. Although the middle ear acts as a linear system, i.e. an increasing input at constant frequency will lead to a proportional increase of the output (Guinan & Peake, 1967; at least at audible frequencies, without the influence of middle ear muscle contractions, and up to moderately high sound pressures, see Dallos, 1973; Aerts & Dirckx, 2010), the middle ear acts as a selective filter, amplifying in a frequency specific manner (Rosowski, 2013). In addition, simple models of middle ear gain do not take into account the significant effect the cochlea exerts on the frequency sensitivity of the auditory apparatus (Ruggero & Temchin, 2002). Therefore, alternative, more complicated models of middle ear function have been developed that use transfer functions instead of transformer ratios and may be summarized under the term "periphery filter hypotheses" (Rosowski, 1994; Coleman & Colbert, 2010). Middle ear transfer functions describe the pressure changes within the scala

vestibuli or the velocity of the stapes in dependence of the sound pressure reaching the tympanic membrane for a broad range of frequencies and thus perfectly describe the frequency dependence of the middle ear system and the cochlear impedance (see below). The functions correlate well with the shape of behavioural audiograms (Dallos, 1973; Zwislocki, 1975; Ehret & Göpfert, 2013). However, obtaining transfer functions is a complicated and invasive procedure that has so far mainly been used on standard laboratory animals such as cat and guinea pig (Møller, 1963; Décory et al., 1990). Because transfer functions obtained from cadavers differ considerably from those measured in vivo (Ruggero & Temchin, 2003), such measurements are almost impossible to get from most wild mammal species. As it is unclear to what extent the transfer functions obtained in laboratory species apply to the ears of other mammalian species, to determine the auditory capacities of these species, we are left with correlation-based models and time consuming behavioural experiments.

Several morphological parameters of the mammalian outer, middle and inner ear correlate well with certain characteristics of behavioural audiograms, as was revealed by studies employing a simple approach: collecting a number of morphological parameters of species with known audiograms or neurophysiological investigations and test for correlations between both parameters (e.g. Rosowski, 1992; Echteler et al., 1994; Vater & Kössl, 2011). Strong correlations have been found and the regression lines can be used to predict the sensitivity of auditory structures. The parameters comprise the whole morphological spectrum including the number of turns of the cochlea (West, 1985), the weight and dimensions of the middle ear ossicles (Hemilä et al., 1995), the length, width, and stiffness of the BM (Vater & Kössl, 2011), the length of the hair cells (Dannhof et al., 1991), as well as the shape of the outer ear (Coleman & Ross, 2004; Coleman & Colbert, 2010). The revealed correlations are of highly variable strength and often heavily dependent on the chosen data set, but in general, a unified understanding of the relationship between mammalian ear diversity and hearing seems in reach. It is necessary to increase the dataset of mammalian species for which parameters of both, auditory morphology and hearing capabilities, are covered in detail to create or refine models of mammalian ear function. This will also reveal differences between the fits of different models and allow for the right choice. Hopefully one day, a simple, correctly chosen model will allow highly accurate predictions of hearing capabilities in extinct and hard to study mammals.

1.2 Material and Methods

1.2.1 Behavioural audiometry

SUBJECTS

Three young (3-8 month old) red foxes (*Vulpes vulpes,* two males and one female) were tested. The experiments were performed in an empty horse stable in a rural area of the Bohemian Forest, Czech Republic (49°9'10.28"N, 13°20'56.45"E). The animals were kept in cages outdoors or within the stable by foresters as pets with permits of the local veterinary medical and Nature and Animal Protection authorities. The daily acoustic environment of the animals consisted mainly of natural environmental sounds and some occasional noise of cars infrequently passing on a nearby small road. The foxes were fed on dry canine diet and were given access to water *ad libitum*. The foxes received at least 80% of their daily food ration during the training and test sessions. Daily monitoring ensured the good health of the animals. One animal (female) was trained and tested in 2012, two other animals in 2013. In addition, one human subject (male, 28 years old) was tested with the same equipment and at the same location.

SETUP

A custom-built semi-anechoic chamber (115 cm x 80 cm x 120 cm, Figure 1.2-1) served to attenuate environmental noise, to house the speaker and other equipment, and to ensure a fixed position of the fox's head within the sound field during test sessions. The walls of the chamber consisted of 80 mm PE-compound panels covered on the inside by a 40 mm layer of heavy weight compound-foam, a 2 mm layer of bitumen paper and an inner layer of acoustical foam. Compound-foam padding (40 mm thickness) below the chamber reduced the transmission of environmental low frequency noise and vibrations. The top of the chamber could be removed to allow for easy manipulation of the equipment inside. No ferromagnetic materials were used in the construction.

The chamber was tightly sealed except for a single opening (25 x 25 cm) on one side wall. A brass-cage (bar-diameter max. 5 mm) mounted on the inside of this opening served as an observing cage and prevented the subjects from climbing into the semi-anechoic chamber. Two infrared (IR) light beams (M18R020PPN-C, Panasonic, Osaka, Japan) automatically detected the en-

trance of the subject and ensured its correct observing position as well as its response after tone presentation. A standard 12 V halogen lamp illuminated the chamber. Closed-circuit video observation via an IR-sensitive webcam (ISlim 321R, Genius, Langenfeld, Germany) equipped with IR-light emitting diodes (LED) mounted above the speaker allowed visual control during the test sessions. An array of blue flashing LEDs mounted on top of the speaker indicated an ongoing trial to the animal (Figure 1.2-1).

For each session I transferred the animals into a wooden start box from which they had access to the observing platform. For one animal, the female, I placed the whole system in front of the home cage, which then served as the start box, so that the fox was free to enter and start trials voluntarily during the session times.
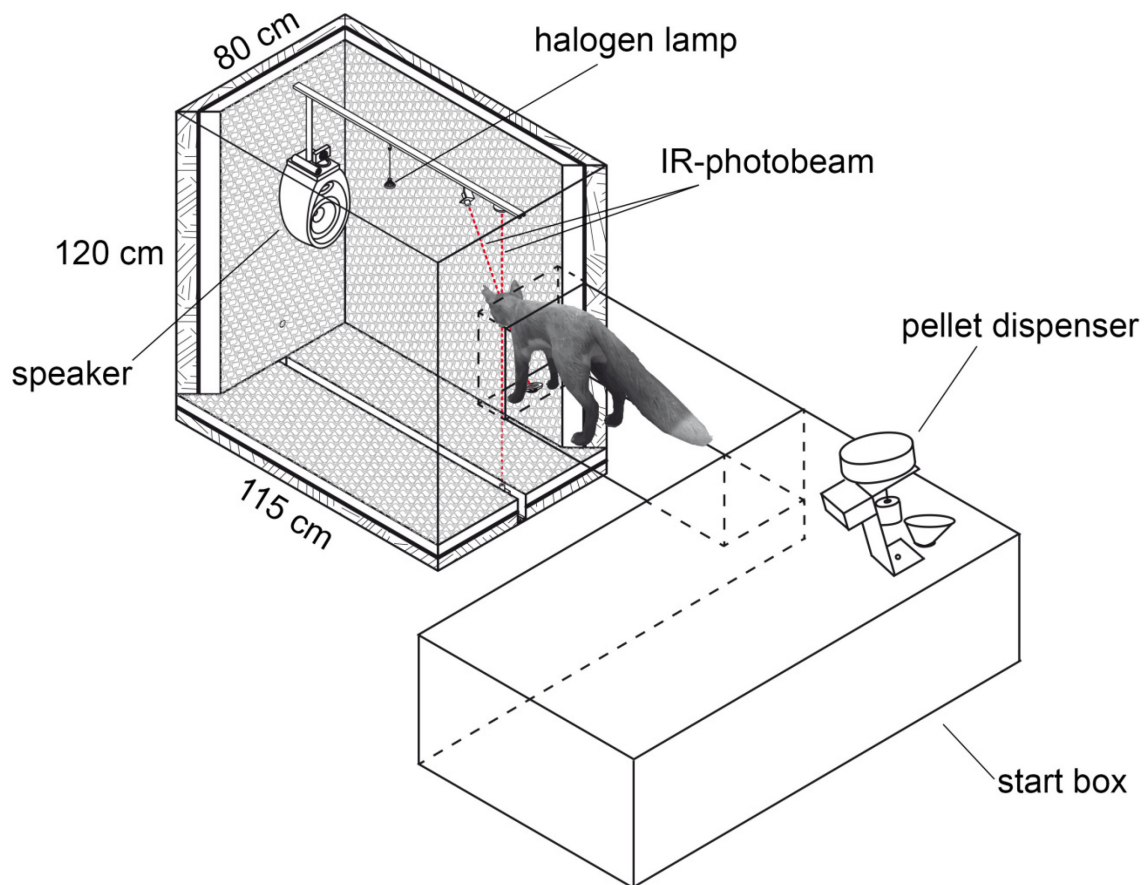
Figure 1.2-1 Setup used to establish the red fox behavioural audiogram. A transportable semi-anechoic chamber was either connected to a wooden start box or placed in front of the cage of the animals. The foxes were trained to wait in the observing position for the presentation of a pure tone upon which they should leave the observing position to obtain a food reward from an automatic pellet dispenser. False alarms were punished with time-outs. Stimulus presentation, subject control through infrared-photobeams, and reward/punishment allocation were fully computerized.

S TIMULUS CONTROL

I used a multi-I/O processor unit (RZ6, Tucker-Davis Technologies (TDT), Alachua, FL, USA)
with a maximal sampling rate of 200 kHz to generate, amplify and attenuate pure tones of
500 ms duration. A software-controlled cosine gate (RPvdsEx V. 74, TDT) created rise and fall
times of 25 ms and 50 ms for frequencies above 63 Hz and up to 63 Hz, respectively. Stimuli
with frequencies higher than 63 Hz were transmitted through a dual concentric loudspeaker
(Arena Satellite, Tannoy, UK; 80 Hz-54 kHz frequency response), for the frequencies 50 Hz and
63 Hz I used a 12" (30 cm) subwoofer (Punch HE, Rockford Fosgate, Tempe, AZ, USA; 28-200
Hz frequency response). The dual concentric loudspeaker was mounted at 0° elevation and at a
distance of 60 cm in front of the animal while the subwoofer was placed on the foam-covered
floor of the chamber with the speaker membrane facing away from the animal.

   I calibrated the sound intensity at the head position for each frequency at 80 dB sound pres-
sure level (SPL, re 20 µPa) with a Precision Sound Level Meter (2231, Brüel & Kjær (B&K),
Naerum, Denmark) equipped with a 1/4" free field microphone (4939, B&K, 4 Hz-100 kHz;
corrected for free field response with protection grid on). The sound level meter was calibrated
before each measurement with a sound level calibrator (4230, B&K; 94 dB re 20 µPa at 1 kHz)
equipped with a 1/4" adaptor (DP-0775, B&K). A flexible extension rod (UA-0196, B&K) min-
imized the risk of measuring reflections from the 2231 case. I used an 1/3-octave filterset (1625,
B&K) to measure sound pressure levels between 50 Hz and 20 kHz, for higher frequencies I
measured with the high pass (>12.5 kHz) filter of an infra- and ultrasound filter set (1627,
B&K). For all sound measurements I used linear frequency weighting. Because the head of the
animal was not fixed within the sound field I controlled the presented sound intensities as fol-
lows. At each frequency I assessed three SPL values within the observing cage: SPL at the observ-
ing position (dBo_b), maximum SPL (dB_{max}) and minimum SPL (dB_{min}). I then took care to meet
the following two criteria during calibration. First, the maximal value at any point within the ob-
serving cage was not higher than + 2 dB SPL above the desired intensity (dSPL). Second, the dif-
ference between dSPL and the mean ($dB_{min, } dB_{max}$) was smaller than 6 dB. This procedure resulted
in homogeneity of the presented sound field of ± 3 dB. Eventually, since most deviations oc-
curred in the corners of the observing cage which were rarely visited by the animal, the actual
sound field experienced by the animal was even more homogenous. To control the sound stimuli
for harmonics and distortion I connected the output of the sound level meter to a digital USB

oscilloscope (PicoScope 4224, Pico Technology, Cambridgeshire, UK) and employed the frequency analyzing FFT-function of the corresponding software (PicoScope 6, Pico Technology).

I determined the ambient noise levels with the same devices that were used to calibrate the stimulus intensity. To assess the attenuation properties of the semi-anechoic chamber I recorded the noise intensities alternately on the inside and outside of the chamber shortly before or after a test session over a period of 10 days. I did not perform these measurements during the experimental procedure since noise created by movement of the experimental animals would have distorted the measurements which were intended to reflect the background noise during the periods of silent listening. For measurements inside of the chamber I inserted the microphone into the chamber through the cable passage at the back (confer Figure 1.2-1). For outside measurements I alternately placed the microphone either on the left or right side of the chamber. I took a single SPL reading in each of 31 1/3-octave bandwidth windows with centre frequencies between 20 Hz and 20 kHz. In addition, I measured ambient noise SPL in the low- (< 20 Hz) and high frequency (> 12.5 kHz-100 kHz) range using the respective filter settings (B&K 1627). It took about 15 min per session to accomplish all ambient noise measurements. Due to the low levels of the ambient noise which were at the lower end of the sensitivity range of the sound level meter, I later corrected the measurements for the internal noise level of the microphone amplifier combination according to the specifications of Brüel & Kjær to avoid overestimations of the noise (personal communication with Ralf Klaerner, B&K).

PSYCHOPHYSICAL PROCEDURE

I employed a simple go/no-go procedure. I trained the foxes to enter the chamber through a window which automatically started a trial and required the animals to wait in a observing position until a tone was presented. Upon tone perception the foxes should leave the observing position to indicate the detection of the stimulus. Correct responses were automatically rewarded with dry dog kibbles delivered directly into the starting box (or home cage for the female) by an electronic pellet dispenser (ENV-203-190 mg, Med associates Inc, St Albans, VT, USA) which was customized to accommodate ordinary dry dog kibbles (Adult Mini, Interquell Happy Dog, Großaitingen, Germany). Punishment was given in form of time-outs during which the foxes had to wait before a new trial could be initiated which were indicated by switched-off chamber lighting.

Presentation of stimuli, subject control, reward delivery and data storage were automatically controlled via a laptop connected to the RZ6 Multi-I/O processor unit and running custom software written in Visual Basic 2010 (Microsoft Corporation). Details on the software and its genesis can be found in Lettmann (2013). The graphical user interface of the software, the hardware configuration as well as a flowchart giving an overview of the psychoacoustic procedure are shown in Figure 1.2-2.
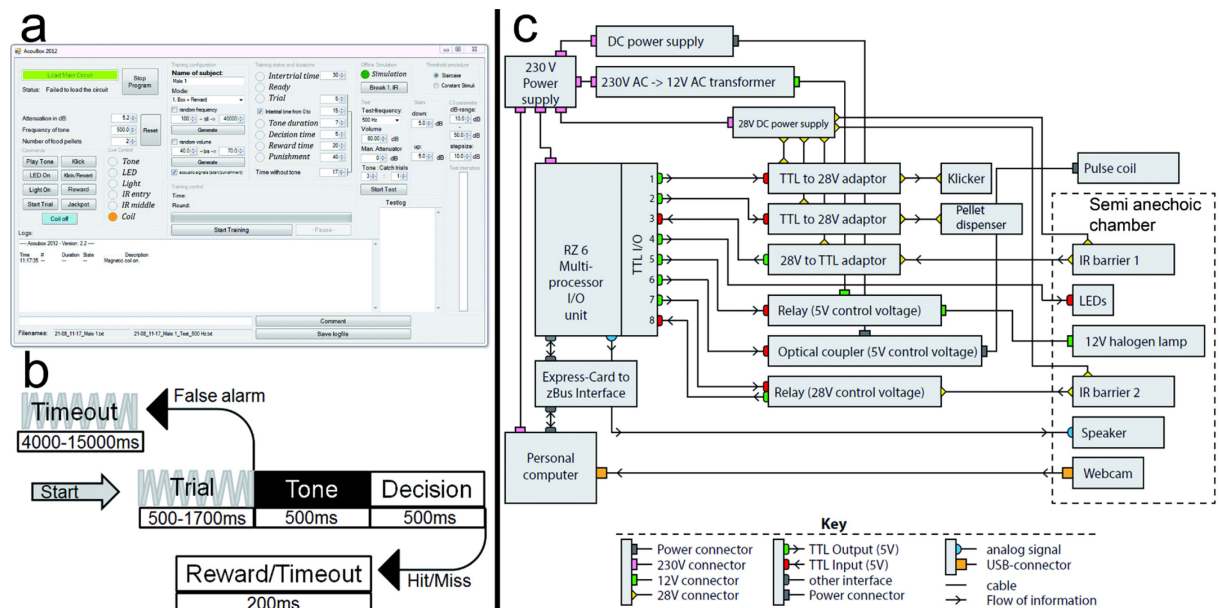
Figure 1.2-2 The psychoacoustic setup. (a) Graphical user interface of the custom-built software used to control the psychoacoustic experiments. (b) Flow chart of a single trial of the psychoacoustic procedure. (c) Diagram of the hardware configuration ((c) after Lettmann 2013)

I used the method of constant stimuli to determine the absolute hearing thresholds (Niemiec and Moody, 1995). In each session, single 500 ms pure tones of one of six intensities that were bracketing the assumed threshold at each frequency were repeatedly presented in random order. I used 10 dB-steps. Before I chose the test intensities, I estimated a rough threshold at each frequency by presenting stimuli decreasing in 10 dB-steps starting from 80 dB until the fox failed to respond (staircase procedure). Then I adjusted the test intensities in such a way that only a single one was lower than the previously estimated threshold of the animal. After the fox entered the chamber, it was detected by the IR-light which automatically started a trial. Every trial began with a variable trial interval lasting 500-1700 ms after which the tone was presented. A 500 ms decision period followed the tone presentation, allowing the fox to leave the box as an indication of sound perception (hit) so as to obtain the food reward. No response during tone presentation or the deci-

sion phase (miss) resulted in a short switch-off of the chamber lighting to indicate the fox to leave the chamber before a new trial could be initiated. Responses during the trial interval or during catch trials where no tone was presented were denoted as false alarms (FA) and followed by a punishment interval of 4-15 s depending on the mood and character of the fox.

I tested the foxes in two to four daily sessions with each session consisting of roughly 100 trials + 25 catch trials. A total of 15 different frequencies from 50 Hz to 54 kHz was tested (50 Hz, 63 Hz, 125 Hz, 250 Hz, 500 Hz, 1 kHz, 2 kHz, 4 kHz, 6.3 kHz, 8 kHz, 16 kHz, 32 kHz, 40 kHz, 46 kHz, 54 kHz). To determine the threshold at each frequency, I first calculated the hit rate at each tested intensity for each session and converted it into a performance measure which I then corrected for false alarms (Heffner & Heffner, 1988b, 1995). I chose the performance measure: performance = hit rate – (hit rate x FA rate), resulting in values between 0 and 1 (with 1 meaning 100% hit rate and no FA; Heffner & Heffner, 1988b). Plotting the performance in each session against the intensity yielded a psychometric function where I calculated the threshold at the tested frequency through interpolation of the intensity where the performance reached a level of 0.5. The final threshold of each animal and frequency was then the mean of the first three sessions that satisfied the following stability criterion: each of the three thresholds lay within ± 5 dB of their respective mean. I discarded test sessions with FA rates higher than 25 %.

1.2.2 Morphometric analysis of the outer and middle ear

The aim of the morphological description of the red fox ear was to reveal correlations between morphometric parameters and properties of the behavioural audiogram, which would ultimately allow for a precise estimation of auditory sensitivity on the basis of morphological data alone. Therefore, the analysis was restricted to the parts of the ear involved in auditory function. I used fresh tissue that was obtained by hunters in the Czech Republic which were instructed and supervised by Dr. Ing. Vlastimil Hart and Prof. Dr. Ing. Jaroslav Červený, Department of Game Management and Wildlife Biology, Faculty of Forestry and Wood Sciences, Czech University of Life Sciences, Prague, Czech Republic. Additionally, I used skulls belonging to my private collection and to the collection of the Senckenberg Museum of Natural History Görlitz (generously provided by Prof. Dr. Hermann Ansorge). All foxes were killed by licensed hunters based on regular shooting schedules; no fox was killed or harmed specifically for this study.

To preserve fresh tissue, the heads of freshly shot red foxes (*Vulpes vulpes*) were immersion fixed by the hunters in the field in either 10 % formalin solution in water or 4 % paraformalde-hyde (PFA)-solution in 0.1 M phosphate buffer (PB). To promote tissue penetration, the fixative was also injected into the ear canal, the muscles surrounding the bulla tympanica, and the eyes for optimal fixation of the retina. The time of fixation of the heads differed between the individuals and ranged from a minimum of two weeks to several years for old specimens from the archive of the Department of General Zoology, University of Duisburg-Essen.

Before preparation of the middle and inner ear the heads were rinsed for several hours with tap water. The eyes were carefully removed with titanium forceps and ceramic scalpels (World precision instruments (WPI), Berlin, Germany) and stored in phosphate buffered saline (PBS, with 0.05 % sodium azide added as a preservative) at 4 °C or for later analysis. Skulls from the collections had been prepared according to standard museum procedures (Mooney et al., 1982). Briefly, the heads were boiled in water with added detergent for several hours after which the soft tissues were easily ablated from the bones. To get a pale finish, the skulls were in most cases bleached for 1-2 minutes in 10 % hydrogen peroxide. The procedure very often left the middle ear ossicles in place and had no significant impact on the ossicle mass or measurements (Nummela, 1995). The ossicles were gathered by opening of the bulla tympanica and removal with a pair of fine forceps.

The total sample comprised material from 54 red foxes (23 fixed individuals and 31 skulls; cf. Tables A1-A8 in the appendix for details on the individuals and the data obtained from them).

OUTER EAR AND BULLA TYMPANICA

I measured the dimensions of the pinnae with a standard ruler. In order to obtain a height to width ratio (Coleman & Colbert, 2010), I determined the maximal width and height of each ear. The fur, skin and mastoid muscles were removed from the skull and the lower jaw was ablated. The bullae tympani were removed with a pair of pincers and the diameter of the proximal end of acoustic meatus was determined with a digital calliper.

After gross preparation, the auditory bullae were cleaned and measurements of height (H), length (L) and width (W) were taken with a digital calliper (Figure 1.2-3). The volume of the bulla was then estimated as an elliptical cone (Schleich & Busch, 2004) according to the formula:

$$\frac{1}{3}\left(\pi \frac{L}{2} \times \frac{W}{2} \times H\right).$$
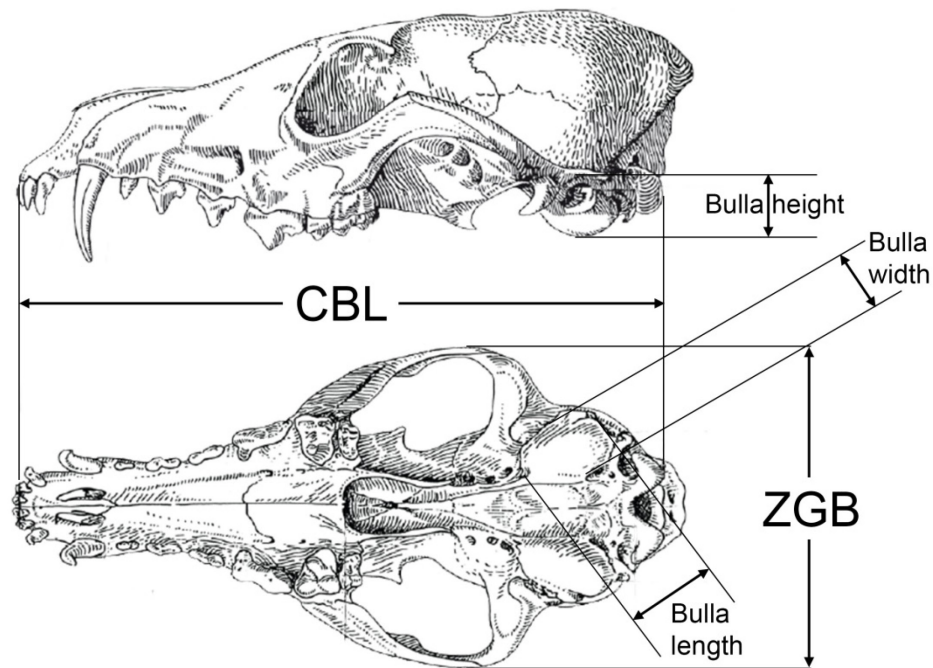
Figure 1.2-3 Parameters that were assessed from the skull and the bulla tympanica. The drawing of the fox skull was taken from Hartová-Nentvichová et al. (2010). CBL, condylobasal length; ZGB, zygomatic breadth.

AREAS OF THE AUDITORY MEMBRANES

The areas of the tympanic membrane (pars tensa), the oval window and the round window were determined by drawing the outlines of each membrane on paper via a camera lucida connected to a stereomicroscope (SZH10 research stereo, Olympus, Hamburg, Germany) (Figure 1.2-4a). The outline of each membrane was drawn at two different magnifications between 7x and 70x and the drawings were digitized at 200 dpi resolution by means of a flatbed scanner. The areas (in mm²) of the membrane drawings were determined in ImageJ (v. 1.48v, National Institutes of Health, Bethesda, USA), and the mean of the drawings at both magnifications was taken as the area value for further calculations.
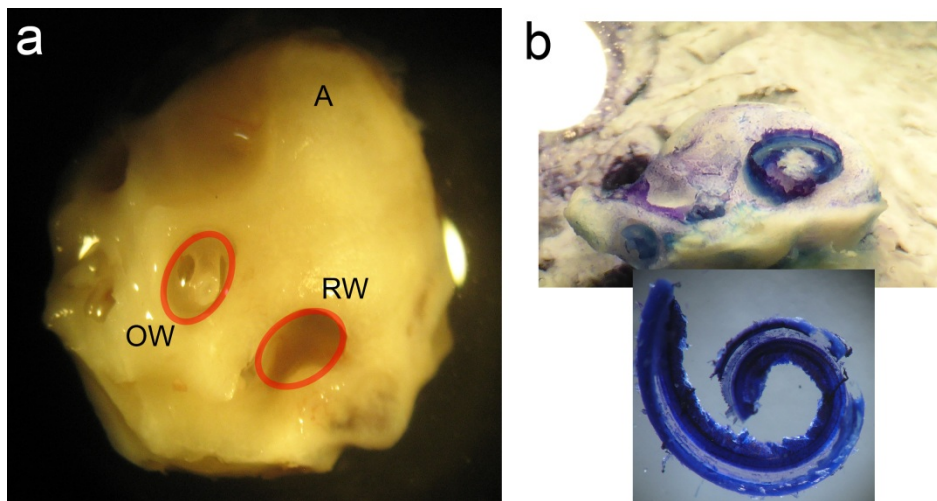
Figure 1.2-4 Cochlear windows and the preparation of the inner ear of the red fox. (a) View onto the inner ear with the stapes sitting within the oval window (OW). The encircled areas indicate how oval and round window (RW) surface were estimated. "A" denotes the approximate region of the apex where the preparation of the cochlea was started. (b) Preparation of the surface specimens. The upper part shows an exposed turn still sitting within the bony labyrinth, the lower picture shows an extracted half-turn.

MEASUREMENTS OF MIDDLE EAR OSSICLES

The auditory ossicles were carefully removed during the middle ear preparation. Whenever necessary (fresh preparations), rests of tympanic membrane and muscle insertions were removed and the ossicles were dried and stored in Eppendorf tubes for later analysis. The weight of each ossicle was determined to the nearest μg with a high precision microbalance (MX5, Mettler-Toledo, Columbus, OH, USA). Each ossicle was weighed twice and the mean was taken as the final weight. High resolution photos were taken of each ossicle (K20D with SMC DFA 50 mm macro objective, Pentax, Tokyo, Japan) and morphometrics were determined with ImageJ (1.48v, NIH).

Table 1 summarizes the assessed measurements as well as the abbreviations used. Two different approximations for the lever arms of the malleus and incus were used. The first followed Hemilä et al. (1995) who defined the arms as the minimal distance between the tips of the manubrium/long process and the pivot of the incudomallear joint (Fig. 1.2-5b). For the second approximation an idealized rotational axis is defined, running from the mallear anterior process through the short process of the incus. The lever arms were then defined as the shortest (perpendicular) distance of the tip of the manubrium/long process to this axis (Figure 1.2-5c; Vrettakos et al., 1988; Mason, 2001). Whenever available, the ossicles of both ears of each red fox specimen were

used to obtain ossicle weight and morphometrics, and the means were taken as the final values for the respective individual.

Table 1 Morphometric measurements taken at the skull and the outer and middle ear.

Morphometric variable		Abbreviation	Description and Unit
Skull	Condylobasal length	CBL	Distance from prosthion to the posterior margin of the condyli occipitales (cf. Figure 1.2-3)
	Zygomatic breadth	ZGB	Distance between both zygion points (cf. Figure 1.2-3)
Pinna	Height	PL	Height (length) of the pinna (mm)
	Width	PW	Basal width of the pinna (mm)
Tympanic membrane	Area	TMA	Area of membrana tympani (pars tensa) defined as the area within the tympanic ring (mm²)
Malleus	Length of manubrium (mallear lever arm)	MLP/MLA	Shortest distance from the tip of the manubrium to the pivot of the incudomallear joint (MLP) or perpendicular to the axis of rotation (MLA) (mm)
	Length of anterior process	MAP	Shortest distance from the tip of the anterior process to its base (mm)
	Length of lateral process	MLP	Shortest distance from the tip of the lateral process to its base (mm)
	Weight	MW	Weight of the dry malleus (mg)
Incus	Length of short process	ISP	Shortest distance from the tip of the short process (crus breve) to the pivot of the incudomallear joint (mm)
	Length of long process (incudal lever arm)	ILP/ILA	Shortest distance from the tip of the long process (crus longum) to the pivot of the incudomallear joint or perpendicular to the axis of rotation (ILA) (mm)
	Weight	IW	Weight of the dry incus (mg)
Stapes	Height	SH	shortest distances from base to head (mm)
	Weight	SW	Weight of the dry stapes (mg)
Oval window	Area	OWA	Oval window area, either measured directly or estimated through stapes footplate area (mm²)
Round window	Area	RWA	Round window area as measured directly (mm²)

1.2.3 Morphometric analysis of the inner ear

The morphology of the cochlea of the red fox was analysed by means of two complementary techniques. First, I used surface specimens to estimate sensory cell numbers and density distributions. Second, mid-modiolar microtome sections served to assess fine morpho-functional properties at different positions along the cochlear duct.

COCHLEAR WHOLE MOUNTS

To obtain whole mounts of the red fox cochlea I carefully liberated the organ of its bony encapsulation with fine forceps. I prepared at a stereoscopic microscope (SZH10 research stereo, Olympus) with a maximum magnification of 70x. The preparation was performed submerged in PBS (Figure 1.2-4b). Starting in the region of the apex, I removed each half-turn, instantly stained it with haematoxylin for one to several minutes and embedded it in glycerol on a standard microscope slide. Occasional toluidine blue-staining facilitated the tissue discrimination during the preparation process.

I analysed the stained half-turns at a light microscope (CM E, Leica, Wetzlar, Germany) at a magnification of 1000x using an oil immersion objective. With help of an eyepiece micrometer, I determined the densities of inner and outer hair cells as well as the width of the row of outer hair cells (Figure 1.2-5) for each field of view over the course of the whole cochlear duct. The distance occupied by ten (minimum of three in fields of view with extensive loss of hair cells) hair cells served to approximate the number of hair cells per mm. By counting the number of non-overlapping fields of view I calculated the total length of the cochlea along the tunnel of Corti, which I then used as an estimate of the length of the basilar membrane. After counting, I assigned all determined parameters to ten percent segments relative to the length of the basilar membrane of the respective individual in order to allow for inter-individual analysis.

I prepared a total of eleven cochleae (seven left ears, four right ears) belonging to eight different animals and counted the hair cells of ten of these surface specimens (the eleventh cochlea showed severe disease related hair cell degeneration which made it impossible to count, but the length of the basilar membrane could still be derived from this specimen). For the animals where both ears where counted (n = 2) I included the mean of both cochleae for each position on the basilar membrane into the final analysis.
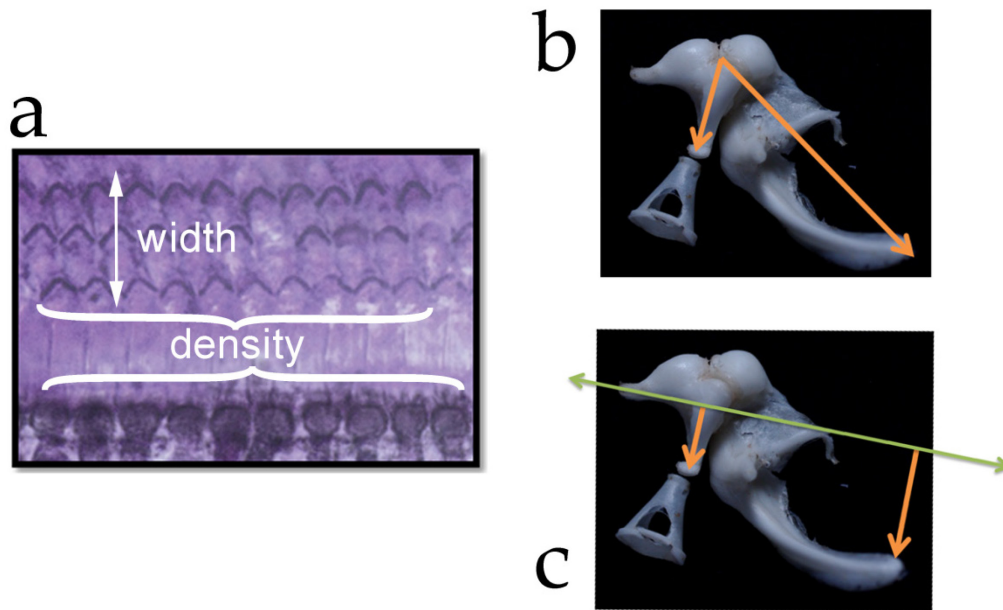
Figure 1.2-5 Cochlear parameters derived from surface specimens and measurement of ossicular lever arms. (a) At 1000x magnification the distance occupied by ten inner and outer hair cells (OHC) as well as the radial width of the OHC triad were determined within each field of view along the whole length of the basilar membrane. The occupied distance by ten hair cells was then transformed into densities which were presented as means of ten segments of equal length from the apex to the base. (b) lever arm lengths measured as the shortest distance between the pivotal point of the incudomallear joint and the tip of the ossicular arms (ILP, MLP; Hemilä et al 1995). (c) lever arm lengths measured as the perpendicular distance between the assumed rotational axis of malleus and the tip of the ossicular arms (ILA, MLA; Vrettakos et al. 1988). Confer Table 1 for more details.

COCHLEAR SECTIONS

To obtain cross-sectional data from cochlear structures, the whole inner ear was first decalcified in 5-10 ml 25 % EDTA (pH 8.0) in PBS for 3-4 weeks at 4 °C. The EDTA-solution was exchanged at least once per week. After decalcification was completed, the cochleae were embedded in paraffin-celloidin (after Ballast, 1984; Burda, Ballast, et al., 1988) and sections of a thickness of 15 μm were cut on a rotary microtome (HM340 E, Microm International, Walldorf, Germany) with disposable blades for hard tissues (N35HR, Feather, Osaka, Japan). Standard paraffin embedding as well as cryosectioning was initially also tested but the combined paraffin-celloidin procedure provided superior results (Figure 1.2-6).

Cryo   Paraffin   Paraffin-Celloidin
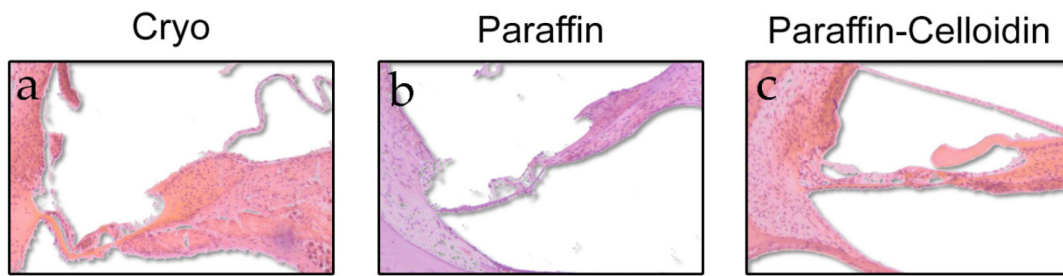
Figure 1.2-6 Comparison of sections of red fox cochleae obtained with three different methods. All sections were HE-stained according to the standard protocol given in the main text. (a) cryosections. (b) microtome slices of a paraffin-embedded specimen (c) combined paraffin-celloidin embedding (after Ballast, 1984). The paraffin-celloidin method yielded the best preserved morphology of the cochlear partition and was therefore chosen throughout this study. All cochleae shown in this figure had been decalcified in 25 % EDTA for the same amount of time before embedding.

Embedding started with incubation of the decalcified cochleae in 5-10 ml of a 1:1 mixture of di-ethyl-ether and absolute ethanol for 4 hours. The cochleae were then incubated for 3 days in 5-10 ml of a 2-4 % Collodion (Fluka Chemie, Buchs, Switzerland) solution, followed by 4 days incubation in 5-10 ml of a 4-8 % Collodion solution. Care was taken to remove all air bubbles from the specimens during these incubation steps. Afterwards, the specimens were hardened in chloroform overnight and cleared for 4 hours in xylene. Paraffin-embedding of the celloidin embedded cochlea specimens was subsequently accomplished in an automated spin tissue processor (STP 120, Microm International) according to the following protocol:

- ⌃ 4 h xylene
- ⌃ 4 h paraffin I
- ⌃ 4 h paraffin II
- ⌃ 4 h paraffin III

The cochleae were then finally embedded in paraffin (Surgipath Paraplast 56 °C, Carl Roth, Karlsruhe, Germany) at an embedding station (EG 1160, Leica). Microtome sections were taken until the plane of the modiolus was passed which was controlled by regular examination under a light microscope (CM E, Leica). The sections were stretched in a water bath (Medax, Neumünster, Germany) containing 10 % ethanol at 40 °C and mounted on uncoated object slides (Carl Roth) as well as positively charged slides (Superfrost Plus°, Menzel, Braunschweig, Germany). Three sections were mounted on each slide and dried on a heat plate (Medax) at 61 °C.

The dried sections were stained with haematoxylin and eosin (HE) according to the following protocol (after Riedelsheimer et al., 2010):

- 3 x 10' Roti-Histol°

- 2 x 3' 99.8 % ethanol

- 2 x 3' 96 % ethanol

- 3' 70 % ethanol

- rinse in aq. dest.

- 3' Ehrlich haematoxylin solution

- rinse in aq. dest.

- 10' rinse in running tap water

- 5' eosin yellow solution

- rinse in aq. dest.

- rinse in 70 % ethanol

- 2 x 1' 96 % ethanol

- 1' 99.8 % ethanol

- 1' 100 % ethanol

- 5' Roti-Histol°

The sections were mounted with Roti Histokit I° and analysed at a light microscope (BX40, Olympus) with an oil immersion objective at a magnification of 1000x. Digital images of the sections were taken with a CCD-camera (XC30, Olympus) and image processing software AnalySIS (V. 5.0, Olympus soft imaging solutions, Münster, Germany).

The ears of eight different red fox individuals were sectioned. From two of these animals I processed both ears and averaged the results. Details about the individuals can be found in the appendix (Table A1). Three mid-modiolar slides were chosen from each specimen and the following parameters were determined for each sectioned half-turn (depicted in Figure 1.2-7):

- length of the IHC and one OHC

- width of the BM

- maximal thickness of the BM homogenous ground substance (zona arcuata, z. pectinata)

- area of the stria vascularis

- area and maximal thickness of the spiral ligament (without stria vascularis)

- area of the tectorial membrane

- presence and length (in % of spiral ligament width) of an osseous spiral lamina

- area of the limbus spiralis
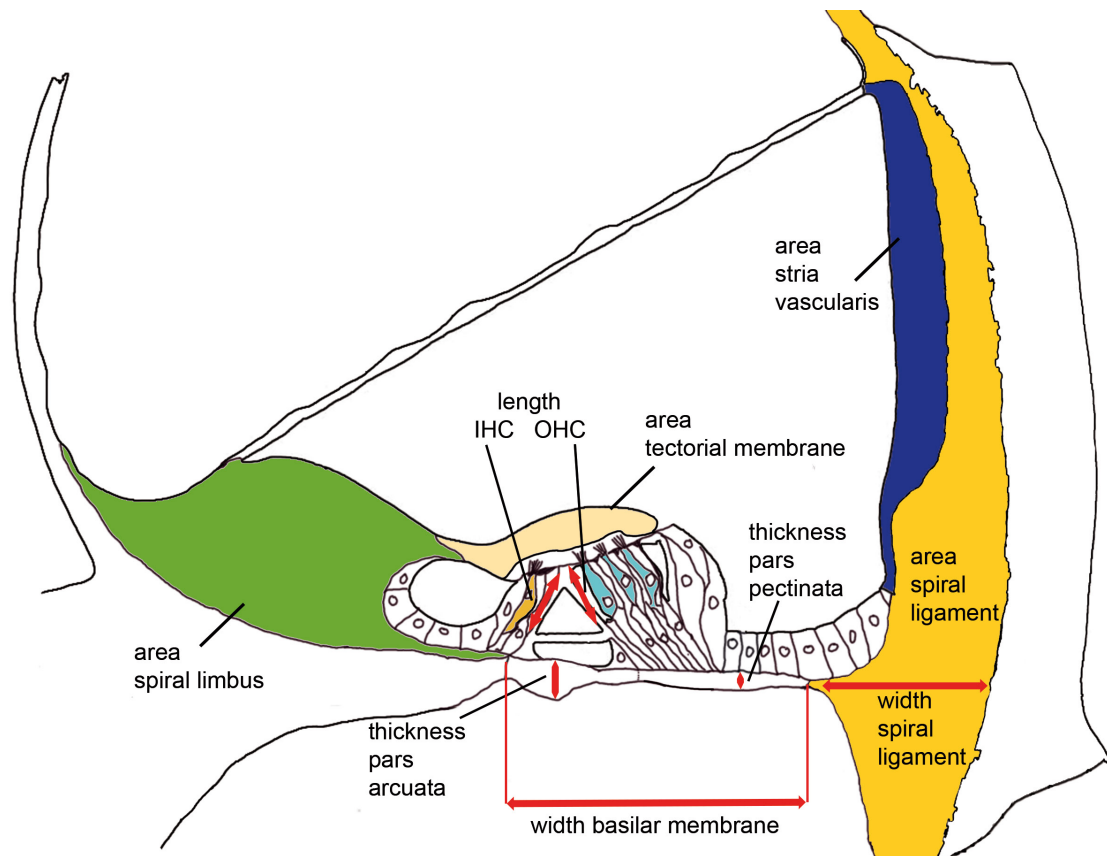
Figure 1.2-7 Cochlear parameters determined for each half-turn of three mid-modiolar sections of each specimen (adapted from Møller 2006).

1.2.4 Statistics

I employed Sigmaplot (V. 12.5, Systat Software Inc., San José, CA, USA) to plot all graphs and perform descriptive statistics and statistical interference. Variance equality and normal distribution were always tested with Bartlett's test and the test procedure by Shapiro-Wilk, respectively. In case of normal distributions I performed t-tests or analyses of variance (ANOVA) depending on the structure of the data (procedure always given in the results section). Nonparametric tests comprised Mann-Whitney U-test and ANOVA on ranks. Advanced statistical tests and analyses are indicated with the respective results in the results section. For tables, standard calculations, and data transformation I used Excel 2010 (Microsoft Corp., Redmond, WA, USA). I prepared graphical illustrations in Photoshop and Illustrator (CS6, Adobe Systems, San José, CA, USA) and performed graphical metrics and cell counts in ImageJ (V. 1.48v, NIH).

1.3 Results

1.3.1 Behavioural audiometry

BEHAVIOURAL AUDIOGRAM

With two daily training sessions the foxes readily learned the behavioural procedure within 2-4 weeks. After the training period, up to two thresholds could be obtained per day, leading to a total experimental period of 8-10 weeks per animal. Complete audiograms could be obtained for two animals, one fox (male 2) escaped from the enclosure during the experimental period. Hence, from male 2 we could only obtain threshold values in the region of highest sensitivity (2 kHz, 4 kHz, 6.3 kHz, 8 kHz) and around the upper limit of hearing (46 kHz, 54 kHz) that were also included in the calculation of the mean red fox audiogram.

The mean false alarm rates of all test sessions used for threshold determination were 13 %, 14 %, and 12 % for each of the three foxes, respectively (cf. Table 2). Furthermore, due to the stability criterion and the correction for false alarms, 93 % of these test sessions had false alarm rates lower than 20 %.

The thresholds of the individual foxes showed high conformity at most frequencies. The mean red fox audiogram shows the typical mammalian V-shape (Figure 1.3-1; Table 2; Fay 1988). At 60 dB SPL, a low frequency limit at 51 Hz was observed, while a gradual decrease in thresholds led to the point of highest sensitivity with a mean of -15 dB SPL at 4 kHz for all three animals. Two of the three animals showed comparable high sensitivity at 2 kHz and 6.3 kHz. The high mean sensitivity at those three frequencies was -10 dB SPL. Above 6.3 kHz, however, sensitivity markedly dropped to 2 dB SPL at 8 kHz followed by a gradual increase of the thresholds with retained sensitivity up to 40 kHz. Above this frequency, a steep increase of thresholds led to a quick approach of the 60 dB SPL high frequency limit at 48 kHz. At 60 dB SPL the red fox audiogram spans 9.84 octaves.
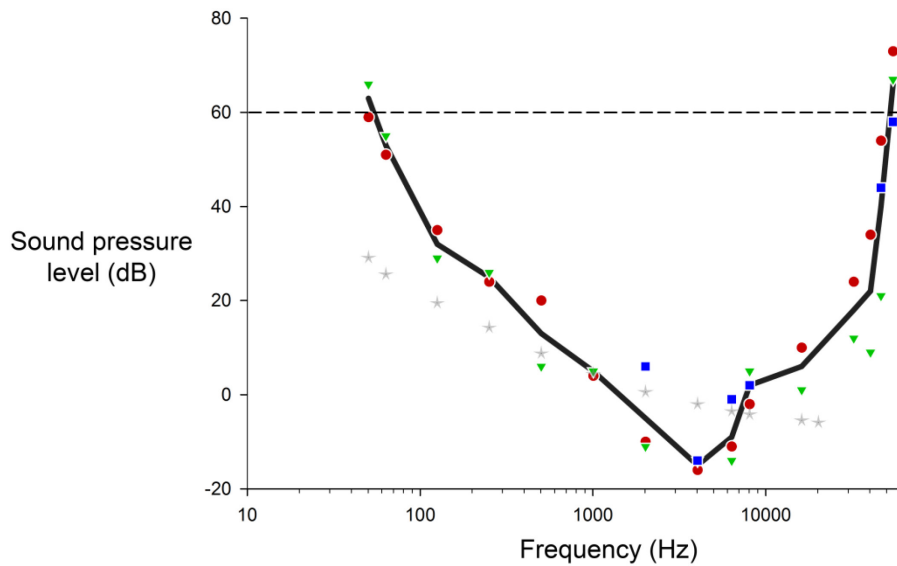
Figure 1.3-1 Behavioural audiogram of three red fox specimens. The symbols represent the different individuals (green triangles: male 1; blue squares: male 2; red circles: female). The solid line represents the mean red fox audiogram calculated through averaging of the individual thresholds. Grey asterisks indicate the average spectrum level of the ambient noise (confer methods for details on the measurements). The dashed line indicates the functional hearing range at 60 dB SPL (51 Hz - 48 kHz).

Table 2 Age, false alarm (FA) rates, and sensitivity thresholds of the three tested red fox specimens. FA rates are given for both the total sessions and the sessions which were finally used for threshold estimation. Due to the stability criterion (see 2.4) the standard deviations of the individual thresholds were always between 1 and 5 dB SPL and are therefore not given in the table.

	Subject			
	Male 1	Male 2	Female	Mean
Age (months)	3-5	3-5	6-8	
Mean FA rate (total)	14 %	15 %	18 %	16 %
Mean FA rate (thresholds)	13 %	14 %	12 %	13 %
Frequency (Hz)	Thresholds in dB SPL			
50	66		60	63
63	55		51	53
125	29		35	32
250	26		24	25
500	6		20	13
1000	5		4	5
2000	-11	6	-10	-5
4000	-14	-14	-16	-15
6300	-14	-1	-11	-9
8000	5	2	-2	2
16000	1		10	6
32000	12		24	18
40000	9		34	22
46000	21	44	54	40
54000	67	58	73	66

AMBIENT NOISE

To determine the degree of comparability of the audiogram presented here and to assess the shielding properties of our semi-anechoic chamber, I conducted several ambient noise measurements. Except for a small region of resonance frequencies between 25 Hz and 31.5 Hz, the ambient noise levels measured inside of the chamber were lower and less erratic than those measured on the outside (Fig. 1.3-2). This was especially true for 1/3-octave windows bracketing the frequencies that were presented in the test sessions (black dots in Figure 1.3-2). The mean ambient noise level within a 1/3-octave window inside of the chamber was 33 ± 5 (SD) dB SPL compared to 35 ± 5 (SD) dB SPL on the outside. The overall difference was highly significant (Two Way ANOVA; $p < 0.001$; Holm-Sidak post-hoc tests: significant differences in 23 of 31 frequency windows). For frequencies higher than 20 kHz no 1/3-octave filter was available, and therefore, no detailed noise levels can be reported for this range, but mean integrated ambient noise intensity in the frequency range from 12.5 kHz to 100 kHz was quantified as 48 ± 0.4 (SD) dB SPL. In the very low frequency range (<20 Hz), mean integrated ambient noise levels inside of the chamber were 57 ± 1.7 (SD) dB SPL.
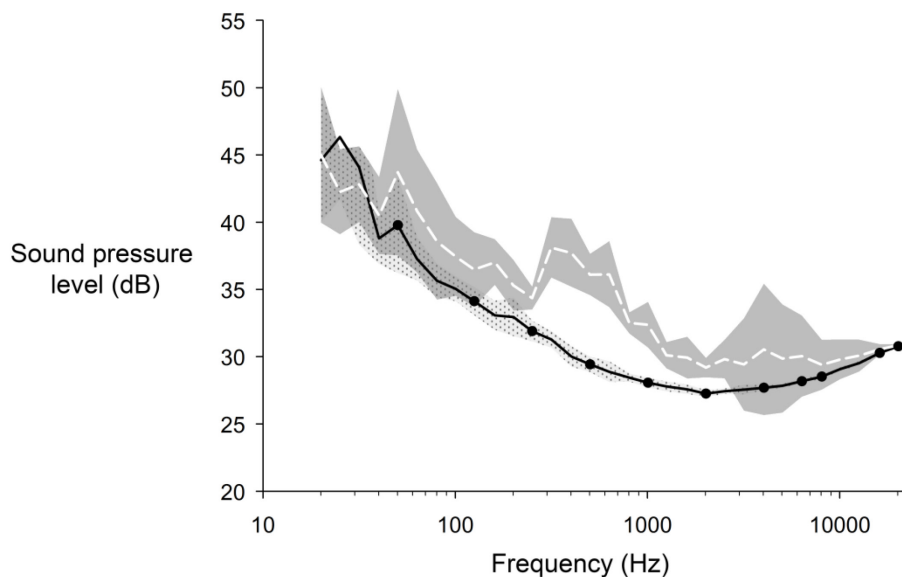
Figure 1.3-2 Mean ambient noise levels in dB SPL. Each line represents averages of 20 sample measurements conducted on different days during the typical time of test sessions. SPL levels were integrated over 1/3-octave windows. The dashed white line indicates the background SPL and the standard deviation (shaded area) measured outside of the semi-anechoic test chamber. The solid line and dotted area confer to the corresponding values measured inside of the chamber. Ambient noise was less erratic inside of the chamber than outside. The same holds for the absolute intensity which was lower at 10 of the 15 frequencies that were assessed in the audiogram and for which the ambient noise could be accurately measured (black dots).

HUMAN AUDIOGRAM

In order to validate the functionality and calibration of the behavioural setup (Coleman, 2009), I used the exact same equipment within the same ambience to generate a human audiogram of one subject. The obtained thresholds were consistent with those of previously published human audiograms (Figure 1.3-3). For example, the low frequency range (<125 Hz) corresponded exactly to data published by Jackson et al. (1999) and to the human ISO free-field threshold curve (ISO, 1961). With the exception of a higher threshold at 1 kHz, the mid-frequency sensitivity fitted well with the audiogram published by Sivian and White (1933) while the high frequency range is again in agreement with the ISO standard. Furthermore, the human audiogram fell always within a 2σ range of published human audiograms by Sivian and White (1933) and Jackson et al. (1999).
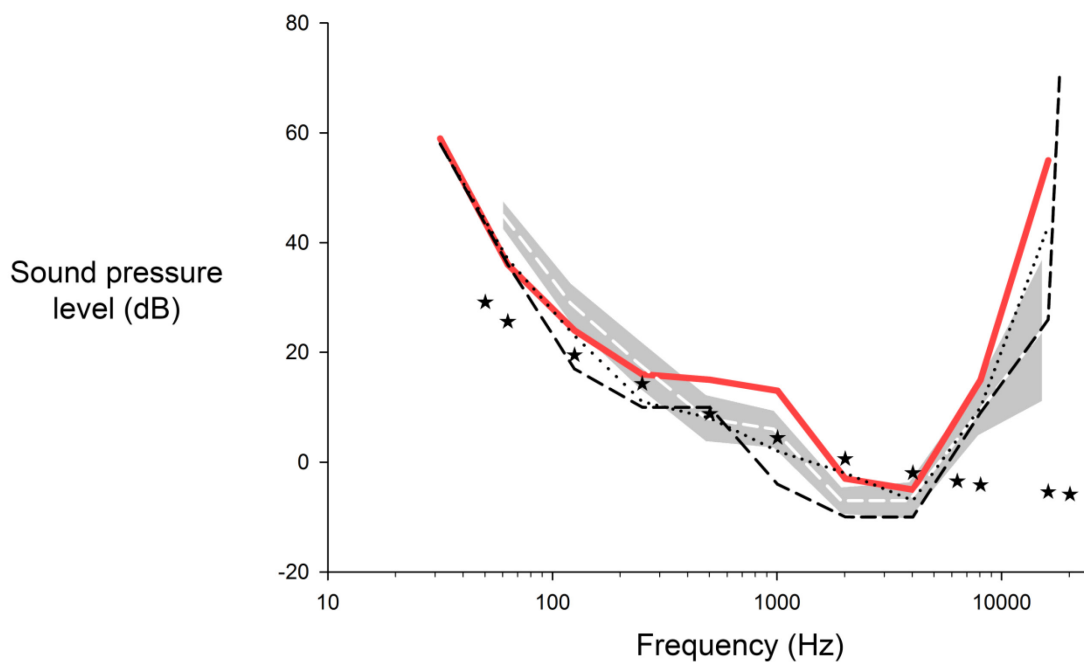
Figure 1.3-3 The human audiogram obtained in this study (bold red line, one person) compared to published human audiograms. The dark dashed line shows the audiogram published by Jackson et al. (1999), the white dashed line represents the mean audiogram of 10 human individuals with the standard deviation given by the shaded area (Group C from Sivian and White, 1933). The dotted line shows the ISO free-field threshold curve (ISO, 1961). Stars indicate the average spectrum level of the ambient noise in the current study.

1.3.2 Anatomy

OUTER EAR

Red foxes have erect pinnae of triangular shape. The mean width measured at the pinna base in seven red foxes (14 ears) amounted to 30.75 ± 3.79 mm (± SD); the mean length was 48.38 ± 15.25 mm. Plotting the width and length of the measured ears against the condylobasal length (CBL) demonstrated a strong positive correlation with ear length, while the width of the base showed more variation and was not correlated with CBL (Pearson product moment correlation; pinna length against CBL, R = 0.833, p = 0.02; width against CBL, R = 0.022, p = 0.963). Thus, the shape of the pinna becomes more elongated as the fox growths (adult height / width ratio 2:1).

Another developmental increase in size could be observed in the basal diameter of the meatus (minimum: 3.8 mm, maximum: 6.75 mm, mean: 5.85 ± 0.68 mm, n = 26 individuals), which significantly increased with increasing CBL (Pearson product moment correlation; meatus diameter against CBL, R = 0.781, p < 0.001).
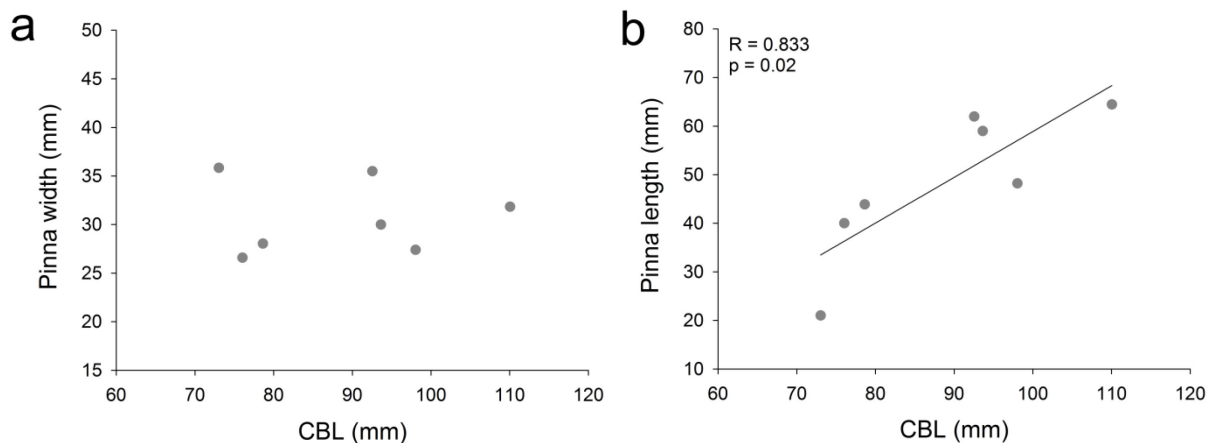
Figure 1.3-4 Lengths and basal widths of the pinnae of seven red foxes plotted against the condylobasal length (CBL) as a proxy of age. When both pinnae of the same fox were measured, the mean values are given. (a) Pinna width against CBL. (b) Pinna length against CBL. Pinna length is positively correlated to CBL while pinna width is not (Pearson product moment correlation; length against CBL, R = 0.833, p = 0.02; width against CBL, R = 0.022, p = 0.963).

MIDDLE EAR

Bulla tympanica and tympanic membrane

The bulla tympanica of the red fox has an oval shape (mean length: 19.8 ± 0.9 mm, mean height: 16.4 ± 0.9 mm, mean width: 11.3 ± 1.1 mm; n = 38 individuals) and distinctly protrudes from the base of the skull. The mean bulla volume calculated from my samples was 967 ± 164 mm³ (n = 38 individuals). The bulla contained a bony septum (S) separating the bulla into two compartments (but not completely as seen in felids, see discussion) as well as several smaller septa at the bulla walls (Figure 1.3-5a).

The tympanic membrane (pars tensa) was of oval shape and had a mean area of 55.7 ± 7.9 mm² (n = 16 individuals). No relationship between the CBL of the animal and the tympanic membrane area was evident (cf. Table A2 in the appendix). The small pars flaccida of the tympanic membrane amounted to less than 10 % of the total tympanic membrane area (Figure 1.3-5b).
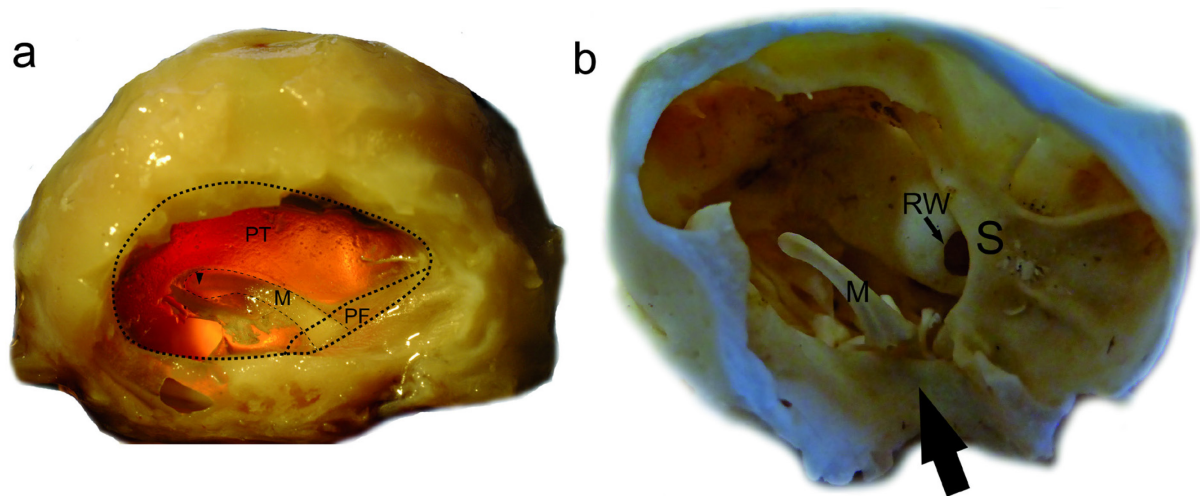
Figure 1.3-5 The bulla tympanica and tympanic membrane of the red fox. (a) View onto the external side of the tympanic membrane. Note the manubrium of the malleus. The arrowhead marks the umbro. (b) Opened bulla tympanica. Note the bony septum (S) separating the bulla into two half-compartments as well as the smaller septa at the bulla walls. The large arrow marks the medial end of the auditory meatus. M, manubrium of malleus; PF, pars flaccida of tympanic membrane; PT, pars tensa of tympanic membrane; RW, round window; S, septum.

Middle ear ossicles

The middle ear ossicles of the red fox (individual VV11, left ear) are shown schematically in Figure 1.3-6. The malleus and incus were not fused but firmly attached to the bulla walls by the middle ear ligaments, giving the apparatus a stiff appearance (see discussion). The handle of the malleus was relatively strong and well curved. The mean weight of the malleus was 10.64 ± 1.18 mg (n = 41 individuals). Measured as the distance from the presumed axis of rotation, the mean lever arm of the malleus was 3.22 ± 0.38 mm (n = 34 individuals), while it was 7.04 ± 0.31 mm (n = 35 individuals) measured from the pivotal point of the malleo-incudal joint. The corresponding mean lever arm lengths of the incus (crus longum) were 1.54 ± 0.15 mm (axis, n = 47 individuals) and 2.06 ± 0.12 mm (pivot, n = 47 individuals). The resulting lever arm ratios were 2.1 ± 0.26 (axis) and 3.26 ± 0.23 (pivot). The anterior and the shorter lateral processes of the malleus had a mean length of 2.25 ± 0.25 mm (n = 39 individuals) and 1.49 ± 0.11 mm (n = 39 individuals), respectively. The short process of the incus (crus breve) was 2.14 ± 0.19 mm (n = 47 individuals) long. Mean incus weight was 5.19 ± 0.63 mg (n = 47 individuals).

The stapes of the red fox specimens had a mean length of 2.11 ± 0.15 mm (n = 26 individuals) and weighed 0.63 ± 0.13 mg (n = 25 individuals). Its footplate was slightly convex, of oval form (cf. Figure 1.3-6), and had a mean area of 1.78 ± 0.38 mm² (n = 36 individuals). The mean ratio between the area of the tympanic membrane and the area of the oval window (stapes footplate) was 32.34 ± 4.33 (n = 15 individuals). When only the estimated effective area of the tympanic membrane is used (2/3 of pars tensa; Wever & Lawrence, 1954; Hemilä et al., 1995), the ratio was reduced to 21.56 ± 2.88 (n = 15 individuals). Combined with the lever arm ratio given above, I calculated the mean middle ear impedance transformer ratio

ITR = (OWA/TMA) × (IL/ML)² (Dallos, 1973; Coleman & Colbert, 2010)

for the red fox:

- ⌃ ITR = 0.0044 ± 0.0009 (using the pivot lever ratio).
- ⌃ ITR = 0.0099 ± 0.0023 (using axis lever ratio).
- ⌃ ITR (mean) = 0.00715.
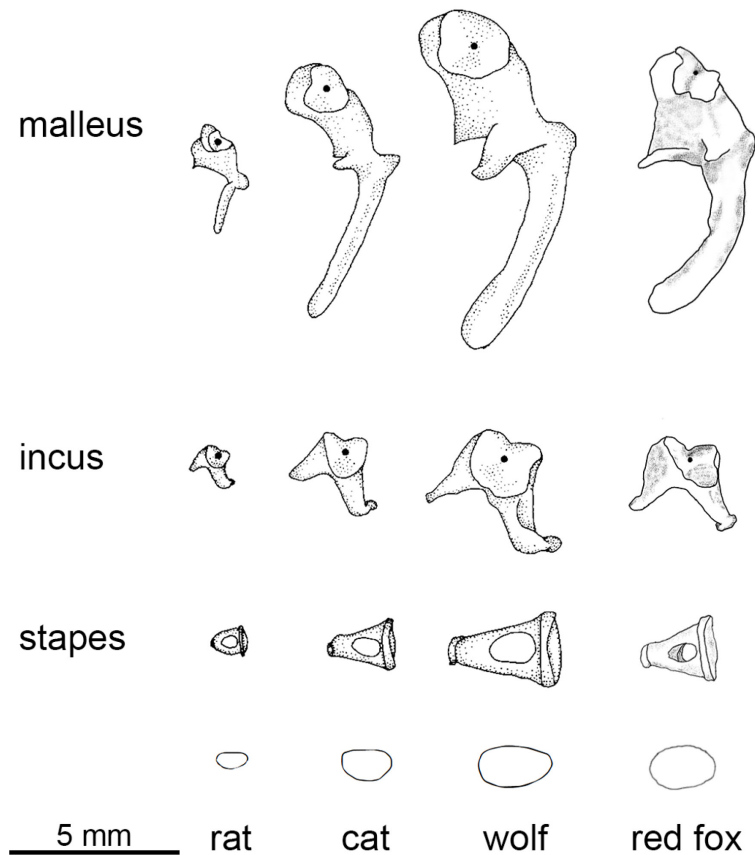
Figure 1.3-6 Schematic drawing of the middle ear ossicles and the area of the stapes foot plate of the red fox (individual VV11) in direct comparison to other species (rat, cat, and wolf). The figure was adopted from Nummela (1995) and complemented with the red fox ossicles drawn to scale.

INNER EAR

General cochlear morphology

The cochleae of the investigated red fox specimens described approximately 3.2 turns. An elongated part in the basal region (cochlear hook) was well developed. The morphology of the cochlear duct closely followed the general mammalian *bauplan* (Vater & Kössl, 2011).

The organ of Corti of the red fox, as assessed by light microscopic inspection, showed all typical mammalian structures and cell types. As in other mammals, the different components of the red fox's auditory partition changed in size and shape along the cochlear duct as I will describe in the following. As not all sections were of equal quality, the following numbers are not always based on the full sample of ten ears stemming from eight different individuals. Therefore, I show the exact mean values and underlying sample sizes in Tables 3.

The base of the cochlea was characterised by an osseous spiral lamina considerably protruding into the cochlear duct, supporting the spiral ligament along almost 100 % of its width, all the way to the outer edge of the BM. This support was retracted further up the cochlear duct and was completely absent somewhere between the fourth and fifth ($\sim$ 16 mm from the base) half-turn (HT). From here on up to the apical end, the basilar membrane was supported on its external edge only by the spiral ligament. In the upper HTs, however, the spiral ligament reached down to the floor of the scala tympani (Figure 1.3-7, inset d), which might substitute for the support of the osseous spiral lamina.

The cross sectional areas of the tectorial membrane and the spiral limbus changed with reversed gradients. The tectorial membrane area increased considerably from the base (835 µm²; confer Table 3 for standard deviations) towards the sixth HT (7,870 µm²) and slightly decreased afterwards (6,457 µm²). The spiral limbus showed relatively constant cross sectional areas up to the second HT and from thereon steadily decreased in size ($\sim$ 22,000-6,500 µm²).

The spiral ligament decreased in size towards the apex of the cochlea, as reflected by a decrease of both width and area. The width declined from a basal value of 424 µm to roughly one fifth of this value at the apex (82 µm). The area decreased accordingly, from more than 160,000 µm² at the base, down to 20,000 µm² in apical regions. Accordingly, also the absolute cross sectional area of the stria vascularis decreased from basal values around 12,000-13,000 µm² down to 2,500-3,000 µm². The proportion of the stria vascularis relative to the spiral ligament, however, doubled from basal $\sim$ 8 % to 15-20 % in apical regions.

The BM reached a maximal thickness (mean: 17.7 µm; both partes pectinata and arcuata) in the region of the first HT. Further basalward the thickness slightly decreased in the order of 1-2 µm. From the first HT towards the apex, the thickness of the BM decreased constantly until it reached minimal thickness of 5-6 µm in apical regions. The slope of the decline was slightly steeper in pars pectinata than pars arcuata. The decrease in BM thickness towards the apical end was accompanied by an increase in BM width, which was smallest in the hook region ($\sim$ 80 µm) and reached widths of more than 380 µm near the apex. The stiffness ratio f (thickness BM / width BM; von Békésy, 1960) decreased constantly from a basal value of $\sim$ 0.19 to an apical value of 0.015 ($f_{basal} : f_{apical}$ = 13:1).

Even though the figures are based on a relatively small sample (cf. Table 3), it was indicated that the length of the IHCs underwent no change along the cochlear duct (stable length around

25 µm), while the length of the OHCs steadily and considerably increased from 21 µm short OHCs in the hook region to 49 µm long OHCs in the apical region.
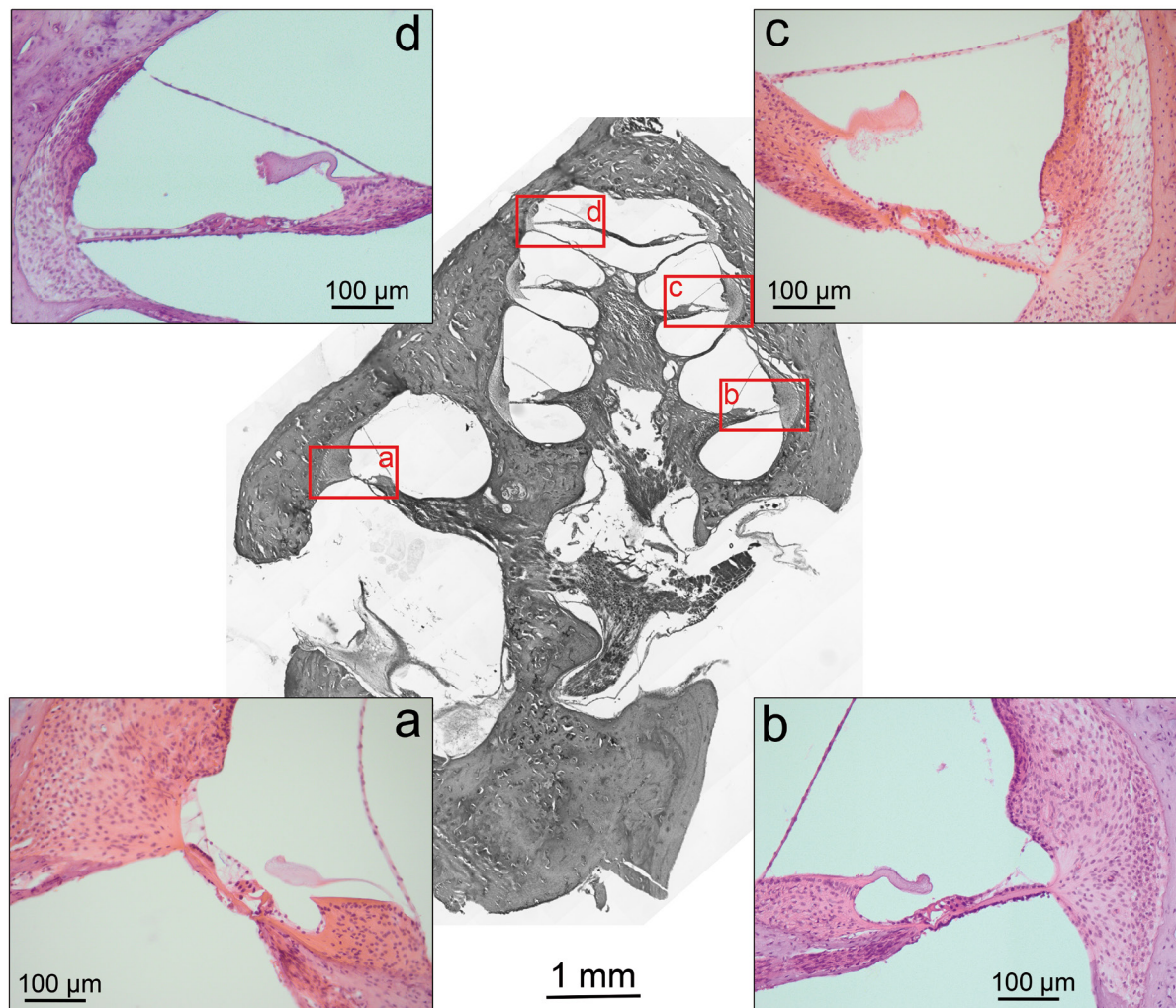
Figure 1.3-7 Mid-modiolar HE stained paraffin-celloidin section of the cochlea of a red fox (individual VV6) and exemplary sections of different positions along the cochlear duct. The shown insets were not of the same individual. The inset (a) depicts the typical situation in the region of the first half-turn (HT), while inset (d) shows the situation in HT7 and the other insets correspondingly at intermediate HTs. For a description of the quantitative changes of the cochlear partition, confer the main text.

Table 3 Cochlear parameters assessed from mid-modiolar sections of eight red fox individuals (ten cochleae). The sample size n denotes the number of individuals the mean was based on. HT, half-turn, P, position in distance from the base.

Parameter		Hook	HT1	HT2	HT3	HT4	HT5	HT6	HT7
	P (mm)	<1	1	6.8	11.3	15.4	18.9	22.1	25
Thickness BM pars arcuata	mean	16.2	17.7	16.8	14.4	11.9	9.5	7.0	5.8
(µm)	n	6	8	8	8	8	8	8	3
	SD	2.1	2.8	3.1	2.6	2.4	2.4	1.7	2.6
Thickness BM pars pectinata	mean	15.9	17.7	14.9	11.8	10.0	8.0	6.5	5.4
(µm)	n	6	8	8	8	8	8	8	3
	SD	1.3	2.2	2.3	2.3	2.0	1.1	1.6	1.8
Width BM	mean	83	188	259	268	282	322	371	384
(µm)	n	6	8	8	8	8	8	8	3
	SD	34	26	33	23	17	33	40	10
Width spiral ligament (radial)	mean	424	334	212	154	125	122	94	82
(µm)	n	5	8	8	8	8	8	8	3
	SD	37	60	35	13	9	15	21	9
Area stria vascularis	mean	12,880	10,324	11,376	9,364	6,666	6,131	6,839	2,876
(µm²)	n	5	8	8	8	8	8	8	3
	SD	1,949	2,720	3,155	1,885	1,569	2,892	4,708	652
Osseous support of spiral ligament	mean	94	75	38	25	13	0	0	0
(%)	n	5	8	8	8	8	8	8	3
	SD	5	14	16	7	13	0	0	0
Cross sectional area spiral ligament	mean	163,471	151,614	129,212	102,857	66,051	51,665	31,964	20,023
(µm²)	n	5	8	8	8	8	8	8	3
	SD	25,183	24,918	18,906	22,058	9,557	10,129	7,786	4,311
Cross sectional area tectorial membrane	mean	835	2,369	4,482	5,109	5,214	7,029	7,870	6,457
(µm²)	n	5	8	8	8	8	8	8	3
	SD	316	1148	1,744	1,979	1,574	2,920	3,648	2,162
Length IHC	mean	21.7	25.4	24.7	25.5	24.6	24.3	27.9	26.8
(µm)	n	1	4	3	2	4	4	5	2
	SD		3.8	2.3	7.2	4.9	3.5	4.6	6.0
Length OHC	mean	21.2	24.1	26.3	29.2	32.3	36.2	37.7	49.3
(µm)	n	3	7	7	7	7	5	4	1
	SD	1.8	2.4	2.9	3.3	4.4	4.4	1.2	
Cross sectional area limbus spiralis	mean	21,649	22,615	22,512	19,602	14,438	13,051	9,346	6,511
(µm²)	n	5	8	8	8	8	8	8	3
	SD	3,268	3,931	3,820	3,619	2,965	2,072	2,150	1,492

Hair cell densities

The cuticular plates and stereocilia of the outer (OHC) and inner hair cells (IHC) as well as the tunnel of Corti were readily identifiable on the toluidine blue and haematoxylin stained cochlear half-turns (Figure 1.3-8). The general arrangement of the cells followed the typical mammalian *bauplan* with three rows of OHCs and a single row of IHCs running along the tunnel of Corti. Infrequently, I observed a fourth row of OHCs, predominantly in the more apical regions (Figure 1.3-8b). The length of the basilar membrane was determined as 25.78 ± 1.6 mm (n = 8 individuals).
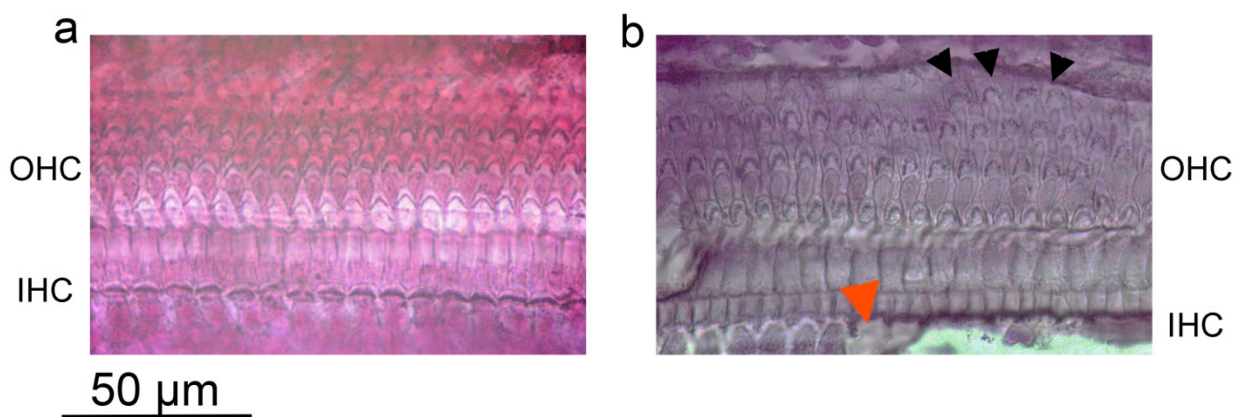
Figure 1.3-8 Surface specimens of red fox cochlea stained with haematoxylin and toluidine blue viewed at 1000x magnification at two different positions along the cochlear duct: near the basal end of the cochlea (a), and in the apical region (b). Note the difference in the width of the OHC triad. A fourth row of OHCs, recognizable in (b) is marked by the black arrowheads. The read arrowhead marks the loss of inner hair cells in (b), most likely due to preparation, which, however, did not interfere with density determination as the insertion sites along the tunnel of Corti were very distinct. Scale bar applies to both inserts. IHC: inner hair cells, OHC: outer hair cells.

In general, the IHC densities in the red fox changed only moderately along the course of the cochlear duct (Figure 1.3-9). Starting at the apex with a mean density of 109.8 ± 4.2 IHC/mm (± SD), the number decreased steadily down to a minimum of 104.0 ± 9.4 IHCs/mm at 51-60 % distance from the apex. Moving further towards the base the number of IHCs increased until it reached a maximum of 113.6 ± 12.1 IHCs/mm at a distance of 71-80 % from the apex. In the basal region the IHC density again slightly decreased to a mean number of 108.2 ± 7.6 IHCs/mm. The overall mean IHC density was 107.2 ± 2.9 IHCs/mm.

The density at different positions of the basilar membrane did not show an overall significant difference (Two Way ANOVA, F = 1.580, p = 0.142) but the peak density of IHCs in the segment 71-80 % was significantly higher than in the adjacent apex-ward region (one-tailed paired t-

test, p = 0.048, tested against the mean of the region 51-70 % = 105.5 IHCs/mm), and the difference towards the more basal region showed a trend towards lower densities (one-tailed paired t-test, p = 0.082, tested against the mean of the region 81-100 % = 108.1 IHCs/mm). Also, the hair cell densities showed significant inter-subject differences (Two Way ANOVA with Holm-Sidak post-hoc test, F = 7.275, p ≤ 0.001). OHC densities were almost constant along the cochlear duct with a mean of 408.0 ± 8.7 OHCs/mm (Figure 1.3-9).
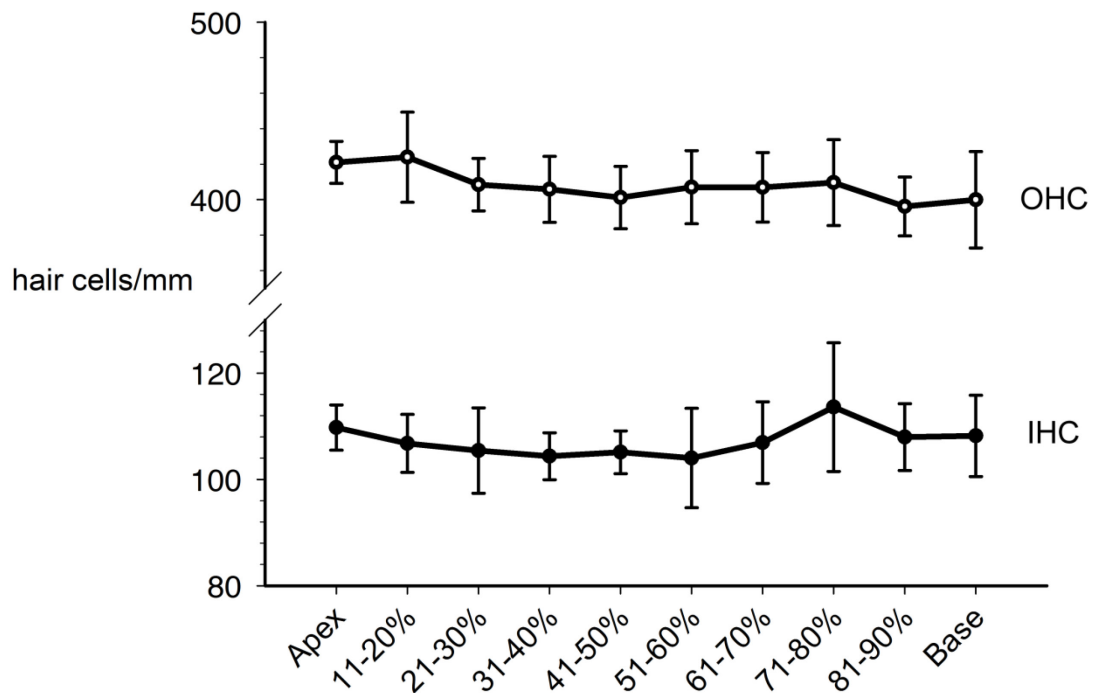
Figure 1.3-9 Mean hair cell densities in relative segments of spiral length along the cochlear duct. Open circles: outer hair cells (OHC), filled circles: inner hair cells (IHC), error bars: SD.

The width of the triad of OHCs first steadily increased from the base (19.22 ± 0.8 μm) towards the apex of the cochlea, reaching a plateau 20-30 % distance from the apex (maximum: 34.1 ± 2.41 μm; Figure 1.3-10). In the final two apical segments, however, the width of the triad slightly decreased again (final segment: 30.82 ± 1.52 μm).
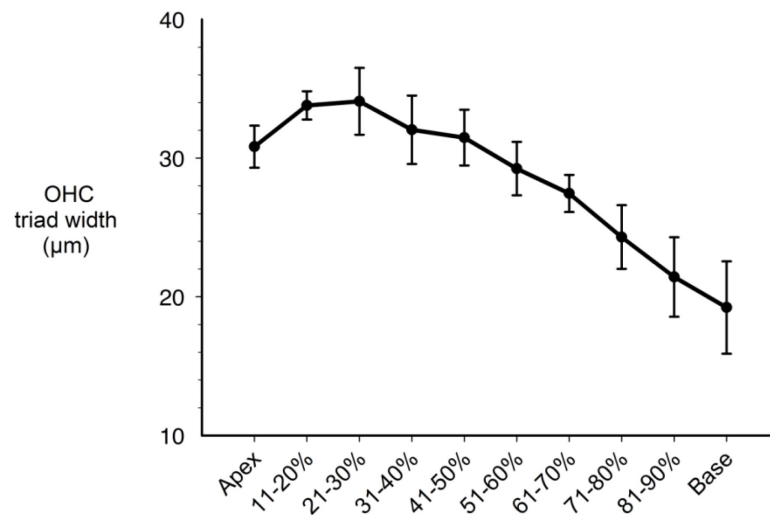
Figure 1.3-10 Mean width of the outer hair cell triad in relative segments of spiral length along the cochlear duct. Error bars: SD.

ONTOGENETIC CONSIDERATIONS OF THE MIDDLE AND INNER EAR

The specimens used in this study were of diverse age classes from several weeks old pups up to several years old adults, even though the exact age is unknown. To see if any developmental processes could be revealed within the middle and inner ear, I tested for correlations between two age-related morphometric variables of the skull (CBL and ZGB as well as their product) and several ossicle dimensions, ossicle weight and cochlear dimensions.

The weight of each ossicle was positively and significantly correlated to CBL, ZGB and their product (Table 4). The correlation was in generally strongest for CBL and showed differences between the ossicles with the weakest correlation for the stapes and the strongest for the malleus. From the ossicle functional dimensions only the incus lever arm measured perpendicular from the axis of rotation (ILA) and stapes height (SH) were positively and significantly correlated to the skull measurements. The relationship between CBL and the weight of the ossicles is shown in Figure 1.3-11.

Table 4 Correlations between the morphometric skull variables and ossicle weight and dimensions. Given are Pearson product-moment correlation coefficients and sample sizes.

	Weight			Length							
	Malleus	Incus	Stapes	MLP	MLA	MAP	MLP	ISP	ILP	ILA	SH
CBL	0.735** (41)	0.641** (47)	0.426* (25)	n.s. (35)	n.s. (34)	n.s. (39)	n.s. (39)	n.s. (47)	n.s. (47)	0.439** (47)	0.439* (26)
ZGB	0.708** (41)	0.602** (47)	0.442* (25)	n.s. (35)	n.s. (34)	n.s (39)	n.s. (39)	n.s. (47)	n.s. (47)	0.425** (47)	0.429* (26)
CBL * ZGB	0.712** (41)	0.604** (47)	0.431* (25)	n.s. (35)	n.s. (34)	n.s (39)	n.s. (39)	n.s. (47)	n.s. (47)	0.429** (47)	0.418* (26)

Pearson correlation coefficients with a superscript "**" were significant with $p < 0.01$; "*" indicates significance with $0.05 > p > 0.01$; n.s. = not significant; the numbers of specimens are given in parentheses
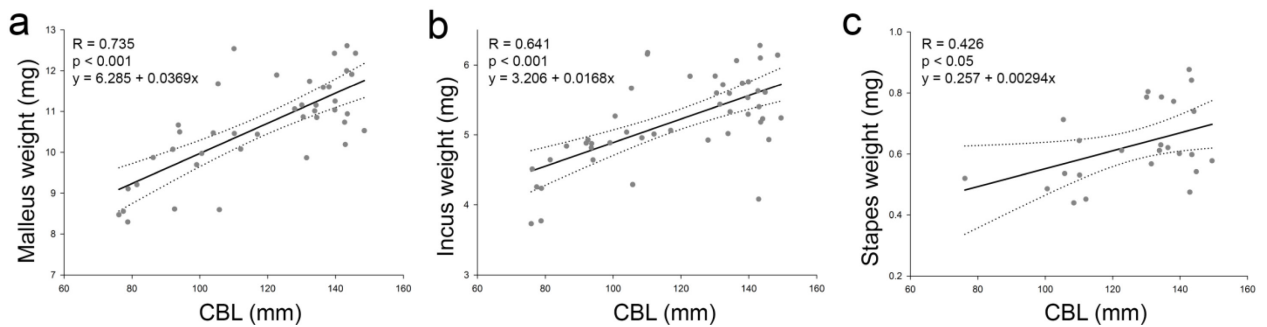
Figure 1.3-11 Weight of the middle ear ossicles in dependence of the condylobasal length (CBL). The weight of all three ossicles ((a) malleus, (b) incus, (c) stapes) was significantly positively correlated with CBL. Regression lines (solid) and corresponding 95 %-confidence intervals are given for each correlation. Pearson correlation coefficients, p-values and the equation of the linear regression are also shown. For sample sizes confer Table 4.

Tests for correlations between ossicle weight and ossicle dimensions revealed that malleus weight was weakly positively correlated to the lever arm measured from the pivot (MLP) and the length of the anterior process (MAP) and strongly correlated to ILA and SH (Table 5). Incus and stapes weight were only but strongly correlated to ILA and SH.

Table 5 Correlations between the weight of the ossicles and respective dimensional measurements. Given are Pearson product-moment correlation coefficients and sample sizes.

	Length							
	Malleus lever (pivot)	Malleus lever (axis)	Malleus anterior process	Malleus lateral process	Incus lever (pivot)	Incus lever (axis)	Incus short process	Stapes height
Malleus weight	0.375* (35)	n.s. (34)	0.366* (36)	n.s. (36)	n.s. (41)	0.473** (41)	n.s. (41)	0.537** (23)
Incus weight	n.s. (35)	n.s. (34)	n.s (39)	n.s. (39)	n.s. (47)	0.530** (47)	n.s. (47)	0.640** (26)
Stapes weight	n.s. (19)	n.s. (18)	n.s (21)	n.s. (21)	n.s. (25)	0.745** (25)	n.s. (25)	0.511* (22)

Pearson correlation coefficients with a superscript "**" were significant with p < 0.01; "*" indicates significance with 0.05 > p > 0.01; n.s. = not significant; the numbers of specimens are given in parentheses

Finally, it was of interest to see how the weight of the skull related to the morphometric measurements and the weight of the ossicles. Skull weight was highly positively correlated to both CBL and ZGB but only to the weight of the malleus while being unrelated to incus and stapes weight (Table 6).

Table 6 Correlations between the weight of the skull, morphometric variables and ossicle weight. Given are Pearson product-moment correlation coefficients and sample sizes. The skull weight does not include the lower jaw.

	CBL	ZGB	Malleus weight	Incus weight	Stapes weight
Skull weight	0.970** (25)	0.950** (25)	0.557** (22)	n.s. (25)	n.s. (19)

Pearson correlation coefficients with a superscript "**" were significant with p < 0.01; "*" indicates significance with 0.05 > p > 0.01; n.s. = not significant; the numbers of specimens are given in parentheses

1.4   Discussion

1.4.1 Behavioural audiometry

FUNCTIONALITY OF THE SETUP AND EFFICIENCY OF THE PSYCHOPHYSICAL PROCEDURE

Several classical and operant conditioning methods are suitable for the assessment of valid animal audiograms (Fay, 1988; Klump et al., 1995). These include both negative conditioning methods such as conditioned avoidance, and positive methods based on reward paradigms. In addition, the method of conditioned suppression represents a powerful combination of both positive and negative reinforcement (Smith, 1970). Each method has its advantages and disadvantages with regards to training time, subject control and the efficiency of data collection. As long as certain standard criteria are met, however, the resulting audiogram data are mostly independent of the conditioning method and provides comparable results (Fujita & Elliott, 1965; Green, 1975; Fay, 1992; Coleman, 2009).

Here, I chose a reward-based (positive) conditioning method because it is more efficient and provides more stable results compared to avoidance procedures, while also avoiding long lasting adverse behavioural consequences (e.g. increased aggressiveness; Stebbins et al., 1984). The latter was of special importance as the subjects were neither laboratory animals nor completely wild and were required to remain affable after completion of the auditory experiments.

Obtaining animal audiograms is a tedious task, consuming considerable time and energy to establish and to stabilize desired behaviours. On the other hand, it is rewarding, as auditory thresholds between healthy individuals of the same species do not differ considerably, so that testing of two to three individuals is sufficient to make generalizations about the species' auditory sensitivity especially in large and non-laboratory animals (Heffner & Heffner, 1988b, 2010).

Recently, Benovitski et al. (2014) developed a mobile apparatus, quite similar to the one I designed, allowing researchers to perform psychoacoustic tests in cats without the need to monitor the experiment continuously and with the great advantage that the animals are free to decide how often and when they would like to perform. The authors also employed a simple go/no-go task with food as a reward. In simple frequency discrimination tasks their technique yielded fast and stable data which were in line with previously published results. As their setup did not provide acoustic shielding, the performing subjects, however, were prone to distractions from other sound

sources (i.e. background noise) and sensitivity tasks could not be performed. This constraint does not exist in my setup. It is transportable and provides a more standardized testing environment within the accompanying semi-anechoic chamber which not only obstructs other visual cues but also significantly reduces ambient noise levels (cf. Figure 1.3-2). Similar to the setup by Benovitzki et al. (2014) it can (but does not have to) directly connected to an animal cage where it automatically records the trials initiated through the subject and controls the presentation of stimuli and allocation of rewards and punishment. Due to the larger size, higher weight and higher costs, however, my setup is not intended for high-throughput parallel screening of the sensory abilities of laboratory animals, but rather for extending the number of species for which we have detailed behavioural data of their sensory adaptations (such as audiograms, but visual tasks are equally conceivable). It is especially suited for testing of rare and sensitive species as it significantly lessens handling and therefore stress of the animals which need not to be removed from their cage for the experiments. Thus, in future studies I plan to employ this novel setup to obtain reliable audiograms in environments previously unsuitable for these types of sensitive measurements (e.g. ancillary cages in a zoo).

THE RED FOX AUDIOGRAM COMPARED TO OTHER CARNIVORE AUDIOGRAMS

Including the red fox audiogram presented here, behavioural audiograms for six different terrestrial carnivore species are currently available (Figure 1.4-1; Table 7). A common characteristic of all these carnivores is the high absolute sensitivity with maximum sensitivities well below the mammalian average of 0.4 dB SPL (Heffner & Heffner, 1990), probably reflecting the need to detect and locate potential prey. The red fox is no exception with overall sensitivities intermediate to those of the other carnivores and a maximum sensitivity which even exceeds those of all others known to date. In contrast to other carnivores, the red fox shows maximum sensitivity around 4 kHz and already markedly lower sensitivity at 8 kHz. This is in line with the best sensitivity reported for the kit fox (*Vulpes marotis*; Bowles & Francine, 1993) and the closely related arctic fox (*Alopex lagopus*; Stansbury et al., 2014). I will not discuss these fox audiograms in detail, however, as they did not comply with some standard criteria for behavioural audiograms. The arctic fox audiogram suffered from high background noise and response biases (Stansbury et al., 2014) while the audiogram of the kit fox was incomplete and based on startle inhibition (Bowles & Francine, 1993), which is a very insensitive testing procedure (Francis, 1975). However, it is

noteworthy that the best sensitivity reported for the kit fox does not only correspond well to that of the red fox in terms of the frequency region but also in terms of absolute sensitivity (-15 dB SPL).
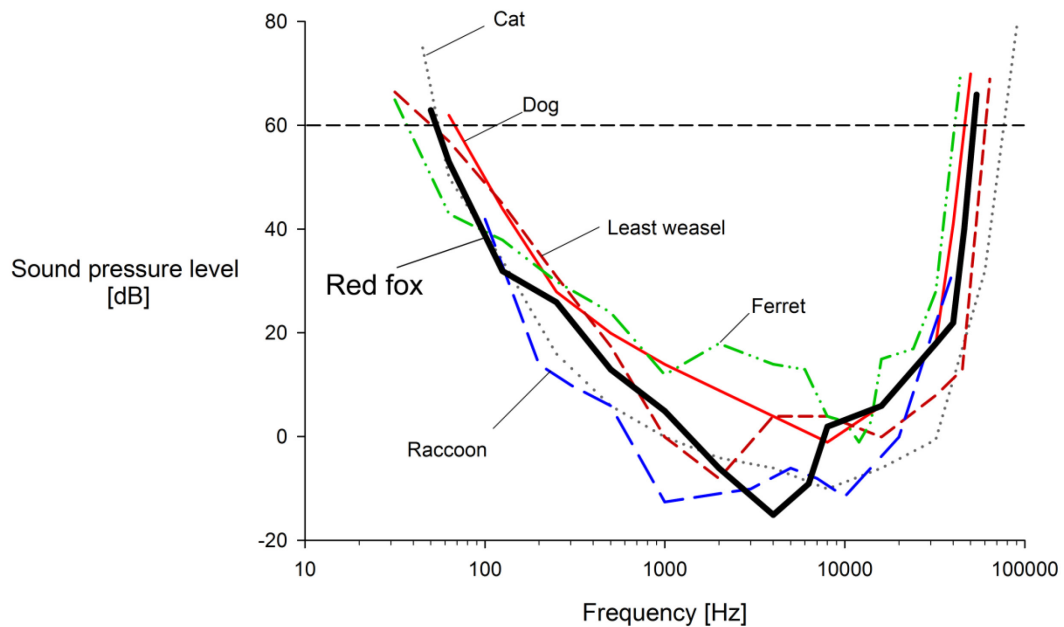
Figure 1.4-1 The red fox (*Vulpes vulpes*) audiogram (solid black line) obtained in this study compared to the known audiograms of several representatives of the order Carnivora. The horizontal dashed line represents the functional hearing range at 60 dB SPL. Domestic cat, *Felis catus* (mean of Neff & Hind, 1955; Heffner & Heffner, 1985b); domestic dog, *Canis familiaris* (mean of 4 dogs of different breeds; Heffner, 1983); ferret, *Mustela putorius* (Kelly et al., 1986); least weasel, *Mustela nivalis* (Heffner & Heffner, 1985a); raccoon, *Procyon lotor* (Wollack, 1965).

Together with the domestic dog (Heffner, 1983), the red fox is now the second representative of the family Canidae for which a behavioural audiogram is available. Furthermore, it is the first non-domesticated canid which allows for a first (albeit highly speculative) assessment of possible domestication effects. The average hearing range at 60 dB SPL of the dog and red fox are alike (9.3 and 9.84 octaves, respectively). The low frequency limits of dog (67 Hz) and red fox (51 Hz) differ by only a quarter octave. At high frequencies this difference is even smaller with only a marginal difference of less than 1/10th of an octave. Differentiation between different dog breeds reveals that the high frequency cutoff of the red fox lies just 1 kHz above the cutoff of the most

sensitive dog breeds (Heffner, 1983). Considerable differences, however, are evident for absolute sensitivities at frequencies below 8 kHz where the red fox is much more sensitive than dogs[1].

Reduced auditory sensitivity as a consequence of domestication has been proposed before (Clutton-Brock, 1995) and anatomical correlates such as reduced middle ear transformer ratios have already been documented in other domesticated species (Fleischer, 1973; Burda, 1985a). Of course, because the dog is not a domesticated red fox, these conjectures have to be treated with caution but are further corroborated by the fact that the domesticated ferret (*Mustela putorius*) also has lower absolute sensitivities compared to its close wild relative the least weasel (*Mustela nivalis*; Heffner & Heffner, 1985a; Kelly et al., 1986). Unfortunately, behavioural audiograms for domesticated silver foxes (*Vulpes vulpes*), wolves (*Canis lupus*) or wild cats (*Felis silvestris*) are not yet available, so until then no further speculations should be made here.

The red fox is sometimes described as combining, at least in its behaviour, typical traits of dogs with characteristics of domestic cats (e.g. Henry, 1996). Anecdotally, in line with these descriptions, the foxes' audiogram shares properties with hearing characteristics with both dogs and cats (Table 7). As already stated, the upper frequency limit of hearing is almost identical to that of the domestic dog (red fox: 45 kHz, dog: 48 kHz). The lower limit, in turn, is practically identical to that of the domestic cat (red fox: 51 Hz, cat: 55 Hz). The overall sensitivity lies between those reported for both species with low and medium frequencies being more similar to the cat and higher frequencies more similar to the dog.

---

[1] An exception can be seen in Lipman & Grassi (1942) who showed clear peak sensitivity at 4 kHz for several dogs. However, the absolute thresholds of these dog audiograms are not included in the present text, because the employed methods do not meet state of the art criteria and the values were given relative to human thresholds; two reasons why the results might differ so considerably from the other dog audiograms published by Heffner (1983).

Table 7 Audiogram characteristics of the red fox compared to other carnivores.

Species	Low frequency limit (at 60 dB) (Hz)	High frequency limit (at 60 dB) (kHz)	Best frequency (kHz)	Maximum sensitivity (dB SPL)	Hearing range (at 60 dB) (octaves)
Red fox *Vulpes vulpes*	51	48	4	-15	9.8
Domestic dog[a] *Canis familiaris*	67	45	8	-1	9.3
Domestic cat[b] *Felis catus*	55	78	8	-10	10.4
Ferret[c] *Mustela putorius*	36	42	12	-1	10.1
Least weasel[d] *Mustela nivalis*	50	60	2	-8	10.2
Raccoon[e] *Procyon lotor*	-	-	1, 10	-15	-

[a] Heffner 1983.

[b] Heffner and Heffner 1985a; Neff and Hind 1955.

[c] Kelly et al. 1986

[d] Heffner and Heffner 1985b

[e] Wollack 1965

VOCALIZATIONS AND PREY SOUNDS

The vocalizations of the red fox have been well characterised. At least 20 call types can be distinguished on the basis of sonograms (Newton-Fisher et al., 1993). Combination calls have also been described for the red fox (Tembrock, 1963) but are not considered here. For most calls the highest energy is invested in frequency bands below 2.5 kHz. Within the adult calls, only the screams contain significant energy proportions within the frequency range of best hearing around 4 kHz. Additionally, pub whines and ratchet calls contain intense harmonics around 4 kHz, too. All of these three calls are used in agonistic encounters as either aggressive or defensive expressions. Even though these calls may convey significant information about the caller, all are usually delivered over close distance, making it unlikely that these calls exerted the primary evolutionary pressure leading to the extreme auditory sensitivity within their frequency range.

Red foxes are crepuscular and nocturnal hunters which heavily rely on their auditory system for localization of prey (Tembrock et al., 1957; Österholm, 1964). It is thus conceivable that their audiogram reveals special adaptations reflecting enhanced perception of prey sounds. Even though the red fox is rather a generalist or sometimes even described as an opportunistic feeder, a considerable proportion of its diet consists of vertebrate prey such as small mammals (in most reports more than 50% rodents, but see Catling, 1988) and birds (maximum 10-20 %) which are assumed to be a constant key resource (Harris, 1981; Hockman & Chapman, 1983; Cavallini & Volpi, 1996; Jankowiak & Tryjanowski, 2013). From these two groups, voles and birds of the Phasianidae family constitute the main proportions (Lever, 1959; Goszczyński, 1974; Hewson & Kolb, 1975; Dell'Arte et al., 2007). Red foxes localize sounds most accurately between 3-4 kHz and this has been proposed to help finding common pheasant-chicks (*Phasianus colchicus*) by their flock call which is pitched around 4 kHz (Heinz & Gysel, 1970; Isley & Gysel, 1975). It is striking that this frequency region of best localization exactly coincides with the highest absolute sensitivity of the red fox. The possibility that the good localization capability might simply be a consequence of the increased perception was already discussed by Isley and Gysel (1975), but seems unlikely as an explanation for the different localization accuracy in the mid-frequency range as the intensity of the presented tones was far above threshold (74 ± 4 dB SPL). Thus, it is plausible that the high hearing sensitivity at 4 kHz aids in finding avian prey over large distances during fox foraging bouts. At this point it is tempting to speculate that the good low frequency sensitivity (in the region around 100 Hz) of the red fox might also be related to the localization of phasanid prey, since many of these bird species communicate in this frequency range over large distance by means of drumming displays (Garcia et al., 2012).

Small mammals emit both vocalizations and involuntary sounds during movement and feeding. Both can potentially be exploited by predators, to identify, track, and locate their prey. Rustling noise is broadband but contains most energy in bands at 8-10 kHz and their first harmonics (Payne, 1971; Konishi, 1973; Marimuthu & Neuweiler, 1987). Even though the ability of the red fox to localize pure tones is lowest at these frequencies, they can still provide reliable spatial information, probably enough to allow for increased hunting success at shorter distance (Isley & Gysel, 1975). In contrast to rustling sounds, the vocalizations of voles and mice are mainly ultrasonic between 50-70 kHz (Sewell, 1968). Ultrasound attenuates very quickly and since thresholds for sounds with frequencies higher than 50 kHz are above 60 dB SPL in the red fox, it seems un-

likely that rodent communications sounds are helpful in prey localization. To sum up, if the high sensitivity to frequencies around 4 kHz developed in response to the pressure of localizing prey items, it was most likely helpful in finding avian prey over larger distances rather than rodents in the grass or below snow cover.

LOW AND HIGH FREQUENCY HEARING

A crucial function of hearing is the ability of localizing sound sources such as prey, mates or predators. Mammals localize sounds with help of monaural and binaural cues (reviewed in Butler, 1975; Gourevitch, 1980; Heffner & Heffner, 1992b). Monaural (pinna) cues mainly aid in the vertical localization of sounds and front/back reversals, whereas binaural cues allow for discriminations in the horizontal plane. Interaural differences are of both temporal nature, arising from the distance between the ears (interaural time difference, ITD), and spectral nature, through the shadowing effect of the head and the pinnae (interaural level difference, ILD).

The maximal ITD depends on the size of an animal's head. Thus, the smaller the head, the smaller the maximal available ITD. Head size is constrained, but at the same time accurate sound localization is crucial, hence mammals improved the efficiency of their second sound localization cue, the ILD. Particularly, it has been suggested that the smaller the mammal, the more it depends on ILD for sound localization (Masterton et al., 1969). High frequencies are better attenuated than low frequencies and larger heads attenuate lower frequencies than smaller heads. As a consequence, a small mammal that relies on ILD needs to hear frequencies that are high enough to be effectively shadowed by its tiny head (Heffner & Heffner, 2008a). This relationship is substantiated by a highly significant negative correlation between the upper limit of hearing and the functional head size of an animal (time of the sound to travel around the head from one auditory meatus to the other; Heffner & Heffner, 1981). With a typical functional head size of 320 µs, the red fox has a predicted high frequency cutoff at 41 kHz (underlying dataset containing 67 species; from Heffner & Heffner, 2008a). This is only marginally lower than the measured limit of 48 kHz; hence the fox further contributes to the good correlation between interaural distance and the upper limit of hearing.

Amongst all factors included so far, the low frequency limit of a species has only been shown to be negatively correlated with the high frequency limit of species (Heffner & Heffner, 2008b). In general, mammals appear to be split in two groups of low frequency hearing characteristics:

those with normal low frequency hearing and those with extended low frequency hearing (retained sensitivity below 125 Hz; Heffner et al., 2001). Since hearing of low frequencies is a common feature of most vertebrates, and only mammals developed high frequency hearing (> 10 kHz), the latter is believed to be the derived state (Heffner et al., 2001). Not all mammals have, however, gained (or retained) the ability to hear both very low and very high frequencies. Amongst "broadband-listeners" are carnivores such as the least weasel (50 Hz-60 kHz) and the domestic cat (55 Hz-79 kHz). The red fox (51 Hz-48 kHz) might also be assorted to this group. Proximately, details of inner and middle ear morphology could reveal anatomical similarities of these species that might be the responsible morphological adaptations contributing to the extended hearing range (see below). Ultimate reasons for retained low frequency hearing might reside in the sound localization abilities of red foxes: The localization of a sound takes place mainly on basis of its high frequency content (Heffner et al., 1995). Therefore, it has been proposed that animals for which the localization of sound is essential might have given up low frequency hearing that might detrimentally mask important high frequencies (Heffner et al., 2001). However, sound localization acuity is outstanding in the domestic cat which also is an auditory hunter that has retained both high and low frequency sensitivity (Casseday & Neff, 1973; Heffner & Heffner, 1988a). Obviously, sound localization is even more important for a non-domesticated auditory predator such as the red fox. Hence it follows that either the extreme absolute sensitivities in the best frequency range (which, as we remember were also localized best; Isley & Gysel, 1975) or some unknown adaptations of sound localization mechanisms have allowed the red fox to keep its high sensitivity in the low frequency range.

Physiological measures of hearing sensitivity

A behavioural audiogram is not the only means of measuring an animal's hearing sensitivity. Electrophysiological responses to sounds that are recorded at the level of the inner ear (cochlear microphonic potentials) or the auditory nerve/brainstem (auditory evoked potentials) are often used to estimate certain characteristics of the audiogram. Peterson et al. (1969) employed cochlear microphonic potentials in several carnivores including six specimens of the red fox. Figure 1.4-2 compares the mean cochlear microphonic audiogram of these foxes to the behavioural audiogram. It is obvious that considerable differences exist between the two audiograms with much higher thresholds in the electrophysiological audiogram and shifted regions of best sensitivity. In contrast

to the behavioural audiogram, no distinct peak of best sensitivity is evident from the cochlear microphonics. The highest correspondence between both audiograms can be seen in the low frequency range. Comparable differences between behavioural audiograms and cochlear microphonics have been reported for other species (e.g. for bats; Pratt & Sohmer, 1978; Heffner et al., 2013) and a meta-analytical comparison between cochlear microphonics and behavioural audiograms led to the suggestion to use the former only for rough estimations of the auditory sensitivity of a species (Raslear, 1974). In spite of that, based on the results of the cochlear microphonic potential measurements, Peterson et al. (1969) assorted the tested carnivores to different sensitivity groups. The red fox was placed in a group with an "inefficient mode of sound reception". In contrast, the domestic cat was placed in the "most efficient sensitivity group" (Peterson et al., 1969). At least with respect to the high absolute sensitivities revealed by the behavioural audiogram presented in this thesis, the grouping needs to be reassessed. Anatomical investigations and behavioural audiograms from additional carnivore species will hopefully shed more light on this matter.
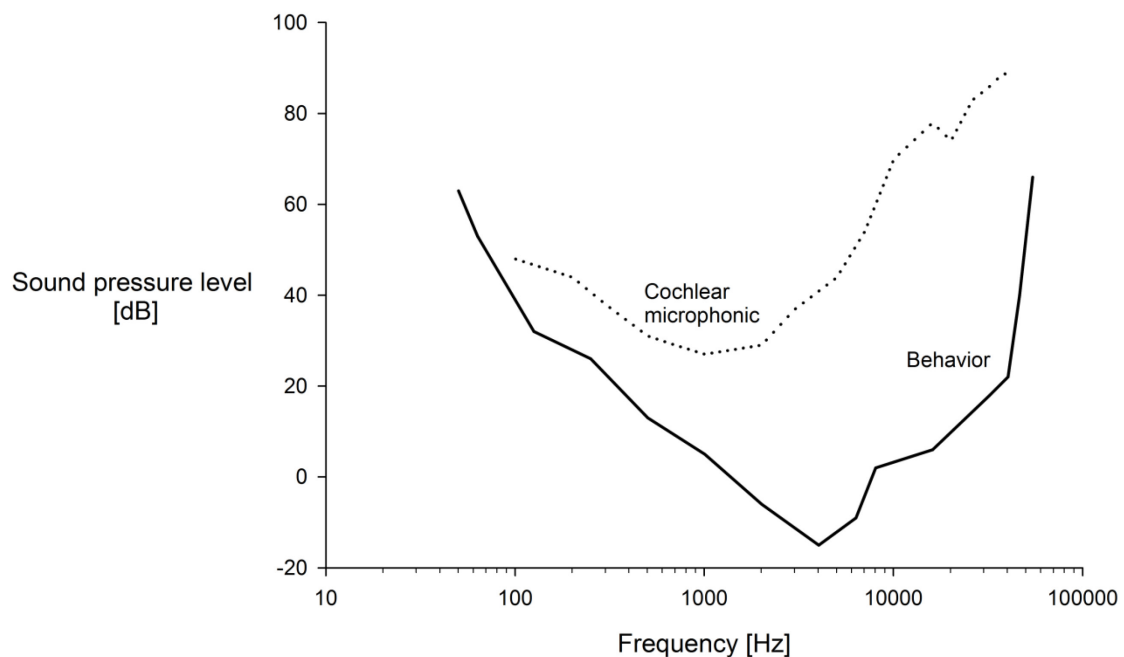
Figure 1.4-2 The behavioural red fox audiogram (solid black line) obtained in this study compared to previously reported data on cochlear microphonic responses (dotted line; data from Peterson et al., 1969). The behavioural thresholds are much lower, show a relatively sharp frequency peak of best hearing, and the sensitivity is shifted towards higher frequencies.

1.4.2 Anatomy

THE RED FOX EAR IN COMPARATIVE CONTEXT OF MAMMALIAN EARS

In the following, I will discuss specific aspects of the red fox ear morphology in comparison to findings in other mammals. The plethora of data that I have collected renders a detailed discussion of all parameters impossible. Therefore, I will dwell on selected characteristics only.

Outer and middle ear

The pinna of mammals is a highly complicated acoustical structure; the essential parameters are hard to put into numbers. Therefore, I only determined a very rough variable, the height to width ratio. I did not collect more variables as the effect of the pinna has been shown to be almost neglectable when it comes to overall sensitivity of the auditory system (Heffner, 1983; Coleman & Colbert, 2010). The ratio might prove useful in a large comparative context (all carnivores), but since no such dataset exists at the moment, any inference on basis of pinna morphology would be mere speculation.

The middle ear of the red fox is of the "transitional or intermediate type" defined by Fleischer (1973, 1978), which is also found in other carnivores such as the cat or the harbour seal (overview in Rosowski, 1992). The malleus is firmly but only ligamentously attached to the tympanic bone. It does not possess an orbicular apophysis, but only a short anterior process and a reduced transversal lamina. The manubrium forms an angle of approximately 45° to the anatomical axis of ossicular rotation. The malleus is about twice the size of the incus. Ears of the intermediate type are characterised by medium stiffness which is supposed to make them suitable to respond over a wide range of frequencies but not in the extremely low and high frequencies. The audiogram of the red fox substantiates this prediction: the red fox is less sensitive in the low frequency range than e.g. primates and subterranean mammals that possess middle ears of the "freely mobile type", and it is also less sensitive in the high frequency range compared to small rodents or bats that possess the stiff "microtype" middle ear.

The size of the auditory bulla is related to the sensitivity in the low frequency range. Animals adapted to hear very low frequencies, such as the kangaroo rat, possess extremely hypertrophied bullae (Webster, 1962; Webster & Webster, 1972). The bulla of the cat is approximately 25% smaller than that of the red fox (Lynch et al., 1981), but this does not seem to have an effect on

the low frequency hearing. With respect to the feline bulla (Keen & Grobbelaar, 1941), it is interesting to know that they are characterised by a septum which divides the bulla. This kind of separation has been related to the 4 kHz-ditch in the cat audiogram. The fact that the fox does not have such a pronounced partition fits well with the high sensitivity at 4 kHz.

Even though we know that the middle ear does not act as an ideal transformer it is still interesting to compare the theoretical middle ear transmission properties of a newly studied species to known values of other well studied animals.

The middle ear impedance transformer ratio (ITR) of the red fox (0.0072) is slightly smaller (i.e. more efficient) than the ITR of the cat (0.0079; cf. Table A9 appendix). This corresponds well to the higher absolute sensitivity found in the red fox audiogram.

The ossicle mass is discussed to have most influence on high frequency middle ear transmission (Dallos, 1973; Manley & Johnstone, 1974; but see e.g. Overstreet & Ruggero, 2002 for a contradicting view). Therefore, I would expect lower ossicle mass in the cat compared to the dog and the red fox. Indeed, the cat ossicles weigh less than those of the adult red fox specimens in my sample and those reported in Nummela (1995), which fits to the better higher frequency hearing in the cat. In contrast, the ossicles of the dog are considerably heavier, although the upper frequency limit is identical to the red fox. Thus, the general trend of lower high frequency limits is supported by those numbers, but it is evident that the body mass as an additional component has to be taken into account (Hunt & Korth, 1980). The relationship between body mass and ossicle weight is also evident in the development of the red fox middle ear reported here. Since the mass changes were not accompanied by linear changes of ossicular dimensions, the influence of ontogeny on hearing is not straightforward to predict on a morphological basis of middle ear parameters.

Inner ear

Before I will start discussing some of the interesting observations on the inner ear of the red fox in a comparative context, some remarks about the general quality of the material and the procedure of cochlear sectioning seem to be appropriate. Establishing a histological procedure for sectioning of the cochlea is by no means a trivial endeavour. The unique combination of very delicate structures embedded within the hardest bone of the body imposes such special requirements that it is impossible to gather good results quickly, especially in larger animals where the time needed to

adapt existing procedures to a new species can very well take several months or even years (Wever et al., 1971). Additionally, even when the sectioning procedure is running, the quality of the material often diminishes the results, as specimens of non-laboratory species are mostly simply immersion-fixed, because perfusion in the field is extremely difficult to accomplish (although not impossible, see Manger et al., 2009 for an impressive example). My red fox specimens were well preserved but not perfused and therefore the quality of inner ear sections could not be expected to be outstanding. I optimized the procedure as much as I could (cf. Figure 1.2-6) and yielded good results. However, the quality differed between individuals and thus on many sections not all parameters could be measured. This was especially problematic for the determination of hair cell lengths, where the presented figures are based on small numbers. This should be kept in mind during the discussion of the functional consequences below.

Some of the morphological parameters of the red fox inner ear are shown in comparison to published figures of other carnivores in Table A9 (appendix). With 3.2 turns, the red fox cochlea is in this respect similar to the dog (3.25 turns; Gray, 1907; Keen, 1939; Le & Keithley, 2007) and the cat (3 turns; Gray, 1907; Keen, 1939). Three or less turns might be a characteristic of the Felidae irrespective of body size, as the tiger and jaguar have 2.75 turns (Burda et al., 1984). Thus, even though BM length is closely correlated with body size (see below), the coiling of the cochlea seems to be decoupled from this development. The number of cochlear turns has been related to the hearing range in octaves (Echteler et al., 1994). Given the small differences in the number of turns between cat, dog, and the red fox, the small difference of (less than) one octave in their hearing ranges supports the relationship.

Compared to the domestic cat, the basilar membrane (BM) of the red fox is slightly longer (cat: 22-25 mm; Retzius, 1884; Schuknecht, 1953; West & Harrison, 1973; Cabezudo, 1978; West, 1985; Sato et al., 1999)[2]. This fits well to the generally observed positive correlation between body weight and BM length (Vater & Kössl, 2011), as the red fox is larger than the cat. The values reported for the BM length of the dog are within the same range as those reported for the cat (22-24.5 mm; Schuknecht et al., 1965; Igarashi et al., 1972; Mair, 1976), seemingly contradicting the BM-body size relationship, as the used dog breeds (Beagle, Dalmatian) considerably outweigh the cat, and it has been shown that at least middle ear morphological parameters are closely related to body size in different dog breeds (Heffner, 1983).

---

[2] Note that unpublished measurements by Burda suggest considerably longer cat BM lengths of 27-28 mm (see below)

It is for this reason highly interesting to note, that for both dog (Branis & Burda, 1985) and cat (Burda, unpublished) longer BM lengths have been found than those published in other studies. The dissent may emerge from the fact that different methods were used for the assessment. Burda (unpublished) and Branis & Burda (1985) used the method of surface specimens which has also been employed in the current study on the red fox. All other studies either used serial sections or mid-modiolar sections and the method of Guild (1921), both of which might be prone to underestimation of the actual BM length (Greenwood, 1990). To my knowledge, the only other study which used surface specimens of the cat cochlea to estimate BM length was the study by Liberman (1982) who reported lengths between 23 and 26.7 mm. A longer BM length in the cat than in the fox would fit the larger hearing range of the former, while a longer BM in the dog might be simply related to the relationship to body size. Even with a BM length comparable to the red fox, the cat probably deviates from the BM–body size relationship, maybe as a result of special sensory adaptations as has already been conjectured for the cat cochlea by Hemilä et al. (1995). Again fitting to the correlation with body size are the reported BM lengths for the jaguar (33.3 mm) and the tiger (35.5 mm; Burda et al., 1984).

A longer BM provides additional surface area to accommodate more sensory hair cells. The total number of IHCs in the red fox matches almost exactly the number that has been found in the cat (red fox: 2,757, cat: 2,723; Burda, unpublished), while it is considerably higher than the number of IHCs reported for the dog (2,603; Branis & Burda, 1985). On the other hand, the number of OHCs is identical between red fox and dog, while being lower in the cat (red fox: 10,503, dog: 10,548, cat: 10,105; Branis & Burda, 1985; Burda, unpublished). Thus, even in inner ear morphology we find a reflection of the cani-feline properties of the red fox hearing system that we already discussed for the audiogram above.

How do these hair cell numbers relate to hearing function? An increased density of sensory hair cells as observed for the IHCs in the red fox and cat compared to the dog, might either lead to increased frequency and amplitude discrimination abilities or to increased sensitivity of the auditory system (Ehret & Frankenreiter, 1977; Burda & Voldřich, 1980; Liberman, 1982; Burda, 1985b). We do not know anything about frequency discrimination in the red fox, but it is striking that the audiogram of red fox and cat are both characterised by a higher number of IHCs and a distinctly higher absolute sensitivity than the one of the dog (cf. Figure 1.4-1).

OHCs, as the driving force of the cochlear amplifier, are known to contribute crucially to the sensitivity of the inner ear (Liberman & Beil, 1979; Dallos, 1992). Hence, we would have expected a higher OHC density in the cat and the red fox than in the dog. As this is not the case, the lower sensitivity of the dog's auditory system is either the consequence of the lower number of inner hair cells or of the inferior transformer efficiency of the middle ear (larger weight of the ossicles).

The length of IHCs stays more or less constant along the cochlear duct for a given species. OHC length, in contrast, significantly increases from base to apex in all species investigated so far (Dannhof et al., 1991; Vater & Kössl, 2011). Furthermore, the length of a particular OHC seems to be strictly related to the represented frequency at its position along the cochlear duct (Dannhof et al., 1991). Short basal OHCs indicate high frequency representations, while long apical OHCs are dominant in low frequency regions (Figure 1.4-3). This pattern is also evident in the red fox. The minimal and maximal lengths of red fox OHCs are almost similar to those reported for the cat (Nadol Jr, 1988; Echteler et al., 1994), with exception of slightly shorter OHCs at the base, which is a good indication of the higher upper limit of hearing in the cat. Accordingly, I would expect the dog to possess slightly shorter OHCs in apical regions but to my knowledge, hair cell lengths of the dog are not available in the literature.
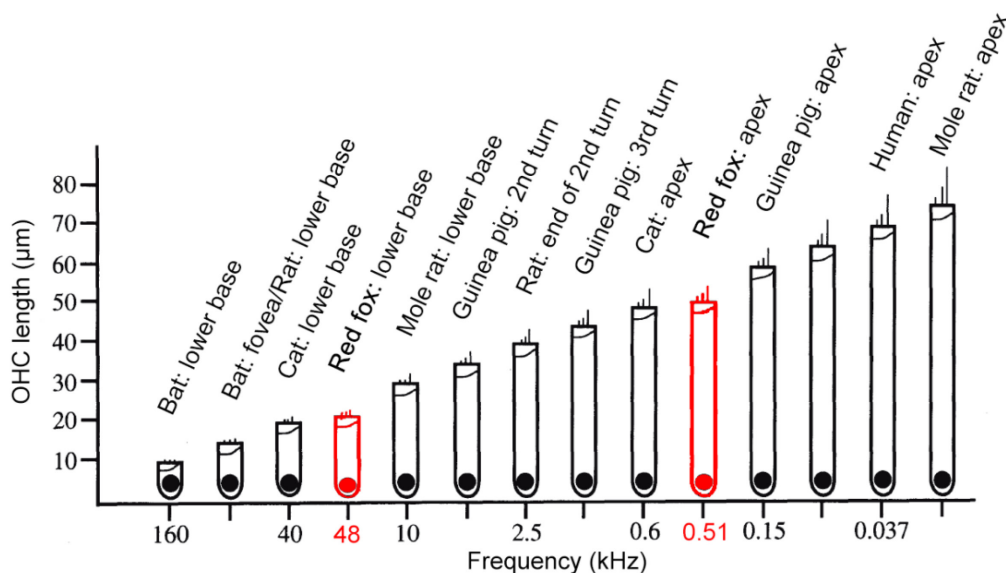
Figure 1.4-3 Illustration of lengths of outer hair cells (OHCs) in different species and at different positions along the cochlear duct and their relationship to their frequency of best response. Above each cell, the species and the region of the cochlea where the cell was derived from, is depicted. The abscissa shows the represented frequencies as obtained from frequency place maps. For the red fox the upper and lower limit of hearing (at 60 dB SPL) are indicated (red numbers). It is obvious that the absolute length of the OHC is strictly related to the adequate frequency at that position independent of species. Also evident, the figures derived from the red fox fit well into the relationship. Modified from Echteler et al. (1994).

The basilar membrane is generally accepted as the crucial part of the cochlea that defines the oscillation behaviour and tonotopic frequency distribution (among other parts discussed to exert a considerable influence are the spiral ligament, the tectorial membrane, and the spiral limbus; Burda, 1982; Henson & Henson Jr, 1991). The BM width, thickness, and the derived stiffness have been widely used for interspecies comparisons and estimates of upper and lower hearing limits (Echteler et al., 1994). With some specialized species as exceptions, BM width decreases and BM thickness increases towards the base of the cochlea. The steepness of this gradient as well as the endpoints vary from species to species and are correlated with lifestyle and body size. High frequency specialists, such as dolphins and bats, are characterised by a very stiff base (Figure 1.4-4). Low frequency specialists, such as mysticete whales or mole-rats, are characterised by a wide and sloppy BM in the apex region. In this context it is evident that the red fox is rather an auditory generalist with neither an extremely stiff base, nor an extremely sloppy apical region, a statement that agrees with the behavioural audiogram (the remarkable absolute sensitivity is not reflected in BM parameters). Except for a slightly thicker basal BM in the red fox, the BM values correspond well to those reported for the cat (Cabezudo, 1978; Echteler et al., 1994). The dog seems to have a somewhat broader BM at the base, which may be related to the lower high frequency limit than in the fox, a possible consequence of domestication, as was already assumed by Fleischer (1973).
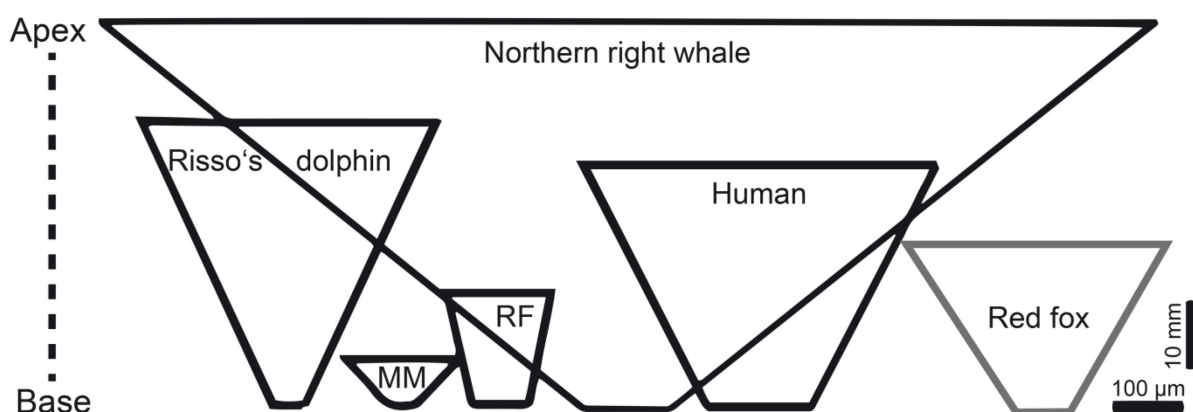
Figure 1.4-4 Basal-apical width gradient of the basilar membrane in different mammalian species including the red fox. MM, M*us musculus*, RF, *Rhinolophus ferrumequinum*. After Vater & Kössl (2011).

The basal stiffness values of the red fox are a bit conspicuous, as they are within a range typical for animals with much higher upper hearing limits (fox: 0.015, mouse: 0.013, horseshoe bat: 0.013, dolphin: 0.014; Echteler et al., 1994). Since I performed the calculation of the stiffness with BM properties found at the very end of the hook region, it might well be that the cochlear partition is not functional in this regions. The BM width decreased considerably in this region and if non-functional anymore, this might have led to a slight overestimation of basal stiffness as a functional variable of red fox hearing. For future calculations of stiffness it is therefore warranted to take the mean values between the hook and first half-turn as the basal BM values of the red fox.

To conclude, the morphology of the red fox inner ear resembles in many parts those of the cat and the dog. Even though direct causality cannot be drawn, the finding is supportive of the conspicuous "sensory-hybridization" that was already suggested by the behavioural audiogram.

COULD I HAVE PREDICTED THE RED FOX AUDIOGRAM FROM THE ANATOMY?

The unique set of detailed anatomical and behavioural data that I have presented within this chapter creates the opportunity to test several of the published correlations between ear morphology and auditory function and thereupon based models and predictions. The goal of this section will be to determine those anatomical parameters that allow the most accurate reproduction of the audiogram of the red fox. For the predictions, I take only morphological parameters of the ear into account but none of the parameters that I obtained from the actual behavioural audiogram. To keep it simple, I will break down the behavioural audiogram into three audiometric variables that have been proven useful in comparative studies of the audiograms in other species (e.g. Rosowski & Graybeal, 1991; Coleman & Colbert, 2010). These variables are:

1. the high frequency limit (at 60 dB SPL and 30 dB SPL above best threshold)
2. the low frequency limit (at 60 dB SPL and 30 dB SPL above best threshold)
3. the frequency of best sensitivity

(1) High frequency limit

According to Rosowski (1992), the high frequency limit (at 30 dB SPL above best threshold) of every mammal can be approximately predicted by three different equations (eq.):

$$F_{max} = 110 \times TM^{-0.37} \qquad \text{(eq. 1)}$$

(TM = area of the tympanic membrane; mm²)

$$F_{max} = 34 \times OW^{-0.4} \qquad \text{(eq. 2)}$$

(OW = area of oval window; mm²)

$$F_{max} = 391 \times BMl^{-0.85} \qquad \text{(eq. 3)}$$

(BMl = length of basilar membrane; mm)

The predicted upper frequency limits (at 30 dB above best threshold) for the red fox are 29.5 kHz (according to eq. 1), 26.9 kHz (eq. 2), and 24.7 kHz (eq. 3), resulting in a mean predicted upper frequency limit of 27 kHz (30 dB SPL above threshold).

West (1985) determined the following equation for estimating the high frequency limit at 60 dB SPL:

$$F_{max} = 10^{(2.42 - 0.994 \times \log(\frac{BMl}{CT})} \times 1000 \qquad \text{(eq. 4)}$$

(at 60 dB SPL); (CT = number of cochlear turns)

which translates into 33 kHz when taking the CT and BMl of the red fox into account.

(2) Low frequency limit

According to Rosowski (1992), the predicted low frequency limit (at 30 dB SPL above best threshold) is:

$$F_{min} = 15 \times TM^{-1.1} \qquad \text{(eq. 5)}$$

(TM = area of the tympanic membrane; mm²)

$$F_{min} = 0.4 \times OW^{-1.1} \qquad \text{(eq. 6)}$$

(OW = area of oval window; mm²)

The predicted lower frequency limits for the red fox are 300 Hz and 210 Hz, using equations 5 and 6 respectively, and thus a mean predicted lower frequency limit of 255 Hz (30 dB SPL above best threshold).

According to West (1985), the lower frequency limit (at 60 dB SPL) can be obtained by:

$$F_{min} = 10^{(1.76-1.66\times \log(BMl\times CT)} \times 1000 \qquad \text{(eq. 7)}$$

(at 60 dB SPL); (CT = number of cochlear turns)

resulting in 38 Hz for the red fox.

(3) Frequency of best sensitivity

The frequency of best sensitivity can be estimated according to Rosowski (1992) by the following equations:

$$F_{best} = 44 \times TM^{-0.61} \qquad \text{(eq. 8)}$$

(TM = area of the tympanic membrane; mm²)

$$F_{best} = 6.2 \times OW^{-0.52} \qquad \text{(eq. 9)}$$

(OW = area of oval window; mm²)

The mean predicted best frequency for the red fox is 4.8 kHz (30 dB SPL above threshold) averaged over 5 kHz (eq. 8) and 4.6 kHz (eq. 9).

The region of best sensitivity in the rat and house mouse is characterised by a distinct peak of highest IHC density (Ehret & Frankenreiter, 1977; Burda & Voldřich, 1980; Burda, 1985b). To test if the peak of higher IHC density seen in the red fox between 71-80 % distance from the apex is of use for predicting the frequency of best sensitivity, I need to assign the characteristic frequency to a known position along the cochlear duct. Therefore, a frequency map (based on neuroethological studies) is needed, which is not available for the red fox. However, the gradual and steady changes in IHC and OHC density along the cochlear duct allow the conclusion that the red fox possesses a generalist cochlea, without highly specialized regions such as the acoustic

foveae reported from bats (Bruns & Schmieszek, 1980) and mole-rats (Müller et al., 1992). Therefore, it is possible to estimate a cochlea frequency map by means of an equation developed by Greenwood (1961, 1974, 1990):

$$f = A \times (10^{ax} - k) \qquad \text{(eq. 10)}$$

where f is the frequency in Hz, A is a scale factor that is dependent on the high frequency limit (60 dB SPL), x is the normalized distance from the apex, a is describing the steepness of the map, and k a constant that serves a better fit for the low frequency data. The constants differ slightly between species (overview in LePage, 2003). The predictive power of the equation was validated in the cat by Liberman (1982) by means of horseradish peroxidase injected into the cochlear nucleus at positions associated with characterised frequencies. Fay (1992) has further simplified and validated equation 10, and ultimately developed the following formula to predict the frequency represented at a specific position p (as a distance (in mm) from the base):

$$p = (1 - \left(log_{10} \left(\frac{f_{Hz}}{0.008 F_{max}} \right) + 1 \right))/2.1)) \qquad \text{(eq. 11)}$$

where F_{max} is the high frequency threshold at 60 dB SPL. Using equation 11 and the predicted high frequency cutoff (eq. 4), I created a position-frequency map from which the represented frequency at the distance 75% away from the apex can be read. The resultant frequency for the position of highest IHC density was 9.5 kHz (eq. 11, F_{max} = 33 kHz).

The position frequency map for the prediction is shown in Figure 1.4-5.

Position-frequency map and IHC-density
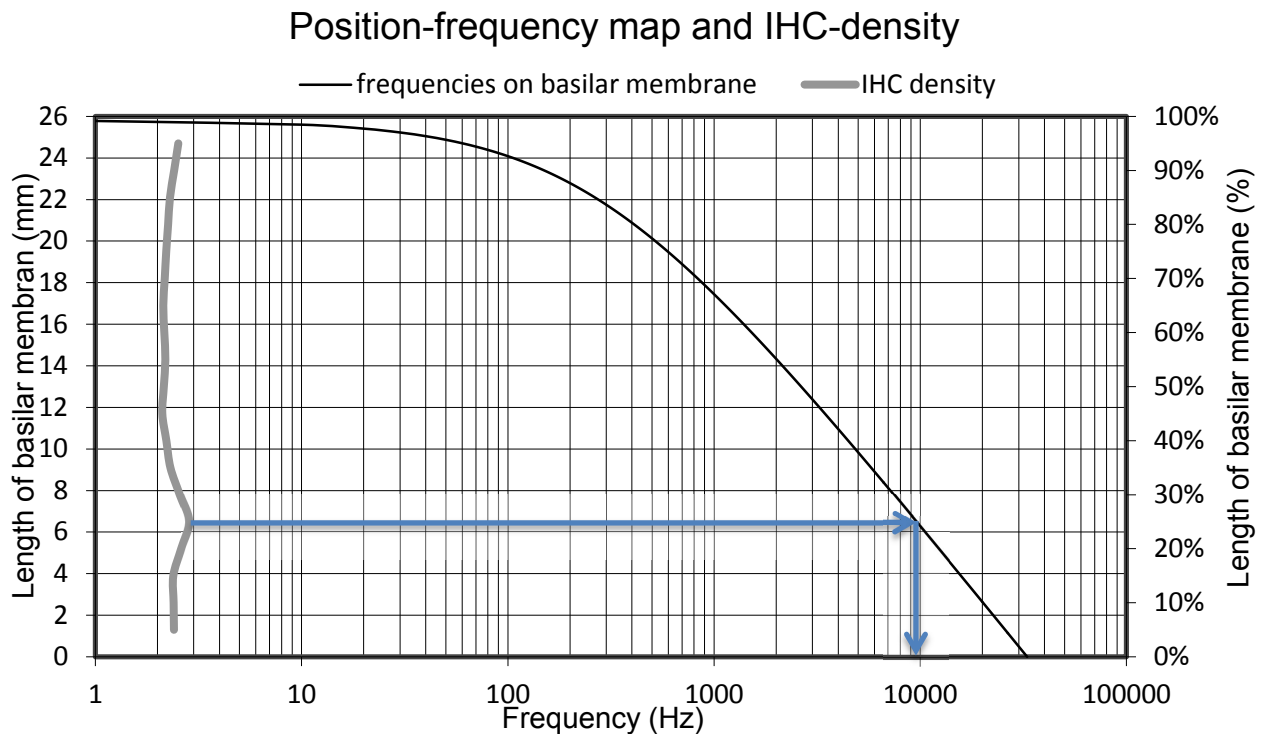
Figure 1.4-5 Position-frequency map of the red fox cochlea using equation 11 by Fay (1992). The map is based on an estimated high frequency limit of 33 kHz (after West 1985, using spiral turns and BM length as the predictor). The vertical curve on the left indicates the mean density of IHC along the cochlear duct. The blue arrows demark the peak of highest IHC density and point to the respective frequency. See text for further explanations.

Now that I have collected a number of predictions for the six audiometric variables, I reconstruct the behavioural audiogram and compare the fit. The result is shown in Figure 1.4-6. Based on the similarities of the middle ear transformer ratio (see above), I assume that the absolute threshold at the best frequency would be comparable to the cat (-10 dB SPL). Thus, the calculated high and low frequency limits after Rosowski (1992) represent the frequencies with an absolute threshold around 20 dB SPL (threshold at best hearing plus 30 dB SPL). Together with the other predicted values (after West, 1985) and in direct comparison to the actual audiogram of the red fox, it becomes quite clear, that the prediction reflects reality (i.e. values obtained by psychoacoustic means) quite well (Figure 1.4-6). The region of best frequency calculated by means of the position frequency map and the region of highest IHC density, however, does not correlate well with the actual best frequency. Maybe in mammals other than rodents the correlation between IHC density and sensitivity is not as simple and the correlation cannot be drawn. For example it was observed, that the innervation density of the IHC rather than the number of cells maximizes in the region of highest sensitivity (Vater & Kössl, 2011). Furthermore, it was recently shown that,

in the chinchilla, IHC loss of up to 80% is not accompanied by a corresponding loss auf auditory sensitivity (Lobarinas et al., 2013). It is also possible, that the position frequency map is not fitting the real distribution on the red fox cochlea. The function by Greenwood (1990) requires species-specific parameters which have only been determined for a handful of species (LePage, 2003). The integration constant of -1 for example, which is assumed in the formula by Fay (1992) (eq. 11), may not be applicable to every species. An absence of functional correlation between IHC density and best sensitivity is further corroborated when we apply the above described relationship between OHC length and best resonance frequency to estimate the position of 4 kHz in the red fox cochlea. Dannhof (1991) reported an OHC length of 36 µm at the position of 4 kHz. In the red fox, outer hair cells of 36 µm length are found in the region of the fifth half-turn, roughly at a distance 19 mm away from the base, or around 25 % away from the apex. As a conclusion, the peak density of IHCs 75 % away from the apex is not related to higher sensitivity but rather to increased frequency and amplitude discrimination abilities as already discussed above.

The predicted audiogram is slightly shifted towards lower frequencies, except for the frequency of best hearing. As the prediction is mostly based on middle ear data (except for BM length), it does not take into account the important influence that has been proposed for the cochlea on high frequency hearing (Ruggero & Temchin, 2002, 2003). It might well be that the cochlea of the fox bears some functional adaptations that reduce the impedance at higher frequencies which would lead to an extended frequency range. With the hair cell data and gross cochlear dimensions collected in the current study, such effects are hardly predicted but obtaining a transfer function for the red fox would be an interesting topic for further research.
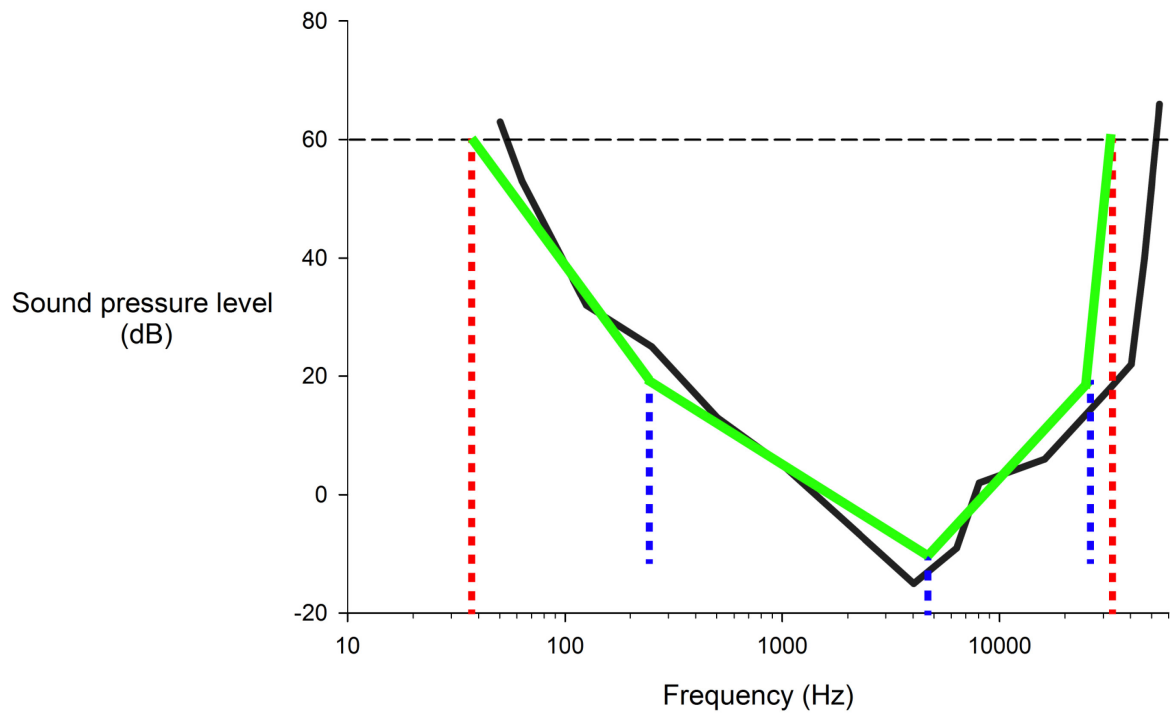
Figure 1.4-6 Predicted and behaviourally determined audiograms of the red fox. The actual audiogram that was determined in the current study is shown in black. The predicted audiogram is shown in light green. The dashed vertical lines indicate the predicted audiometric variables that define the predicted audiogram. The blue lines represent the predictions by the equations of Rosowski (1992), the red lines the predictions made after West (1985). The prediction fits the real situation quite accurately. See main text for the exact values and further explanation.

2. VISION

2.1   Introduction

2.1.1 Anatomy of the mammalian eye and retina

Mammals, as all vertebrates and in contrast to most invertebrates, possess lens eyes (detailed reviews on eye anatomy and function can be found in Land & Nilsson, 2012; Kretzberg & Ernst, 2013). The cornea which is covering the eye at the most anterior pole provides most of the refraction that is needed to gather light rays, which are subsequently focussed onto the back of the eyecup by the relatively flat lens suspended by the ciliary body within the anterior part of the eye. The shape (and to some degree the position) of the lens can be modified by ciliary muscles to allow focussing of objects at varying distances (accommodation; Hughes, 1977). Additionally, anterior to the lens, a circular structure of muscles and fibres, the iris, controls the amount of light that enters the eye through the pupil, the eye's aperture. The posterior half sphere of the eye is lined on the inside with the retina, a multi-layered neuronal outgrowth of the brain that contains the receptor cells that translate photon arrivals into neuronal excitation. The eyecup is filled with vitreous humour, a gelatinous mass which keeps the eye in shape and the retina in place. The outer shell of the eye is built of a strong, opaque layer, the sclera. Six extraocular muscles attach to the sclera and mediate eye movements.

The mammalian retina contains a variety of cell types arranged in distinct layers (excellently reviewed in Wässle & Boycott, 1991). Light hitting the retina has to pass most of these layers of neurons and glia cells before reaching the actual photoreceptors (cf. Figure 2.1-1). According to the appearance in vertical sections, the retina is divided into nuclear layers, containing mainly neuronal somata, and plexiform layers, where nerve fibres predominate. When a photon reaches the photoreceptor outer segments, that contain the light-sensitive pigments, the transduced signal is sent through the cell bodies of the photoreceptors (outer nuclear layer, ONL) via the outer plexiform layer (OPL) to the horizontal, bipolar, and amacrine cells in the inner nuclear layer (INL), and from here on via the fibres within the inner plexiform layer (IPL) to the retinal ganglion cells (RGCs), the axons of which form the optic nerve that leaves the eye and enters the brain.

The mammalian photoreceptors can be divided into two distinct populations, rods and cones. This duplex nature of the retinal receptor layer (Schultze, 1866) is a general property of all species studied so far (Peichl, 2005). Rods are far more sensitive than cones and therefore serve scotopic (night) vision. In the majority of retinae the rods predominate, which is interpreted as a remnant of the strictly nocturnal mammal ancestors (Ahnelt & Kolb, 2000; Peichl, 2005; Heesy & Hall, 2010). Cones are less sensitive and mainly used for photopic (daylight) vision. The occurrence of cone types with different absorbance spectra is the basis of colour vision. By comparing the coincident activity status of different cones at every point in time, colour is perceived in the central nervous system (Dusenbery, 1992). The spectrum of light visible to mammals ranges approximately from 340 nm to 800 nm, with the amount of this spectrum visible for a given species being defined by the transmissivity of the optical apparatus and the cone properties (Dusenbery, 1992; Jacobs, 1992). As a consequence, most mammals only see a part of this spectrum. The majority of mammals are dichromats, possessing two types of cones that peak in the blue and green part of the visual spectrum, respectively (see below for details). Only catarrhines (including humans), a few marsupials and some females of platyrrhine species possess a third cone type, making them trichromats.
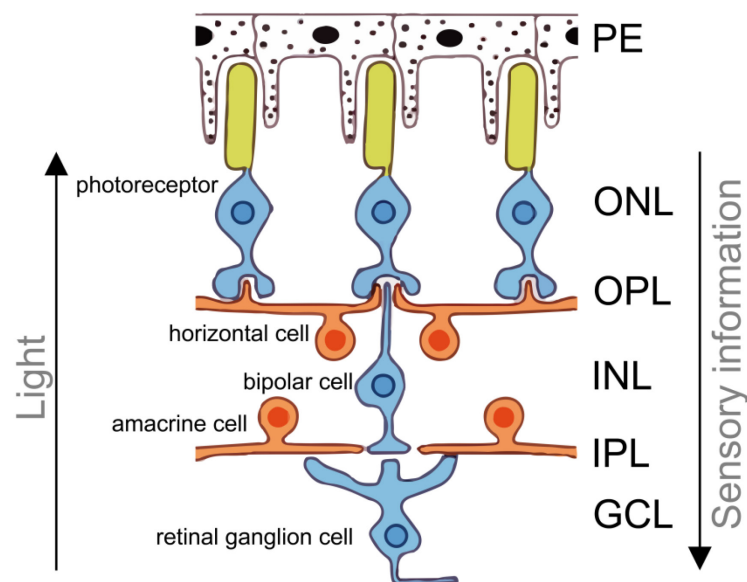
Figure 2.1-1 Simplified scheme of the cellular architecture of the mammalian retina (modified from Roth, 2013). The way of light through the different retinal layers and the flow of sensory information towards the central nervous system are indicated by the arrows. Note that the sensory flow is not exclusively vertical (see text) and that eventually all information has to pass the "bottle neck" of the retinal ganglion cells. GCL: ganglion cell layer, INL: inner nuclear layer, IPL: inner plexiform layer, ONL: outer nuclear layer, OPL: outer plexiform layer, PE: pigment epithelium.

2.1.2 Receptor properties and densities

Every visual system has to deal with a trade-off between spatial resolution and sensitivity (Land & Nilsson, 2012). Enhancing one domain goes along with reduction in the other, so within the mammalian retina the two types of photoreceptors are specialized to fulfil mainly one of both tasks each. The rod system provides high sensitivity, both intrinsically through rod properties and through spatial integration, while the cone system is not only responsible for colour vision but also for providing maximal visual acuity (spatial resolution).

The receptor mosaic of the retina is specialized to optimize the visual perception within the species' habitat, diurnal rhythm and feeding strategy. Nocturnal and crepuscular mammals possess mainly rods, while the proportion of cones increases with the diurnality of the species (Peichl, 2005). The lowest mammalian rod proportions of less than 10 % have been found in the diurnal ground squirrel and the tree shrew (West & Dowling, 1975; Müller & Peichl, 1989; Kryger et al., 1998). In line with this general rule of thumb, fissiped carnivores possess rod dominated retinae (Ahnelt & Kolb, 2000). For example in the cat, the absolute number of rods outnumbers the cones by a factor of at least 10 and up to 100, depending on the position within the retina (Steinberg et al., 1973). Although rather spectacular adaptations of the cellular architecture exist (cf. Solovei et al., 2009) we do not distinguish between different types of rods.

In general, rod and cone photosensitivity is based on the protein opsin linked to a light sensitive chromophore, the retinal (Hunt & Peichl, 2014). Rhodopsin, the visual pigment of rods, absorbs maximally in the blue-green range around 500 nm in all species (Jacobs, 1993; however, the peak sensitivity differs slightly between species, Kelber et al., 2003). Small changes in the amino acid composition of the opsin can shift the absorption maximum of the visual pigment. By this means, evolution has produced four different classes of cone pigments with peaks in the ultraviolet (360 nm; short wavelength-sensitive type 1, SWS1), blue (400-470 nm, SWS2), green-yellow (480-530 nm; medium wavelength-sensitive, MWS), and red (570 nm; long wavelength-sensitive, LWS) part of the visual spectrum (Hunt & Peichl, 2014). Only two of these classes have been retained by extant mammals: the LWS class and one of the SWS classes (SWS2 in monotremes, SWS1 in all other mammals; reviewed in Davies et al., 2012). Mammalian trichromacy is the result of a *de novo* duplication of the LWS class opsin, leading to two types of L pigments which are then commonly referred to as M (530 nm, green) and L (560 nm, red) opsins (Jacobs et al., 1996; Dulai et al., 1999). All other mammals possess a set of S and M/L cones, al-

lowing them dichromatic colour vision (Peichl et al., 2001). In some species even cones expressing both S and L opsins occur or even predominate (e.g. Lukáts et al., 2002; reviewed in Lukáts et al., 2005). Aquatic mammals (including aquatic carnivores) are characterised by a secondary loss of S cones (Peichl & Moutairou, 1998; Peichl et al., 2001), as are a few strictly nocturnal terrestrial mammals (e.g. the racoon, Jacobs & Deegan, 1992; reviewed in Szél et al., 1996).

In most species the photoreceptors show specific density gradients across the retina, and this is believed to reflect the properties of the environment relevant to each species (Hughes, 1977; Szél et al., 1996; Peichl, 2005; Ahnelt et al., 2006; Schiviz et al., 2008; Temple, 2011). Primates for instance possess a fovea, a central depression and region of cone peak density, responsible for sharp central colour vision. Even though most mammals do not have a fovea, they possess a region of higher receptor density, slightly inaccurately coined as the central area, or area centralis (Müller, 1861; Hughes, 1977). In addition, many species are characterised by a horizontal medial stripe of higher photoreceptor density, the visual streak. Broadly speaking, most mammals possess this centroperipheral density gradient of photoreceptors. In the majority of species, both S and M/L cones follow this pattern, the M/L cones being the vast majority outnumbering the S cones approximately ten times (Peichl, 2005). In several species, however, the pattern of S cones seems to be decoupled from the M/L cone distribution (Peichl, 2005). This is particularly obvious in several *Mus* species where the S cones predominate the ventral retina, while M/L cones prevail in the dorsal part (Szél et al., 1994). A closely related pattern with high ventral S cone density was observed in several carnivores, such as cat, tiger, and lion (Linberg et al., 2001; Ahnelt et al., 2006). Figure 2.1-2 gives an overview of the most common cone distribution patterns found in mammalian retinae.
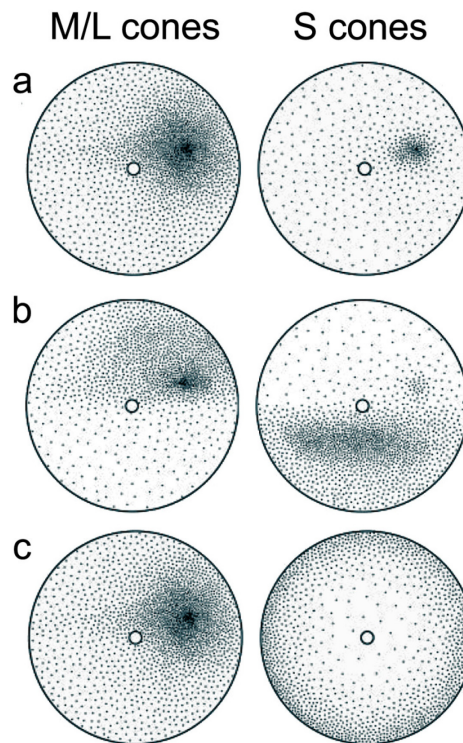
Figure 2.1-2 Schemes of typical S and M/L cone distribution patterns occurring in mammals. The retina is represented by the circles with dorsal always being on the upper side and temporal being on the right. (a) Most commonly found centroperipheral gradient with the lower S cone density closely following the pattern of M/L cone distribution. (b) Normal topography of M/L cones and ventral concentration of S cones (e.g. domestic cat, common shrew). (c) Normal M/L cone distribution and inverted S cone gradient with highest densities in the periphery (e.g. tarsier). From Peichl (2005).

In the red fox, even though colour vision had been doubted on the basis of observational studies (Lloyd, 1980), two different functional visual pigments have been identified by electroretinogram flicker photometry, one with peak sensitivity around 555 nm and the other around 438 nm (Jacobs et al., 1993). Thus, the red fox is supposed to possess the same photoreceptor types as other terrestrial and not strictly nocturnal carnivores (Jacobs et al., 1993; Linberg et al., 2001; Peichl et al., 2001). So far, however, nothing is known about the absolute numbers and topography of cone types in the red fox.

2.1.3 Retinal ganglion cell distributions

All excitatory input originating in the rods and cones eventually has to be transmitted via the retinal ganglion cells (RGC) to reach the higher processing centres in the brain (Figure 2.1-1). As the number of cones and rods considerably exceeds the number of RGCs, the information has to pass a bottleneck where input of several photoreceptors converges in a single RGC. It is only in

the primate fovea that every cone is connected to a single or even several ganglion cells (cone-to-ganglion cell convergence 1:1; Wässle et al., 1990). In all other animals, the absolute number and density distribution of RGCs rather than photoreceptors defines the overall resolution and field of best vision, respectively. For this reason, counts of RGCs, which can easily be performed on Nissl stained retinal whole mounts, have found wide acceptance as estimates of visual acuity of animal species which have not been tested behaviourally (e.g. Hughes, 1975; Peichl, 1992; Gonzalez-Soriano et al., 1997; Harman et al., 2001; Ullmann et al., 2012). As discussed above for the photoreceptors, the distribution pattern of the RGCs reflects certain demands within the ecology of a species. For instance, animals living in large unstructured habitats with high visibility of the horizon, such as many ungulates, tend to have a high RGC density along a nasal-temporal line, the so called visual streak, with only an indistinctive area of highest density close to the temporal end of the streak (e.g. Hebel, 1976). In contrast, animals that inhabit rather three dimensional environments, such as forest-dwelling species tend to have a more pronounced area centralis. This relationship between habitat and RGC distribution was first clearly formulated by Hughes (1977) and coined as the "terrain hypothesis" which is still the most parsimonious hypothesis for the functional significance of different RGC distributions in mammalian species.

Retinal ganglion cells have been quantified in several carnivores: cat (Stone, 1965; Hughes, 1975; Stone, 1978), cheetah (Hughes, 1977), dog and wolf (Hebel, 1976; Peichl, 1992), gray fox (Rapaport et al., 1979), ferret (Henderson, 1985), and spotted hyena (Calderone et al., 2003). Heffner & Heffner (1992c) added the maximal RGC density of the least weasel (*Mustela nivalis*) to this collection. Peichl (1997) has published a qualitative map of the RGC densities of the red fox retina. In line with the terrain hypothesis, the forest-dwelling red fox showed a distinctive area centralis and only an inconspicuous visual streak, as for example in comparison to the arctic fox (*Alopex lagopus*) which inhabits vast landscapes where the horizon is the most prominent feature. The findings were contradicting the report of a prominent visual streak from very coarse and subjective initial description of the red fox retina by Slonaker (Slonaker, 1897). As the assessment by Slonaker was highly subjective and the qualitative RGC maps by Peichl were based on gross estimations only (Peichl, personal communication) the absolute RGC numbers of the red fox still await determination.

2.2   Material and Methods

2.2.1   Gross anatomy of the eye

Eyes for retinal whole mounts and sectioning were taken from immersion fixed heads in either 10 % formalin-solution in water or 4 % PFA-solution in 0.1 M PB (see 1.2.2 for further details). I carefully removed the eyes from the orbits by means of titanium forceps and ceramic scalpels and cut the optic nerve close to the sclera. I detached remaining eye muscles and connective tissues and inflated the eyes by means of a gentle injection of PBS with a syringe (Vakkur et al., 1963). This procedure allowed for accurate measurements of the outer dimensions with a digital calliper. I determined the maximal diameter and the axial length of the eye as well as the diameter of the cornea. Additionally, I measured the thickness and diameter of the extracted lens in some of the specimens. Figure 2.2-1 gives an overview of the ocular dimensions I assessed.
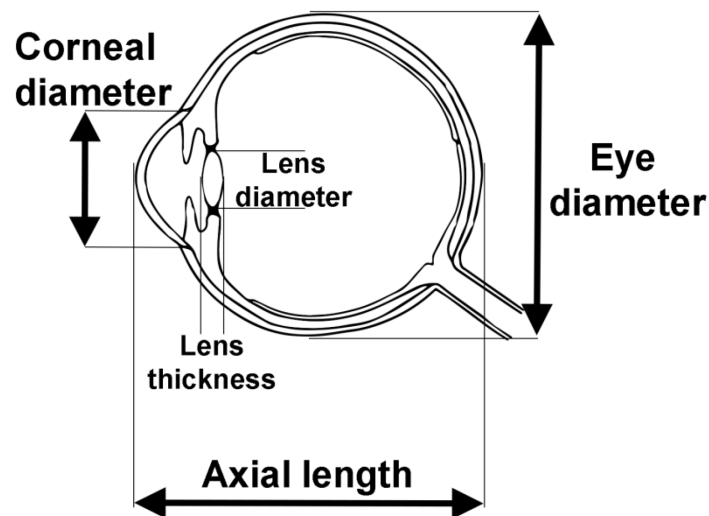
Figure 2.2-1 Simplified scheme of the mammalian eye with the dimensions that were measured prior to retina preparation.

Retinal whole mount preparation

The dissection of the eyes and mounting of retinae followed the description by Stone (1981) and the comprehensive review by Ullmann et al. (2012). First, I set a small cut behind the limbus with a ceramic scalpel, followed by the dissection of the anterior part of the eye (cornea, ciliary body, and lens) with titanium scissors and forceps. I stored the cornea and lens in PBS at 4 °C for

later analysis. A small triangular incision allowed for later reorientation. To extract the retina from the eyecup, I first carefully removed the vitreous body with help of titanium forceps and soft brushes. Next, I freed the retina in small steps beginning at the margins by carefully inserting a custom-sharpened and custom-bent raspatory (AF-Medical, Kreuzlingen, Switzerland) between the retina and the pigment epithelium. When reaching the optic disc, I cut the optic nerve and removed the retina from the eyecup. If pigment epithelium was still attached to the retina, I bleached it for up to 45 minutes in a hydrogen peroxide bleaching solution (recipe given in the appendix). After bleaching, I thoroughly washed the retina in 0.1 M PB.

OPSIN IMMUNOHISTOCHEMISTRY

The preparation of the retinae followed the same protocol as for the RGC staining, but for immunohistochemistry I processed the retinae free floating in a plastic petri dish (3.5 cm diameter) before mounting them upside down onto an untreated microscope slide to promote visual access to the photoreceptor layers after staining was completed. The visualization of the different cone types was accomplished by immunohistochemistry of the S and L opsins according to the following steps (all performed at ambient temperature):

- wash the fixed and prepared retina in PB (0.1 M pH = 7.4; several times if the retina had been bleached before)
- incubate the retina in sucrose solutions of increasing concentrations (10 %, 20 %, 30 % in PB) until the retina sinks to the bottom of the vial; at least 2 h in the 30 % solution
- cracking: transfer the retina from the 30 %-sucrose solution onto a clean microscope slide and quickly freeze it by holding it over a -80 °C metal cooling block; allow the retina to thaw and repeated the procedure two more times
- wash in 0.1 M PB
- block with 1 ml 10 % normal goat serum (NGS) or normal donkey serum (NDS), 1 % bovine serum albumin (BSA), 0.5 % Triton-X-100, 0.05 % sodium azide (NaN_3) in PB for 1 h
- wash in 0.1 M PB
- incubate with the first antibody diluted in 1 ml 3 % NGS or NDS, 1 % BSA, 0.5 % Triton-X-100, 0.05 % sodium azide in 0.1 M PB on a lab shaker for 3 days
- wash in PB for at least 1 h

Diaminobenzidine (DAB)-staining:

- ⚔ incubate with the secondary antibodies diluted in 1 ml 3 % NGS or NDS, 1 % BSA, 0.5 % Triton-X, 0.05 % sodium azide in 0.1 M PB on a lab shaker overnight in darkness

- ⚔ wash for several hours in 0.1 M PB

- ⚔ incubate with xx-peroxidase anti peroxidase (xx-PAP with xx being the host species of the primary antibodies) diluted in 1 ml 3 % NGS or NDS, 1 % BSA, 0.5 % Triton-X-100, in 0.1 M PB (without sodium azide) on a lab shaker overnight

- ⚔ wash several times for several hours in 0.1 M PB (without sodium azide)

- ⚔ transfer retinae in 0.05 M Tris-buffer (pH = 7.6); change the buffer two times

- ⚔ 15' incubation in 1 ml 0.05 % DAB in 0.05 M Tris-buffer

- ⚔ 5-8' incubation in 1 ml 0.05 % DAB, 0.01 % H_2O_2 in 0.05 M Tris-buffer until staining was sufficient

- ⚔ wash in 0.05 M Tris-buffer

- ⚔ wash 2-3 h in 0.1 M PB; change buffer several times

I mounted the retinae with Roti Histokit II® (Carl Roth) and analysed them at a bright field microscope (Olympus BX40 or Zeiss Axio Observer Z1).

The following primary antibodies were used:

1. Rabbit antiserum JH 455 raised against the last 38 amino acids of the human S (blue) cone opsin (kindly provided by J. Nathans; characterised by Wang et al., 1992).

2. Rabbit antiserum JH 492 raised against the last 38 amino acids of the human L (red) cone opsin (kindly provided by J. Nathans; characterised by Wang et al., 1992).

I determined the outer dimensions of 37 eyes from 19 different foxes. As in the previous chapter, I assorted the animals to three age classes (juvenile, subadult, adult) according to their CBL values (interpolated from the findings by Hartová-Nentvichová et al., 2010). The sample distribution was skewed towards younger animals with ten juveniles and seven subadults, while the eyes of only three adult specimens could be studied.

RETINAL GANGLION CELL STAINING

For staining of RGCs, I mounted the retinae with their anterior side (RGC layer) up on a gelatinized (5 %) microscope slide (76 mm x 52 mm, Carl Roth). Three to four radial cuts served to flatten the retina. I carefully removed remaining vitreous humour with a soft brush.

To attach the retina to the gelatinized slide, I employed the sandwich method (Figure 2.2-2, Peichl, personal communication). I covered the retina with two sheets of lens cleaning paper (Olympus) with a single layer of filter paper (Whatman, Kent, UK) in between. An uncoated microscope slide and a 54 g brass weight covered the top, and the whole sandwich was placed overnight in a 9:1 solution of 96 % ethanol and 37 % formalin. I soaked all paper sheets and cover slides with the ethanol-formalin solution before usage.

I used a Nissl stain for RGC visualization according to the following protocol:

- 45' incubation of the mounted retina in a solution of 95 % ethanol + 5 % acetic acid
- rinse in aq. dest.
- staining with 0.1 % cresyl violet until RGC layer (only) is clearly recognizable → depending on the freshness of the dye solution incubate between 30" and 5'
- control staining success under the microscope and stop in time by rinsing in aq. dest.
- 30" 70 % ethanol
- 5-7' 100 % ethanol
- 20' xylen

I mounted the retinae with Roti Histokit II® (Carl Roth) and analysed them at a bright field microscope (BX40, Olympus or Axio Observer Z1, Carl Zeiss AG, Jena, Germany).
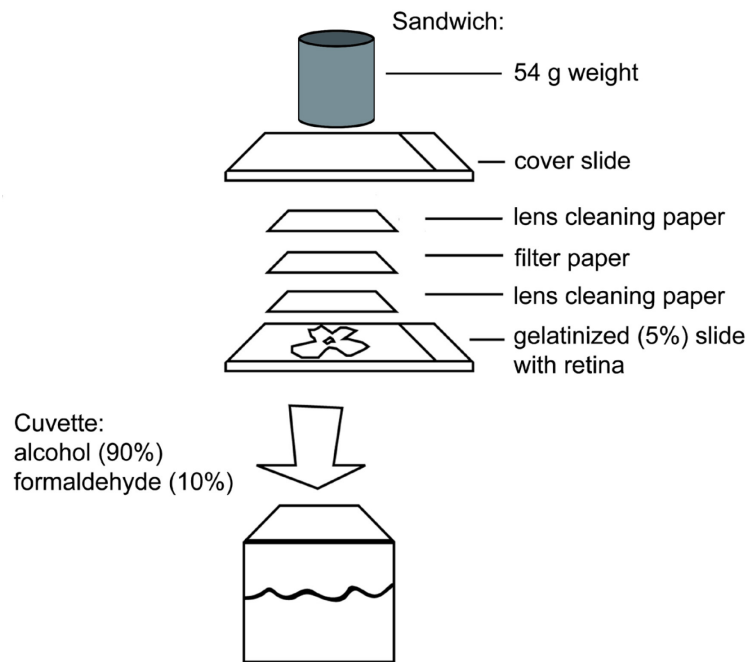
Figure 2.2-2 Overview of the sandwich method that was used to flat and mount the retinal whole mounts (modified after Peichl, personal communication).

MAPPING OF RETINAL GANGLION CELL AND CONE DENSITIES

To analyse the RGC distribution, I first drew the outlines and distinctive features of the retina under 12.5-16x magnification on graph paper via a camera lucida connected to a bright field microscope (BX40 Olympus). I added a grid onto the map and determined the RGC density at every point of the grid, each corresponding to a single sampling point every 1.8 mm of the retina. In regions of exceptionally high RGC density (e.g. area centralis) I increased the resolution of the grid to add further counting points. In total, around 120 sampling points were counted per retina. At each point I determined the number of RGCs within a 0.144 mm² area (0.0324 mm² in area centralis) under 400x magnification. The identification of RGC followed the guidelines given by Hughes (1975). Hence, I identified RGCs by their clearly visible Nissl granules, the right size and the correct topography (focus layer). I transformed the RGC densities at each point into cells/mm² and mapped them onto the retinal overview. After digitizing I inserted isodensity contour lines through manual interpolation in Illustrator CS6 (Adobe Systems). Within the area centralis, I determined the area containing 75 % or more of the maximal RGC density with the respective maximal ventrocaudal and nasotemporal width. For the determination I transferred the coordinates and cell densities of each sampling point into the statistics software Sigmaplot (V. 12.5, Systat Software Inc.), created a contour plot and set the threshold accordingly to display

the boundaries of the 75 % area. ImageJ (1.48v, NIH) then allowed the measurement of the area and linear dimensions. As the retina had been fixed to the gelatinized slide already at the beginning of the staining procedure, I assumed, referring to other reports (Wässle et al., 1975, 1981), shrinkage artefacts to be neglectable and did not correct for it.

The procedure of mapping the distribution of photopigments (S and M/L cones) was different from the RGC procedure. I scanned the whole immunostained retina at high-magnification with help of an inverted microscope with an automated stage (Zeiss Axio Observer Z1) at 200x magnification. To ensure sharp imaging of the desired plane at all positions, a Z-stack was created of 5-8 planes with 6-8 μm spacing at each sampling point. Additionally, as the surface of the specimens was not fully even, the focus had to be adjusted by setting 50-60 focus points between which the microscope automatically used interpolated values. The resulting image of the retina consisted of approximately 2,000 single images (each at 200x magnification) which were automatically stitched together with the image processing software ZEN (V. 2012., Zeiss) to yield a coherent and non-overlapping image of the retinal specimen. To map the density of the cones, I overlaid a grid (spacing 1.8 mm) within the ZEN software and counted all immunopositive cells at each of the approximately 120 grid positions within a 0.04 mm² area at 200x magnification. I interpolated the respective cone densities per mm² and mapped them onto the retinal overview. Finally, to visualize the distribution, I transferred the coordinates and cell densities of each sampling point into the statistics software Sigmaplot (V. 12.5, Systat Software Inc.) to create contour plots which I subsequently fitted into outlines of the retina. Here, to achieve full mapping coverage of the whole retina, I added a few additional points with slightly lower values relative to those sampled along the retinal periphery and placed these beyond the retinal outlines. I did not correct for tissue shrinkage (cf. Calderone et al., 2003; Schiviz et al., 2008).

2.2.2 Estimates of visual acuity

The external measurements of the eye and retinal cell densities were used to estimate the visual acuity of the red fox. As no schematic eye exists for the red fox and the establishment of such a model was beyond the scope of this thesis (cf. Vakkur & Bishop, 1963; Hughes, 1977, 1979; Coile & O'Keefe, 1988 for the technical and computational demands of developing such a model), I determined the retinal magnification factor (RMF) by two different approximate methods and used the mean for all further calculations. First, as comparative studies have shown that

the RMF is linearly related to the axial length of the eye (Hughes, 1977), I calculated the respective RMF for the red fox by placing the mean axial length (AL) into the equation of the regression line:

$$\text{RMF} \left(\frac{\text{mm}}{\text{deg}}\right) = 0.011 \left(\frac{1}{\text{deg}}\right) \times \text{AL(mm)} \text{ (Hughes, 1977)}.$$

Additionally, I determined the RMF with help of the estimated posterior nodal distance (PND) by multiplying the axial length of the eye by 0.54, the axial length/PND ratio (Pettigrew et al., 1988). I chose this specific ratio for the red fox because the published ratios of strictly nocturnal animals ranged from 0.51-0.54, while the respective ratios of crepuscular animals were between 0.54 and 0.6 (Pettigrew et al., 1988). Within this spectrum I assorted the red fox to the upper end of the nocturnal and the lower end of the crepuscular range, properly reflecting its ecology. Using the PND, the RMF can be estimated as:

$$\text{RMF (mm/deg)} = 2\pi \times \frac{\text{PND (mm)}}{360 \text{ (deg)}} \text{ (Harman et al., 2001)}.$$

The number of cycles per mm can be calculated by dividing the number of ganglion cells per mm (assuming a square sample array, the number can be estimated from the square root of the maximal density) in the region of highest density by two:

$$\frac{\text{cyc}}{\text{mm}} = \frac{\sqrt{\text{maximal ganglion cell density}}}{2 \text{ cyc mm}^{-1}}.$$

Finally, I calculated the visual acuity in cycles per degree:

$$\text{Visual acuity (cyc/deg)} = \text{RMF} \left(\frac{mm}{deg}\right) \times \frac{\text{cyc}}{\text{mm}}.$$

2.2.3 Estimates of sound localization ability

The area of best vision, defined as the horizontal width (in degree) of the retinal area where the density of RGCs reaches at least 75 %, is strongly inversely correlated to the sound localization ability of mammals (Heffner & Heffner, 1992c). To estimate this value for the red fox, I determined the horizontal width of the 75 % RGC density area (measurement described above) and the species-specific RMF as described above. The resulting value of the field of best vision in degrees served then to estimate the sound localization threshold of the red fox (in degrees) by means of the regression that I obtained by plotting the field of vision and sound localization threshold data published in Heffner & Heffner (1992c) on a double-logarithmic scale:

sound localization threshold (deg) = $1.8422 \times$ (field of best vision (deg)$^{0.5588}$).

2.2.4 Statistics and graphics

I employed Sigmaplot (V. 12.5, Systat Software Inc.) to plot all graphs and perform descriptive statistics and statistical interference. Variance equality and normal distribution were always tested with Bartlett's test and test procedure by Shapiro-Wilk, respectively. In case of normal distributions, I performed t-tests or analyses of variance (ANOVA) depending on the structure of the data (procedure always given in the results section). Nonparametric tests comprised Mann-Whitney U-test and ANOVA on ranks. Advanced statistical tests and analyses are indicated with the respective results in the results section. For tables, standard calculations, and data transformation I used Excel 2010 (Microsoft Corp.). I prepared graphical illustrations in Photoshop and Illustrator CS6 (Adobe Systems) and performed graphical metrics and cell counts in ImageJ (V. 1.48v, NIH).

2.3   Results

2.3.1 Gross anatomy of the eye

Figure 2.3-1 shows the eye of a red fox. The eye is of spherical shape and characterised by a large corneal diameter and a distinctive tapetum lucidum, both adaptations to scotopic vision. The prominent optic nerve enters the eye almost centrally at the posterior pole.
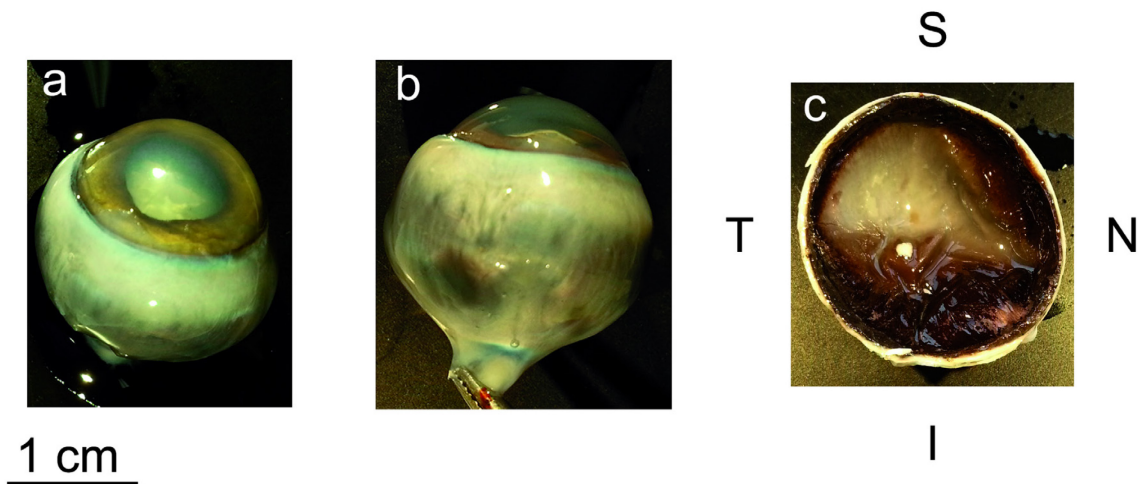
Figure 2.3-1 Eye of a red fox. (a) Side-frontal view. Note the large corneal diameter with respect to the total eye diameter. (b) Side view with the optic nerve at the bottom. (c) View into the eyecup after removal of the cornea, lens, vitreous body, and retina. Note the prominent tapetum lucidum superior and temporal to the optic disc and as a small streak extending into the nasal proportion of the eye. I, inferior; N, nasal; S, superior; T, temporal.

All measured outer eye dimensions (but not lens dimensions) were positively correlated to the age of the animals (Table 8). The relationship is exemplarily shown for the axial length in Figure 2.3-2. Least square regression analysis revealed that the development of the axial length is best described by a polynomial quadratic function ($r^2 = 0.638$, $p = 0.003$; Figure 2.3-2), which is approaching the asymptote at adult CBL within the range of my adult samples (for one adult fox the CBL could not be measured as the skull was incomplete). Therefore, I calculated the respective means for all age groups, but only used the adult mean for further calculations of the performance of the visual system.
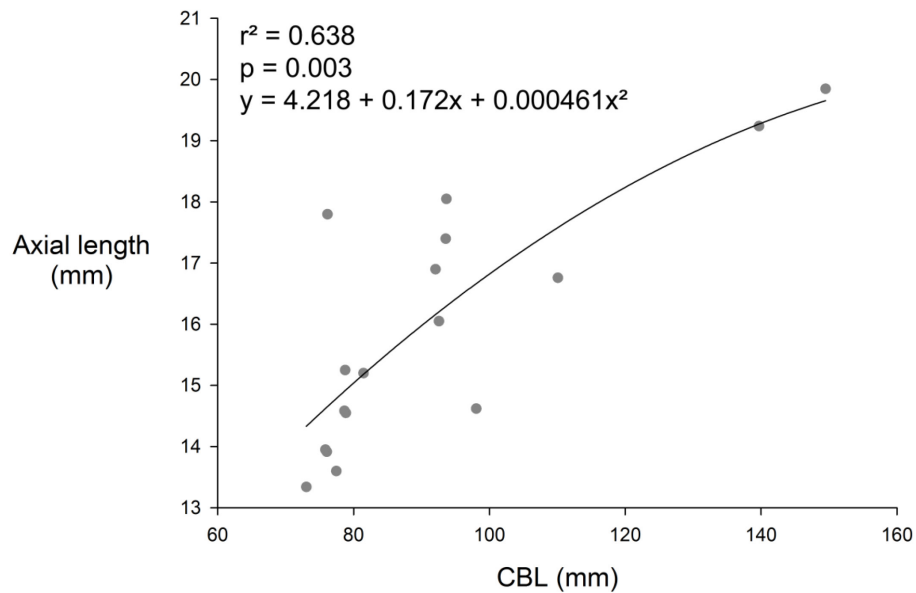
Figure 2.3-2 Axial length of the eye plotted against the condylobasal length (CBL). The axial length increased with increasing length of the skull (which served as a proxy of age). The positive correlation was best described by a polynomial quadratic regression function (parameters of which are given in the upper left of the diagram).

Table 8 Correlations between the condylobasal length (CBL) as a proxy of age and the dimensions of the eye. Pearson product-moment correlation coefficients and sample sizes (individuals) are given.

	Length (mm)				
	Axial length	Diameter	Corneal diameter	Lens diameter	Lens thickness
CBL	0.791** (17)	0.877** (17)	0.900** (17)	n.s. (8)	n.s. (8)

Pearson correlation coefficients with a superscript "**" were significant with $p < 0.01$; n.s. = not significant; the numbers of specimens are given in parentheses

The mean axial eye length was increasing with age from 14.91 ± 1.45 mm (± SD) in juveniles (n = 10), over 16.52 ± 1.19 mm in subadults (n = 6) to 19.16 ± 0.73 mm (n =3) in adult individuals (Table 9). The mean diameter of the eye was nearly identical to the axial length, reflecting the almost perfect spherical shape of the eye (juveniles: 14.65 ± 0.98 mm; subadults: 15.71 ± 1.33 mm; adults: 19.44 ± 0.81 mm). The cornea had a mean diameter of 11.30 ± 0.77 mm (juveniles), 12.53 ± 1.17 (subadults) and 16.04 ± 0.99 mm (adults). Increase in lens size seemed not to be correlated with age, as both mean diameter and thickness were larger in juveniles than in subadults (cf. Table 9). Adult lens dimensions (n = 2) were 11.58 ± 0.12 mm diameter and 6.82 ± 0.18 mm maximal thickness.

Table 9 Ocular dimensions of several red fox specimens of different age classes. The age estimation was based on the data published in Hartová-Nentvichová et al. (2010).

Specimen	Age class**	Axial length (mm)	Diameter (mm)	Corneal diameter (mm)	Lens diameter (mm)	Lens thickness (mm)
VV18	adult	19.24*	18.5*	14.9*	11.66	6.69
VV8	adult	19.85	19.91	16.56	11.49	6.95
VV22	adult	18.40	19.90	16.65		
VV6	subadult	17.40	15.90	13.60		
VV7	subadult	18.05	16.90	12.90	8.68	5.29
VV29	subadult	14.62	14.65	11.16		
VV30	subadult	16.76	17.60	14.06		
VV11	subadult				8.24	4.57
VV12	subadult	16.05	14.95	11.90	8.00	4.49
VV17	subadult	16.25	14.25	11.55		
VV1	juvenile	13.60	13.95	10.90	7.8*	4.76*
VV2	juvenile	15.20	14.50	11.65		
VV3	juvenile	14.55	15.20	11.25		
VV4	juvenile	15.25	14.20	10.95		
VV5	juvenile	13.95	14.40	10.60	11.54	6.83
VV9	juvenile	17.80	16.80	12.70		
VV10	juvenile	16.90	15.70	12.55	9.06*	5.06*
VV26	juvenile	13.34	13.60	11.06		
VV27	juvenile	13.92	13.84	10.60		
VV28	juvenile	14.59	14.31	10.71		
Mean ± SD (juvenile)		14.91 ± 1.45	14.65 ± 0.98	11.30 ± 0.77	9.47 ± 1.90	5.55 ± 1.12
Mean ± SD (subadult)		16.52 ± 1.19	15.71 ± 1.33	12.53 ± 1.17	8.31 ± 0.34	4.78 ± 0.44
Mean ± SD (adult)		19.16 ± 0.73	19.44 ± 0.81	16.04 ± 0.99	11.58 ± 0.12	6.82 ± 0.18
Mean ± SD (all)		16.1 ± 1.98	15.74 ± 2.00	12.43 ± 1.92	9.56 ± 1.71	5.58 ± 1.06

*measurements were derived from a single eye, all other values are means of both eyes

**age classification: CBL

juvenile   < 90 mm

subadult   90-110 mm

Adult   > 110 mm

2.3.2 Cone density distribution

Both S and M/L cones could readily be identified within the red fox retinae by the applied immunostaining. The cone distributions and absolute densities differed considerably between both types (Figure 2.3-3). The predominant M/L cones were concentrated along a medial horizontal streak, reaching highest densities in a region slightly temporodorsal to the optic disc (area centralis). The mean peak M/L cone density of the two stained retinae was 22,619 cells/mm² (Table 10). Minimal encountered M/L cone densities were 3,491 cells/mm² and 3,281 cells/mm², resulting in a mean of 3,386 cells/mm².

The far less numerous S cones were concentrated within the ventral half of the retina in all three retinal specimens. A single individual also showed a distinctive region of higher S cone density in the dorsotemporal retina, but no clear increase was observed in this region in the other stained retinae. The absolute peak densities showed considerable interindividual differences (Table 10). The highest densities found in each of the specimens were 2,373 cells/mm², 2,887 cells/mm², and 3,437 cells/mm², yielding a mean of 2,899 cells/mm². The corresponding lowest densities were 300 cells/mm², 567 cells /mm², and 491 cells/mm², with a mean of 453 cells/mm². It was striking that the lowest S cone densities were found in an individual of advanced age (approximately 10-12 years, see discussion). The M/L cone densities determined in the other eye of the same individual were, however, in the range of the other test red fox specimen (Figure 2.3-3).

Table 10 Retinal areas and numbers of S and M/L cones stained in the red fox specimens.

Specimen	Cone type / Antibody	Cones			Retina
		Peak density (cells/mm²)	Lowest density (cells/mm²)	Total cone numbers (approximate)	Area (mm²)
VV1R	S cones JH 455	3,437	491	574,107	332.4
VV4L		2,887	567	603,515	352.1
VV8R		2,373	300	404,518	455.3
VV8L	M/L cones JH 492	23,377	3,281	3,400,239	400.4
VV12L		21,861	3,491	4,224,226	407.0
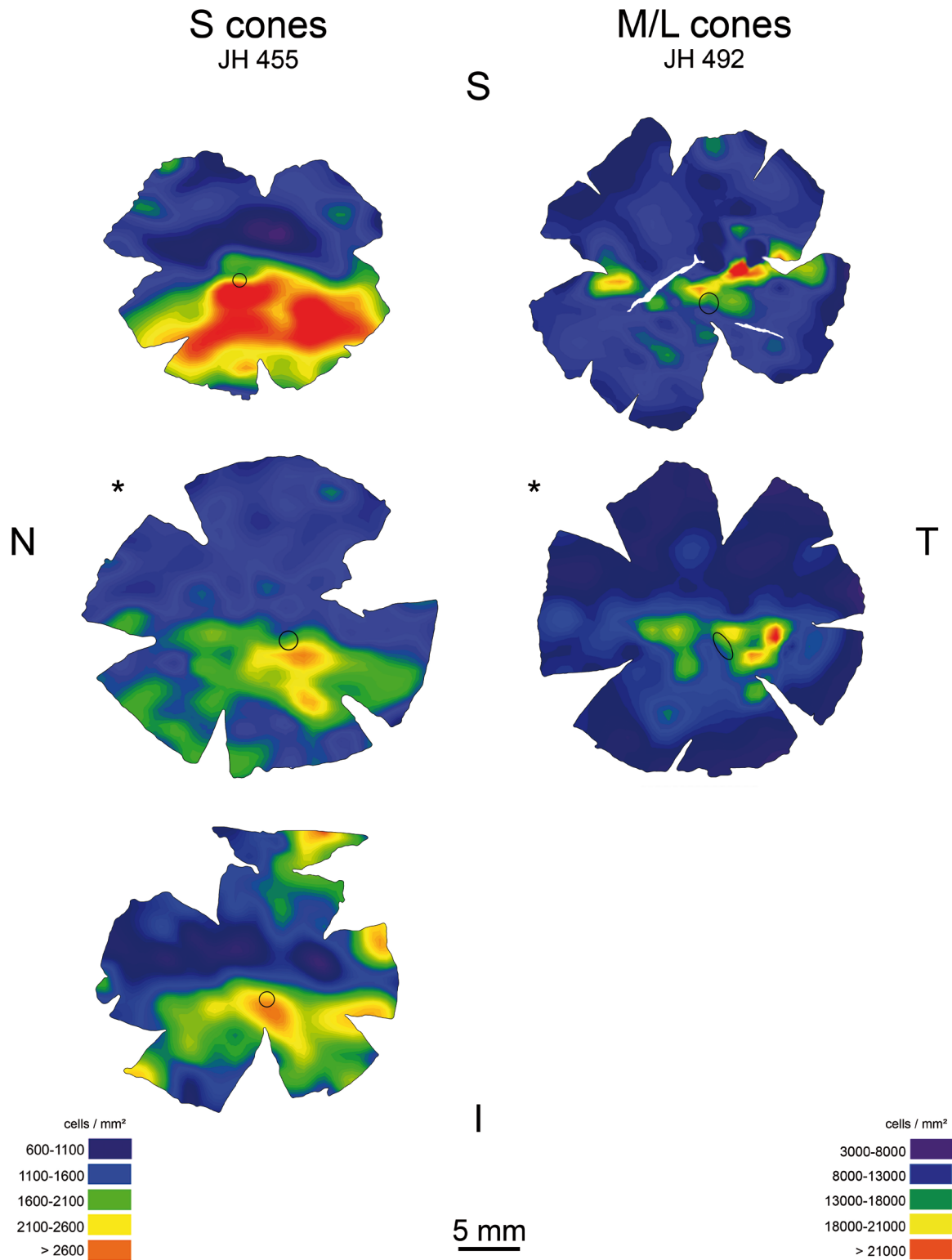
Figure 2.3-3 Distribution of S and M/L cones in red fox retinae as determined by immunostaining (S cones, JH 455, M/L cones, JH 492). The S cones showed a clear dorsoventral gradient with high densities in the lower retina, while the predominant M/L cones exhibited a medial aggregation along a horizontal streak with maximum densities in a small area temporodorsal to the optic disc. The retinae in the middle row (asterisks) both stemmed from a single red fox individual (VV8) of highly advanced age (approximately 10-12 years). The densities of S cones were considerably lower in this specimen than in the other two specimens. I, inferior; N, nasal; S, superior; T, temporal.

2.3.3 Ganglion cell density distribution

The RGCs in the three investigated red fox retinae displayed a distinct centroperipheral gradient with highest densities in an area centralis just temporally to the optic disc. Additionally, a notable visual streak extends almost to the nasal margin of the retina. In the fully mapped specimen VV21446R the peripheral RGC densities fluctuated between 40-50 cells/mm² and 200-300 cells/mm² (Figure 2.3-4). Within the visual streak, the densities reached values around 500-1,000 cells/mm². Within the small area centralis I determined a maximal RGC density of 7,253 cells/mm². The two other red fox retinae had maximal RGC densities of 7,747 cells/mm² and 7,593 cell/mm², therefore I calculated the average peak RGC density of the red fox as 7,531 ± 253 cells/mm² (± SD). The average dorsoventral and temporonasal extent of the area containing at least 75 % of the highest RGC density (area of best vision) was 329 µm and 559 µm, respectively. The respective values for the single arctic fox specimen were 215 µm and 863 µm. Detailed values for each of the investigated red fox retinae are given in Table 11.

Table 11 Peak retinal ganglion cell (RGC) densities in three red fox retinae. The area of best vision was defined as the region with at least 75 % of the peak RGC density. n.d., not determined.

Specimen	Species	Retinal ganglion cells		Area of best vision		
		Peak density (cells/mm²)	Lowest density (cells/mm²)	Area (mm²)	Horizontal extent (mm)	Vertical extent (mm)
VV5R	*Vulpes vulpes*	7,747	n.d.	0.119	0.534	0.287
VV10L		7,593	n.d.	0.178	0.753	0.313
VV21946R		7,253	21	0.113	0.389	0.387
AL25447R	*Alopex lagopus*	8,827	128	0.123	0.863	0.215
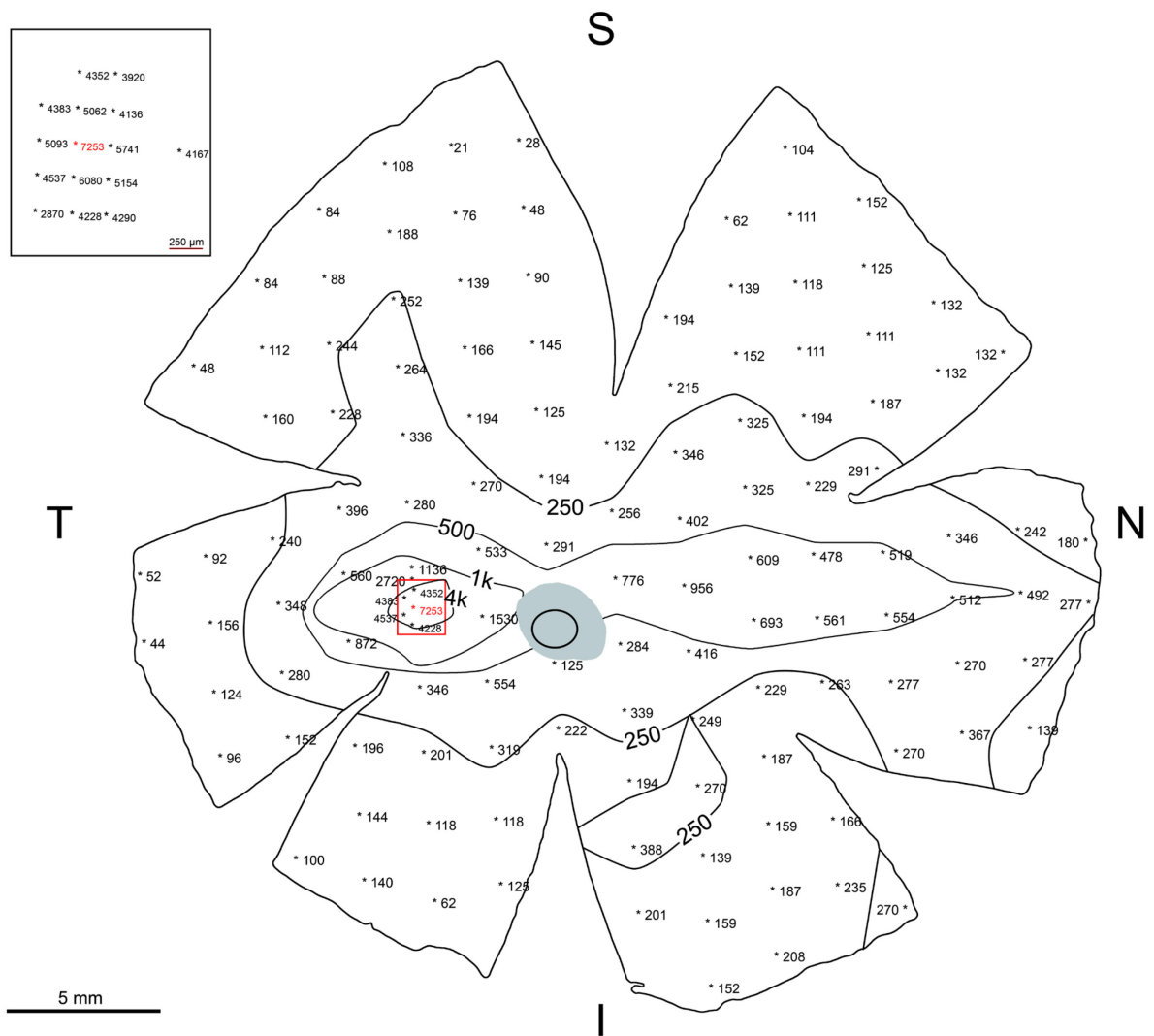
Figure 2.3-4 Distribution of retinal ganglion cells (RGCs) in the right retina of a red fox (VV21946R) determined by Nissl stain. The numbers indicate the RGC density in cells/mm². Cell densities in the periphery were too inhomogeneous to allow for meaningful isodensity contours, therefore only the visual streak and area centralis are illustrated with isodensity regions. The inset in the upper left shows the counts within the area centralis in higher detail. I, inferior; N, nasal; S, superior; T, temporal.

In the single arctic fox retinal specimen (AL25447R) a highly distinct medial visual streak was discernible already with the naked eye. The streak extends from the very outer nasal margin almost to the temporal border of the retina. In the periphery, the RGC densities were slightly higher than in the red fox specimen, with minimal densities between 150-200 cells/mm² (Figure 2.3-5). In the nasal part of the visual streak, the densities were between 1,000-4,000 cells/mm², steadily increasing towards and behind the optic disc. The area centralis was less distinct as in the red fox but still the RGC densities rose considerably up to a maximal value of 8,827 cells/mm. The area containing at least 75 % of the highest RGC density comprised 215 µm x 863 µm (dorsoventral x temporonasal). Detailed values of the arctic fox retina can be found in Table 11.

Using the temporonasal extension, converted into degrees of visual arc and entering these values into the equation of the regression line from Heffner & Heffner (1992c), the estimated sound localization abilities of the red fox and arctic fox were 3.32° and 4.57°, respectively.
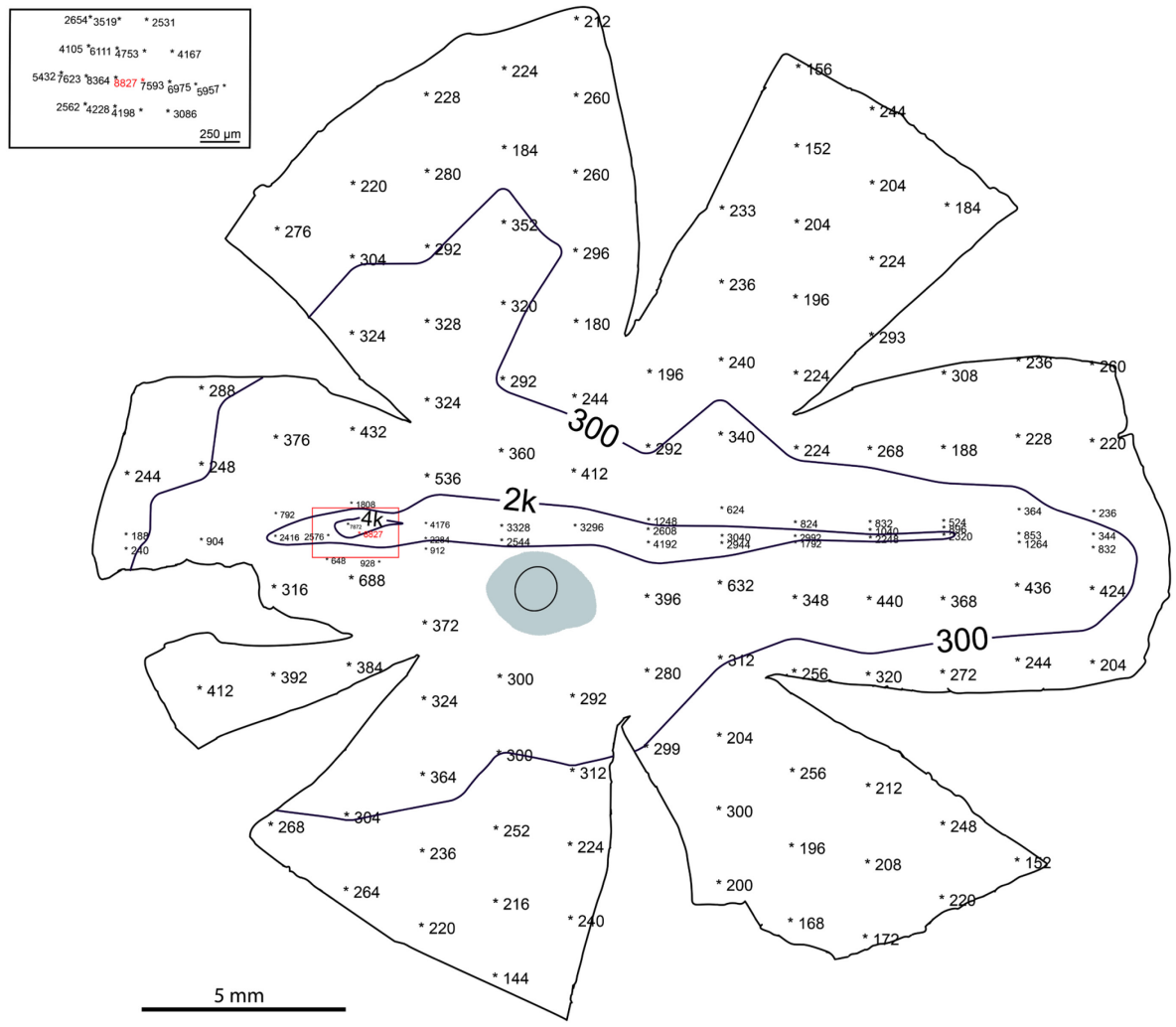
Figure 2.3-5 Distribution of retinal ganglion cells (RGCs) in the right retina of an arctic fox (AL25447R) determined by Nissl stain. The numbers indicate the RGC density in cells/mm². The inset in the upper left shows the counts within the area centralis in higher detail. Map orientation as in Figure 2.3-4.

2.3.4 Visual acuity of the red fox

Using the adult mean axial length of 19.16 mm, yielded red fox RMF estimations of 0.21 mm/deg (Hughes, 1977) and 0.18 mm/deg (Pettigrew et al., 1988; Harman et al., 2001), resulting in a mean of 0.195 mm/deg. With the averaged peak RGC density of the three investigated red fox specimens of 7,531 cells/mm² the cycle number calculated as 43.39 cyc/mm, which totalled in a visual acuity of 8.46 cyc/deg of viewing angle.

Performing the same calculations with the data for the single arctic fox eye (axial length: 17 mm) yielded an estimated RMF of 0.17 mm/deg (I chose the same axial length/PND ratio of 0.54, based on the predominant nocturnal activity pattern reported by Audet et al., 2002). With a maximal RGC density of 8,827 cells/mm², the visual acuity of the arctic fox specimen thus was estimated as 7.99 cyc/deg.

2.4 Discussion

2.4.1 General ocular dimensions and ontogenetic development

The eyes of the red fox are typical for a nocturnal carnivore, with a relatively large cornea and a well-developed tapetum lucidum. Details on the optical apparatus of lens and pupil of the red fox have been described elsewhere (Malmström & Kröger, 2006), so I will not elaborate on this here. Compared to the cat, the eyes of the red fox are a bit smaller but of the same globular shape (axial length to diameter ratio 1:1.02; in the cat 1:1.03 (Vakkur et al., 1963). Because eye size strongly correlates with body size, the smaller eyes in the larger red fox underline the supposition that it relies more on other senses, such as olfaction and hearing than the cat (Österholm, 1964; Nummela et al., 2013). The smaller eye size of the arctic fox compared to the red fox, on the other hand, is most probably not related to ecological factors but a simple consequence of its smaller body size (Larivière & Pasitschniak-Arts, 1996; Audet et al., 2002; Nummela et al., 2013).

Eye growth during ontogenetic development extends well into adulthood in the Mongolian gerbil (Wilkinson, 1986), the cat (Olson & Freeman, 1980), and even in humans (Scammon & Armstrong, 1925), and might be a general mammalian trait during development. Changes in the weight of the lens have already been reported for the red fox and were suggested to serve as a means of age determination (Cavallini & Santini, 1995; in accordance with the results presented here, lens weight alone was not an accurate predictor). Therefore, the strong correlation between eye size and CBL in my fox sample is not astonishing. As to the use of CBL as a proxy of age, Figure 2.3-2 shows that the growth rate of red foxes' eyes decreases considerably for foxes with CBLs ranging between 110 and 140 mm, and together with the good correspondence with axial eye lengths of adult red foxes given by other authors (e.g. 20.55 mm; Nummela et al., 2013; 19 mm, 20 mm; Peichl, personal communication), the use of data from foxes with CBL > 110 mm as an estimate of the visual acuity of adult red foxes can be justified.

The significant developmental changes in the axial length of the eyes strongly alter the retinal magnification factor (RMF) and consequently should affect visual acuity. In kittens, adult visual acuity is reached earlier than adult eye size (Mitchell et al., 1976), so that mechanisms compensating for the changes in ocular morphology can be assumed. It has been reported that distribution and absolute RGC density undergo significant changes during postnatal development in the rat (McCall et al., 1987) and the cat (Alfred & Stone, 1982; Wong & Hughes, 1987). Therefore,

it would be interesting to study whether the density of RGCs in red foxes follows this developmental pattern and maybe compensates for the reduced RMF, thus keeping the visual acuity more or less constant. In doing so, also the development of the corneal curvature would have to be taken into account. However, this would require studying the RGC distribution in a sufficiently large number of foxes of different age, which was not feasible within the scope of the current study.

2.4.2 Opsin distribution

The topography of S and M/L cones within the red fox retina follows a similar pattern as in other carnivores, such as the cat (Linberg et al., 2001), the spotted hyena (Calderone et al., 2003), the lion (Ahnelt et al., 2006), and the dog (beagle; Mowat et al., 2008). In all these species the highest densities of S cones are found in the ventral half-retina, while M/L cones predominate more dorsally and often along a horizontal streak and within the area centralis. Ahnelt et al. (2006) argued that this pattern seems to be typical for animals living in open habitats such as the African savannah, while forest-dwelling animals such as lynx, tiger, or deer exhibit a more concentric arrangement of S cones. Both the (wild) cat and the red fox contradict this hypothesis. With respect to the three most common stereotypical S cone distributions among mammals (Figure 2.1-2), they possess a pattern which is in general quite common among small mammals as seen in numerous rodents (Szél et al., 1994; Calderone & Jacobs, 2003; Haverkamp et al., 2005; Williams et al., 2005), the rabbit (Juliusson et al., 1994), as well as all insectivores studied so far (Peichl et al., 2000; Glösmann et al., 2008). The most common and intuitive explanation for this peculiar cone arrangement is based on the close match between the dominant wavelengths reaching each hemisphere of the visual field from the environment with the peak absorption of the S and M/L cones. According to this hypothesis, in small rodents the upper hemisphere will mainly be excited by longer wavelengths reflected from grass, earth, and leaf litter, while the lower hemisphere will receive a considerably higher amount of short wavelengths from the sky (Veilleux & Kirk, 2014). The higher sensitivity for short wavelengths in this part of the retina would hence be an adaptation to enhance the contrast between the sky and objects within the sky, such as aerial predators (coined as the "skylight hypothesis"; Szél et al., 1996). This simple "colour-match" explanation has lately been questioned by Baden et al. (2013), demonstrating that the achromatic response properties of the S cones rather than the spectral sensitivity makes them more suitable for detect-

ing dark objects in front of a bright background, while M/L cones respond equally to light and dark stimuli (with opposite gain). Regardless of the underlying physiological mechanism, the assumption for the ultimate evolutionary mechanism supported by the findings is enhanced survival (or reduced mortality) by avoiding aerial predation. This explanation does not hold for the red fox. Even though smaller fox species can under highly unnatural circumstances become the main prey of aerial predators (Roemer et al., 2002), this factor is highly improbable to have driven the evolution of photoreceptors in the red fox. The red fox is the largest fox species and in general rather predator than prey of birds (e.g. Chavko et al., 2007), let alone the much larger hyena and lion. Ahnelt et al. (2006) therefore proposed, that in these species the ventral S cone gradient is related to the low head position during stalking and search for carrion. As the eye height might be approximately similar for a fox and a stalking lion, this hypothesis seems plausible.

Another alternative explanation discussed for the variations in cone patterns confers to the retinal areas that show variability are under relaxed evolutionary pressure and might represent an ancestral state of opsin evolution. Developmental and phylogenetic constraints might have led to interspecies differences in opsin patterns without actual functional relevance (Szél et al., 1996; Temple, 2011). Supporting this theory, while contradicting the "visual environment" theory is the fact that in some closely related mice species, apparently inhabiting the same visual environment, the S cone distributions differ considerably (Szél et al., 1994). It is quite certain that the debate will be continued as cone distributions of more and more species as well as good data about the visual environments relevant to individual species are revealed (an overview is given by Temple, 2011).

In both the cat (Linberg et al., 2001; Ahnelt et al., 2006) and one of the fox specimens analysed here a second region of high S cone density is found along the temporodorsal rim of the retina. Since the other two red fox retinae of my sample did not reveal such a secondary peak region and no factor such as age, sex, or general cone densities consistently varies and might explain the difference, it remains open for speculation and future studies, whether it simply reflects interindividual differences and/or has functional implications.

The cone densities of the red fox fall within a range typical for canine and felid retinae (Table 12). In particular, the density fits well to those reported for the wolf and cat (Steinberg et al., 1973; Linberg et al., 2001; Peichl et al., 2001), with the M/L cone minimal density being higher than in the cat but lower than in the wolf, while maximal M/L densities are higher in the cat and

lower in the wolf. The lowest S cone density of the red fox is identical to smaller cats (including the lynx) and wolves but the peak density is almost twice as high. It is unclear what the functional relevance of this higher density is, but it is not unusual among carnivores, as comparable peak densities have been reported in ferret (but see the lower densities reported by Peichl et al., 2001; Calderone & Jacobs, 2003), cheetah (Ahnelt & Kolb, 2000), and hyena (Calderone et al., 2003).

Table 12 Minimal and maximal densities of S and M/L cones in the red fox and other carnivores (cf. Calderone et al., 2003 and the main text for original references).

Family	Species	M/L cone density (1,000/mm²)	S cone density (1,000/mm²)
Canidae	Red fox	3.4-22.6	0.45-2.8
	Wolf	5.7-19.0	0.4-1.5
Felidae	Cat	2.2-26.0	0.5-1.5
	European lynx	18.0	1.4
	Cheetah	30.0	7.0
Mustelidae	Ferret	10.3-28.8	0.1-3.7
Procyonidae	Raccoon	2.0-5.6	none
	Coati	18.6	1.4
Hyaenidae	Spotted hyena	0.6-7.5	<0.1-3.3

The total number of cones is rarely given in reports of opsin distributions of carnivorous species. Calderone et al. (2003) have calculated the total numbers of M/L cones and S cones in the hyena retina to approximate 2.3 and 0.3 million, respectively. The estimated totals of the red fox are 50 % higher for both, M/L and S cones (and, interestingly, also the RGCs, see below). With 10 %, the proportion of S cones in the red fox is within the standard range reported for carnivore retinae (Ahnelt & Kolb, 2000).

Interestingly, in one of my specimens (VV8) the overall density of S cones and the peripheral density of M/L cones was approximately 30 % lower than in the other specimens (cf. Table 10). Even though the eyes of this specimen had been stored in formalin for approximately two years, the fact that the peak density of M/L cones was not reduced makes it unlikely that impeded antibody penetration explains the discrepancy. Rather it seems as if the individual suffered from age related cone loss which seemed slightly higher in the S than in the M/L cones. Although the exact age of the individual still has to be determined by analysing the annular cementum rings of the molars, it has been approximated that the animal was around ten years old when it was shot (Hart, personal communication). Given that the maximal lifespan of wild foxes has been reported

as 8.6 years (Larivière & Pasitschniak-Arts, 1996) it seems reasonable to assume that the individual had suffered from age related degenerations. Peripheral, but not central cone loss of up to 23 % has been reported in aged human individuals (Gao & Hollyfield, 1992; Curcio et al., 1993) and S cones have been reported to be more vulnerable than the other cone types (Haegerstrom-Portnoy et al., 1989). Therefore, I conclude that age related photoreceptor loss is witnessed in the old red fox specimen.

2.4.3 Ganglion cell density and estimated sound localization acuity

In most mammals, the distribution of the ganglion cells closely follows the distribution of the M/L cones (Ahnelt & Kolb, 2000). This holds true for the red fox, where both distributions are characterised by a distinct density-increase around the area centralis and within a moderate horizontal streak. The generally accepted hypothesis by Hughes (1977) states that the degree of the expression of a visual streak is closely related to the environment the species is inhabiting. Species in open habitats show generally prominent visual streaks as their predominant visual feature is the horizon. The ganglion cell distribution of the arctic fox shows a very prominent streak and thus perfectly fits to this theory. Also fittingly, the red fox RGC distribution is much more concentrated within the area centralis, reflecting the more silvicolous lifestyle of this species (Larivière & Pasitschniak-Arts, 1996).

The peak RGC densities of the red fox and the arctic fox are approximately located in the middle of the range reported for carnivores (cf. Table 13). They correspond well to the densities reported for the cat (Hughes, 1975; Stone, 1978) while other canids tend to have considerably higher peak densities, even though numbers in different dog breeds are highly variable (Peichl, 1992). RGC densities in many non-carnivores tend to be considerably lower.

The horizontal extent of the area containing at least 75 % of the peak RGC density allows drawing inferences about the sound localization ability of a species (Heffner & Heffner, 1992c). For the field of best vision determined in this study, the red fox would be predicted to have sound localization acuity of 3-4°. At first glance this seems not to be in line with the reports of the maximal acuity of 1° given by Österholm (1964). However, having a closer look at the methods used in the study by Österholm reveals several flaws that might explain the divergence. First, the presented sounds were much longer (2 s) than those used in contemporary studies of sound localization acuity (100 ms). This is of importance as the former allows the fox to move the head and the

pinnae during the tone presentation which increases the acuity but hampers the correct interpretation of the results. Second, the angle between the speakers in the Österholm study is given relative to the midline and not as the angle between the speakers, which is the standard definition. Therefore, the minimal angle of localization needs to be doubled. Finally, in a two-choice procedure, as used by Österholm, the threshold is defined as the 75 % level of correct choices, which Österholm did not take into account. Correcting for this last factor yields a behaviourally determined sound localization ability of 4°, well in line with the prediction based on RGC distribution (3.32°) and better than the reported values of 5.7° for cats (Casseday & Neff, 1973; Heffner & Heffner, 1988a) and 8° for dogs (Heffner & Heffner, 1992c).

2.4.4 Estimates of visual acuity

Morphological estimates of the visual acuity based on peak RGC densities are available for several mammalian species. Table 13 shows some figures for different mammals that were originally collected and calculated by Gianfranceschi et al. (1999). Even though estimated and behavioural visual acuity values correlate quite well, it is salient that the visual acuity determined from maximal RGC densities tends to overestimate the actual behaviourally determined visual acuity. For example, the visual acuity in the cat estimated from the mean RGC peak density of ~ 8,250 cells/mm² (Stone, 1978) and a RMF of 0.22 mm/deg (Vakkur & Bishop, 1963), is 10 cyc/deg, while the actual visual acuity determined in behavioural experiments was reported as 6 cyc/deg. The reason for this discrepancy might reside in the assumption that every RGC counted on Nissl stained whole mounts contributes to visual acuity. Due to differences in the extent of the receptive fields, however, only beta type RGCs contribute significantly to visual acuity (Wässle et al., 1981; Wässle & Boycott, 1991). In the cat, these make up approximately 55 % of all RGCs (Wässle et al., 1981). Taking this correction factor into account yields an estimated visual acuity for the cat of 7.4 cyc/deg, considerably closer to the behavioural threshold listed in Table 13 (originally from Blake et al., 1974) and well corresponding to the acuity of 8-9 cyc/deg reported by other authors (Jacobson et al., 1976). Under the assumption that the red fox and arctic fox do not deviate strongly from this pattern, the corrected visual acuity would be 6.27 cyc/deg and 5.92 cyc/deg, respectively. As no behavioural visual acuities have been reported for both species, I list these values as predicted in Table 13. Interestingly, the estimated visual acuity of the red fox is almost identical to the value calculated for the spotted hyena (Calderone et al., 2003), a predator

that presumably also relies more on other senses than vision (olfaction) to find its main food items (carrion). Thus, even though a strong positive correlation between the axial length of mammal eyes and their visual acuity has been revealed (Veilleux & Kirk, 2014) and the hyena eye (axial length: 25.4 mm) is considerably larger than the red fox eye, it is a nice example of how evolution has equipped the hyena eye with the optical properties just fitting the requirements of its lifestyle. Having larger eyes than the red fox allowed the hyena to reduce the cone and RGC densities, which reduces computational demands and saves energy. The opposite might have happened to the arctic fox, which had to increase the ganglion cell density (compared to the red fox) in order to achieve comparable visual acuity with smaller eyes.

Table 13 Visual acuity in different mammalian species as estimated from their peak ganglion cell densities and ocular axial length, together with corresponding visual acuities determined behaviourally. I took the data shown in this table from Gianfranceschi et al. (1999), see the paper for references to the original studies. I corrected the data for the cat peak RGC densities reported by Gianfranceschi et al. (1999) as they did not correspond to those originally reported by Stone (1978). Also, the RMF of the rat and the estimates of the visual acuity of the dog and horse were corrected as they were wrongly calculated or cited by Gianfranceschi et al. (1999). Data on spotted hyena are taken from Calderone et al. (2003). I predicted the behavioural thresholds of both foxes by correcting the peak RGC density for the proportion of beta RGCs (see main text). n.d., not determined.

Species	Peak RGC density (cells/mm²)	RMF (mm/deg)	Estimated visual acuity (cyc/deg)	Behavioural visual acuity (cyc/deg)
Cat *Felis catus*	8,250	0.22	10.0	6.0
Dog (beagle) *Canis familiaris*	12,200	0.18	9.9	6.3
Spotted hyena *Crocuta crocuta*	4,200	0.26	8.4	n.d.
Rabbit *Oryctolagus cuniculus*	2,500	0.17	4.3	3.4
Horse *Equus ferus caballus*	6,500	0.47	18.9	22.3
Rat *Rattus norvegicus*	2,000	0.059	1.3	1.0
Arctic fox *Alopex lagopus*	8,800	0.17	8.0	5.9 (predicted)
Red fox *Vulpes vulpes*	7,500	0.195	8.5	6.3 (predicted)

3. MAGNETORECEPTION

3.1   Introduction

3.1.1 Magnetic orientation

The ability to perceive the geomagnetic field (GMF) and use it as a universal reference for orientation has so far been demonstrated in more than 30 species of vertebrates with new ones being reported regularly (reviewed in Wiltschko & Wiltschko, 1995; Wiltschko & Wiltschko, 2012a; Begall et al., 2014). In the past, the majority of studies were done on birds. These studies have given valuable insights into the functional properties of the magnetoreceptors (Wiltschko & Wiltschko, 2010). In mammals, research on magnetoreception is far less advanced, but recently the list of mammalian species expressing magnetosensitive behaviours is steadily growing (reviewed in Begall et al., 2014).

The first mammals reported to have a magnetic sense were rodents. Early homing and orientation experiments with small epigeic rodents suggested that these mammals possess a magnetic compass which they use for navigational purposes (Mather & Baker, 1981; August et al., 1989). Later studies, however, challenged these findings with negative results and failed experimental replications (Madden & Phillips, 1987; Sauvé, 1988) so that it was not until the early 1990s that a robust behavioural assay was developed which provided solid and replicable evidence for magnetoreception in mammals: the nest building assay (Burda et al., 1990). This paradigm, in which the directions of nests built in a radial symmetrical arena are analysed, has been used ever since with a variety of different species and has yielded first insights into the mechanisms of magnetoreception in mammals (Burda et al., 1991; Marhold, 1997a, b, 2000; Kimchi & Terkel, 2001; Muheim et al., 2006; Wegner et al., 2006; Thalau et al., 2008; Oliveriusová et al., 2012).

3.1.2 Receptor mechanisms of magnetoreception in mammals[3]

Receptors for the detection of magnetic fields have not yet been conclusively demonstrated in any animal. However, findings from behavioural, histological and electrophysiological studies have led to several physically viable conjectures that might also apply to mammals. Here, I focus on the three most supported and most vividly discussed mechanisms: a magnetite-based mechanism, the radical-pair mechanism and electromagnetic inductions. Several other mechanisms, such as induced fluid streaming (Bamberger et al., 1978) and cyclotron resonance (Liboff & Jenrow, 2000) have been suggested, but since they have not received substantial support from behavioural experiments I will not further elucidate them within the framework of this thesis.

MAGNETITE

Perhaps the most intuitive (at least to the human imagination) mechanism to explain magneto-sensitivity in animals is the idea of a small permanent magnet inside the animal that acts like a compass needle (Yorke, 1979). It is therefore not surprising that after the initial discovery of biogenic magnetic material in the teeth of chitons (Lowenstam, 1962) and the subsequent demonstration of magnetite (Fe_3O_4) chains and their crucial role in the magnetotactic behaviour of certain bacteria (Blakemore, 1975; Frankel et al., 1979), a rigorous search was performed to map the distribution of this new biogenic material. Within a period of less than 20 years, suitable magnetic particles were demonstrated in different tissues of a variety of animals. The occurrence of these ferrimagnetic particles in rodents (Mather, 1985), bats (Buchler & Wasilewski, 1982), marine mammals (Zoeger et al., 1981; Bauer et al., 1985) and even humans (Kirschvink et al., 1992) makes it tempting to speculate that magnetite is a common mammalian feature and perhaps serves a magnetoreceptive function. Indeed, it has been speculated that a magnetic sense based on magnetite evolved so early in animal history that it is a common feature of all animal phyla (Kirschvink et al., 2001). Consequently, the theory of a magnetite-based mechanism of magnetoreception has found general acceptance today even though many details are still unknown (Kirschvink et al., 2010; Wiltschko & Wiltschko, 2012a).

In general, two different types of magnetite particles suitable for an animal magnetoreceptor can be distinguished: larger (> ~ 50 nm) particles are called single domain (SD) particles and pos-

---

[3] This section has already been published in Begall, Burda, Malkemper (2014) and was only marginally adapted to fit to this thesis.

sess a permanent magnetic moment, while smaller super-paramagnetic (SPM) particles (~ 3-5 nm) obtain their magnetic moment from an external magnetic field (Kirschvink & Gould, 1981; Kirschvink & Walker, 1985). Theoretically, both particle types might constitute an animal magnetoreceptor either independently or arranged as hybrid detectors (Kirschvink & Gould, 1981; Davila et al., 2003; Solov'yov & Greiner, 2007), and both types have been found to occur in animal tissues (e.g. Walcott et al., 1979; Diebel et al., 2000; Hanzlik et al., 2000). Still unsolved, however, are questions about how the magnetic stimulus is transduced into nerve signals and where exactly the receptors are located.

Nerve cell excitation is always accomplished by transient changes in the conductivity of nerve cell membranes. There are several possibilities as to how ferromagnetic particles might accomplish this task. With respect to the size and magnetic properties of the particles found in animals, two hypotheses about the transduction mechanism are widely acknowledged by the scientific community. The first hypothesis states that SD magnetite, either alone or in combination with SPM agglomerations, is embedded in the cell membrane. Presuming that these particles are partially electrically isolated and/or elongate, an interaction with an external magnetic field will alter their orientation and thus directly modify the electron conductivity of the membrane (Figure 3.1-1a) (Kirschvink & Gould, 1981). Due to the fact that nerve cells are generally excited by the opening/closing of ion channels and the movement of ions rather than just electrons, a second theory of the transductive mechanism has received stronger support. This theory is that cytosolic or actin filament anchored SD magnetite chains control ion channels either directly via a torque mechanism or indirectly through membrane deformation (Figure 3.1-1b, c) (Kirschvink & Gould, 1981; Winklhofer & Kirschvink, 2010). Based on histological findings in pigeons a direct coupling of magnetite particles to highly sensitive muscle spindles has also been suggested (Presti & Pettigrew, 1980) but this mechanism has not gained further evidence so far.
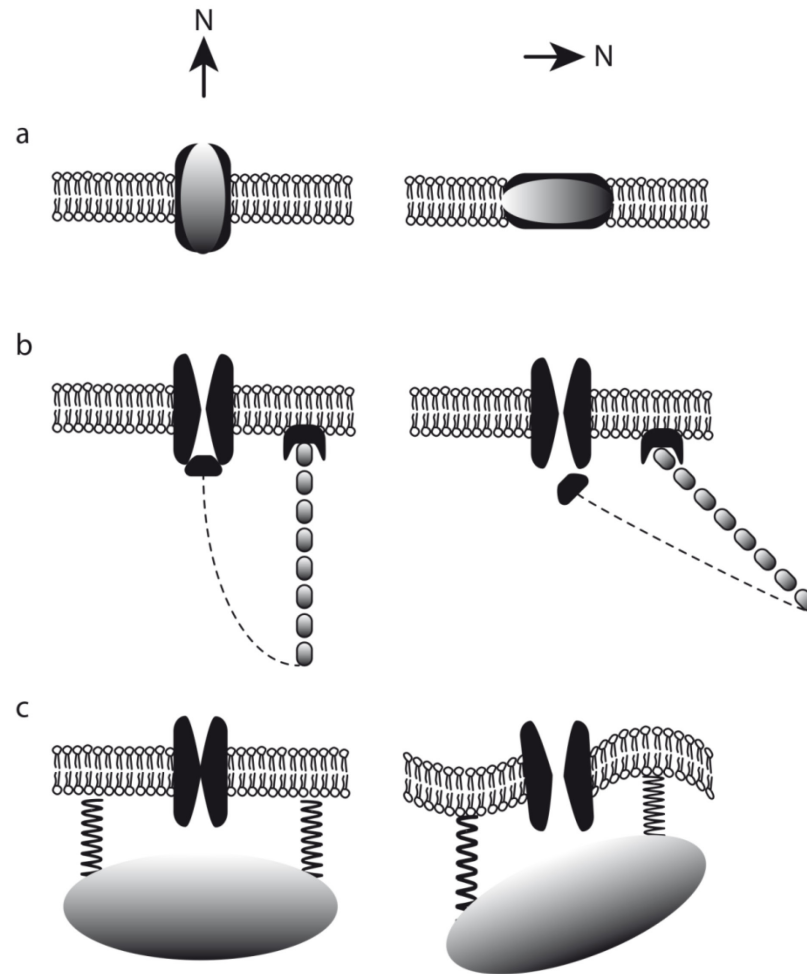
Figure 3.1-1 Three suggested models of the cellular signal transduction in a magnetite based mechanism of magnetoreception. (a) The membrane-short model. An elongated magnetite particle is embedded in the cell membrane. The particle is partially isolated (black layer) and aligns within a superimposed magnetic field. Only in a certain alignment, the particle creates an electric shortcut which leads to de- or hyperpolarization of the cell. (b) The torque-transducer model. A chain of SD-magnetite particles is anchored at the cell membrane. The tip of the chain is connected to several gaiting filaments, which control the flow of intermembrane ion channels (note that only one channel is exemplified in the figure). Depending on the direction of the magnetic field, the chain is variably deflected and opens ion channels while closing others, ultimately changing the membrane potential. (c) The membrane deformation model. A magnetite cluster exerts a pressure on the cellular membrane and deforms it in a manner that is dependent on the alignment of the cluster with respect to an external magnetic field. The deformation directly opens or closes ion channels. The figure is not drawn to scale.
(a) After Kirschvink and Gould (1981); (b) after Walker, Dennis, and Kirschvink (2002), and Winklhofer and Kirschvink (2010); (c) after Solov'yov and Greiner (2007). The figure has already been published in Begall, Burda, Malkemper (2014).

Yet another mechanism for magnetite magnetoreception has been proposed by Edmonds (1996).

According to his idea, a group of SD-magnetite particles is embedded in a liquid crystal of a photoreceptor. Within this crystal the SD-particles will be able to rotate freely and align with superimposed magnetic fields. The model further assumes that the liquid crystal also contains dye molecules with anisotropic absorption (e.g. carotenoids), which means that they absorb light only

under a specific angle of incidence. The oil droplets that are found in the cones of some birds and reptiles fulfill these requirements (Goldsmith et al., 1984; Edmonds, 1996). With this arrangement of magnetite and pigments, light of the wavelength-band absorbed by the pigment would only reach the photoreceptor if the cone is aligned parallel or anti-parallel to the magnetic field lines. Many behavioural findings on magnetoreception in birds, such as its strong wavelength dependency (Wiltschko & Wiltschko, 2001), could be explained by the liquid crystal mechanism. However, so far it lacks one crucial aspect: magnetic particles have not been found in oil droplets. Furthermore, within the scope of this review the mechanism seems even more unlikely, since mammalian cones do not possess oil droplets (Kelber et al., 2003).

For mammals, aside from the detailed realization of the transduction mechanism, a bulk of behavioural and histological data supports the involvement of ferromagnetic particles in the magnetic sense. Firstly, as mentioned above, magnetite has been demonstrated to occur in many mammals, but this finding alone does not prove anything about its significance.

An SD magnetite magnetoreceptor enables an animal to perceive the polarity of the magnetic field and is insensitive to low intensity oscillating magnetic fields in the MHz-range (radiofrequency; RF). In contrast, RF magnetic fields do interfere with radical pairs (Henbest et al., 2004b; Ritz et al., 2004), thus disabling a radical-pair mechanism (see next section). In addition, SD magnetite receptors have a unidirectional permanent magnetic moment and their polarity can be flipped by a short but strong magnetic pulse (Kalmijn & Blakemore, 1978). Each of these intrinsic and delimiting properties can be exploited in behavioural experiments to determine whether magnetite receptors are involved.

The first experimental paradigm that yielded replicable, reliable results, and thus could be used to investigate the properties of the magnetoreceptor in a mammal, was the nest-building assay with mole-rats of the genus *Fukomys* (cf. 2.4). When mole-rats were treated with a strong magnetic pulse prior to testing, they changed the direction of their nest-building preference by 90°, an effect that lasted for several weeks (Marhold, et al., 1997). A long lasting effect of pulse treatment is in accordance with the SD character of magnetite particles – but since no recovery from the effect was reported in the mole-rat experiment, unspecific effects on the receptors cannot be ruled out. However, the same authors showed that mole-rats respond to the polarity of the magnetic field rather than to its inclination (Marhold, et al., 1997a, 1997b) and both of these findings combined strongly suggest the involvement of SD magnetite.

Sensitivity to the polarity of the magnetic field was subsequently demonstrated in another subterranean rodent species, the blind mole-rat *Spalax ehrenbergi* (Kimchi & Terkel, 2001). Two epigeic rodents, the Siberian hamster *Phodopus sungorus* and laboratory C57Bl/6J mice, have also shown clear magnetic orientation but the experiments performed so far do not allow any conclusive statement about the underlying receptor mechanism (Deutschlander et al., 2003; Muheim et al., 2006). The latter is also true for the controversial homing experiments on the European wood mouse (Mather & Baker, 1981).

Even though pulsing experiments had indicated magnetite as the basis of magnetoreception in mole-rats, it took almost 10 years until the possible localization of the magnetoreceptor cells was shown by an elegant combination of histological and behavioural investigations. Here, in spite of the fact that the subterranean mole-rats have strongly reduced eyes, iron staining (Prussian blue) revealed small particles in the corneal epithelium (Wegner et al., 2006). Congruently with an involvement of these particles in magnetoreception, corneal anesthesia abolished the natural preference of the animals to build nests in the south-eastern sector of a circular arena. As opposed to sham-treated control animals, the nests of the anesthetized animals were randomly distributed even though the visual sense was not impaired by the treatment (Wegner et al., 2006). In agreement with comparable impairment of magnetoreception in beak-anaesthetized birds (Wiltschko et al., 2009), these findings on the cornea constitute the best evidence for the seat of the mammalian magnetoreceptors so far. Moreover, the mammalian cornea is innervated by the trigeminal nerve, which has also been proposed to carry sensory information from (magnetite-based) magnetoreceptors in birds (e.g. Mora et al., 2004; Heyers et al., 2010; Wu & Dickman, 2011; but see Treiber et al., 2012; Wu & Dickman, 2012). Finally, neuronal activation studies in mole-rats revealed magnetic field-dependent activity in a layer of the superior colliculus that dominantly receives trigeminal input (Němec et al., 2001).

Bats, the only group of non-rodent mammals studied in this respect so far, also use a polarity compass rather than an inclination compass (Wang et al., 2007). In accordance with this, pulsing also disrupted the homeward orientation of displaced big brown bats *Eptesicus fuscus* (Holland et al., 2008).

To sum up, magnetite-based magnetoreception is a highly promising candidate in mammals. All species that have been specifically tested so far responded to the polarity of the magnetic field and are disturbed by magnetic pulses but not by weak RF-fields (see below). However, this

should not be taken as an argument against other mechanisms, since the existence of one receptor mechanism does not rule out the involvement of others. In birds it is generally accepted that magnetite receptors are complemented by a chemical magnetoreceptor mechanism, most probably located in the eye, with the two mechanisms being used in different tasks (Wiltschko & Wiltschko, 2012b). Two distinct magnetoreceptors have also been found in amphibians (Phillips, 1986b).

CHEMICAL MAGNETORECEPTION

More recently another mechanism for magnetoreception in animals has been proposed (Ritz et al., 2000), which goes down to the quantum mechanical level of a chemical reaction and requires radical pairs. It is widely accepted that these radical pairs are produced by the oxidation of a light-sensitive molecule after photo-excitation and that this reaction most likely takes place in the retina (Ritz et al., 2010).

The observation of a physiochemical interaction between radical pairs and weak magnetic fields and its putative use in biomagnetic sensors was published years before theories of magnetite magnetoreception were formulated in detail (Schulten et al., 1976; Leask, 1977; Schulten et al., 1978). These early considerations, however, suffered from several intrinsic requirements that were not met by any known biological molecule. Therefore, it was not until the beginning of this century that the idea was reassessed and a coherent and plausible theory of chemical magnetoreception in birds was formulated (Ritz et al., 2000).

The mechanism proposed by Ritz and colleagues (2000, 2010) requires that a donor molecule is excited by light and consequently transfers an electron to a nearby acceptor molecule (Figure 3.1-2a). In the following intermediate state of the reaction, both molecules possess an unpaired electron, thus forming a radical pair (Figure 3.1-2b). The free electrons of the radical pair switch between two different spin states, the singlet (antiparallel spin) and triplet (parallel spin) state. These spin states are basically small magnetic moments and they can be influenced by external magnetic fields (Figure 3.1-2c). If an external magnetic field is applied, the interconversion between the two spin states is dependent on the alignment with, and the general intensity of, the magnetic field. In the final step (Figure 3.1-2d), the radical pairs react and form distinct products for each of the intermediate states. Ultimately, the yield of triplet products allows the animal to extract information about the intensity of the magnetic field and the alignment of the receptor

molecules with respect to the magnetic field lines. In particular, the critical transition between the spin states can specifically be affected through resonance effects with weak (nT-range) oscillating magnetic fields in the range between 0.1-10 MHz, a property that can be utilized as a diagnostic tool in behavioural experiments (Ritz et al., 2004).
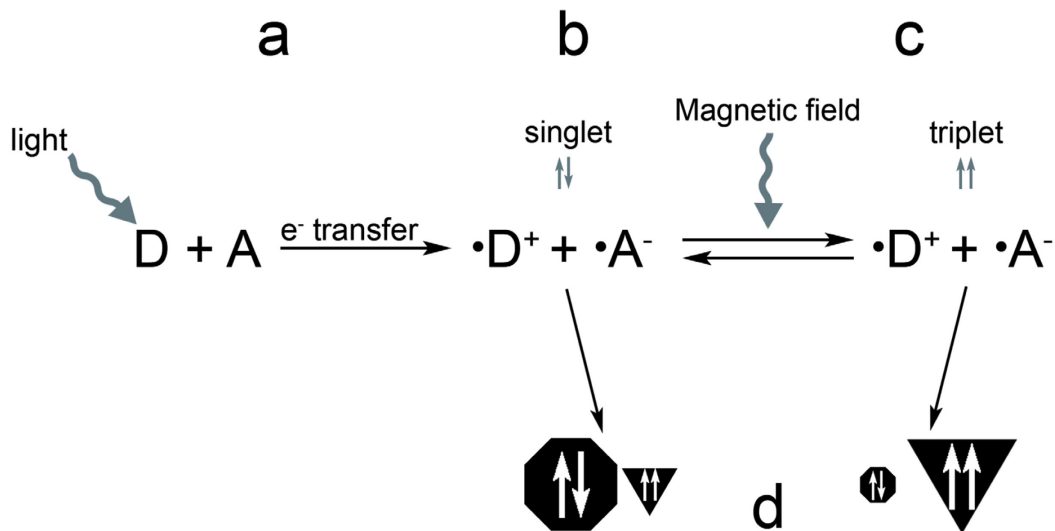
Figure 3.1-2 A simplified scheme of the radical-pair mechanism of magnetoreception. (a) A donor molecule (D) is excited by light (of specific wavelengths) and subsequently transfers an electron to a nearby acceptor molecule (A). (b) This leads to the generation of a radical pair where both molecules possess a single unpaired electron. (c) The unpaired electrons of both radical-pair partners can exist in two different states (singlet and triplet). Depending on the intensity and direction of an external magnetic field, the interconversion between the states is shifted to one direction. (d) The switching state of the radical-pair spin state leads to varying yields of respective products. The comparison of the product yield enables the animal to extract information about the parameters of the magnetic field. Modified from Ritz et al. (2009). The figure has already been published in Begall, Burda, Malkemper (2014).

Cryptochrome, a blue-light sensitive photoreceptor molecule, is at present the most promising candidate for the magnetoreceptor (Ritz et al., 2000, 2010; Liedvogel & Mouritsen, 2010). It is present in cells of a variety of plant and animal species, including mammals, where it is known to be responsible for the maintenance of circadian rhythms (Cashmore et al., 1999; Horst et al., 1999). The orbital arrangement of the retinal cells fulfils a critical prerequisite for the radical-pair compass to work: the cryptochrome molecules of the different cells are aligned into distinct directions (Ritz et al., 2000). If we further assume that within any sensory cell the alignment of the cryptochrome molecules is uniform, the triplet product yield at any given moment will vary across the retina. This pattern is believed to be perceived by the animal as a light-dark pattern superimposed on the normal visual scene (Ritz et al., 2000; Solov'yov et al., 2010). The pattern is complex but axially symmetrical, which means that if an animal is looking parallel to the field

lines it cannot distinguish between "looking north" and "looking south". This is in accordance with the behaviour of migratory birds, which also do not respond to a change in the polarity of the magnetic field but rather to its inclination (Wiltschko & Wiltschko, 1972).

The description of the radical-pair mechanism given above is a rather simplified and general version of a very complex model. The simplification was chosen on the one hand in consideration of the scope of this thesis but also and importantly because many basic parameters of the reaction mechanism are still unclear. For example, it is not resolved what exactly is the signalling state of cryptochrome in animals (Nießner et al., 2013), which radical-pairs are involved and essential for magnetoreception (Ritz et al., 2009; Müller & Ahmad, 2011), which anisotropy accounts for the directional sensitivity of the radical-pair (Lambert et al., 2013), or whether the chemical or physical properties of the radical-pair are responsible for the sensation (Stoneham et al., 2012).

In mammals, no direct evidence for the use of a radical-pair based mechanism of magnetoreception exists so far. For mole-rats, in addition to the above-mentioned findings that indicate a magnetite magnetoreceptor (pulse effect, response to polarity), experiments with radiofrequency oscillating fields did not affect the directional preference in the nest-building assay (Thalau et al., 2006). This indicates that mole-rats either do not possess a light-dependent radical-pair based magnetoreceptor, which would make sense in a lightless subterranean environment (cf. Moritz et al., 2007), or that they do not use it in the nest-building task.

For epigeic rodents, there are some indirect clues that hint towards the existence of a radical-pair based magnetoreceptor. The first is related to the complexity and the axial symmetry of the visual pattern that is assumed to be created by the retinal magnetoreceptors. Mice that were trained to build their nests in one of the four cardinal magnetic directions behaved differently when they were trained to build in N or S than when they were trained to build in E or W. While the nests of N-S mice were clustered in the trained direction, the nests of E-W mice formed two distinct clusters around the trained direction (Muheim et al., 2006; Painter et al., 2013). This discrepancy suggests the perception of a complex pattern, rather than a simple compass direction (Painter et al., 2013).

Further indirect evidence for the involvement of radical pairs in mammal magnetic orientation stems from very recent findings of mouse water-maze experiments. Mice in a plus water-maze task can quickly be trained to search for a hidden platform in a specific magnetic direction (Phillips et al., 2013). Yet, before these elegant experiments yielded stable results the authors had

to struggle with a variety of confounding factors. One of these factors were RF fields between 0.2 and 200 MHz, which had to be significantly lowered inside the test buildings for the mice to be reliably oriented (Phillips et al., 2013). The authors state that these precautions were also crucial for the experiments on mice and hamster nest-building published earlier (Madden & Phillips, 1987; Phillips & Deutschlander, 1997b; Deutschlander et al., 2003; Muheim et al., 2006; Phillips et al., 2013). If the mice were using a magnetite-based mechanism for these tasks, the weak RF magnetic fields that are typical of laboratory environments would not have had any effect.

Early experiments on pineal physiology that indicated involvement of the retina in rodent magnetoreception fit well to the suggestion of an RPM in mammals (reviewed in Olcese, 1990). A single 30-min change in the ambient magnetic field during the night resulted in a depression of pineal melatonin synthesis in rats (Welker et al., 1983). This effect was abolished when the rats' optic nerves were cut before the MF-treatment, thus indicating retinal involvement (Olcese et al., 1985). A later study confirmed that this effect was indeed light-dependent as rats kept under dim red light were sensitive to the effect, in contrast to rats kept in total darkness (Reuss & Olcese, 1986).

Interestingly, the MF effect was also abolished by degeneration of the outer segments of the rat photoreceptors (Olcese et al., 1988), a region which in birds contains activated cryptochrome 1a under influence of light of specific wavelengths, such that it strongly suggests its involvement in magnetoreception (Nießner et al., 2011; Nießner et al., 2013). Yet the results remain puzzling, since even though they prove the light dependency of the MF-effect, they are not consistent with the behavioural results in migratory birds, which were disoriented in dim red light of comparable intensity (Wiltschko et al., 1993). The presence of a cryptochrome-based system that mediates magnetosensitivity via two antagonistic channels, as has been proposed for amphibians by Phillips and Borland (1992), would resolve this inconsistency. At least on a theoretical level the observations are also explicable with a receptor based on magnetite particles suspended in nematic liquid crystals as proposed by Edmonds (1996), if suitable liquid crystals could be found in mammalian retinae. Finally, doubts have been raised about the magnetosensitivity of the pineal gland in the rat experiments, since the effects are most likely the result of induced currents through the rapid switching of the magnetic field (Lerchl et al., 1991). However, this does not rule out the possibility that retinal magnetoreceptors were the site of action (Phillips & Deutschlander, 1997a).

To summarize, it is still unclear whether or not a radical-pair based mechanism is used in mammalian magnetoreception. Further behavioural and physiological experiments should primarily address the effects of RF-fields and different light wavelengths as well as darkness on mammal magnetoreception, especially on epigeic rodents. RF-fields will have to be shielded and then reintroduced into the test environment, allowing determination of the exact frequencies and minimal intensities needed. In addition, future studies should make precise distinctions between different behavioural tasks to determine whether effects are context dependent. For example, this might reveal a division of labour between radical pair and magnetite receptors as has been proposed in birds (Wiltschko & Wiltschko, 2007). Thus it seems reasonable also to expect different properties for the magnetoreceptors of mammals, e.g. for those involved in learned spatial navigation tasks compared to more innate behaviours such as magnetic alignment or the still enigmatic nest-building preferences (Begall et al., 2013).

3.1.3 Magnetic alignment

Magnetic alignment (MA) constitutes the simplest directional response to the geomagnetic field (GMF). In contrast to magnetic compass orientation, MA is not goal directed and represents a spontaneous, fixed directional response, that is being documented in increasing numbers of, especially mammalian, species (reviewed in Begall et al., 2013). A preference for certain compass directions has already been observed in various behaviours of several species (flies, goldfish) during the 1960s and 70s but no great importance was attached to the findings as they were hard to explain in adaptive terms, and remarkable studies on magnetic orientation and navigation in birds were attracting more attention at that time (summarized in Wiltschko & Wiltschko, 1995). New interest in MA was gained by the spectacular finding of magnetic alignment in several mammals, such as cattle and deer (Begall et al., 2008; Burda et al., 2009), dogs (Hart et al., 2013), and red foxes (Červený et al., 2011), suggesting that these mammals possess a magnetic sense. So far, it is, however, enigmatic why they align with the geomagnetic field. The finding of MA in red foxes offers the unique opportunity to test several hypotheses two of which will be elucidated below.

3.1.4 Magnetic alignment in the red fox[4]

The finding that cattle and deer align their body axis approximately along the field lines of the geomagnetic field led to more intense inspections of different behaviours of mammalian species. One of these behaviours was the mousing of red foxes, which is a specific behaviour shown during hunting of small mammals. The fox approaches its prey carefully and slowly to avoid making noise; it stops at a certain point; then it jumps high in the air and virtually attacks its prey from above. Jumping directions were determined by direct observation (23 experienced wildlife biologists and hunters provided independent recordings). The direction in which red foxes jump during mousing is significantly different from random (Červený et al., 2011): circular analysis of the angular data (head direction of jumps) revealed a significant preference for NE. Since this preference was independent of the observer, time of day, season, wind direction, etc., it is proposed that the mousing behaviour is another case of alignment with respect to GMF. Interestingly, red foxes mousing in high cover (i.e., when the prey is hidden in high vegetation or under snow cover), where visually guided attacks are not possible, had higher hunting success when the jumps were oriented toward north (segment: 340°-40°; 72.5 % hunting success) or south (160°-220°; 60 % hunting success) compared to other directions (success rate in other segments less than 18 %) (Figure 3.1-3). Here, approximately 82 % of all successful jumps were directed toward N or NE. Unsuccessful jumps were more scattered. By contrast, red foxes mousing in low cover can spot their prey visually and might not necessarily rely on aid from the field lines of the geomagnetic field. Accordingly, the mousing jumps in low cover showed high directional scatter (Červený et al., 2011). The sensory aspects of this peculiar behaviour can be explained by the so-called "range finder hypothesis," which provides a theoretical basis for the differential hunting success in dependence of the MA of the red fox and is described in detail in Červený et al. (2011). The hypothesis proposes a direction-dependent improvement of target-distance estimation by the fox, mediated by a photoreceptor-based magnetoreception system, maybe based on cryptochrome, the magnetoreceptor found in the visual system of birds. An alternative hypothesis states, that the sense of hearing is influenced by the alignment of the body within the geomagnetic field. For example, hearing sensitivity might be enhanced, when facing N or S, but reduced when facing E or W.

---

[4] Large parts of this section have already been published in Begall, Burda, Malkemper (2014) and were only marginally adapted to fit to this thesis.
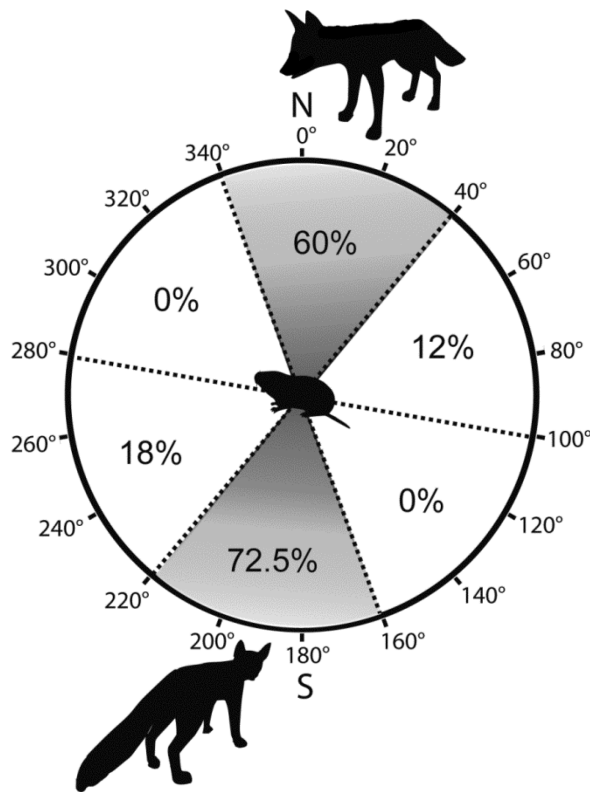
Figure 3.1-3 Hunting success of red foxes. The hunting success of mousing red foxes is dependent on the direction of the jumps with respect to the GMF lines. When vision is obstructed by snow or high vegetation, jumps from south–southwest and from north- northeast directions are much more successful than from other directions (percentage of successful jumps given in each sector; calculation based on 200 observed fox mousing jumps). Congruently, the foxes prefer to jump from these directions (shaded sectors) in high cover. Data from Červený et al.(2011). The figure has already been published in Begall, Burda, Malkemper (2014).

The aim of this third chapter of my thesis on the sensory biology of the red fox is to yield further insight into the probabilities of the two hypotheses for red fox MA. Therefore, I will present data on red fox hearing sensitivity in disturbed magnetic fields and in different magnetic alignments. In parallel, I performed iron staining on the inner ear of the fox to check for iron particles within the sensory hair cells that have been found in birds (Lauwers et al., 2013). If magnetic fields would exert an influence on hearing sensitivity, cochlear hair cells equipped with magnetic parti-cles would make the perfect receptor cells (Burda, personal communication).

I also searched for evidence to support the range finder hypothesis. A prerequisite of this hy-pothesis would be a magnetosensor within the visual system of the red fox. Therefore, I per-formed immunohistological staining of cryptochrome on the red fox retina.

As a side project, I performed experiments with wood mice addressing two questions. First, do wood mice, *Apodemus sylvaticus*, have a magnetic sense as was suggested by early orientation ex-periments (Mather & Baker, 1981)? Second, if they do have a magnetic sense, is it RPM-based, i.e. can it be influenced by weak RF-magnetic fields? To yield answers I tested captured animals with the classic nest building assay and exposed them to different RF-fields.

3.2   Material and Methods

3.2.1 Magnetic coil systems

STATIC FIELDS

To alter the direction of the ambient magnetic field under certain experimental conditions (red fox alignment experiments, wood mice experiments), I used a pair of double-wrapped Helmholtz-coils (2.15 m diameter, 10+10 turns of copper wire wrapped on a wooden frame, current 1.76 A) powered by a current-regulated power supply (DPD-3030, Manson, Hong Kong, China). Parallel current flow through both wires on each coil created a magnetic field while with the current flowing antiparallel no magnetic field was created but possible side effects originating from the equipment used (heat, vibrations, electric fields) where the same in both conditions (Kirschvink, 1992). The coils were arranged in such a way that magnetic north could be shifted by 90° counterclockwise without changing the intensity or inclination of the local geomagnetic field (Phillips, 1986a) (Figure 3.2-2). The intensities of the static field and of extremely low frequency (mainly 50 Hz) oscillating fields were measured with a 3-axial magnetometer (NFA 1000, Gigahertz Solutions, Langenzenn, Germany) equipped with an additional magnetostatic probe (MS-NFA, Gigahertz Solutions). The intensity of the local magnetic field within the arena was 49.05 µT. With antiparallel current flow (control condition) and in west fields (parallel current flow), the overall intensity was 49.03 µT and 49.20 µT, respectively. The output of the power supply ran through an EMI filter (5500.2058, Schurter, Endingen, Germany) to reduce low radiofrequency fields. Oscillating magnetic fields mainly in the 150-180 Hz range, with intensities around 60 nT (parallel current flow) and 6 nT (antiparallel current flow) were detectable.

In one set of experiments, a short magnetic pulse was created in the region of the head of the foxes. The magnetic treatment consisted of a short (700 ms) pulse that was created with a single double-wrapped coil (30 cm diameter, 20+20 turns of copper wire wrapped on a plastic frame) powered by a current-regulated power supply (DPD-3030, Manson). As with the set of Helmholtz coils, parallel current flowing through both wires on each coil created a magnetic field while no magnetic field was created with antiparallel flow, but possible side effects (heat, vibrations, electric fields) where the same in both conditions (Kirschvink, 1992).

RADIOFREQUENCY MAGNETIC FIELDS

Split-shield magnetic-field loops for RF experiments were constructed using coaxial cable (Air-cell 7). One loop was designed with a sharp resonance at about 1.3 MHz for application of a magnetic field oscillating at the local Larmor frequency (1.33 MHz) with a 47 Ohm resistance at the feed for impedance matching, the other cable had a broad resonance between 0.9-5 MHz, with maximum at 4 MHz, where the magnetic field was two times stronger than at 0.9 MHz. The coils (60 cm diameter) were powered using a Wavetek 144 function generator (Wavetek, San Diego, CA, USA) for a 1.33 MHz continuous sine wave and a Wavetek 193 sweep generator used for generating a wideband-frequency modulated (FM) field, where the frequency sweep (0.9 MHz to 5 MHz) was repeated at intervals of 1 msec. The RF field produced by the coils was measured with an ETS-Lindgren split-shield magnetic-field probe (7405 E&H 6 cm diameter near field loop probe) connected by a coaxial cable to an oscilloscope (Picoscope 4224). The intensities in the LF condition had maximum values of 1.26 μT in the periphery of the arena and minimum values of 785 nT in the centre, while in the wideband-FM condition, due to the frequency response characteristics of the coil, the intensities varied between 25 nT and 50 nT in the centre of the coil to twice these values at the periphery of the arena. An induction coil connected to a HAMEG (HMO 3524) oscilloscope was used (in FFT mode) to monitor low frequency magnetic noise. Neither single-frequency nor the sweeping conditions were found to cause enhanced noise levels in the low frequency range.

3.2.2 Effects of a weak magnetic pulse on hearing sensitivity

I performed two experiments to investigate the possible influence of a short magnetic pulse on hearing sensitivity, which only differed in the used psychoacoustic procedure. Both experiments were conducted within the framework of the psychoacoustic experiments, and I used exactly the same equipment and procedures for threshold determination as described in chapter 1. The only exception is a single fox (female) for which I used a different psychoacoustic procedure for threshold determination. Instead of using the method of constant stimuli described in chapter one, I employed an adapted staircase procedure (Cornsweet, 1962). Here, the tones are presented with intensity decreasing in 10 dB SPL steps until the animal fails to respond, which automatically increases the next tone presentation by 10 dB SPL. In each session, I determined the intensity

of ten such reversals in each condition. The final threshold was calculated as the mean of three sessions in each condition.

I placed the coil in such a way on top of the semi-anechoic chamber, that in the parallel mode the coil created a field strength of approximately 8 µT in the region of the foxes' head (Figure 3.2-1a). The horizontal direction of the geomagnetic field was not visibly affected by the pulse. In each trial, a single magnetic pulse was given in always the same temporal relationship to the acoustic stimulus (Figure 3.2-1 b). The magnetic stimulus was automatically controlled by the custom-made psychoacoustic software via the RZ6 multi-I/O processor unit and an optical coupler (POK 2,5/3, Appoldt GmbH, Düsseldorf, Germany; cf. 1.2-2 for wiring), which prevented the occurrence of switching noise.

I randomly interspersed two types of control conditions between the magnetic test trials. First, I switched the coil into the antiparallel mode so that no change in magnetic field was created. In this condition, however, there was still a temporal electric field change. In the second condition, I removed the cable between power supply and optical coupler, so that no current was flowing through the coil anymore. I always performed the magnetic anomaly tests at a fixed acoustic stimulus frequency of 8 kHz, as this is the dominant frequency in the rustling noise of small rodents (Payne 1971).
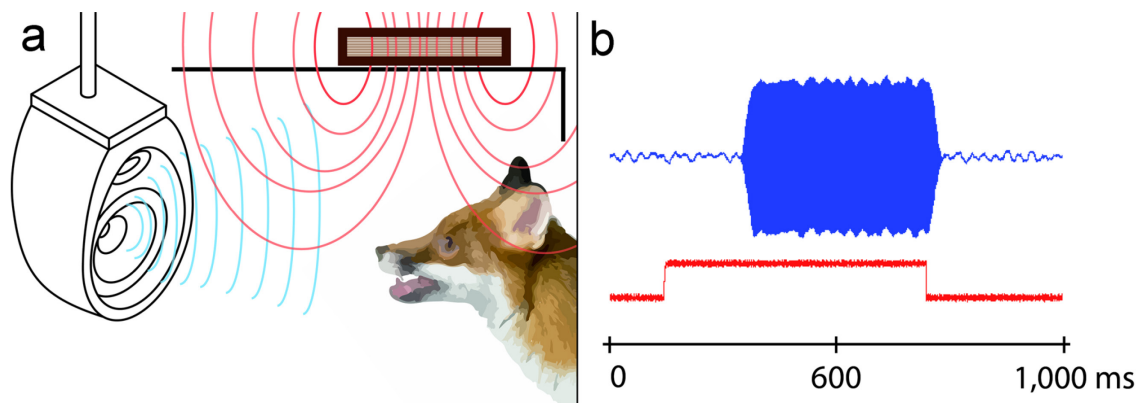
Figure 3.2-1 Scheme of the setup used to test for the influence of a temporal magnetic anomaly on red fox hearing sensitivity. For an overview of the complete behavioural setup cf. Figure 1.2-1. (a) The position of the magnetic coil with respect to the fox's head and the loudspeaker is schematically shown. The coil was placed on top of the semi-anechoic chamber at a distance of 35 cm from the head of the listening fox. The blue waves indicate the sound stimulus, the red circles stylize the magnetic field lines. The loudspeaker was placed 60 cm in front of the animal, the coil was placed 35 cm above its head. For details on the behavioural setup cf. Figure 1.2-1. (b) Temporal relationship between the magnetic and acoustic stimuli. The magnetic stimulus (red line) preceded the sound (blue line) by 200 ms and lasted for 700 ms until the acoustic stimulus diminished.

3.2.3 Experiment on the effect of magnetic alignment on hearing sensitivity

To reveal a possible influence of the alignment between the magnetic field and the direction to-wards the fox was listening, all behavioural experiments with male 1 described in chapter 1 were performed within a pair of double-wrapped Helmholtz-coils that I set up around the semi-anechoic chamber and operated in antiparallel mode (cf. section on static fields and Figure 3.2-2a, b). Additionally, for some frequencies (1 kHz, 4 kHz, 6.3 kHz, 8 kHz, and 16 kHz) the final threshold was determined twice, once in antiparallel and once in parallel mode, the latter rotating magnetic north towards west, leaving the red fox listening into magnetic east direction (Figure 3.2-2a, b). The intensity of the magnetic field did not considerably differ between both conditions (49.03 µT in antiparallel mode (control), 49.20 µT in parallel mode). To account for effects of training and season (temperature), the test sessions with rotated magnetic north were intermingled in between the standard test sessions. Current was flowing through the magnetic coils in all tests, the only difference was the direction of the magnetic field.

3.2.4 Histology: Where are the magnetoreceptors?

IRON STAINING

To check for the occurrence of ferric iron particles in the sensory hair cells of the red fox inner ear, I stained whole mounts and paraffin-celloidin sections with Prussian blue (PrB). The cochlear whole mount preparation followed the procedures described in chapter 1, with the only differ-ence that I used no haematoxylin and toluidine blue but instead performed the iron staining on the intact cochlea in order to avoid staining of artifacts that might have been introduced during the preparation. I exclusively used titanium and ceramic instruments that were rinsed in 5 % HCl for at least 10' before the start of the preparation.

To rinse the cochlea with PrB, I opened the bony capsule of the cochlea in the region of the apex and the oval window and injected the PrB solution (1:1 mixture of 5 % potassium-hexacyanoferrate and 5 % HCl) into the apical opening with a syringe. Then I submerged the whole specimen for 30' in the PrB solution. After staining I rinsed the cochlea with PBS and con-tinued with the preparation as already described. I mounted the exposed half-turns in glycerol on an untreated microscope slide.

After the first observation and documentation at the light microscope (BX 40, Olympus), I removed the coverslip and rinsed the cochlea thoroughly in PBS to wash away the embedding medium. A second incubation step in PrB for another 30' and light-microscopic documentation followed.

Cochlear sections were prepared as described in chapter 1. To avoid contamination, I used ceramic coated microtome blades (DuraEdge BLM00103P (7203) High Profile, Crescent Manufacturing, Fremont, OH, USA). I counterstained every second slice with nuclear fast red (NFR) for 1-3 minutes.

CRYPTOCHROME IMMUNOHISTOCHEMISTRY

Immunostaining against Cry1 was performed together with Christine Nießner in the laboratories of Prof. Dr. Leo Peichl at the Max-Planck-Institute for Brain Research, Frankfurt am Main, Germany. We used the retinae of two red fox specimens and one eye of a European wood mouse.

The preparation of the retinae followed the same protocol as describe for the opsin immunohistochemistry in chapter 2. We processed the retinae for whole mounts free floating in a 6-well plate before mounting them upside down onto an untreated microscope slide to promote visual access to the photoreceptor layers after staining was completed.

Retinal sections of a red fox retina were kindly provided by Prof. Dr. Leo Peichl. The sections originated from an adult specimen killed by a hunter. The eyes were immersion fixed in 4 % PFA in PB for 28 h starting 30' postmortem. 14 µm thick cryosections were prepared and stored at -20°C until usage.

The visualization of Cry1 and S cones was accomplished by immunohistochemistry according to the following steps (all performed at ambient temperature):

- wash the fixed and prepared retina in PB (0.1M pH = 7.4; several times, if retina had been bleached before, see chapter 2)
- block with 1 ml 10 % normal donkey serum (NDS), 2 % bovine serum albumin (BSA), 0.25 % Triton-X-100 in PB for 1 h
- wash in 0.1 M PB
- incubate with the first antibody diluted in 1 ml 3 % NDS, 2 % BSA, 0.25 % Triton-X-100, 0.05 % sodium azide in 0.1 M PB on a lab shaker for 3 days (sections overnight)

- wash in PB for at least 1 h
- incubate with the secondary antibody (dk-anti-gp Cy3 and dk-anti-gt Cy5; Dianova, Hamburg, Germany) diluted in 1 ml 3 % NDS, 2 % BSA, 0.25 % Triton-X-100 in 0.1 M PB on a lab shaker for 1 h.

We mounted the retinae with Aqua-Poly Mount (Polysciences Europe, Eppelheim, Germany) and analysed them under a confocal laser-scanning microscope (Zeiss Typ 510 META) or a Zeiss Axioplan 2 microscope.

The following primary antibodies were used:

1. Guinea pig Cry1 antiserum (produced by GENOVAC GmbH, Freiburg, Germany), raised against amino acids 601–621 of Cryptochrome 1a in chicken: (C-) RPNPE EETQS VGPKV QRQST (-N), characterised in Nießner et al. (2011). The amino acid sequence is very similar to the predicted Cry1 from *Canis lupus familiaris* and *Felis catus domestica* as well as the sequence from two rodents (Table 14).

2. Goat antiserum sc-14363 raised against a 20-aa N-terminal epitope of the human S (blue) cone opsin (Santa Cruz Biotechnology Inc., Santa Cruz, CA, USA), characterised by Schiviz et al. (2008).

Table 14 Amino acid sequence of the antigen of the bird Cry1a antiserum compared with the sequences of Cry1 in two mammalian species closely related to the red fox and the wood mouse. Identical amino acids are given in red. Sequences for red fox and wood mouse were not available, so the respective sequences of cat, dog and two rodents are shown.

Species	Part of sequence	GenBank
Epitope recognized by antiserum anti-Cry1	RPNPEEETQSVGPKVQRQST	
Felis catus domestica (AA 567 – 585)	RPSQEEDTQSIGPKVQRQS[1]	XP_003989258.1
Canis lupus familiaris (AA 567 – 586)	RPSEEEDTQTISPKVQRQST[1]	XP_862753.1
Mus musculus (AA 586 - 604)	RPSQEEDAQSVGPKVQRQS	NP_031797.1
Rattus norvegicus (AA 568 – 586)	RPSQEEDAQSVGPKVQRQS	EDM17107.1

[1] predicted

3.2.5 Magnetic nest building experiments with wood mice

The experiments were performed in a horse stable in a rural area of the Bohemian Forest, Czech Republic (49°9'10.28"N, 13°20'56.45"E) in summer and autumn of 2013. The wood mice (*Apodemus sylvaticus*) were live-trapped in the vicinity of the stable by means of trap-door traps. Until testing they were kept in a rectangular wooden crate (approximately 2 m x 0.8 m) based in an adjacent part of the stable (Figure 3.2-2a) and fed apples and grain *ad libitum*. Each mouse was kept for at least one night in the crate before being tested.
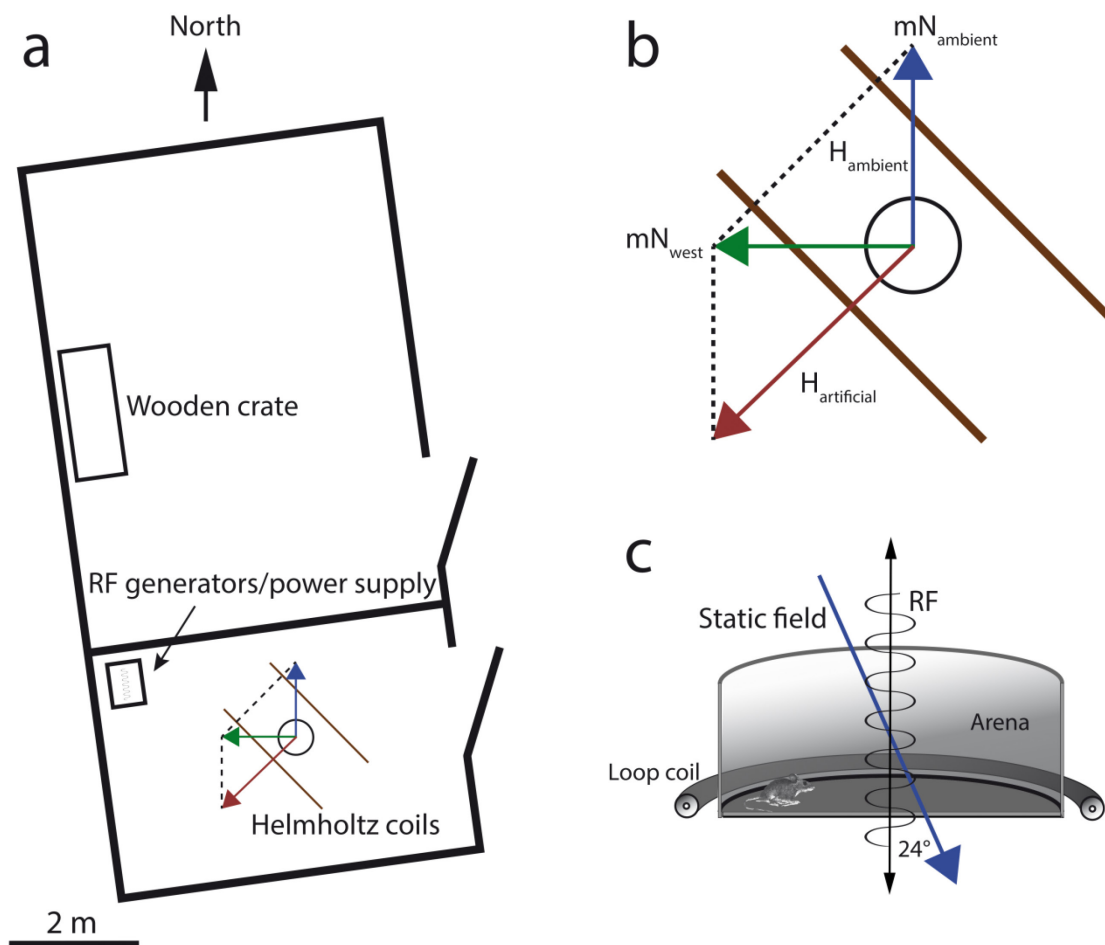
Figure 3.2-2 Overview of the testing site, the coil-setup and the nest-building arena. (a) Top view of the empty horse stable that consisted of two compartments. One compartment contained the wooden enclosure, the other one the testing setup and coil systems. (b) Production of the artificial static magnetic field (top view). In the control condition (mN$_{ambient}$) the horizontal of the ambient magnetic field (H$_{ambient}$) was left unchanged. To shift magnetic north by 90° counterclockwise (mN$_{west}$), an artificial magnetic field was added with a 135° clockwise aligned Helmholtz-coil pair (H$_{artificial}$) to produce a 90° shifted resultant field of the same inclination and total intensity as the ambient magnetic field. The circle in the middle indicates either the arena (nest building experiments) or the observing position of the red fox (experiments on the influence of magnetic alignment on hearing sensitivity) (c) Profile of the test arena and the loop coil used to produce the oscillating magnetic fields in the RF range. The oscillating fields were aligned vertically at an angle of 24° to the static field lines. The scale only applies to part (a) of the figure.

The animals were tested in a circular arena (diameter 50 cm) made of black PVC. The floor of the arena was evenly covered with sawdust and hay which served as nest building material. An apple slice place in the centre of the arena served as food (Figure 3.2-3). All experiments started in the evening and were conducted overnight. Before the mouse was introduced into the arena the magnetic conditions (control, 90° shift, RF, no RF) were set. The condition for each day was randomly chosen. The mice were then gently placed in the middle of the arena and the arena was quickly covered with a frosted white PVC-sheet. On the next morning the direction of the nest was measured with a hand-held compass (Figure 3.2-3) and the mouse was released. Only clearly recognizable nests that were built at the wall of the arena (max. 10 cm away) were counted. Nights with thunderstorms were also excluded from the analysis (cf. Phillips et al., 2013). After each test the arena was emptied and thoroughly cleaned with 70 % ethanol. To control for a possible observer bias, pictures were taken of a subset of the nests (n = 24) and analysed by a person unaware of magnetic north and the experimental conditions. The mean difference between the nest directions obtained from direct compass measurements and those taken from the pictures was 3.7° (circular SD = 7.4°).

Figure 3.2-3 The nest building assay. (a) The arena (50 cm diameter) was prepared with saw dust and hay as nest building material and an apple slice and grain as food. (b) After the mouse had been released, the arena was covered with a frosted white PVC-sheet. (c) On the next day the direction of the nest was measured as from the centre of the arena (arrow).

3.2.6 Statistics and graphics

I employed Sigmaplot (V. 12.5, Systat Software Inc.) to plot all non-circular graphs and perform descriptive statistics and statistical interference. Variance equality and normal distribution were always tested with Bartlett's test and the test procedure by Shapiro-Wilk, respectively. In case of normal distributions, I performed t-tests or analyses of variance (ANOVA) depending on the data (procedure always given in the results section). Nonparametric tests comprised Mann-Whitney U-test and ANOVA on ranks. Advanced statistical tests and analyses are indicated with the re-

spective results in the results section. For tables, standard calculations, and data transformation I used Excel 2010 (Microsoft Corp.). I prepared graphical illustrations in Photoshop and Illustrator CS6 (Adobe Systems).

For analysis of the distributions of nest directions I used standard circular statistics (Batschelet, 1981). All calculations were carried out in Oriana (V. 4.02, Kovach Computing Services, Anglesey, Wales, UK). I treated each nest direction as an independent data point. The likelihood of retesting a mouse was low because wood mice avoid traps for some time after they have been captured (unpublished observations). Furthermore, any mouse that was recaptured had only a 25 % chance of being tested in the same experimental condition. For the calculation of mean vectors the software employs simple vector addition. For axial analysis, the method of doubling the angles was used to convert angular data in axial ones prior to statistical analysis. I used the Rayleigh test with $p < 0.05$ as the threshold of statistical significance to test the data for significant deviation from random distribution. The Watson U^2 test compared distributions of different experimental groups.

3.3   Results

3.3.1 Temporal magnetic anomaly during psychoacoustic testing

The mean thresholds obtained in three sessions (at 8 kHz) with one female red fox, under three magnetic conditions are shown in the box plots in Figure 3.3-1. The thresholds did not differ statistically between the conditions (ANOVA on ranks; p = 0.056, H= 5.754). Mean thresholds were: *coil off*: -0.7 ± 7 dB SPL (± SD), *coil on*: -1.3 ± 6 dB SPL (± SD), *antiparallel*: 0.9 ± 6 dB SPL (± SD).
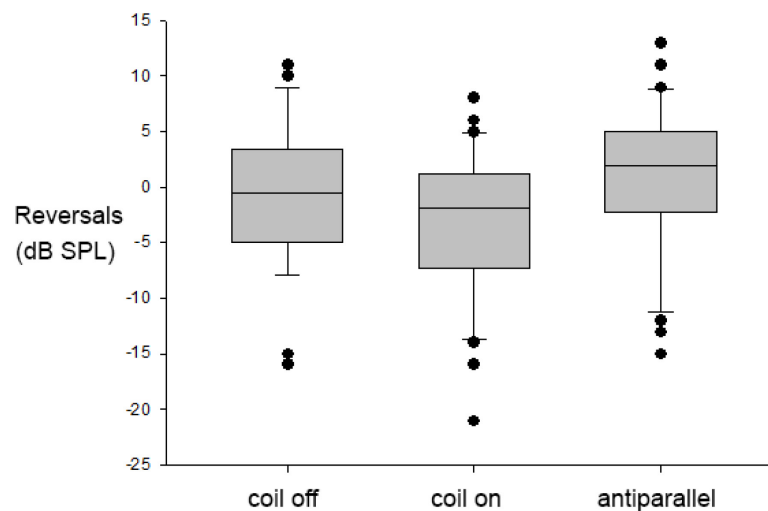
Figure 3.3-1 Testing the effect of a short magnetic pulse on hearing of 8 kHz pure tones in the red fox. Box plots (means and 95% confidence intervals) of thirty reversals obtained from a single red fox for each of three different conditions during three sessions are shown: *coil on*: a 700 ms magnetic pulse of 8 μT was given. The pulse preceded the tone presentation by 200 ms; *antiparallel*: current was sent through the *coil on* but no magnetic field was created (cf. method section); *coil off*: no current was sent through the coil. The mean thresholds were not significantly different between the conditions (ANOVA on ranks; p = 0.056, H = 5.754).

The psychoacoustic functions obtained under the three different conditions for male 1, were not significantly different (Figure 3.3.-2). However, the performance of male 2 was significantly different in the conditions (Two Way ANOVA, F = 6.404, p = 0.032; Holm-Sidak post-hoc test: difference between *antiparallel* and *coil on*, p = 0.035; Figure 3.3-2). The performance of male 2 was better in the *coil on* condition than in the antiparallel condition. The response latencies of male 1 and male 2 did not differ significantly under different magnetic conditions (male 1: *coil off*: 0.64 ± 0.27 s; *coil on*: 0.6 ± 0.28 s; antiparallel: 0.63 ± 0.3 s; male 2: *coil off*: 0.61 ± 0.98 s; *coil on*: 0.63 ± 0.2 s; antiparallel: 0.58 ± 0.22 s).
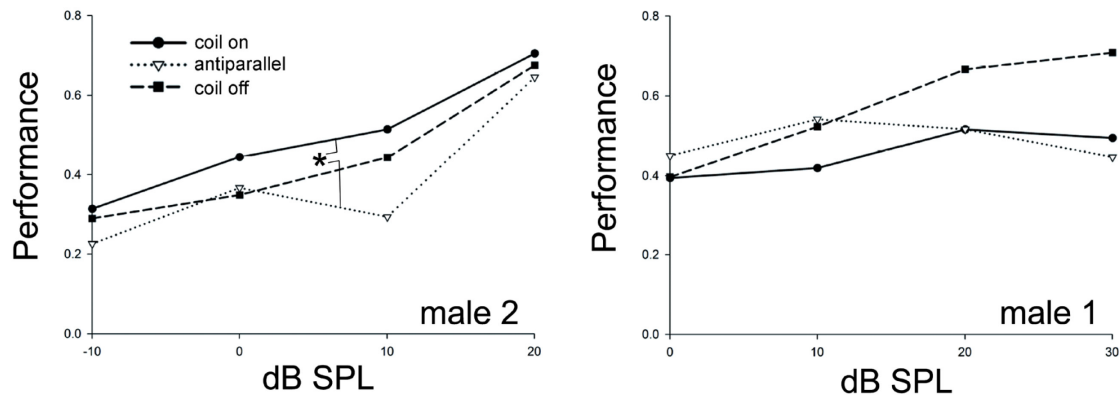
Figure 3.3-2 The effect of a short magnetic pulse on hearing of 8 kHz pure tones in two red foxes. The psychometric functions of two foxes (male 1, male 2) obtained under three different conditions are shown: *coil on*: a 700 ms magnetic pulse of 8 μT was given. The pulse preceded the tone presentation by 200 ms; *antiparallel*: current was sent through the *coil on* but no magnetic field was created (cf. method section); *coil off*: no current was sent through the coil. The psychometric functions in each condition were calculated on the basis of ~100 trials per condition assessed in four sessions on four consecutive days. The asterisk indicates a significant difference of the psychometric functions of male 2 (Two Way ANOVA; p = 0.032, F = 6.404) The post hoc comparison (Holm-Sidak) revealed that the significance is based on the differences between the lower performance in the *antiparallel* condition in comparison to the performance in the *coil on* condition. No significant differences were found between the psychometric functions of male 1. For details on the psychoacoustic procedure cf. chapter 1.

3.3.2 Experiment on the effect of magnetic alignment on hearing sensitivity

The audiogram of a single red fox individual (male 1) tested in two different magnetic alignments is shown in Figure 3.3-3. The audiogram obtained under magnetic-north condition is identical to the data shown in Figure 1.3-1 (Helmholtz coils in antiparallel mode). The "east-audiogram" (Helmholtz coils in parallel mode) only comprised the region of best hearing sensitivity from 1-16 kHz (tests at 2 kHz could not be completed). The sensitivity in the east-field was not significantly different from the north-audiogram (Two Way ANOVA; $p = 0.404$, $F = 0.722$), the mean difference between the thresholds being 1.4 ± 0.9 dB.
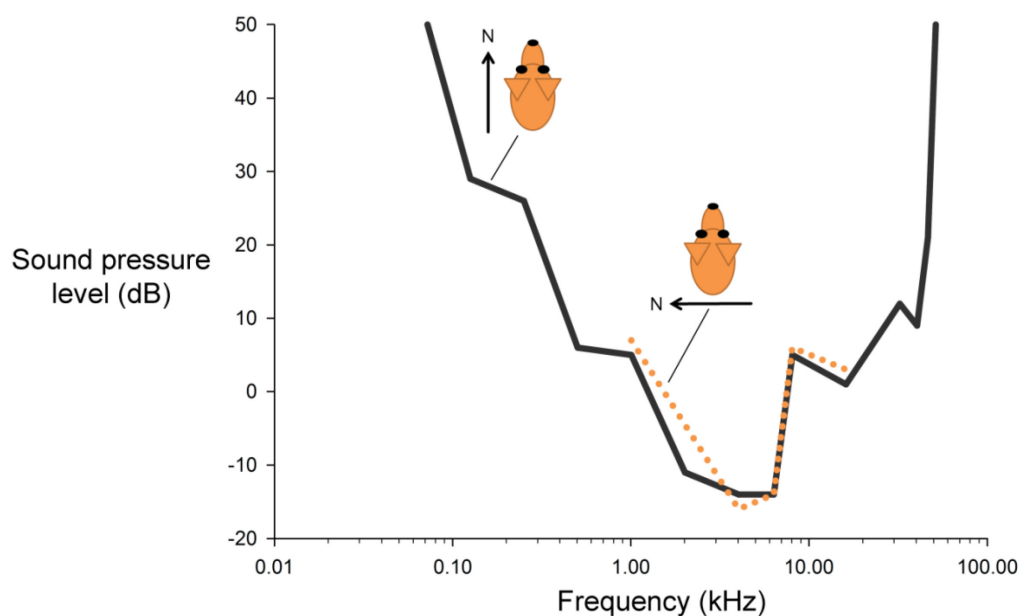
Figure 3.3-3 Audiogram of a single fox (male 1) obtained in two different magnetic alignments. The black solid line indicates the whole audiogram established with the fox facing magnetic north (N). The orange dotted line indicates the region of best hearing sensitivity assessed with the fox facing magnetic east (but topographic north). There was no significant difference between the thresholds obtained under both conditions. As I used double-wrapped coils in the experiments, the only parameter that differed between the conditions was the direction of the magnetic field with respect to the listening direction of the fox (confer the methods section for details on the coil system).

3.3.3 Histology: Where are the magnetoreceptors?

PRUSSIAN BLUE STAINING

No specific Prussian blue stain was detected in any of the three studied red fox cochlea specimens. In both sections and whole mounts, however, regions of unspecific staining (outside of cells) were visible, indicating that the general staining procedure was successful.

CRYPTOCHROME IMMUNOHISTOCHEMISTRY

In the retina of both fox specimens (whole mount and sections) all S cones were also immuno-positive for Cry1 (Figure 3.3-4). Cry1 was always localized in the outer segments of the cones, which was shown by double-labeling with antibodies against S opsin. On the other hand, in the wood mouse, no Cry1 immunopositive cells could be detected (Figure 3.3-5).
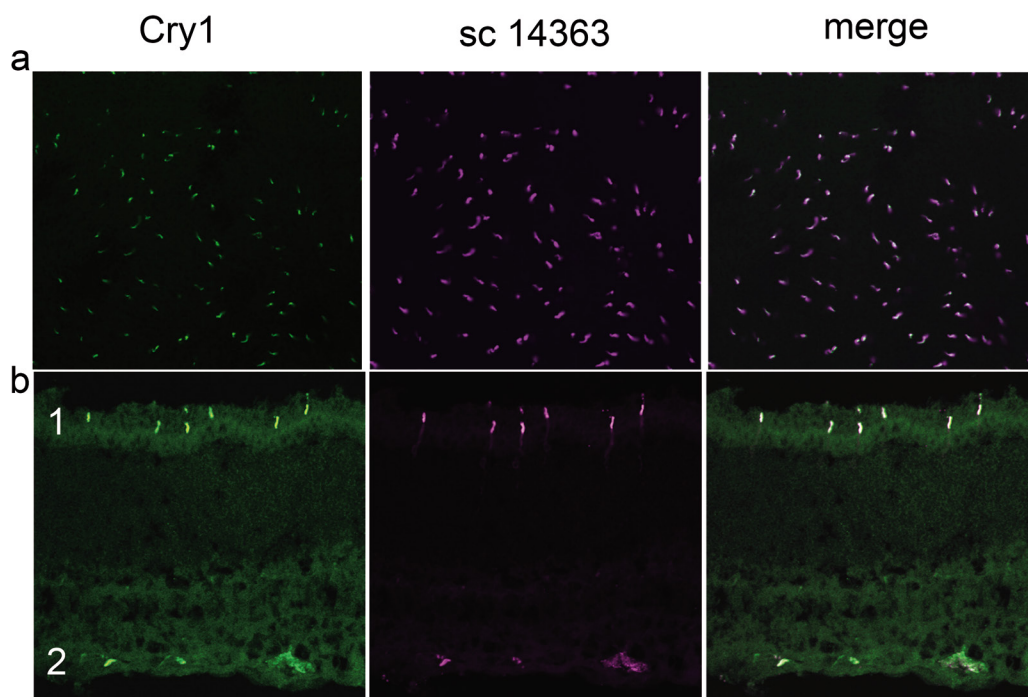
Figure 3.3-4 Cry1 label in the S cones of the red fox retina. (a) Whole mount and (b) vertical section of red fox retina. Cry1 immunofluorescence (rendered in green) is present in all S cones (rendered in magenta) of the red fox retina. Middle column: S opsin immunofluorescence (rendered in magenta) in the same sections and fields, respectively. Right column: merge of the images, indicating that Cry1 and the S opsin co-localize in the red fox retina. For orientation, two different layers in the vertical sections are indicated: 1: photoreceptor layer, 2: ganglion cell layer.
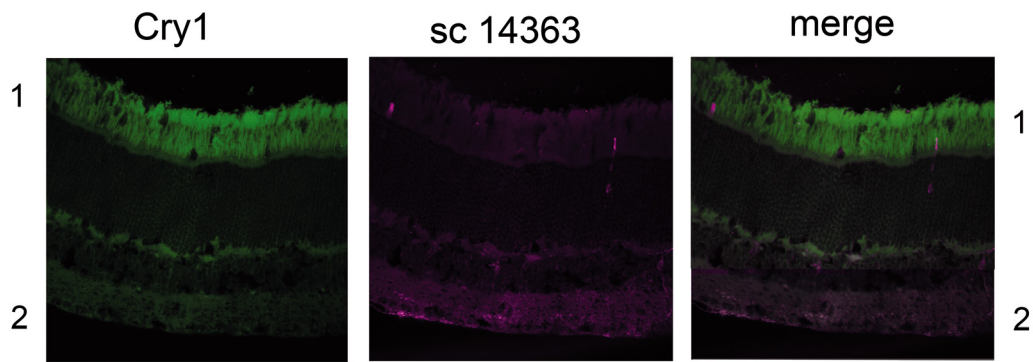
Figure 3.3-5 Absence of Cry1 label in wood mouse retina (vertical section). Cry1 immunofluorescence (would be green) is not visible within the S cones (rendered in magenta) of the wood mouse retina (only stained background visible). Middle column: S opsin immunofluorescence (rendered in magenta) in the same sections and fields, respectively. Right column: merge of the images. For orientation, two different layers are indicated: 1: photoreceptor layer, 2: ganglion cell layer.

3.3.4 Experiments on the magnetic sense of the red fox prey

NEST BUILDING PREFERENCES IN WOOD MICE

In the unchanged geomagnetic field (antiparallel current flow) the wood mice showed a significant preference to build their nests in the north-east and south-west quadrant of the arena (Figure 3.3-7a; n = 24, μ = 27°/207° ± 37° (mean vector orientation angle; circular standard deviation), r = 0.43 (mean vector length); Rayleigh test: p = 0.01, Z = 4.441). When north was shifted by 90° westwards the nests where built predominantly in the new magnetic north and south quadrants even though the distribution was not significantly different from random (Figure 3.3-7b; n = 21, μ = 106°/286° ± 47°, r = 0.262; Rayleigh test: p = 0.238, Z = 1.445). The distributions in both conditions were significantly different from each other (Watson U²: p < 0.01, U² = 0.293). Plots of the pooled data from both conditions with respect to a) magnetic north or b) topographic north revealed a highly significant preference for magnetic north-east and south-west (Figure 3.3-6a; n = 45, μ = 23°/203° ± 42°, r = 0.346; Rayleigh test: p = 0.004, Z = 5.386) while the nests were randomly distributed with respect to topographic north (Figure 3.3-6b; n = 45, μ = 38°/218° ± 58°, r = 0.125; Rayleigh test: p = 0.499, Z = 0.701).
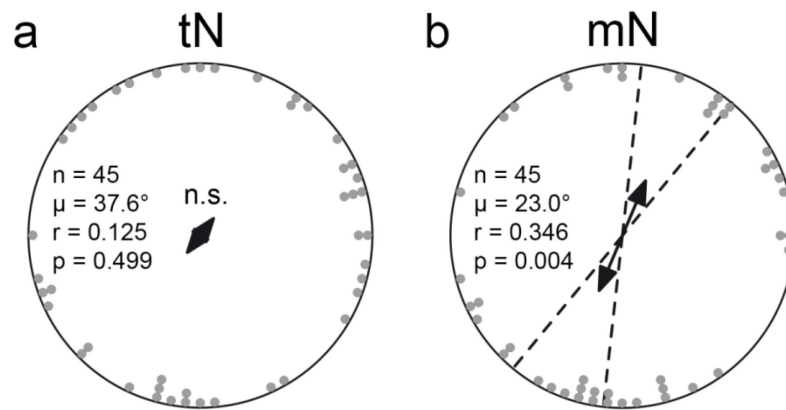
Figure 3.3-6 Orientation of wood mice nests built in a visually symmetrical circular arena without superimposed RF magnetic fields. Each data point represents the position of a nest built by an individual mouse. The figure shows the pooled nest positions of mice tested in the ambient field and with magnetic north shifted 90° counterclockwise. (a) Absolute bearings in the arena. (b) Bearings relative to magnetic north (mN) in the arena. Arrows give the mean vector for the distribution of the nests, the dotted lines are the 95 % confidence intervals for the mean bearing (μ) of nonrandom distributions (p-value of the Rayleigh test is given for each distribution). The double-headed arrows indicate bimodal distributions; the lengths of the arrows represent the mean vector length r (scaled so the radius of the circles corresponds to r = 1), which provides a measure of the degree of clustering in the distribution of the bearings. n.s. = not significant.

INFLUENCE OF RF MAGNETIC FIELDS ON WOOD MICE NEST BUILDING BEHAVIOUR

Nests built under the influence of a single-frequency (SF) RF-magnetic field (1.33 MHz) still showed a significant axial non-random distribution with clusters in the north-east and south-west (Figure 3.3-7c; n = 22, μ = 8°/188° ± 37°, r = 0.439; Rayleigh test: p = 0.013, Z = 4.233). There was no significant difference between the distributions of nests in the control condition (antiparallel mode) and the SF RF-condition (Figure 3.3-7; Watson U²: p > 0.5, U² = 0.05).

Animals tested in a broadband RF-magnetic field (1-5 MHz) displayed an axial south-east and north-west preference with a high concentration in the south-east (Figure 3.3-7d, n = 17, μ = 127°/307° ± 37°, r = 0.443; Rayleigh test: p = 0.033, Z = 3.335). The distributions in both conditions were significantly different from each other (Watson U²: p < 0.005, U² = 0.294). The distributions of the nests in the broadband RF-condition and the condition with the static field shifted by 90° were not significantly different from each other (Figure 3.3-7; Watson U²: 0.5 > p < 0.2, U² = 0.074).
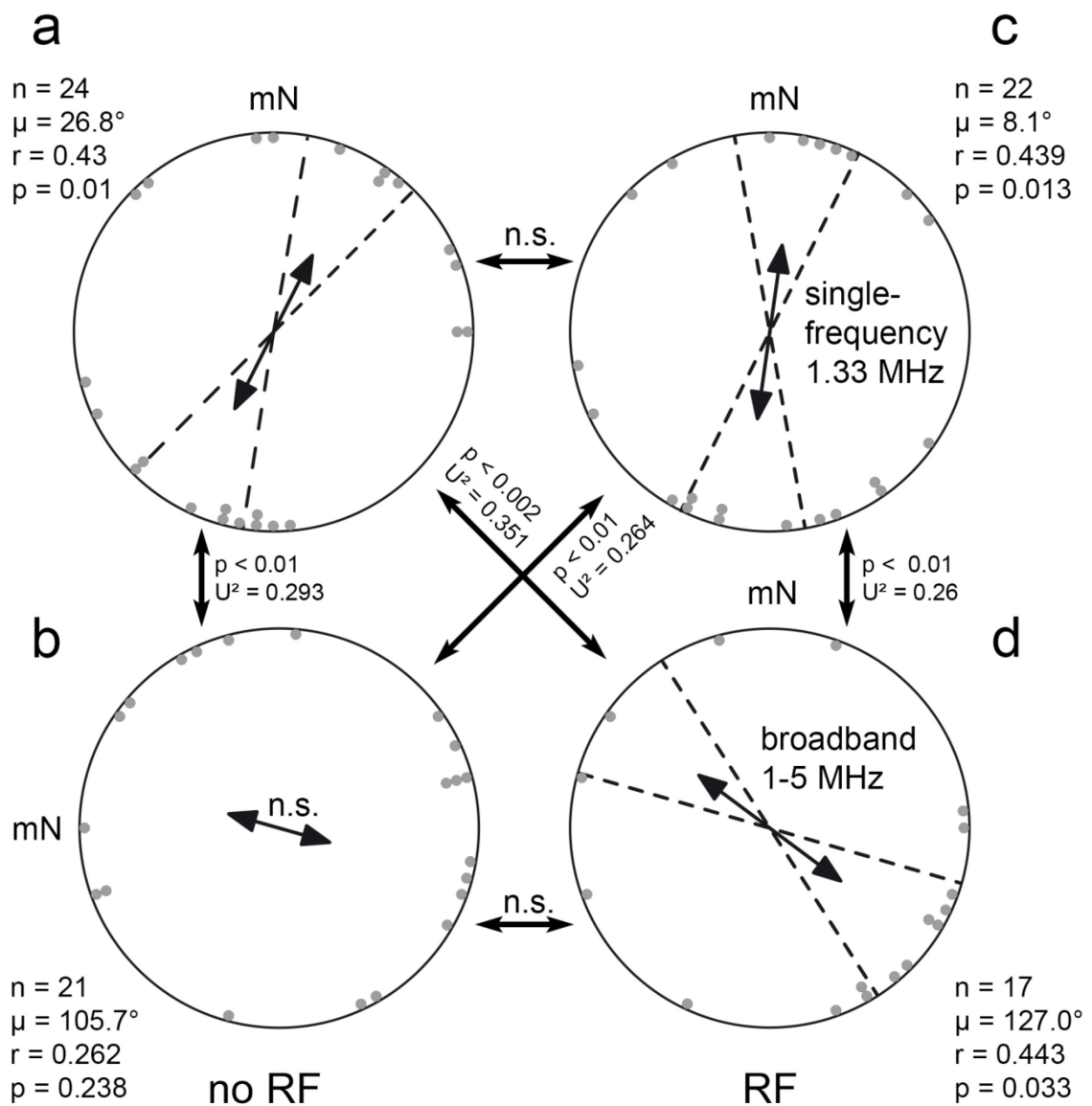
Figure 3.3-7 Orientation of wood mice nests built in a visually symmetrical circular arena under different magnetic conditions. Each data point represents the position of a nest built by an individual mouse. (a) Bearings relative to magnetic north (mN) in the arena in the ambient magnetic field. (b) Bearings relative to magnetic north (mN) in the arena with magnetic north shifted 90° counterclockwise. (c) Bearings relative to magnetic north (mN) in the arena in the ambient magnetic field with a superimposed Larmor frequency oscillating field (785 nT-1.26 μT). (d) Bearings relative to magnetic north (mN) in the arena in the ambient magnetic field with a superimposed broadband (0.9-5 MHz) oscillating field (25-100 nT). Arrows give the mean vector for the distribution of the nests, the dotted lines are the 95 % confidence intervals for the mean bearing (μ) of nonrandom distributions (p-value of the Rayleigh test is given for each distribution). The double-headed arrows indicate bimodal distributions; the lengths of the arrows represent the mean vector length r (scaled so the radius of the circles corresponds to r = 1), which provides a measure of the degree of clustering in the distribution of the bearings. Significant differences between the distributions are indicated by the p- and U²-values of the Watson U² test. n.s. = not significant.

3.4   Discussion

3.4.1   Pulse experiment

At this point it seems appropriate to clarify, that this experiment was not designed to test for the involvement of magnetite in red fox magnetoreception, as this is the usual purpose of pulse experiments in magnetoreception research (e.g. Holland et al., 2008). The pulse used here was of far too less intensity to remagnetize single-domain magnetite and was simply intended to test for the occurrence of magnetoreception in foxes in general.

The interpretation of the results of the pulse experiment is not straightforward. On the one hand, statistically significant effects of the magnetic field changes were detectable in one of the three tested foxes. On the other hand, the results do not reveal any consistencies and can at best be interpreted as a very cautious hint that magnetoreception might exist in red foxes. Clearly, there is no consistent or biologically relevant effect on hearing thresholds. Furthermore, since the response latencies were not different between the conditions, foxes do not (at least not consciously) perceive the magnetic pulse, otherwise they would have had quickly learned the connection between the reward and the magnetic stimulus, and therefore would have been expected to become quicker under *coil on* condition with each subsequent session. In sum, the data does not allow to conclude that the foxes' auditory system is affected by pulsed magnetic fields. A much larger dataset obtained in a completely acoustically shielded room might yield different results, but would be even further away from the natural situation in the wild.

3.4.2   Horizontal shift experiment

The thresholds of the single fox listening towards magnetic north were not different from the thresholds obtained when the fox was listening towards magnetic east. Therefore, it is highly unlikely, that the magnetic alignment observed in hunting red foxes (Červený et al., 2011) is the consequence of enhanced hearing sensitivity, leaving room to provide evidence for the alternative hypotheses. One might argue that with north and east the magnetic directions were inappropriately chosen, as the foxes clearly preferred the mean direction of these two, north-east and thus no differential effect of north and east would have been expected. However, as magnetic alignment is beginning of being recognized as a quite universally distributed phenomenon amongst mammali-

an species and furthermore most species prefer the north-south axis (Begall et al., 2013), I assumed that the east shift in the red fox MA would simply be based on scatter of the relatively small sample in the study by Červený et al. (2011; at least for a MA study) and therefore decided to test magnetic east versus magnetic north. It can, however, not be excluded that alignment with anticardinal directions would show an effect.

Also, it is theoretically possible that only frequencies lower or higher than the tested spectrum are affected by magnetic fields. In light of the working hypothesis that magnetic alignment influences acoustic prey detection, this would not be of relevance as the rustling noise of mice and voles contains most energy in bands around 8-10 kHz (Payne, 1971; Konishi, 1973; Marimuthu & Neuweiler, 1987). However, chewing noise seems to be more shifted into higher frequencies (Payne, 1971), and future experiments should be conducted to determine whether foxes prefer rustling or chewing noise for the detection of prey.

3.4.3 Histology: Where are the magnetoreceptors?

I was not able to demonstrate the occurrence of iron particles (cuticulosomes) in the inner ear of the red fox by means of the Prussian blue staining of surface specimens and paraffin sections which is in line with the absence of an effect of magnetic alignment on hearing sensitivity. It is not a surprising finding, given that Lauwers et al. (2013) also tested several mammalian species (rat, mice, guinea pig, human) without the appearance of any stained structures. Nevertheless, the absence of staining does not prove that the particles do not exist, as several factors might have complicated their discovery. First of all, the particles shown by Lauwers et al. (2013) were so small (300-600 nm) that they might have been easily overlooked under the light microscope if they would have been only sparsely distributed. Furthermore, it is not clear whether the Prussian blue stain penetrates cell membranes, which might be the reason of the absence of staining in the surface specimens. On the other hand, I could not stain every paraffin section of each cochlea (as they were needed for the general ear morphology) and often the hair cells were disrupted or totally missing. Another possibility might be related to the evolution of the auditory organ in mammals. Lauwers et al (2013) demonstrated the occurrence of the iron particles in hair cells of both the cochlear and vestibular hair cells. The sense of hearing has gained a considerably higher importance during mammalian evolution that it would seem at least plausible that, assumed the particles would be sensors of magnetic fields, they might have been relocalized in order to avoid dis-

turbing sensory crosstalk. As a conclusion, it still seems promising to search within the vestibular system of the red fox.

The finding of Cry1 in the S cone outer segments of the red fox retina is a highly surprising finding. In birds, even though the transduction process is still enigmatic, Cry1, localized with the UV-cones of robins and chickens, is the most probable receptor molecule for the magnetic compass in birds (Bischof et al., 2011; Nießner et al., 2011, 2013). The absence of staining in the wood mouse suggests, that interspecies differences exist, which is suggestive of a rather specific function in the red fox. Cry1 is known to be involved in circadian rhythms (Sancar, 2000), but this seems unlikely to be the cause for cryptochromes being seated in the cone outer segments, since for controlling circadian rhythms it needs to be able to exert influence on transcription processes. Thus, a new role seems possible and given the findings in birds, this new role might be magnetoreception.

At this point, however, it needs to be stated that as the experiment was preliminary and the results are only based on three specimens (two foxes, one wood mouse), not too far reaching speculations should be made. Nevertheless, if shown in future that cryptochrome is involved in a magnetic sense of the red fox, the hypothesis of a magneto-visual range finder would gain considerable new support. Furthermore, as Cry1 is exclusively found in S cones, the distribution pattern of those and the retinal ganglion cell densities provided in this thesis, might prove very useful in developing a model of the "magnetic pattern" a fox might see, similar as it has been done in birds (Ritz et al., 2000; Solov'yov et al., 2010).

3.4.4 Magnetic orientation in wood mice

The results provide clear evidence for a magnetic sense in wood mice. When deciding where to build a nest in an otherwise featureless environment, the animals revealed a preference for the magnetic north-northeast and south-southwest axis and when the alignment of the magnetic field was rotated by 90°, the bimodal clustering of bearings, although not significant, was rotated by a comparable extent. The increased scatter of nest positions in the 90° shifted field may have been due to the inhomogeneity in the artificial magnetic field or, alternatively, to a cue conflict between magnetic cues and non-magnetic (e.g. sound) cues that may have been accessible for the mice in the holding enclosure and arena. Thus, for example, the irregular creaking sound produced by the stable doors might have provided an orientation cue to the mice. During the night

before the test (when the animals were kept in the enclosure) and in control condition this creaking came from ~magnetic east, but from magnetic south in changed magnetic field condition (see Figure 3.2-2a). Evidence consistent with a cue conflict between magnetic and non-magnetic cues, and higher scatter in shifted magnetic field conditions, have been reported in other studies of rodent magnetic orientation (Burda et al., 1990; Deutschlander et al., 2003; Oliveriusová et al., 2012, 2014). Nevertheless, the results clearly confirm the presence of a magnetic sense in wood mice, a prerequisite for a magnetic compass, which supports the findings by Mather and Baker (Mather & Baker, 1981). A magnetic compass would be highly beneficial for nocturnal wood mice that perform regular foraging bouts over distances of more than 200 m, show remarkable homing ability from unfamiliar locations after displacements of up to 350 m (Hacker & Pearson, 1951; Jamon & Bovet, 1987), occupy comparatively large home ranges of 1-2 ha (Tew & MacDonald, 1994), and show remarkable navigational strategies, including way-marking behaviour using portable, visual landmarks (Stopka & MacDonald, 2003).

It is unclear why mice exhibit a preference to build their nests along the magnetic ~north-south axis, but there are two general proximate explanations: either the preference is learned (e.g., corresponding to the direction of some feature of the environment) or innate (consistent with spontaneous northward magnetic orientation, or axial orientation along the north-south magnetic axis, found in other vertebrates; Begall et al., 2013). Laboratory mice can be trained to orient in the direction of a nest box placed at one end of the cage in which they are held prior to testing (Muheim et al., 2006). The wood mice tested in the current study were kept in a rectangular enclosure for up to three nights before being tested, but this pre-exposure was shorter than in earlier studies of learned compass responses (e.g. 5-24 days in Muheim et al., 2006) and no features of the cage environment relative to the magnetic field or to topographic cues (cage axis, shadows, etc.) appeared to coincide with the axis of orientation exhibited by the mice. Hence it is unlikely that the observed axial preference was learned even though "magnetic imprinting" with respect to other cues, i.e. a response that was learned prior to the mouse being captured that was subsequently transferred to non-magnetic (topographic) cues, cannot be fully excluded. Also an effect of the displacement direction cannot be ruled out as many animals were caught north-northeast of the testing site.

Laboratory mice, in addition to showing learned compass orientation relative to the magnetic field, also exhibit a weak, presumably innate (i.e., independent of any learned direction) axial

preference along the magnetic north-south axis (Muheim et al., 2006). Recently, such a preference was also revealed in the semi-fossorial bank vole (*Clethrionomys glareolus*), which Oliveriusová et al., (2014) suggested is likely to be innate although the voles were kept in approximately north-south aligned cages in the laboratory for at least 8 weeks before testing (Oliveriusová et al., 2014). Consequently, although there is insufficient information to determine if the observed preference in wood mice is innate or learned, it appears likely that at least some component of the response is innate.

We can only speculate about the ultimate reasons for an innate preference to build nests along the north-south axis of the Earth's magnetic field. As for the more general phenomenon of magnetic alignment, several functions for nest position preferences seem plausible (discussed in Begall et al., 2013). It might provide a constant directional reference for the use of a (visual) map-sense (see below), or enhance selective attention through the facilitation of cross-modal integration (Phillips et al., 2010). Further experiments will hopefully shed light on this issue.

3.4.5 Mechanisms of magnetoreception and the influence of RF fields

The responses of the mice under RF exposure are not straightforward to interpret in view of the current theories on magnetoreception. The available evidence indicates that subterranean microphthalmic mole-rats rely on a light-independent MPM (Thalau et al., 2006), while the properties of learned magnetic compass orientation by epigeic rodents may point to the involvement of a RPM (Phillips et al., 2013). It is therefore possible that macrophthalmic, epigeic wood mice also have a RPM, in which case we expect a specific sensitivity to weak RF magnetic fields (Henbest et al., 2004a; Ritz et al., 2004). Analogous to the experiments performed in birds and mole-rats (Ritz et al., 2004, 2009; Thalau et al., 2006), we tested the wood mice in both Larmor frequency (LF) and wideband-FM (comparable to broadband-RF) oscillating magnetic fields. Contrary to the predictions of the RPM made earlier by other investigators (Ritz et al., 2004, 2009), wood mice exhibited non-random directional preferences in both conditions: The distribution of bearings under the LF condition was indistinguishable from controls (i.e., nests were bimodally distributed along the ∼north-south magnetic axis; Figure 3.3-7c). In contrast, under wideband-FM conditions it was rotated by roughly 90° relative to control. As the angle between the static field and the RF fields was the same in both conditions (see Figure 3.2-2c), the only differences were the overall intensity, the temporal pattern, and the frequency spectrum. The in-

tensities in the LF condition had maximum values of 1.26 μT in the periphery of the arena and minimum values of 785 nT in the centre and therefore greatly exceeded those shown to affect the inclination compass of birds (Ritz et al., 2009; Engels et al., 2014). In the wideband-FM condition, due to the frequency response characteristics of the coil, the intensities varied between 25-50 nT in the centre of the coil to twice these values at the periphery of the arena. These field strengths are comparable to the ones used in Engels et al. (2014), who were able to perturb the magnetic compass of European robins by broadband electromagnetic noise with spectral intensity of 0.1-0.2 nT per 10 kHz in the range 600 kHz-3 MHz, which upon integration over the frequency domain translates into a typical RF magnetic field amplitude of 30-35 nT in the time domain.

The fact that we observed an effect under wideband-FM field but no visible effect on nest building under LF conditions is consistent with a RPM mechanism in which both electron spins have an anisotropic coupling to their respective host molecules, due either to nuclear hyperfine interactions (Schulten et al., 1978; Ritz et al., 2000) or to spin-orbit coupling (Lambert et al., 2013). In any case, we can rule out that wood mice use a so-called optimal reference-probe RPM model (where one of the two unpaired electrons in the radical pair - the probe spin - is devoid of anisotropy), which was suggested by Ritz et al. (2009, 2010) to explain disorientation in birds under very weak fields (15 nT) oscillating at the Larmor frequency. Under the assumption that cryptochrome 1a (Nießner et al., 2011, 2013) is the responsible molecule for RPM magnetoreception in mammals, the radical partner of the flavin adenine dinucleotide (FAD) cofactor thus cannot be a reactive oxygen species (superoxide) as has been suggested for birds (Solov'yov & Schulten, 2009; Ritz et al., 2010), because superoxide is free of hyperfine interactions, but it could be tryptophan as in the original model (Ritz et al., 2000) or ascorbyl as recently proposed by Lee et al. (2014). Alternatively, although it is unclear whether the RPM is an evolutionary relatively new invention (Gould, 2008) or was present in a common ancestor of arthropod and chordate lineages, and perhaps modified in the bird lineage, the results render it possible that mammals and perhaps other taxa might utilize a different host molecule for their RPM than birds. Either way, a large number of resonance frequencies below and above the LF are possible in a RPM in which both members of the radical pair have hyperfine interactions, which would have been covered by the frequency window in the wideband-FM conditions.

Interestingly, however, while RF magnetic fields so far have been found to cause disorientation in birds (and also in insects; Vácha et al., 2009), in the present experiments the wideband-FM field caused re-orientation in mice, with nest-building positions shifted by 90° relative to the axis of orientation observed in the ambient magnetic field. To our knowledge, the possibility of this type of RF effect (i.e., altering rather than eliminating the pattern of response) has not been addressed by the available models of the RPM. For simple reference-probe RPM models, either with a single hyperfine coupling to one of the electron spins (Gauger et al., 2011), or alternatively with a slightly anisotropic uniaxial *g*-factor of one spin due to spin-orbit coupling (Lambert et al., 2013), it is the lifetime of the spin-correlated radical pair ("spin correlation time") that determines the magnitude of the effect of weak RF magnetic field on the radical pair dynamics: long correlation times, on the order 100 μs (i.e. an order of magnitude longer than the ones found in *ex vivo* studies on CRY-DASH; Biskup et al., 2009) allow weak RF magnetic fields to fully perturb the singlet-triplet interconversion, which leads to a flattened angular response (suppression of the compass), while shorter correlation times alter the absolute values of the yield without flattening the angular response (Gauger et al., 2011; Lambert et al., 2013). Theoretically it is possible that the RPM in rodents is based on a radical pair with shorter spin coherence time than the ones in migratory birds, so that the effect of an RF magnetic field could be different in the two taxa. Regardless, the altered response in the short-lived radical pair would be equivalent to the response produced by an intensity shift in the static magnetic field (Gauger et al., 2011), which could produce a change in pattern of response. Based on the idea that vertebrates might exploit this pattern as a global reference system (Phillips et al., 2010), being useful in a variety of daily challenges from integrating spatial information from multiple sensory modalities, to distance estimations (Červený et al., 2011) and landing angle assessment (Hart, et al., 2013), the mice might position themselves and/or their nests in the arena in a specific alignment with respect to the pattern generated by the RPM. Consequently, the alignment of the mice might change when the visual pattern is altered by the RF treatment. When exposed to such an unfamiliar pattern of response, recalibration of the static field direction may be required as suggested to occur in migratory birds exposed to a change in magnetic field intensity (Wiltschko et al., 2006; Winklhofer et al., 2013). This recalibration might require the animal to switch to a different compass mechanism, which under natural conditions would be mediated by a MPM or by a non-magnetic cue; see also (Phillips et al., 2010).

It is widely believed that RF magnetic fields influence exclusively a RPM, not a MPM. This is certainly true for single-domain magnetite, where the inertia of the particles surrounded by the viscous cytoplasm is generally believed to hinder motion and thus transduction of oscillating fields in the radiofrequency range (Kirschvink, Kuwajima, et al., 1992; Rodgers & Hore, 2009). However, a different type of MPM may indeed be affected by RF magnetic fields. According to Shcherbakov & Winklhofer (2010), a MPM based on magnetic susceptibility, such as the maghemite-superparamagnetic magnetite hybrid magnetoreceptor proposed by Fleissner et al. (2007) (for which there is little if any histological evidence, however), would represent an antenna for RF magnetic fields and should convert the radiation into thermal agitation. As with the putative effect on a RPM, it is not clear why such a heating effect would cause re-orientation, not disorientation. Importantly, however, due to the stronger magnetic field amplitude used for the LF condition compared to the broadband situation, the hyperthermia effects would have been more pronounced for the LF conditions. Instead the absence of an effect at the LF can be taken as a control for unspecific RF-effects (not acting on the receptor mechanism).

3.4.6 Summary and outlook of the wood mice experiments

In sum, I could show that wood mice possess a magnetic sense and display a probably innate directional preference for the NE-SW axis. It was demonstrated that this preference is not altered by weak RF fields of the Larmor frequency but shifted by 90° in broadband RF. The results suggest the involvement of a RPM or a related quantum process, but do not allow definite conclusions about the underlying mechanism of magnetoreception. Essentially, the influence of low frequency fields on nest building preferences has to be specifically tested while pulsing experiments should allow a clear distinction between RPM and MPM. If wood mice respond to the low frequency fields with a 90° shift and if furthermore the animals would show the normal NE-SW preference when treated with a strong (0.5 T) magnetic pulse before testing in these low frequency fields it would be clear that the behavioural response is mediated by a MPM (Wiltschko et al., 2009). The newly developed wood mouse assay is well-suited for future experiments to determine whether epigeic rodents have a MPM or a RPM. Finally and importantly, the RF magnetic fields applied here have peak intensities below the ICNIRP guidelines for general public exposure (i.e., Brms=0.92 µT/f (MHz), or Bpeak=1.30 µT/f (MHz); ICNIRP, 1998), considered as harmless for human health. Yet, they are sufficient to affect behaviour in a mammalian system.

General conclusions

The goal of this study was to extend the knowledge about the sensory biology of the red fox with a focus on the senses of hearing, vision, and magnetoreception. In summary, with this study we have gained a behavioural audiogram of the red fox, a comprehensive morphological description of its auditory system, a detailed map of two important components of its visual system, and first insights into the role of magnetic alignment in red foxes.

In addition, I could provide evidence for magnetoreception in another small rodent possibly using a magnetoreceptor that has so far been thought to be unique to non-mammalian species.

The results about the auditory system of the red fox obtained in this study are valuable because they provide the basic knowledge needed before any other behaviour in relation to auditory stimuli can be properly interpreted. The behavioural audiogram presented here, will be useful in all kind of future auditory studies on the red fox and other canids, but also for studies of vocalization and pest control (acoustic repellence). The morphological results have provided further insights into the general relationship between morphology and function in auditory systems and will be valuable as they add to the still small database of (non-laboratory) mammals of which both hearing has been studied accurately and the morphology of the middle and inner ear is described in detail.

The results on the visual system add to the growing database of mammalian photoreceptor distributions, ganglion cell densities, and visual acuity in wild mammals and revealed the strong effects a differing ecology can have on the sensory equipment of two closely related species, the red fox and the arctic fox. As there is still debate about the ultimate mechanisms underlying the diversity of photoreceptor distributions, every new species investigated is of high value.

Finally, the results on magnetoreception lead the way to new and very promising directions of research. Although the magnetic sense in red foxes could not be proven and the function of its magnetic alignment during hunting remains an enigma, at least one hypothesis concerning the function of magnetic alignment in the red fox could be disproven. Furthermore, the finding of cryptochrome in the red fox retina is in favour of an alternative hypothesis, which can now be specifically tested as more accurate predictions can be made (e.g. in combination with the results on the visual system).

The discovery of radiofrequency sensitive magnetoreceptive behaviour in a small rodent is spectacular and will lead to a series of further investigations. The absence of cryptochrome in the retina of RF-sensitive species is intriguing and does not fit to the predictions. If reproducible, the search for magnetoreceptors in mammals will have to be adjusted into new directions.

Acknowledgements

References

Aerts, J. R. M., & Dirckx, J. J. J. (2010). Nonlinearity in eardrum vibration as a function of frequency and sound pressure. *Hearing Research, 263*, 26-32

Ahnelt, P. K., & Kolb, H. (2000). The mammalian photoreceptor mosaic-adaptive design. *Progress in Retinal and Eye Research, 19*, 711-777

Ahnelt, P. K., Schubert, C., Kübber-Heiss, A., Schiviz, A., & Anger, E. (2006). Independent variation of retinal S and M cone photoreceptor topographies: A survey of four families of mammals. *Visual Neuroscience, 23*, 429-435

Aibara, R., Welsh, J. T., Puria, S., & Goode, R. L. (2001). Human middle-ear sound transfer function and cochlear input impedance. *Hearing Research, 152*, 100-109

Alfred, Y. K., & Stone, J. (1982). The optic nerve of the cat: Appearance and loss of axons during normal development. *Developmental Brain Research, 5*, 263-271

Anderson, R. M., Jackson, H. C., May, R. M., & Smith, A. M. (1981). Population dynamics of fox rabies in Europe. *Nature, 289*, 765-771

Andriashek, D., & Spencer, C. (1989). Predation on a ringed seal, *Phoca hispida*, pup by a red fox, *Vulpes vulpes*. *Canadian field-naturalist. Ottawa ON, 103*, 600

Au, W. W. (2000). Hearing in whales and dolphins: An overview. In W. W. Au, A. N. Popper & R. R. Fay (Eds.), *Hearing by Whales and Dolphins* (pp. 1-42). New York: Springer.

Audet, A. M., Robbins, C. B., & Larivière, S. (2002). *Alopex lagopus*. *Mammalian Species, 713*, 1-10

August, P. V., Ayvazian, S. G., & Anderson, J. G. T. (1989). Magnetic orientation in a small mammal, *Peromyscus leucopus*. *Journal of Mammalogy, 70*, 1-9

Baden, T., Schubert, T., Chang, L., Wei, T., Zaichuk, M., Wissinger, B., & Euler, T. (2013). A tale of two retinal domains: Near-optimal sampling of achromatic contrasts in natural scenes through asymmetric photoreceptor distribution. *Neuron, 80*, 1206-1217

Ballast, L. (1984). *Funktionelle und vergleichende Morphologie der Cochlea von Wildformen und Laborstämmen der Muridae.* PhD thesis, Johann Wolfgang Goethe-Universität, Frankfurt am Main.

Bamberger, S., Valet, G., Storch, F., & Ruhenstroth-Bauer, G. (1978). Electromagnetically induced fluid streaming as a possible mechanism of the biomagnetic orientation of organisms. *Zeitschrift fur Naturforschung, 33c*, 59-60

Batschelet, E. (1981). *Circular Statistics in Biology*. London: Academic Press.

Bauer, G. B., Fuller, M., Perry, A., Dunn, J. R., & Zoeger, J. (1985). Magnetoreception and biomineralization of magnetite in cetaceans. In J. L. Kirschvink, D. S. Jones & B. J. MacFadden (Eds.), *Magnetite Biomineralization and Magnetoreception in Organisms* (pp. 489-507). New York: Plenum Press.

Begall, S., Burda, H., & Malkemper, E. P. (2014). Magnetoreception in mammals. In M. Naguib (Ed.), *Advances in the Study of Behavior* (Vol. 46, pp. 45-88). Amsterdam: Elsevier.

Begall, S., Lange, S., Schleich, C. E., & Burda, H. (2007). Acoustics, audition and auditory system. In S. Begall, H. Burda & C. E. Schleich (Eds.), *Subterranean Rodents - News from Underground* (pp. 97-111). Heidelberg: Springer.

Begall, S., Červený, J., Neef, J., Vojtêch, O., & Burda, H. (2008). Magnetic alignment in grazing and resting cattle and deer. *Proceedings of the National Academy of Sciences, 105*, 13451-13455

Begall, S., Malkemper, E. P., Červený, J., Němec, P., & Burda, H. (2013). Magnetic alignment in mammals and other animals. *Mammalian Biology, 78*, 10-20

Benovitski, Y. B., Blamey, P. J., Rathbone, G. D., & Fallon, J. B. (2014). An automated psychoacoustic testing apparatus for use in cats. *Hearing Research, 309*, 1-7

Bischof, H. J., Nießner, C., Peichl, L., Wiltschko, R., & Wiltschko, W. (2011). Avian ultraviolet/violet cones as magnetoreceptors: The problem of separating visual and magnetic information. *Communicative and Integrative Biology, 4*, 0--1

Biskup, T., Schleicher, E., Okafuji, A., Link, G., Hitomi, K., Getzoff, E. D., & Weber, S. (2009). Direct observation of a photoinduced radical pair in a cryptochrome blue-light photoreceptor. *Angewandte Chemie International Edition, 48*, 404-407

Blake, R., Cool, S. J., & Crawford, M. L. J. (1974). Visual resolution in the cat. *Vision Research, 14*, 1211-1217

Blakemore, R. (1975). Magnetotactic bacteria. *Science, 190*, 377-379

Blevins, C. E. (1964). Studies on the innervation of the stapedius muscle of the cat. *The Anatomical Record, 149*, 157-171

Bobbin, R. P. (1979). Glutamate and aspartate mimic the afferent transmitter in the cochlea. *Experimental Brain Research, 34*, 389-393

Bowles, A. E., & Francine, J. K. (1993). Effects of simulated aircraft noise on hearing, food detection, and predator avoidance behavior of the kit fox, *Vulpes marotis*. *The Journal of the Acoustical Society of America, 93*, 2378-2378

Branis, M., & Burda, H. (1985). Inner ear structure in the deaf and normally hearing Dalmatian dog. *Journal of Comparative Pathology, 95*, 295-299

Bruns, V., & Schmieszek, E. (1980). Cochlear innervation in the greater horseshoe bat: demonstration of an acoustic fovea. *Hearing Research, 3*, 27-43

Bruns, V., Müller, M., Hofer, W., Heth, G., & Nevo, E. (1988). Inner ear structure electrophysiological audiograms of the subterranean mole rat, *Spalax ehrenbergi*. *Hearing Research, 33*, 1-9

Buchler, E. R., & Wasilewski, P. J. (1982). Bats have magnets. *EOS, Transactions American Geophysical Union, 63*, 156

Burda, H. (1982). *Relation of the spiral ligament form to the auditory function.* Paper presented at the VI. Symposium Cochlea Forschung, Halle (Saale).

Burda, H. (1985a). Effects of domestication on morphometry of ear structures in Norway rats. *Fortschritte der Zoologie, 30*, 657-659

Burda, H. (1985b). Qualitative assessment of postnatal maturation of the organ of Corti in two rat strains. *Hearing Research, 17*, 201-208

Burda, H., & Voldřich, L. (1980). Correlation between the hair cell density and the auditory threshold in the white rat. *Hearing Research, 3*, 91-93

Burda, H., Ulehlova, L., & Branis, M. (1984). Morphology of the middle and inner ear in two *Panthera* species - *P. tigris* and *P. onca* (Felidae, Carnivora, Mammalia). *Vestnik Ceskoslovenske Spolecnosti Zoologicke, 48*, 9-14

Burda, H., Ballast, L., & Bruns, V. (1988). Cochlea in old world mice and rats (Muridae). *Journal of Morphology, 198*, 269-285

Burda, H., Fiedler, J., & Bruns, V. (1988). The receptor and neuron distribution in the cochlea of the bat, *Taphozous kachhensis*. *Hearing Research, 32*, 131-135

Burda, H., Marhold, S., Westenberger, T., Wiltschko, R., & Wiltschko, W. (1990). Evidence for magnetic compass orientation in the subterranean rodent *Cryptomys hottentotus* (Bathyergidae). *Experientia, 46*, 528-530

Burda, H., Begall, S., Červený, J., Neef, J., & Němec, P. (2009). Extremely low-frequency electromagnetic fields disrupt magnetic alignment of ruminants. *Proceedings of the National Academy of Sciences, 106*, 5708-5713

Burda, H., Beiles, A., Marhold, S., Simson, S., Nevo, E., & Wiltschko, W. (1991). Magnetic orientation in subterranean mole rats of the superspecies *Spalax ehrenbergi*: Experiments, patterns, and memory. *Israel Journal of Zoology, 37*, 182-183

Butler, R. A. (1975). The influence of the external and middle ear on auditory discriminations. In W. D. Keidel & W. D. Neff (Eds.), *Auditory System* (Vol. 5/2, pp. 247-260). Berlin Heidelberg: Springer.

Cabezudo, L. M. (1978). The ultrastructure of the basilar membrane in the cat. *Acta Oto-Laryngologica, 86*, 160-175

Calderone, J. B., & Jacobs, G. H. (2003). Spectral properties and retinal distribution of ferret cones. *Visual Neuroscience, 20*, 11-17

Calderone, J. B., Reese, B. E., & Jacobs, G. H. (2003). Topography of photoreceptors and retinal ganglion cells in the spotted hyena (*Crocuta crocuta*). *Brain, Behavior and Evolution, 62*, 182-192

Cashmore, A., Jarillo, J. A., Wu, Y., & Liu, D. (1999). Cryptochromes: blue light receptors for plants and animals. *Science, 284*, 760–765

Casseday, J., & Neff, W. (1973). Localization of pure tones. *The Journal of the Acoustical Society of America, 54*, 365-372

Catling, P. C. (1988). Similarities and contrasts in the diets of foxes, *Vulpes vulpes*, and cats, *Felis catus*, relative to fluctuating prey populations and drought. *Wildlife Research, 15*, 307-317

Cavallini, P., & Santini, S. (1995). Age determination in the red fox in a Mediterranean habitat.

Cavallini, P., & Volpi, T. (1996). Variation in the diet of the red fox in a Mediterranean area. *Revue d'Ecologie (Terre Vie), 51*, 173-189

Červený, J., Begall, S., Koubek, P., Nováková, P., & Burda, H. (2011). Directional preference may enhance hunting accuracy in foraging foxes. *Biology Letters, 7*, 355-357

Chavko, J., Danko, Š., Obuch, J., & Mihók, J. (2007). The food of the imperial eagle (*Aquila heliaca*) in Slovakia. *Slovak Raptor Journal, 1*, 1-18

Clutton-Brock, J. (1995). Origins of the dog: domestication and early history. In J. Serpell (Ed.), *The Domestic Dog: Its Evolution, Behaviour and Interactions with People* (pp. 7-20). Cambridge: Cambridge University Press.

Coile, D. C., & O'Keefe, L. P. (1988). Schematic eyes for domestic animals. *Ophthalmic and Physiological Optics, 8*, 215-219

Coleman, M. N. (2009). What do primates hear? A meta-analysis of all known nonhuman primate behavioral audiograms. *International Journal of Primatology, 30*, 55-91

Coleman, M. N., & Ross, C. F. (2004). Primate auditory diversity and its influence on hearing performance. *The Anatomical Record A, 281*, 1123-1137

Coleman, M. N., & Colbert, M. W. (2010). Correlations between auditory structures and hearing sensitivity in non-human primates. *Journal of Morphology, 271*, 511-532

Cornsweet, T. N. (1962). The staircase-method in psychophysics. *The American Journal of Psychology, 75*, 485-491

Curcio, C. A., Millican, C. L., Allen, K. A., & Kalina, R. E. (1993). Aging of the human photoreceptor mosaic: evidence for selective vulnerability of rods in central retina. *Investigative Ophthalmology & Visual Science, 34*, 3278-3296

Dallos, P. (1973). *The Auditory Periphery*. New York: Academic Press.

Dallos, P. (1992). The active cochlea. *The Journal of Neuroscience, 12*, 4575-4585

Dallos, P., & Harris, D. (1978). Properties of auditory nerve responses in absence of outer hair cells. *Journal of Neurophysiology, 41*, 365-383

Dallos, P., Harris, D., Özdamar, Ö., & Ryan, A. (1978). Behavioral, compound action potential, and single unit thresholds: Relationship in normal and abnormal ears. *The Journal of the Acoustical Society of America, 64*, 151-157

Dannhof, B. J., Roth, B., & Bruns, V. (1991). Length of hair cells as a measure of frequency representation in the mammalian inner ear? *Naturwissenschaften, 78*, 570-573

Davies, W. I. L., Collin, S. P., & Hunt, D. M. (2012). Molecular ecology and adaptation of visual photopigments in craniates. *Molecular Ecology, 21*, 3121-3158

Davila, A. F., Fleissner, G., Winklhofer, M., & Petersen, N. (2003). A new model for a magnetoreceptor in homing pigeons based on interacting clusters of superparamagnetic magnetite. *Physics and Chemistry of the Earth, 28*, 647-652

Davis, H. (1958). Transmission and transduction in the cochlea. *The Laryngoscope, 68*, 359-382

Décory, L., Franke, R. B., & Dancer, A. L. (1990). Measurement of the middle ear transfer function in cat, chinchilla and guinea pig. In P. Dallos, C. D. Geisler, J. W. Matthews, M. A. Ruggero & C. R. Steele (Eds.), *The Mechanics and Biophysics of Hearing* (Vol. 87, pp. 270-277). New York: Springer.

Decraemer, W. F., & Khanna, S. M. (2004). Measurement, visualization and quantitative analysis of complete three-dimensional kinematical data sets of human and cat middle ear. In K. Gyo, H.

Wada, N. Hato & T. Koike (Eds.), *Middle Ear Mechanics in Research and Otology* (pp. 3-10). Singapore: World Scientific.

Decraemer, W. F., Khanna, S. M., & Funnell, W. R. J. (1995). Bending of the manubrium in cat under normal sound stimulation. In H. J. Foth, A. Lewis, H. Podbielska, M. Robert-Nicoud, H. Schneckenburger & A. J. Wilson (Eds.), *Proceedings SPIE, Optical and Imaging Techniques in Biomedicine* (Vol. 2329, pp. 74-84).

Dell'Arte, G. L., Laaksonen, T., Norrdahl, K., & Korpimäki, E. (2007). Variation in the diet composition of a generalist predator, the red fox, in relation to season and density of main prey. *Acta Oecologica, 31*, 276-281

Deutschlander, M. E., Freake, M. J., Borland, S. C., Phillips, J. B., Madden, R. C., Anderson, L. E., & Wilson, B. W. (2003). Learned magnetic compass orientation by the Siberian hamster, *Phodopus sungorus. Animal Behaviour, 65*, 779-786

Diebel, C. E., Proksch, R., Green, C. R., Neilson, P., & Walker, M. M. (2000). Magnetite defines a vertebrate magnetoreceptor. *Nature, 406*, 299-302

Dooling, R. J., Lohr, B., & Dent, M. L. (2000). Hearing in birds and reptiles. In R. J. Dooling, R. R. Fay & A. N. Popper (Eds.), *Comparative Hearing: Birds and Reptiles*. New York: Springer.

Doran, A. (1879). Morphology of the mammalian ossicula auditus. *Journal of Anatomy and Physiology, 13*, 401-406

Dulai, K. S., von Dornum, M., Mollon, J. D., & Hunt, D. M. (1999). The evolution of trichromatic color vision by opsin gene duplication in New World and Old World primates. *Genome Research, 9*, 629-638

Dusenbery, D. B. (1992). *Sensory Ecology. How Organisms Acquire and Respond to Information*. New York: W. H. Freeman and Company.

Dyson, M. L., Klump, G. M., & Gauger, B. (1998). Absolute hearing thresholds and critical masking ratios in the European barn owl: a comparison with other owls. *Journal of Comparative Physiology A, 182*, 695-702

Echteler, S. M., Fay, R. R., & Popper, A. N. (1994). Structure of the mammalian cochlea. In R. R. Fay & A. N. Popper (Eds.), *Comparative Hearing: Mammals* (Vol. 4, pp. 134-171). New York: Springer.

Edmonds, D. T. (1996). A sensitive optically detected magnetic compass for animals. *Proceedings of the Royal Society B, 263*, 295-298

Ehrenberger, K., & Felix, D. (1991). Glutamate receptors in afferent cochlear neurotransmission in guinea pigs. *Hearing Research, 52*, 73-80

Ehret, G. (1978). Stiffness gradient along the basilar membrane as a basis for spatial frequency analysis within the cochlea. *The Journal of the Acoustical Society of America, 64*, 1723-1726

Ehret, G., & Frankenreiter, M. (1977). Quantitative analysis of cochlear structures in the house mouse in relation to mechanisms of acoustical information processing. *Journal of Comparative Physiology, 122*, 65-85

Ehret, G., & Göpfert, M. C. (2013). Auditory systems. In G. G. Galizia & P.-M. Lledo (Eds.), *Neurosciences - From Molecule to Behavior: a University Textbook* (pp. 337-362). Berlin, Heidelberg: Springer.

Engels, S., Schneider, N. L., Lefeldt, N., Hein, C. M., Zapka, M., Michalik, A., Elbers, D., Kittel, A., Hore, P. J., & Mouritsen, H. (2014). Anthropogenic electromagnetic noise disrupts magnetic compass orientation in a migratory bird. *Nature, 509*, 353-356

Fattu, J. (1969). Acoustic orientation by the rabbit pinna and external auditory meatus. *The Journal of the Acoustical Society of America, 46*, 124

Fay, J. P., Puria, S., & Steele, C. R. (2006). The discordant eardrum. *Proceedings of the National Academy of Sciences, 103*, 19743-19748

Fay, R. R. (1974). Auditory frequency discrimination in vertebrates. *Journal of the Acoustical Society of America, 56*, 206-209

Fay, R. R. (1988). *Hearing in Vertebrates: A Psychophysics Databook*. Winnetka, IL: Hill-Fay Associates.

Fay, R. R. (1992). Structure and function in sound discrimination among vertebrates. In D. Webster, R. R. Fay & P. A. N. (Eds.), *The Evolutionary Biology of Hearing* (pp. 229-263). Berlin, Heidelberg, New York: Springer.

Feng, A. S., Narins, P. M., Xu, C.-H., Lin, W.-Y., Yu, Z.-L., Qiu, Q., Xu, Z.-M., & Shen, J.-X. (2006). Ultrasonic communication in frogs. *Nature, 440*, 333-336

Fleischer, G. (1973). Studien am Skelett des Gehörorgans der Säugetiere, einschließlich des Menschen. *Säugetierkundliche Mitteilungen, 21*, 131-239

Fleischer, G. (1978). Evolutionary principles of the mammalian middle ear. *Advances in the Study of Anatomy, Embryology and Cell Biology, 55*, 1-70

Fleissner, G., Stahl, B., Thalau, P., & Falkenberg, G. (2007). A novel concept of Fe-mineral-based magnetoreception: histological and physicochemical data from the upper beak of homing pigeons. *Naturwissenschaften, 94*, 631-642

Francis, R. (1975). *Behavioural audiometry in mammals: Review and evaluation of techniques*. Paper presented at the Symposia of the Zoological Society of London.

Frankel, R. B., Blakemore, R. P., & Wolfe, R. S. (1979). Magnetite in freshwater magnetotactic bacteria. *Science, 203*, 1355-1356

Fujita, S., & Elliott, D. (1965). Thresholds of audition for three species of monkey. *The Journal of the Acoustical Society of America, 37*, 139-144

Funnell, W. R. J., Decraemer, W. F., & Khanna, S. M. (1987). On the damped frequency response of a finite-element model of the cat eardrum. *The Journal of the Acoustical Society of America, 81*, 1851-1859

Funnell, W. R. J., Khanna, S. M., & Decraemer, W. F. (1992). On the degree of rigidity of the manubrium in a finite-element model of the cat eardrum. *The Journal of the Acoustical Society of America, 91*, 2082-2090

Funnell, W. R. J., Heng Siah, T., McKee, M. D., Daniel, S. J., & Decraemer, W. F. (2005). On the coupling between the incus and the stapes in the cat. *Journal of the Association for Research in Otolaryngology, 6*, 9-18

Galambos, R., & Rupert, A. (1959). Action of the middle ear muscles in normal cats. *The Journal of the Acoustical Society of America, 31*, 349-355

Gao, H., & Hollyfield, J. G. (1992). Aging of the human retina. Differential loss of neurons and retinal pigment epithelial cells. *Investigative Ophthalmology & Visual Science, 33*, 1-17

Garcia, M., Charrier, I., Rendall, D., & Iwaniuk, A. N. (2012). Temporal and spectral analyses reveal individual variation in a non-vocal acoustic display: The drumming display of the ruffed grouse (*Bonasa umbellus*, L.). *Ethology, 118*, 292-301

Gauger, E. M., Rieper, E., Morton, J. J. L., Benjamin, S. C., & Vedral, V. (2011). Sustained quantum coherence and entanglement in the avian compass. *Physical Review Letters, 106*, 040503

Gianfranceschi, L., Fiorentini, A., & Maffei, L. (1999). Behavioural visual acuity of wild type and bcl2 transgenic mouse. *Vision Research, 39*, 569-574

Glösmann, M., Steiner, M., Peichl, L., & Ahnelt, P. K. (2008). Cone photoreceptors and potential UV vision in a subterranean insectivore, the European mole. *Journal of Vision, 8*

Goldsmith, T. H., Collins, J. S., & Licht, S. (1984). The cone oil droplets of avian retinas. *Vision Research, 24*, 1661-1671

Gonzalez-Soriano, J., Mayayo-Vicente, S., Martinez-Sainz, P., Contreras-Rodriguez, J., & Rodriguez-Veiga, E. (1997). A quantitative study of ganglion cells in the goat retina. *Anatomia, Histologia, Embryologia, 26*, 39-44

Goszczyński, J. (1974). Studies on the food of foxes. *Acta Theriologica, 19*, 1-18

Gould, J. L. (2008). Animal navigation: the evolution of magnetic orientation. *Current Biology, 18*, R482-R484

Gourevitch, G. (1980). Directional hearing in terrestrial mammals. In A. N. Popper & R. R. Fay (Eds.), *Comparative studies of hearing in vertebrates* (pp. 357-373). New York: Springer.

Gray, A. A. (1907). *The Labyrinth of Animals. Including Mammals, Birds, Reptiles and Amphibians. [With Plates and a Hand Stereoscope.]*. London: J. & A. Churchill.

Green, S. (1975). Auditory sensitivity and equal loudness in the squirrel monkey (*Saimiri sciureus*). *Journal of the Experimental Analysis of Behavior, 23*, 255-264

Greenwood, D. D. (1961). Critical bandwidth and the frequency coordinates of the basilar membrane. *The Journal of the Acoustical Society of America, 33*, 1344-1356

Greenwood, D. D. (1974). Critical bandwidth in man and some other species in relation to the traveling wave envelope. In H. R. Moskowitz, B. Scharf & J. C. Stevens (Eds.), *Sensation and Measurement* (pp. 231-239). Dordrecht, NL: D. Reidel Publishing.

Greenwood, D. D. (1990). A cochlear frequency-position function for several species - 29 years later. *Journal of the Acoustical Society of America, 87*, 2592-2605

Guild, S. R. (1921). A graphic reconstruction method for the study of the organ of Corti. *The Anatomical Record, 22*, 140-157

Guinan, J. J., & Peake, W. T. (1967). Middle-ear characteristics of anesthetized cats. *The Journal of the Acoustical Society of America, 41*, 1237-1261

Hacker, H. P., & Pearson, H. S. (1951). Distribution of the long-tailed field mouse, *Apodemus sylvaticus*, on South Haven Peninsula, Dorset, in 1937, with some observations on its wandering and homing powers. *Journal of the Linnean Society of London, Zoology, 42*, 1-17

Haegerstrom-Portnoy, G., Hewlett, S., & Barr, S. N. (1989). S Cone Loss with Aging. In B. Drum & G. Verriest (Eds.), *Colour Vision Deficiencies IX* (Vol. 52, pp. 345-352): Springer Netherlands.

Hanzlik, M., Heunemann, C., Holtkamp-Rötzler, E., Winklhofer, M., Petersen, N., & Fleissner, G. (2000). Superparamagnetic magnetite in the upper beak tissue of homing pigeons. *Biometals, 13*, 325-331

Harman, A., Dann, J., Ahmat, A., Macuda, T., Johnston, K., & Timney, B. (2001). The retinal ganglion cell layer and visual acuity of the camel. *Brain, Behavior and Evolution, 58*, 15-27

Harris, S. (1981). The food of suburban foxes (*Vulpes vulpes*), with special reference to London. *Mammal Review, 11*, 151-168

Harris, S., & Smith, G. (1987). Demography of two urban fox (*Vulpes vulpes*) populations. *Journal of Applied Ecology*, 75-86

Harrison, J. M., & Downey, P. (1970). Intensity changes at the ear as a function of the azimuth of a tone source: A comparative study. *The Journal of the Acoustical Society of America, 47*, 1509-1518

Hart, V., Malkemper, E. P., Kušta, T., Begall, S., Nováková, P., Hanzal, V., Pleskač, L., Ježek, M., Policht, R., Husinec, V., Červený, J., & Burda, H. (2013). Directional compass preference for landing in water birds. *Frontiers in Zoology, 10*, 38

Hart, V., Nováková, P., Malkemper, E. P., Begall, S., Hanzal, V., Ježek, M., Kušta, T., Němcová, V., Adámková, J., Benediktová, K., Červený, J., & Burda, H. (2013). Dogs are sensitive to small variations of the Earth's magnetic field. *Frontiers in Zoology, 10*, 80

Hartová-Nentvichová, M., Anděra, M., & Hart, V. (2010). Cranial ontogenetic variability, sex ratio and age structure of the red fox. *Central European Journal of Biology, 5*, 894-907

Haverkamp, S., Wässle, H., Duebel, J., Kuner, T., Augustine, G. J., Feng, G., & Euler, T. (2005). The primordial, blue-cone color system of the mouse retina. *The Journal of Neuroscience, 25*, 5438-5445

Hebel, R. (1976). Distribution of retinal ganglion cells in five mammalian species (pig, sheep, ox, horse, dog). *Anatomy and Embryology, 150*, 45-51

Heesy, C. P., & Hall, M. I. (2010). The nocturnal bottleneck and the evolution of mammalian vision. *Brain, Behavior and Evolution, 75*, 195-203

Heffner, H., & Heffner, R. (1981). Functional interaural distance and high-frequency hearing in the elephant. *The Journal of the Acoustical Society of America, 70*, 1794-1795

Heffner, H., & Heffner, H. E. (2010). The behavioral audiogram of whitetail deer (*Odocoileus virginianus*). *The Journal of the Acoustical Society of America, 127*, 111-114

Heffner, H. E. (1983). Hearing in large and small dogs: Absolute thresholds and size of the tympanic membrane. *Behavioral Neuroscience, 97*, 310-318

Heffner, H. E., & Heffner, R. S. (1992a). Auditory perception. *Farm Animals and the Environment*, 159-184

Heffner, H. E., & Heffner, R. S. (1995). Conditioned avoidance. In G. M. Klump, R. J. Dooling, R. R. Fay & W. C. Stebbins (Eds.), *Biomethods* (Vol. 6, pp. 79-79). Basel: Birkhäuser.

Heffner, H. E., & Heffner, R. S. (2008a). High-frequency hearing. In P. Dallos & D. Oertel (Eds.), *The Senses: A Comprehensive Reference* (Vol. 3: Audition, pp. 55-60). Amsterdam: Elsevier.

Heffner, H. E., & Heffner, R. S. (2008b). Audition. In S. F. Davis (Ed.), *Handbook of Research Methods in Experimental Psychology* (pp. 413-440). Malden, MA: Blackwell.

Heffner, H. E., & Heffner, R. S. (2014). The behavioral study of mammalian hearing. In A. N. Popper & R. R. Fay (Eds.), *Perspectives on Auditory Research* (pp. 269-285). New York: Springer.

Heffner, R. S., & Heffner, H. E. (1985a). Hearing in mammals: the least weasel. *Journal of Mammalogy, 66*, 745-755

Heffner, R. S., & Heffner, H. E. (1985b). Hearing range of the domestic cat. *Hearing Research, 19*, 85-88

Heffner, R. S., & Heffner, H. E. (1988a). Sound localization acuity in the cat - effect of azimuth, signal duration, and test procedure. *Hearing Research, 36*, 221-232

Heffner, R. S., & Heffner, H. E. (1988b). Sound localization in a predatory rodent, the northern grasshopper mouse (*Onychomys leucogaster*). *Journal of Comparative Psychology, 102*, 66-71

Heffner, R. S., & Heffner, H. E. (1990). Hearing in domestic pigs (*Sus scrofa*) and goats (*Capra hircus*). *Hearing Research, 48*, 231-240

Heffner, R. S., & Heffner, H. E. (1992b). Evolution of sound localization in mammals. In D. B. Webster, R. R. Fay & A. N. Popper (Eds.), *The Evolutionary Biology of Hearing* (pp. 691-715). New York: Springer.

Heffner, R. S., & Heffner, H. E. (1992c). Visual factors in sound localization in mammals. *The Journal of Comparative Neurology, 317*, 219-232

Heffner, R. S., Heffner, H. E., & Koay, G. (1995). Sound localization in chinchillas. II. Front/back and vertical localization. *Hearing Research, 88*, 190-198

Heffner, R. S., Koay, G., & Heffner, H. E. (2001). Audiograms of five species of rodents: implications for the evolution of hearing and the perception of pitch. *Hearing Research, 157*, 138-152

Heffner, R. S., Koay, G., & Heffner, H. E. (2013). Hearing in American leaf-nosed bats. IV: The Common vampire bat, *Desmodus rotundus*. *Hearing Research, 296*, 42-50

Heffner, R. S., Koay, G., & Heffner, H. E. (2014). Hearing in alpacas (*Vicugna pacos*): Audiogram, localization acuity, and use of binaural locus cues. *The Journal of the Acoustical Society of America, 135*, 778-788

Heinz, G. H., & Gysel, L. W. (1970). Vocalization behavior of the ring-necked pheasant. *The Auk, 87*, 279-295

Hellström, S., & Stenfors, L.-E. (1983). The pressure equilibrating function of pars flaccida in middle ear mechanics. *Acta Physiologica Scandinavica, 118*, 337-341

Hemilä, S., Nummela, S., & Reuter, T. (1995). What middle ear parameters tell about impedance matching and high frequency hearing. *Hearing Research, 85*, 31-44

Henbest, K. B., Kukura, P., Rodgers, C. T., Hore, P., & Timmel, C. R. (2004a). Radio frequency magnetic field effects on a radical recombination reaction: a diagnostic test for the radical pair mechanism. *Journal of the American Chemical Society, 126*, 8102-8103

Henbest, K. B., Kukura, P., Rodgers, C. T., Hore, P. J., & Timmel, C. R. (2004b). Radio frequency magnetic field effects on a radical recombination reaction: a diagnostic test for the radical pair mechanism. *Journal of the American Chemical Society, 126*, 8102-8103

Henderson, Z. (1985). Distribution of ganglion cells in the retina of adult pigmented ferret. *Brain Research, 358*, 221-228

Henry, J. D. (1996). *Red Fox: The Catlike Canine.* Washington: Smithsonian Institution Press.

Henson, M. M., & Henson Jr, O. W. (1991). Specializations for sharp tuning in the mustached bat: The tectorial membrane and spiral limbus. *Hearing Research, 56*, 122-132

Hewson, R., & Kolb, H. H. (1975). The food of foxes (*Vulpes vulpes*) in Scottish forests. *Journal of Zoology, 176*, 287-292

Heyers, D., Zapka, M., Hoffmeister, M., Wild, J. M., & Mouritsen, H. (2010). Magnetic field changes activate the trigeminal brainstem complex in a migratory bird. *Proceedings of the National Academy of Sciences, 107*, 9394-9399

Hockman, J. G., & Chapman, J. A. (1983). Comparative feeding habits of red foxes (*Vulpes vulpes*) and gray foxes (*Urocyon cinereoargenteus*) in Maryland. *American Midland Naturalist, 110*, 276-285

Holland, R. A., Kirschvink, J. L., Doak, T. G., & Wikelski, M. (2008). Bats use magnetite to detect the Earth's magnetic field. *PLoS ONE, 3*, e1676

Horst, G. T. J. v. d., Muijtjens, M., Kobayashi, K., Takano, R., Kanno, S.-i., Takao, M., Wit, J. d., Verkerk, A., Eker, A. P. M., Leenen, D. v., Buijs, R., Bootsma, D., Hoeijmakers, J. H. J., & Yasui, A. (1999). Mammalian Cry1 and Cry2 are essential for maintenance of circadian rhythms. *Nature, 398*, 627-630

Hughes, A. (1975). A quantitative analysis of the cat retinal ganglion cell topography. *The Journal of Comparative Neurology, 163*, 107-128

Hughes, A. (1977). The topography of vision in mammals of contrasting life style: comparative optics and retinal organisation. In F. Crescitelli (Ed.), *Handbook of Sensory Physiology* (Vol. VII/5, pp. 613-756). New York: Springer.

Hughes, A. (1979). A schematic eye for the rat. *Vision Research, 19*, 569-588

Hunt, D. M., & Peichl, L. (2014). S cones: Evolution, retinal distribution, development, and spectral sensitivity. *Visual Neuroscience, 31*, 115-138

ICNIRP guidelines for limiting exposure to time-varying electric, magnetic, and electromagnetic fields (up to 300 GHz). 74 C.F.R. (1998).

Igarashi, M., Alford, B. R., Cohn, A. M., Saito, R., & Watanabe, T. (1972). Inner ear anomalies in dogs. *The Annals of otology, rhinology, and laryngology, 81*, 249-255

Isley, T. E., & Gysel, L. W. (1975). Sound-source localization by the red fox. *Journal of Mammalogy, 56*, 397-404

ISO. (1961). Normal equal-loudness level contours. *International Organization for Standardization, Switzerland, R. 226*

IUCN/SSC Canid Specialist Group. (2004). *Canids: Foxes, Wolves, Jackals and Dogs. Status Survey and Conservation Action Plan.* Gland, Switzerland and Cambridge, UK: IUCN Publications Services Unit.

Jackson, L. L., Heffner, R. S., & Heffner, H. E. (1999). Free-field audiogram of the Japanese macaque (*Macaca fuscata*). *The Journal of the Acoustical Society of America, 106*, 3017-3023

Jacobs, G., & Deegan, J., II. (1992). Cone photopigments in nocturnal and diurnal procyonids. *Journal of Comparative Physiology A, 171*, 351-358

Jacobs, G. H. (1992). Ultraviolet vision in vertebrates. *American Zoologist, 32*, 544-554

Jacobs, G. H. (1993). The distribution and nature of colour vision among the mammals. *Biological Reviews, 68*, 413-471

Jacobs, G. H., Deegan, J. F., Crognale, M. A., & Fenwick, J. A. (1993). Photopigments of dogs and foxes and their implications for canid vision. *Visual Neuroscience, 10*, 173-173

Jacobs, G. H., Neitz, M., Deegan, J. F., & Neitz, J. (1996). Trichromatic colour vision in New World monkeys. *Nature, 382*, 156-158

Jacobson, S. G., Franklin, K. B. J., & McDonald, W. I. (1976). Visual acuity of the cat. *Vision Research, 16*, 1141-1143

Jamon, M., & Bovet, P. (1987). Possible use of environmental gradients in orientation by homing wood mice, *Apodemus sylvaticus*. *Behavioural Processes, 15*, 93-107

Janko, C., Schröder, W., Linke, S., & König, A. (2012). Space use and resting site selection of red foxes (*Vulpes vulpes*) living near villages and small towns in Southern Germany. *Acta Theriologica, 57*, 245-250

Jankowiak, L., & Tryjanowski, P. (2013). Cooccurence and food niche overlap of two common predators (red fox *Vulpes vulpes* and common buzzard *Buteo buteo*) in an agricultural landscape. *Turkish Journal of Zoology, 37*, 157-162

Jerison, H. J. (1973). *Evolution of the Brain and Intelligence*. New York: Academic Press.

Juliusson, B., Bergström, A., Röhlich, P., Ehinger, B., van Veen, T., & Szél, A. (1994). Complementary cone fields of the rabbit retina. *Investigative Ophthalmology & Visual Science, 35*, 811-818

Kalmijn, A. J., & Blakemore, R. P. (1978). The magnetic behavior of mud bacteria. In K. Schmidt-Koenig & W. T. Keeton (Eds.), *Animal Migration, Navigation and Homing* (pp. 354 -355.). Berlin, Heidelberg, New York: Springer Verlag.

Kandel, E. R., Schwartz, J. H., Jessell, T. M., Siegelbaum, S. A., & Hudspeth, A. J. (2013). *Principles of Neural Science 5th Edn*. New York: McGraw-Hill.

Keen, J. A. (1939). A note on the comparative size of the cochlear canal in mammals. *Journal of Anatomy, 73*, 592

Keen, J. A., & Grobbelaar, C. S. (1941). The comparative anatomy of the tympanic bulla and auditory ossicles, with a note suggesting their function. *Transactions of the Royal Society of South Africa, 28*, 307-329

Kelber, A., Vorobyev, M., & Osorio, D. (2003). Animal colour vision - behavioural tests and physiological concepts. *Biological Reviews, 78*, 81-118

Kelly, J. B., Kavanagh, G. L., & Dalton, J. C. (1986). Hearing in the ferret *Mustela putorius*: Thresholds for pure tone detection. *Hearing Research, 24*, 269-275

Kermack, D. M., & Kermack, K. A. (1984). *The Evolution of Mammalian Characters*. London: Croom Helm.

Ketten, D. R. (2000). Cetacean Ears. In W. W. L. Au, A. N. Popper & R. R. Fay (Eds.), *Hearing by Whales and Dolphins* (pp. 43-108). New York: Springer.

Khanna, S. M., & Tonndorf, J. (1972). Tympanic membrane vibrations in cats studied by time-averaged holography. *The Journal of the Acoustical Society of America, 51*, 1904-1920

Kikuchi, T., Kimura, R. S., Paul, D. L., Takasaka, T., & Adams, J. C. (2000). Gap junction systems in the mammalian cochlea. *Brain Research Reviews, 32*, 163-166

Kimchi, T., & Terkel, J. (2001). Magnetic compass orientation in the blind mole rat *Spalax ehrenbergi*. *Journal of Experimental Biology, 204*, 751-758

Kirschvink, J. L. (1992). Uniform magnetic fields and double wrapped coil systems: Improved techniques for the design of bioelectromagnetic experiments. *Bioelectromagnetics, 13*, 401-411

Kirschvink, J. L., & Gould, J. L. (1981). Biogenic magnetite as a basis for magnetic field detection in animals. *Biosystems, 13*, 181-201

Kirschvink, J. L., & Walker, M. M. (1985). Particle-size considerations for magnetite-based magnetoreceptors. In J. L. Kirschvink, D. S. Jones & B. J. MacFadden (Eds.), *Magnetite Biomineralization and Magnetoreception in Organisms* (pp. 243-256). New York: Plenum Press.

Kirschvink, J. L., Walker, M. M., & Diebel, C. E. (2001). Magnetite-based magnetoreception. *Current Opinion in Neurobiology, 11*, 462-467

Kirschvink, J. L., Winklhofer, M., & Walker, M. M. (2010). Biophysics of magnetic orientation: strengthening the interface between theory and experimental design. *Journal of the Royal Society Interface, 7*, S179-S191

Kirschvink, J. L., Kobayashi-Kirschvink, A., Diaz-Ricci, J., & Kirschvink, S. J. (1992). Magnetite in human tissues: A mechanism for the biological effects of weak ELF magnetic fields. *Bioelectromagnetics Supplement, 1*, 101–114

Kirschvink, J. L., Kuwajima, T., Ueno, S., Kirschvink, S. J., Diaz-Ricci, J. C., Morales, A., Barwig, S., & Quinn, K. (1992). Discrimination of low-frequency magnetic fields by honeybees: Biophysics and experimental tests. In D. P. Corey & S. D. Roper (Eds.), *Sensory Transduction* (pp. 225-240.). New York: Society of General Physiologists, 45th Annual Symposium, Rockefeller University Press.

Klump, G. M., Dooling, R. J., Fay, R. R., & Stebbins, W. C. (1995). *Methods in Comparative Psychoacoustics* (Vol. 6). Basel, Boston, Berlin: Birkhäuser.

Koay, G., Heffner, R. S., Bitter, K. S., & Heffner, H. E. (2003). Hearing in American leaf-nosed bats. II: *Carollia perspicillata*. *Hearing Research, 178*, 27-34

Kohllöffel, L. (1984). Notes on the comparative mechanics of hearing. III. On Shrapnell's membrane. *Hearing Research, 13*, 83-88

König, A. (2008). Fears, attitudes and opinions of suburban residents with regards to their urban foxes. *European Journal of Wildlife Research, 54*, 101-109

Konishi, M. (1973). How the owl tracks its prey: Experiments with trained barn owls reveal how their acute sense of hearing enables them to catch prey in the dark. *American Scientist, 61*, 414-424

Kretzberg, J., & Ernst, U. (2013). Vision. In C. G. Galizia & P.-M. Lledo (Eds.), *Neurosciences - From Molecule to Behavior: A University Textbook* (pp. 363-407). Berlin Heidelberg: Springer.

Kryger, Z., Galli-Resta, L., Jacobs, G. H., & Reese, B. E. (1998). The topography of rod and cone photoreceptors in the retina of the ground squirrel. *Visual Neuroscience, 15*, 685-691

Kurokawa, H., & Goode, R. L. (1995). Sound pressure gain produced by the human middle ear. *Otolaryngology - Head and Neck Surgery, 113*, 349

Labhardt, F. (1996). *Der Rotfuchs* (2nd ed.). Hamburg: Paul Parey.

Lambert, N., De Liberato, S., Emary, C., & Nori, F. (2013). Radical-pair model of magnetoreception with spin-orbit coupling. *New Journal of Physics, 15*, 083024

Land, M. F., & Nilsson, D.-E. (2012). *Animal Eyes*. New York: Oxford University Press.

Larivière, S., & Pasitschniak-Arts, M. (1996). *Vulpes vulpes*. *Mammalian Species, 537*, 1-11

Lauwers, M., Pichler, P., Edelman, Nathaniel B., Resch, Guenter P., Ushakova, L., Salzer, Marion C., Heyers, D., Saunders, M., Shaw, J., & Keays, David A. (2013). An iron-rich organelle in the cuticular plate of avian hair cells. *Current Biology, 23*, 924-929

Le, T., & Keithley, E. M. (2007). Effects of antioxidants on the aging inner ear. *Hearing Research, 226*, 194-202

Leask, M. J. M. (1977). A physiochemical mechanism for magnetic field detection by migratory birds and homing pigeons. *Nature, 267*, 144–145

Lee, A. A., Lau, J. C. S., Hogben, H. J., Biskup, T., Kattnig, D. R., & Hore, P. J. (2014). Alternative radical pairs for cryptochrome-based magnetoreception. *Journal of the Royal Society Interface, 11*

LePage, E. L. (2003). The mammalian cochlear map is optimally warped. *The Journal of the Acoustical Society of America, 114*, 896-906

Lerchl, A., Nonaka, K. O., & Reiter, R. J. (1991). Pineal gland "magnetosensitivity" to static magnetic fields is a consequence of induced electric currents (eddy currents). *Journal of Pineal Research, 10*, 109-116

Lettmann, R. (2013). *Entwicklung und Validierung einer Versuchsapparatur zur Erstellung von Verhaltensaudiogrammen kleiner Karnivoren.* State examination, University of Duisburg-Essen, Essen.

Lever, R. J. A. W. (1959). The diet of the fox since myxomatosis. *Journal of Animal Ecology, 28*, 359-375

Liberman, M. C. (1982). The cochlear frequency map for the cat: Labeling auditory-nerve fibers of known characteristic frequency. *The Journal of the Acoustical Society of America, 72*, 1441-1449

Liberman, M. C., & Beil, D. G. (1979). Hair cell condition and auditory nerve response in normal and noise-damaged cochleas. *Acta Oto-Laryngologica, 88*, 161-176

Liberman, M. C., Gao, J., He, D. Z. Z., Wu, X., Jia, S., & Zuo, J. (2002). Prestin is required for electromotility of the outer hair cell and for the cochlear amplifier. *Nature, 419*, 300-304

Liboff, A. R., & Jenrow, K. A. (2000). New model for the avian magnetic compass. *Bioelectromagnetics, 21*, 555-565

Liedvogel, M., & Mouritsen, H. (2010). Cryptochromes—a potential magnetoreceptor: what do we know and what do we want to know? *Journal of the Royal Society Interface, 7*, S147-S162

Linberg, K. A., Lewis, G. P., Shaaw, C., Rex, T. S., & Fisher, S. K. (2001). Distribution of S- and M-cones in normal and experimentally detached cat retina. *The Journal of Comparative Neurology, 430*, 343-356

Lipman, E. A., & Grassi, J. R. (1942). Comparative auditory sensitivity of man and dog. *The American Journal of Psychology, 55*, 84-89

Lloyd, H. G. (1980). *The Red Fox*. London: BT Batsford.

Lobarinas, E., Salvi, R., & Ding, D. (2013). Insensitivity of the audiogram to carboplatin induced inner hair cell loss in chinchillas. *Hearing Research, 302*, 113-120

Long, G. R. (1994). Psychoacoustics. In R. R. Fay & A. N. Popper (Eds.), *Comparative Hearing: Mammals* (Vol. 4, pp. 18-56). New York: Springer.

Lowenstam, H. A. (1962). Magnetite in denticle capping in recent chitons (Polyplacophora). *Geological Society of America Bulletin, 73*, 435–438

Lukáts, Á., Szabó, A., Röhlich, P., Vigh, B., & Szél, A. (2005). Photopigment coexpression in mammals: comparative and developmental aspects. *Histology and Histopathology, 20*, 551-574

Lukáts, Á., Dkhissi-Benyahya, O., Szepessy, Z., Röhlich, P., Vígh, B., Bennett, N. C., Cooper, H. M., & Szél, Á. (2002). Visual pigment coexpression in all cones of two rodents, the Siberian hamster, and the pouched mouse. *Investigative Ophthalmology & Visual Science, 43*, 2468-2473

Madden, R. C., & Phillips, J. B. (1987). An attempt to demonstrate magnetic compass orientation in two species of mammals. *Learning & Behavior, 15*, 130-134

Mair, I. (1976). Hereditary deafness in the Dalmatian dog. *European Archives of Oto-Rhino-Laryngology, 212*, 1-14

Malmström, T., & Kröger, R. H. (2006). Pupil shapes and lens optics in the eyes of terrestrial vertebrates. *Journal of Experimental Biology, 209*, 18-25

Manger, P. R., Pillay, P., Maseko, B. C., Bhagwandin, A., Gravett, N., Moon, D.-J., Jillani, N., & Hemingway, J. (2009). Acquisition of brains from the African elephant (*Loxodonta africana*): Perfusion-fixation and dissection. *Journal of Neuroscience Methods, 179*, 16-21

Manley, G. A., & Johnstone, B. M. (1974). Middle-ear function in the guinea pig. *The Journal of the Acoustical Society of America, 56*, 571-576

Mann, D. A., Lu, Z., & Popper, A. N. (1997). A clupeid fish can detect ultrasound. *Nature, 389*, 341-341

Mann, D. A., Higgs, D. M., Tavolga, W. N., Souza, M. J., & Popper, A. N. (2001). Ultrasound detection by clupeiform fishes. *The Journal of the Acoustical Society of America, 109*, 3048-3054

Marhold, S., Wiltschko, W., & Burda, H. (1997a). A magnetic polarity compass for direction finding in a subterranean mammal. *Naturwissenschaften, 84*, 421-423

Marhold, S., Burda, H., Kreilos, I., & Wiltschko, W. (1997b). *Magnetic orientation in common mole-rats from Zambia.* Paper presented at the RIN 97 Orientation & Navigation - Birds, Humans and Other Animals, Oxford University.

Marhold, S., Beiles, A., Burda, H., & Nevo, E. (2000). Spontaneous directional preference in a subterranean rodent, the blind mole-rat, *Spalax ehrenbergi*. *Folia Zoologica, 49*, 7-18

Marimuthu, G., & Neuweiler, G. (1987). The use of acoustical cues for prey detection by the Indian false vampire bat, *Megaderma lyra*. *Journal of Comparative Physiology A, 160*, 509-515

Mason, M. J. (2001). Middle ear structures in fossorial mammals: a comparison with non-fossorial species. *Journal of Zoology, 255*, 467-486

Masterton, B., Heffner, H., & Ravizza, R. (1969). The evolution of human hearing. *The Journal of the Acoustical Society of America, 45*, 966-985

Mather, J. G. (1985). Magnetoreception and the search for magnetic material in rodents. In J. L. Kirschvink, D. S. Jones & B. J. MacFadden (Eds.), *Magnetite Biomineralization and Magnetoreception in Organisms* (pp. 509-533). New York: Plenum Press.

Mather, J. G., & Baker, R. R. (1981). Magnetic sense of direction in woodmice for route-based navigation. *Nature, 291*, 152-155

McCall, M. J., Robinson, S. R., & Dreher, B. (1987). Differential retinal growth appears to be the primary factor producing the ganglion cell density gradient in the rat. *Neuroscience Letters, 79*, 78-84

Mitchell, D. E., Giffin, F., Wilkinson, F., Anderson, P., & Smith, M. L. (1976). Visual resolution in young kittens. *Vision Research, 16*, 363-366

Mohl, B. (1968). Auditory sensitivity of the common seal in air and water. *Journal of Auditory Research, 81*, 27-38

Møller, A. R. (1963). Transfer function of the middle ear. *The Journal of the Acoustical Society of America, 35*, 1526-1534

Møller, A. R. (2006). *Hearing: Anatomy, Physiology, and Disorders of the Auditory System* (2nd ed.). London, UK: Academic press.

Møller, A. R. (2013). *Hearing: Anatomy, Physiology, and Disorders of the Auditory System* (3rd ed.). San Diego, CA, USA: Plural Publishing, Incorporated.

Mooney, M. P., Kraus, E. M., Bardach, J., & Snodgass, J. I. (1982). Skull preparation using the enzyme-active detergent technique. *The Anatomical Record, 202*, 125-129

Moore, P. W. B., & Schusterman, R. J. (1987). Audiometric assessment of northern fur seals, *Callorhinus ursinus*. *Marine Mammal Science, 3*, 31-53

Mora, C. V., Davison, M., Wild, J. M., & Walker, M. M. (2004). Magnetoreception and its trigeminal mediation in the homing pigeon. *Nature, 432*, 508-511

Moritz, R. E., Burda, H., Begall, S., & Němec, P. (2007). Magnetic compass: A useful tool underground. In S. Begall, B. H. & S. C. E. (Eds.), *Subterranean Rodents - News from Underground:* (pp. 161-174). Heidelberg: Springer.

Mowat, F. M., Petersen-Jones, S. M., Williamson, H., Williams, D. L., Luthert, P. J., Ali, R. R., & Bainbridge, J. W. (2008). Topographical characterization of cone photoreceptors and the area centralis of the canine retina. *Molecular Vision, 14*, 2518-2527

Muheim, R., Edgar, N. M., Sloan, K. A., & Phillips, J. B. (2006). Magnetic compass orientation in C57BL/6J mice. *Learning & Behavior, 34*, 366-373

Müller, B., & Peichl, L. (1989). Topography of cones and rods in the tree shrew retina. *The Journal of Comparative Neurology, 282*, 581-594

Müller, H. (1861). Ueber das ausgedehnte Vorkommen einer dem gelben Fleck der Retina entsprechenden Stelle bei Thieren. *Wurzburger naturwissenschaftliche Zeitschrift, 2*, 139-140

Müller, M., Laube, B., Burda, H., & Bruns, V. (1992). Structure and function of the cochlea in the African mole rat *(Cryptomys hottentotus*): evidence for a low frequency acoustic fovea. *Journal of Comparative Physiology A, 171*, 469-476

Müller, P., & Ahmad, M. (2011). Light-activated cryptochrome reacts with molecular oxygen to form a flavin-superoxide radical pair consistent with magnetoreception. *Journal of Biological Chemistry, 286*, 21033-21040

Mulsow, J., Finneran, J. J., & Houser, D. S. (2011). California sea lion (*Zalophus californianus*) aerial hearing sensitivity measured using auditory steady-state response and psychophysical methods. *The Journal of the Acoustical Society of America, 129*, 2298-2306

Nadol Jr, J. B. (1988). Comparative anatomy of the cochlea and auditory nerve in mammals. *Hearing Research, 34*, 253-266

Nedzelnitsky, V. (1980). Sound pressures in the basal turn of the cat cochlea. *The Journal of the Acoustical Society of America, 68*, 1676-1689

Neff, W. D., & Hind, J. E. (1955). Auditory thresholds of the cat. *The Journal of the Acoustical Society of America, 27*, 480-483

Němec, P., Altmann, J., Marhold, S., Burda, H., & Oelschlager, H. H. A. (2001). Neuroanatomy of magnetoreception: The superior colliculus involved in magnetic orientation in a mammal. *Science, 294*, 366-368

Newton-Fisher, N., Harris, S., White, P., & Jones, G. (1993). Structure and function of red fox *Vulpes vulpes* vocalisations. *Bioacoustics, 5*, 1-31

Nießner, C., Denzau, S., Stapput, K., Ahmad, M., Peichl, L., Wiltschko, W., & Wiltschko, R. (2013). Magnetoreception: activated cryptochrome 1a concurs with magnetic orientation in birds. *Journal of the Royal Society Interface, 10*, 20130638

Nießner, C., Denzau, S., Gross, J. C., Peichl, L., Bischof, H. J., Fleissner, G., Wiltschko, W., & Wiltschko, R. (2011). Avian ultraviolet/violet cones identified as probable magnetoreceptors. *PLoS ONE, 6*, e20091

Nowak, R. M. (1999). *Walker's Mammals of the World* (6th ed.). Baltimore, MD: The Johns Hopkins University Press.

Nummela, S. (1995). Scaling of the mammalian middle ear. *Hearing Research, 85*, 18-30

Nummela, S., & Sánchez-Villagra, M. R. (2006). Scaling of the marsupial middle ear and its functional significance. *Journal of Zoology, 270*, 256-267

Nummela, S., Pihlström, H., Puolamäki, K., Fortelius, M., Hemilä, S., & Reuter, T. (2013). Exploring the mammalian sensory space: co-operations and trade-offs among senses. *Journal of Comparative Physiology A, 199*, 1077-1092

Nuttall, A. L. (1974). Tympanic muscle effects on middle-ear transfer characteristic. *The Journal of the Acoustical Society of America, 56*, 1239-1247

Olcese, J. (1990). The neurobiology of magnetic field detection in rodents. *Progress in Neurobiology, 35*, 325-330

Olcese, J., Reuss, S., & Vollrath, L. (1985). Evidence for the involvement of the visual system in mediating magnetic field effects on pineal melatonin synthesis in the rat. *Brain Research, 333*, 382-384

Olcese, J., Reuss, S., Stehle, J., Steinlechner, S., & Vollrath, L. (1988). Responses to the mammalian retina to experimental alteration of the ambient magnetic field. *Brain Research, 448*, 325–330

Oliveriusová, L., Němec, P., Králová, Z., & Sedláček, F. (2012). Magnetic compass orientation in two strictly subterranean rodents: learned or species-specific innate directional preference? *Journal of Experimental Biology, 215*, 3649-3654

Oliveriusová, L., Němec, P., Pavelková, Z., & Sedláček, F. (2014). Spontaneous expression of magnetic compass orientation in an epigeic rodent: the bank vole, *Clethrionomys glareolus*. *Naturwissenschaften, in press*

Olson, C. R., & Freeman, R. D. (1980). Rescaling of the retinal map of visual space during growth of the kitten's eye. *Brain Research, 186*, 55-65

Olson, E. S. (1998). Observing middle and inner ear mechanics with novel intracochlear pressure sensors. *The Journal of the Acoustical Society of America, 103*, 3445-3463

Österholm, H. (1964). The significance of distance receptors in the feeding behaviour of the fox: *Vulpes vulpes* L. *Acta Zoologica Fennica, 106*, 1-31

Overstreet, E. H., & Ruggero, M. A. (2002). Development of wide-band middle ear transmission in the Mongolian gerbil. *The Journal of the Acoustical Society of America, 111*, 261-270

Painter, M. S., Dommer, D. H., Altizer, W. W., Muheim, R., & Phillips, J. B. (2013). Spontaneous magnetic orientation in larval *Drosophila* shares properties with learned magnetic compass responses in adult flies and mice. *Journal of Experimental Biology, 216*, 1307-1316

Pang, X. D., & Peake, W. T. (1986). How do contractions of the stapedius muscle alter the acoustic properties of the ear? In J. B. Allen, J. L. Hall, A. E. Hubbard, S. T. Neely & A. Tubis (Eds.), *Peripheral Auditory Mechanisms* (Vol. 64, pp. 36-43). Berlin Heidelberg: Springer.

Payne, R. S. (1971). Acoustic location of prey by barn owls (*Tyto alba*). *Journal of Experimental Biology, 54*, 535-573

Peichl, L. (1992). Topography of ganglion cells in the dog and wolf retina. *The Journal of Comparative Neurology, 324*, 603-620

Peichl, L. (1997). Die Augen der Säugetiere: Unterschiedliche Blicke in die Welt. *Biologie in Unserer Zeit, 27*, 96-105

Peichl, L. (2005). Diversity of mammalian photoreceptor properties: Adaptations to habitat and lifestyle? *The Anatomical Record A, 287*, 1001-1012

Peichl, L., & Moutairou, K. (1998). Absence of short-wavelength sensitive cones in the retinae of seals (Carnivora) and African giant rats (Rodentia). *European Journal of Neuroscience, 10*, 2586-2594

Peichl, L., Künzle, H., & Vogel, P. (2000). Photoreceptor types and distributions in the retinae of insectivores. *Visual Neuroscience, 17*, 937-948

Peichl, L., Behrmann, G., & Kroeger, R. H. (2001). For whales and seals the ocean is not blue: a visual pigment loss in marine mammals. *European Journal of Neuroscience, 13*, 1520-1528

Peterson, E. A., Heaton, W. C., & Wruble, S. D. (1969). Levels of auditory response in fissiped carnivores. *Journal of Mammalogy, 50*, 566-578

Pettigrew, J. D., Dreher, B., Hopkins, C. S., McCall, M. J., & Brown, M. (1988). Peak density and distribution of ganglion cells in the retinae of microchiropteran bats: Implications for visual acuity (Part 1 of 2). *Brain, Behavior and Evolution, 32*, 39-47

Phillips, J., & Deutschlander, M. (1997a). Magnetoreception in terrestrial vertebrates: implications for possible mechanisms of EMF interaction with biological systems. *The melatonin hypothesis: Electric power and the risk of breast cancer*, 111-172

Phillips, J. B. (1986a). Magnetic compass orientation in the eastern red-spotted newt (*Notophthalmus viridescens*). *Journal of Comparative Physiology A, 158*, 103-109

Phillips, J. B. (1986b). Two magnetoreception pathways in a migratory salamander. *Science, 233*, 765-767

Phillips, J. B., & Borland, S. C. (1992). Behavioural evidence for use of a light-dependent magnetoreception mechanism by a vertebrate. *Nature, 359*, 142-144

Phillips, J. B., & Deutschlander, M. E. (1997b). Magnetoreception in terrestrial vertebrates: Implications for possible mechanisms of EMF interaction with biological systems. In R. G. Stevens, L. E. Andrews & B. W. Wilson (Eds.), *The Melatonin Hypothesis: Electric Power and the Risk of Breast Cancer* (pp. 111‑172.). Columbus, OH: Battelle Press.

Phillips, J. B., Muheim, R., & Jorge, P. E. (2010). A behavioral perspective on the biophysics of the light-dependent magnetic compass: a link between directional and spatial perception? *Journal of Experimental Biology, 213*, 3247-3255

Phillips, J. B., Youmans, P. W., Muheim, R., Sloan, K. A., Landler, L., Painter, M. S., & Anderson, C. R. (2013). Rapid learning of magnetic compass direction by C57BL/6 mice in a 4-armed 'plus' water maze. *PLoS ONE, 8*, e73112

Pratt, H., & Sohmer, H. (1978). Comparison of hearing threshold determined by auditory pathway electric responses and by behavioural responses. *International Journal of Audiology, 17*, 285-292

Presti, D., & Pettigrew, J. D. (1980). Ferromagnetic coupling to muscle receptors as a basis for geomagnetic field sensitivity in animals. *Nature, 285*, 99-101

Puria, S., Peake, W. T., & Rosowski, J. J. (1997). Sound-pressure measurements in the cochlear vestibule of human-cadaver ears. *The Journal of the Acoustical Society of America, 101*, 2754-2770

Puria, S., & Allen, J. B. (1998). Measurements and model of the cat middle ear: evidence of tympanic membrane acoustic delay. *The Journal of the Acoustical Society of America, 104*, 3463-3481

Rapaport, D. H., Sesma, M. A., & Rowe, M. H. (1979). Distribution and central projections of ganglion cells in the retina of the gray fox (*Urocyon cinereoargenteus*) (Vol. 5, pp. 804): Society for Neuroscience.

Raslear, T. G. (1974). The use of the cochlear microphonic response as an indicant of auditory sensitivity: review and evaluation. *Psychological Bulletin, 81*, 791-803

Retzius, G. (1884). *Das Gehörorgan der Wirbelthiere: morphologisch-histologische Studien. 2, Das Gehörorgan der Reptilien, der Vögel und der Säugethiere*. Stockholm: Samson & Wallin.

Reuss, S., & Olcese, J. (1986). Magnetic field effects on rat pineal gland: role of retinal activation by light. *Neuroscience Letters, 64*, 97–101

Riedelsheimer, B., Wegerhoff, R., van den Boom, F., & Welsch, U. (2010). *Romeis - Mikroskopische Technik*. Heidelberg: Spektrum Akademischer Verlag.

Ritz, T., Adem, S., & Schulten, K. (2000). A model for photoreceptor-based magnetoreception in birds. *Biophysical Journal, 78*, 707-718

Ritz, T., Thalau, P., Phillips, J. B., Wiltschko, R., & Wiltschko, W. (2004). Resonance effects indicate a radical-pair mechanism for avian magnetic compass. *Nature, 429*, 177-180

Ritz, T., Ahmad, M., Mouritsen, H., Wiltschko, R., & Wiltschko, W. (2010). Photoreceptor-based magnetoreception: optimal design of receptor molecules, cells, and neuronal processing. *Journal of the Royal Society Interface, 7*, 135-146

Ritz, T., Wiltschko, R., Hore, P. J., Rodgers, C. T., Stapput, K., Thalau, P., Timmel, C. R., & Wiltschko, W. (2009). Magnetic compass of birds is based on a molecule with optimal directional sensitivity. *Biophysical Journal, 96*, 3451-3457

Rodgers, C. T., & Hore, P. J. (2009). Chemical magnetoreception in birds: the radical pair mechanism. *Proceedings of the National Academy of Sciences, 106*, 353-360

Roemer, G. W., Donlan, C. J., & Courchamp, F. (2002). Golden eagles, feral pigs, and insular carnivores: How exotic species turn native predators into prey. *Proceedings of the National Academy of Sciences, 99*, 791-796

Rosowski, J. J. (1991). The effects of external-and middle-ear filtering on auditory threshold and noise-induced hearing loss. *The Journal of the Acoustical Society of America, 90*, 124-135

Rosowski, J. J. (1992). Hearing in transitional mammals: predictions from the middle-ear anatomy and hearing capabilities of extant mammals. In D. B. Webster, R. R. Fay & A. N. Popper (Eds.), *The Evolutionary Biology of Hearing* (pp. 615-631). New York: Springer.

Rosowski, J. J. (1994). Outer and middle ears. In R. R. Fay & A. N. Popper (Eds.), *Comparative Hearing: Mammals* (Vol. 4, pp. 172-247). New York: Springer.

Rosowski, J. J. (2010). External and middle ear function. In P. A. Fuchs (Ed.), *Oxford Handbook of Auditory Science: The Ear* (pp. 49-91). New York: OUP Oxford.

Rosowski, J. J. (2013). Comparative middle ear structure and function in vertebrates. In S. Puria, R. R. Fay & A. N. Popper (Eds.), *The Middle Ear* (Vol. 46, pp. 31-65). New York: Springer.

Rosowski, J. J., & Graybeal, A. (1991). What did *Morganucodon* hear? *Zoological Journal of the Linnean Society, 101*, 131-168

Roth, G. (2013). *The Long Evolution of Brains and Minds*. New York: Springer.

Ruggero, M. A., & Temchin, A. N. (2002). The roles of the external, middle, and inner ears, in determining the bandwidth of hearing. *Proceedings of the National Academy of Science, 99*, 13206-13210

Ruggero, M. A., & Temchin, A. N. (2003). Middle-ear transmission in humans: wide-band, not frequency-tuned? *Acoustics Research Letters Online, 4*, 53-58

Salih, W. H. M., Buytaert, J. A. N., Aerts, J. R. M., Vanderniepen, P., Dierick, M., & Dirckx, J. J. J. (2012). Open access high-resolution 3D morphology models of cat, gerbil, rabbit, rat and human ossicular chains. *Hearing Research, 284*, 1-5

Sancar, A. (2000). Cryptochrome: the second photoactive pigment in the eye and its role in circadian photoreception. *Annual Review of Biochemistry, 69*, 31-67

Sato, M., Leake, P. A., & Hradek, G. T. (1999). Postnatal development of the organ of Corti in cats: a light microscopic morphometric study. *Hearing Research, 127*, 1-13

Sauvé, J. P. (1988). Analyse de l'orientation initiale dans une expérience de retour au gîte chez le mulot, *Apodemus sylvaticus*. *Sciences et Techniques de l'Animal de Laboratoire, 13*, 89-91

Scammon, R. E., & Armstrong, E. L. (1925). On the growth of the human eyeball and optic nerve. *The Journal of Comparative Neurology, 38*, 165-219

Schiviz, A. N., Ruf, T., Kuebber-Heiss, A., Schubert, C., & Ahnelt, P. K. (2008). Retinal cone topography of artiodactyl mammals: influence of body height and habitat. *The Journal of Comparative Neurology, 507*, 1336-1350

Schleich, C. E., & Busch, C. (2004). Functional morphology of the middle ear of *Ctenomys talarum* (Rodentia: Octodontidae). *Journal of Mammalogy, 85*, 290-295

Schmidt, R. S., & Fernandez, C. (1963). Development of mammalian endocochlear potential. *Journal of Experimental Zoology, 153*, 227-235

Schuknecht, H. F. (1953). Techniques for study of cochlear function and pathology in experimental animals *AMA Archives of Otolaryngology, 58*, 377-397

Schuknecht, H. F., Icarashi, M., & Gacek, R. R. (1965). The pathological types of cochleo-saccular degeneration. *Acta Oto-Laryngologica, 59*, 154-170

Schulten, K., Swenberg, C., & Weller, A. (1978). A biomagnetic sensory mechanism based on the geminate recombination of radical ion pairs in solvents. *Zeitschrift für Physikalische Chemie, NF101*, 371-390

Schulten, K., Staerk, H., Weller, A., Werner, H., & Nickel, B. (1976). Magnetic field dependence of the geminate recombination of radical ion pairs in polar solvents. *Zeitschrift für Physikalische Chemie. NF101*, 371–390

Schultze, M. (1866). Zur Anatomie und Physiologie der Retina. *Archiv für mikroskopische Anatomie, 2*, 175-286

Sewell, G. D. (1968). Ultrasound in rodents. *Nature, 217*, 682-683

Shaw, E. A. G. (1974). The external ear. In W. D. Keidel & W. D. Neff (Eds.), *Auditory System* (Vol. 5/1, pp. 455-490). Berlin Heidelberg: Springer.

Shcherbakov, V. P., & Winklhofer, M. (2010). Theoretical analysis of flux amplification by soft magnetic material in a putative biological magnetic-field receptor. *Physical Review E, 81*, 031921

Sidorovich, V., Sidorovich, A. A., & Izotova, I. V. (2006). Variations in the diet and population density of the red fox *Vulpes vulpes* in the mixed woodlands of northern Belarus. *Mammalian Biology, 71*, 74-89

Sivian, L., & White, S. (1933). On minimum audible sound fields. *The Journal of the Acoustical Society of America, 4*, 288-321

Slepecky, N. B. (1996). Structure of the mammalian cochlea. In P. Dallos, A. N. Popper & R. R. Fay (Eds.), *The Cochlea* (Vol. 8, pp. 44-129). New York: Springer.

Slonaker, J. R. (1897). A comparative study of the area of acute vision in vertebrates. *Journal of Morphology, 13*, 445-502

Smith, J. (1970). Conditioned suppression as an animal psychophysical technique. In W. C. Stebbins (Ed.), *Animal Psychophysics: The Design and Conduct of Sensory Experiments* (pp. 125-159). New York: Appleton-Century-Crofts.

Solov'yov, I. A., & Schulten, K. (2009). Magnetoreception through cryptochrome may involve superoxide. *Biophysical Journal, 96*, 4804-4813

Solov'yov, I. A., Mouritsen, H., & Schulten, K. (2010). Acuity of a cryptochrome and vision-based magnetoreception system in birds. *Biophysical Journal, 99*, 40-49

Solov'yov, I. A., & Greiner, W. (2007). Theoretical analysis of an iron mineral-based magnetoreceptor model in birds. *Biophysical Journal, 93*, 1493-1509

Solovei, I., Kreysing, M., Lanctôt, C., Kösem, S., Peichl, L., Cremer, T., Guck, J., & Joffe, B. (2009). Nuclear architecture of rod photoreceptor cells adapts to vision in mammalian evolution. *Cell, 137*, 356-368

Spoendlin, H. (1985). Anatomy of cochlear innervation. *American Journal of Otolaryngology, 6*, 453-467

Stansbury, A., Thomas, J., Stalf, C., Murphy, L., Lombardi, D., Carpenter, J., & Mueller, T. (2014). Behavioral audiogram of two Arctic foxes (*Vulpes lagopus*). *Polar Biology, 37*, 417-422

Stebbins, W. C. (1980). The evolution of hearing in the mammals. In A. N. Popper & R. R. Fay (Eds.), *Comparative studies of hearing in vertebrates* (pp. 421-436). New York: Springer.

Stebbins, W. C., Brown, C. H., & Petersen, M. R. (1984). Sensory function in animals. *Comprehensive Physiology, Supplement 3*, 123-148

Steinberg, R. H., Reid, M., & Lacy, P. L. (1973). The distribution of rods and cones in the retina of the cat (*Felis domesticus*). *The Journal of Comparative Neurology, 148*, 229-248

Stevens, M. (2013). *Sensory Ecology, Behaviour, and Evolution*. Oxford: Oxford University Press.

Stone, J. (1965). A quantitative analysis of the distribution of ganglion cells in the cat's retina. *The Journal of Comparative Neurology, 124*, 337-352

Stone, J. (1978). The number and distribution of ganglion cells in the cat's retina. *The Journal of Comparative Neurology, 180*, 753-771

Stone, J. (1981). *The Whole Mount Handbook: A Guide to the Preparation and Analysis of Retinal Whole Mounts*. Sydney: Maitland Publications.

Stoneham, A. M., Gauger, Erik M., Porfyrakis, K., Benjamin, Simon C., & Lovett, Brendon W. (2012). A new type of radical-pair-based model for magnetoreception. *Biophysical Journal, 102*, 961-968

Stopka, P., & MacDonald, D. W. (2003). Way-marking behaviour: an aid to spatial navigation in the wood mouse (*Apodemus sylvaticus*). *BMC Ecology, 3: 3*

Storm, G. L., Andrews, R. D., Phillips, R. L., Bishop, R. A., Siniff, D. B., & Tester, J. R. (1976). Morphology, reproduction, dispersal, and mortality of midwestern red fox populations. *Wildlife Monographs, 49*, 3-82

Szél, Á., Röhlich, P., Caffé, A. R., & van Veen, T. (1996). Distribution of cone photoreceptors in the mammalian retina. *Microscopy Research and Technique, 35*, 445-462

Szél, Á., Csorba, G., Caffé, A. R., Szél, G., Röhlich, P., & Veen, T. (1994). Different patterns of retinal cone topography in two genera of rodents, *Mus* and *Apodemus*. *Cell and Tissue Research, 276*, 143-150

Tembrock, G. (1963). Mischlaute beim Rotfuchs (*Vulpes vulpes* L.). *Zeitschrift fur Tierpsychologie, 20*, 616-623

Tembrock, G., Helmcke, J.-G., & Kükenthal, W. (1957). *Das Verhalten des Rotfuchses.* Berlin: De Gruyter.

Temple, S. E. (2011). Why different regions of the retina have different spectral sensitivities: A review of mechanisms and functional significance of intraretinal variability in spectral sensitivity in vertebrates. *Visual Neuroscience, 28*, 281-293

Tew, T. E., & MacDonald, D. W. (1994). Dynamics of space use and male vigour amongst wood mice, *Apodemus sylvaticus*, in the cereal ecosystem. *Behavioral Ecology and Sociobiology, 34*, 337-345

Thalau, P., Ritz, T., Burda, H., Wegner, R. E., & Wiltschko, R. (2006). The magnetic compass mechanisms of birds and rodents are based on different physical principles. *Journal of the Royal Society Interface, 3*, 583-587

Thalau, T., Ritz, T., Burda, H., Stapput, K., Moritz, R. E., Wiltschko, R., & Wiltschko, W. (2008). *The magnetic compass mechanisms of birds and mammals are based on different physical principles.* Paper presented at the RIN 08 Orientation & Navigation Birds Humans & Other Animals, Reading University UK.

Tonndorf, J., & Khanna, S. M. (1970). The role of the tympanic membrane in middle ear transmission. *The Annals of otology, rhinology, and laryngology, 79*, 743-753

Tonndorf, J., & Khanna, S. M. (1972). Tympanic-membrane vibrations in human cadaver ears studied by time-averaged holography. *The Journal of the Acoustical Society of America, 52*, 1221-1233

Treiber, C. D., Salzer, M. C., Riegler, J., Edelman, N., Sugar, C., Breuss, M., Pichler, P., Cadiou, H., Saunders, M., Lythgoe, M., Shaw, J., & Keays, D. A. (2012). Clusters of iron-rich cells in the upper beak of pigeons are macrophages not magnetosensitive neurons. *Nature, 484*, 367-370

Ulehlová, L., Burda, H., & Voldřich, L. (1984). Involution of the auditory neuro-epithelium in a tiger (*Panthera tigris*) and a jaguar (*Panthera onca*). *Journal of Comparative Pathology*, 94, 153-157

Ullmann, J. F., Moore, B. A., Temple, S. E., Fernández-Juricic, E., & Collin, S. P. (2012). The retinal wholemount technique: a window to understanding the brain and behaviour. *Brain, Behavior and Evolution, 79*, 26-44

Vácha, M., Půžová, T., & Kvíćalová, M. (2009). Radio frequency magnetic fields disrupt magnetoreception in American cockroach. *Journal of Experimental Biology, 212*, 3473-3477

Vakkur, G. J., & Bishop, P. O. (1963). The schematic eye in the cat. *Vision Research, 3*, 357-381

Vakkur, G. J., Bishop, P. O., & Kozak, W. (1963). Visual optics in the cat, including posterior nodal distance and retinal landmarks. *Vision Research, 3*, 289-314

Van Dijk, T. (1972). A comparative study of hearing in owls of the family Strigidae. *Netherlands Journal of Zoology, 23*, 131-167

Vater, M., & Kössl, M. (2011). Comparative aspects of cochlear functional organization in mammals. *Hearing Research, 273*, 89-99

Veilleux, C. C., & Kirk, E. C. (2014). Visual acuity in mammals: effects of eye size and ecology. *Brain, Behavior and Evolution, 83*, 43-53

von Békésy, G. (1960). *Experiments in Hearing*. New York: McGraw-Hill.

von Helmholtz, H. (1863). *Die Lehre von den Tonempfindungen als physiologische Grundlage für die Theorie der Musik*. Braunschweig: Vieweg.

von Helmholtz, H. (1868). Die Mechanik der Gehörknöchelchen und des Trommelfells. *Pflügers Archiv European Journal of Physiology, 1*, 1-60

Voss, S. E., Rosowski, J. J., & Peake, W. T. (1996). Is the pressure difference between the oval and round windows the effective acoustic stimulus for the cochlea? *The Journal of the Acoustical Society of America, 100*, 1602-1616

Vrettakos, P. A., Dear, S. P., & Saunders, J. C. (1988). Middle ear structure in the chinchilla: A quantitative study. *American Journal of Otolaryngology, 9*, 58-67

Walcott, C., Gould, J. L., & Kirschvink, J. L. (1979). Pigeons have magnets. *Science., 205*, 1027-1028

Walker, M. M., Dennis, T. E., & Kirschvink, J. L. (2002). The magnetic sense and its use in long-distance navigation by animals. *Current Opinion in Neurobiology, 12*, 735-744

Wang, Y., Pan, Y., Parsons, S., Walker, M., & Zhang, S. (2007). Bats respond to polarity of a magnetic field. *Proceedings of the Royal Society of London B, 274*, 2901-2904

Wang, Y., Macke, J. P., Merbs, S. L., Zack, D. J., Klaunberg, B., Bennett, J., Gearhart, J., & Nathans, J. (1992). A locus control region adjacent to the human red and green visual pigment genes. *Neuron, 9*, 429-440

Wässle, H., & Boycott, B. B. (1991). Functional architecture of the mammalian retina. *Physiological Reviews, 71*, 447-480

Wässle, H., Levick, W. R., & Cleland, B. G. (1975). The distribution of the alpha type of ganglion cells in the cat's retina. *The Journal of Comparative Neurology, 159*, 419-437

Wässle, H., Boycott, B. B., & Illing, R.-B. (1981). Morphology and mosaic of on-and off-beta cells in the cat retina and some functional considerations. *Proceedings of the Royal Society of London B, 212*, 177-195

Wässle, H., Grünert, U., Röhrenbeck, J., & Boycott, B. B. (1990). Retinal ganglion cell density and cortical magnification factor in the primate. *Vision Research, 30*, 1897-1911

Webster, D. B. (1962). A function of the enlarged middle-ear cavities of the kangaroo rat, *Dipodomys*. *Physiological Zoology, 3*, 248-255

Webster, D. B., & Webster, M. (1972). Kangaroo rat auditory thresholds before and after middle ear reduction. *Brain, Behavior and Evolution, 5*, 41-53

Wegner, R. E., Begall, S., & Burda, H. (2006). Magnetic compass in the cornea: local anaesthesia impairs orientation in a mammal. *Journal of Experimental Biology, 209*, 4747-4750

Welker, H. A., Semm, P., Willig, R. P., Commentz, J. C., Wiltschko, W., & Vollrath, L. (1983). Effects of an artificial magnetic field on serotonin N-acetyltransferase activity and melatonin content in the rat pineal gland. *Experimental Brain Research, 50*, 426–432

West, C. D. (1985). The relationship of the spiral turns of the cochlea and the length of the basilar membrane to the range of audible frequencies in ground dwelling mammals. *The Journal of the Acoustical Society of America, 77*, 1091-1101

West, C. D., & Harrison, J. M. (1973). Transneuronal cell atrophy in the congenitally deaf white cat. *The Journal of Comparative Neurology, 151*, 377-398

West, R. W., & Dowling, J. E. (1975). Anatomical evidence for cone and rod-like receptors in the gray squirrel, ground squirrel, and prairie dog retinas. *The Journal of Comparative Neurology, 159*, 439-459

Wever, E. G., & Lawrence, M. (1950). The acoustic pathways to the cochlea. *The Journal of the Acoustical Society of America, 22*, 460-467

Wever, E. G., & Lawrence, M. (1954). *Physiological Acoustics*. Princeton: Princeton University Press.

Wever, E. G., McCormick, J. G., Palin, J., & Ridgway, S. H. (1971). The cochlea of the dolphin, *Tursiops truncatus*: General morphology. *Proceedings of the National Academy of Sciences, 68*, 2381-2385

Wiener, F. M., Pfeiffer, R. R., & Backus, A. S. N. (1966). On the sound pressure transformation by the head and auditory meatus of the cat. *Acta Oto-Laryngologica, 61*, 255-269

Wilkinson, F. (1986). Eye and brain growth in the mongolian gerbil (*Meriones unguiculatus*). *Behavioural Brain Research, 19*, 59-69

Willi, U. B., Ferrazzini, M. A., & Huber, A. M. (2002). The incudo-malleolar joint and sound transmission losses. *Hearing Research, 174*, 32-44

Williams, G. A., Calderone, J. B., & Jacobs, G. H. (2005). Photoreceptors and photopigments in a subterranean rodent, the pocket gopher (*Thomomys bottae*). *Journal of Comparative Physiology A, 191*, 125-134

Wiltschko, R., & Wiltschko, W. (1995). *Magnetic Orientation in Animals*. Berlin, Heidelberg, New York: Springer.

Wiltschko, R., & Wiltschko, W. (2010). Avian magnetic compass: Its functional properties and physical basis. *Current Zoology, 56*, 265-276

Wiltschko, R., & Wiltschko, W. (2012a). Magnetoreception. In C. López-Larrea (Ed.), *Sensing in Nature* (pp. 126-141). New York: Springer.

Wiltschko, R., & Wiltschko, W. (2012b). The magnetite-based receptors in the beak of birds and their role in avian navigation. *Journal of Comparative Physiology A, 199*, 89-98

Wiltschko, W., & Wiltschko, R. (1972). The magnetic compass of European robins. *Science, 176*, 62-64

Wiltschko, W., & Wiltschko, R. (2001). Light-dependent magnetoreception in birds: the behavior of European robins, *Erithacus rubecula*, under monochromatic light of various wavelengths. *The Journal of Experimental Biology, 204*, 3295-3302

Wiltschko, W., & Wiltschko, R. (2007). Magnetoreception in birds: two receptors for two different tasks. *Journal of Ornithology, 148*, 61-76

Wiltschko, W., Munro, U., Ford, H., & Wiltschko, R. (1993). Red light disrupts magnetic orientation of migratory birds. *Nature, 364*, 525 - 527

Wiltschko, W., Stapput, K., Thalau, P., & Wiltschko, R. (2006). Avian magnetic compass: fast adjustment to intensities outside the normal functional window. *Naturwissenschaften, 93*, 300-304

Wiltschko, W., Munro, U., Ford, H., & Wiltschko, R. (2009). Avian orientation: the pulse effect is mediated by the magnetite receptors in the upper beak. *Proceedings of the Royal Society B, 276*, 2227-2232

Winklhofer, M., & Kirschvink, J. L. (2010). A quantitative assessment of torque-transducer models for magnetoreception. *Journal of the Royal Society Interface, 7*, 273-289

Winklhofer, M., Dylda, E., Thalau, P., Wiltschko, W., & Wiltschko, R. (2013). Avian magnetic compass can be tuned to anomalously low magnetic intensities. *Proceedings of the Royal Society Biological Sciences Series B, 280*, 20130853

Wollack, C. H. (1965). Auditory thresholds in the raccoon (*Procyon lotor*). *Journal of Auditory Research, 5*, 139-144

Wolski, L. F., Anderson, R. C., Bowles, A. E., & Yochem, P. K. (2003). Measuring hearing in the harbor seal (*Phoca vitulina*): Comparison of behavioral and auditory brainstem response techniques. *The Journal of the Acoustical Society of America, 113*, 629-637

Wong, R. O. L., & Hughes, A. (1987). Developing neuronal populations of the cat retinal ganglion cell layer. *The Journal of Comparative Neurology, 262*, 473-495

Wu, L.-Q., & Dickman, J. á. (2011). Magnetoreception in an avian brain in part mediated by inner ear lagena. *Current Biology, 21*, 418-423

Wu, L.-Q., & Dickman, J. D. (2012). Neural correlates of a magnetic sense. *Science, 336*, 1054-1057

Yorke, E. D. (1979). A possible magnetic transducer in birds. *Journal of Theoretical Biology, 77*, 101-105

Zheng, J., Shen, W., He, D. Z. Z., Long, K. B., Madison, L. D., & Dallos, P. (2000). Prestin is the motor protein of cochlear outer hair cells. *Nature, 405*, 149-155

Zoeger, J., Dunn, J. R., & Fuller, M. (1981). Magnetic material in the head of the common Pacific dolphin. *Science, 213*, 892-894

Zwislocki, J. J. (1975). The role of the external and middle ear in sound transmission. In D. B. Tower (Ed.), *The nervous system* (Vol. 3, pp. 45-55). New York: Raven Press.

Figures

Tables

Solutions and chemicals

SOLUTIONS

Ethylenediamine tetraacetic acid (EDTA, 25 %, pH 8.0; Riedelsheimer et al., 2010):

- ⚐ dissolve 250 g EDTA in 200 ml aq. dest.

- ⚐ add 50 ml NaOH (40 %)

- ⚐ stir and heat

- ⚐ add up to 800 ml with aq. dest.

- ⚐ adjust pH to 8.0 with NaOH (40%); EDTA should now dissolve completely

- ⚐ add up to 1000 ml with aq. dest.

Ehrlich-haematoxylin (Riedelsheimer et al., 2010):

- ⚐ dissolve 4 g haematoxylin in 200 ml 96 % ethanol

- ⚐ dissolve 6 g potassium alum in 200 ml aq. dest. and boil the solution

- ⚐ add 200 ml glycerin to the warm potassium alum solution

- ⚐ add 20 ml glacial acetic acid

- ⚐ mix all solutions

- ⚐ wait two weeks for the solution to oxidize or add 0.35 g of sodium iodate as oxidant

Cresyl violet (Nissl):

- ⚐ dissolve 0.5 g cresyl violet in 500 ml aq. dest.

- ⚐ filtrate before usage

Eosin yellow (Riedelsheimer et al., 2010):

- ⚐ dissolve 0.2 g eosin Y in 200 ml aq. dest.

- ⚐ add two drops of glacial acetic acid

- ⚐ filtrate before usage

Gelatine coating of microscope slides (adapted from Riedelsheimer et al., 2010):

- dissolve 2 g gelatine (20 g for mounting of retinae) in 400 ml aq. dest. at 60 °C
- add 0.2 g chrome (III) potassium sulphate
- clean untreated microscope slides with 96 % ethanol
- dip the slides two times in the gelatine solution
- dry slides overnight at 37 °C

Nuclear fast red (Riedelsheimer et al., 2010)

- dissolve 10 g aluminium sulphate in boiling 200 ml aq. dest.
- add 0.2 g nuclear fast red
- cool down and filtrate before usage

4 % Paraformaldehyde (PFA) in 0.1 M PB:

- solute 40 g paraformaldehyde in 800 ml 0.1M PB at 60 °C
- add two to three pellets of NaOH until the solution clears
- add up to 1000 ml with 0.1M PB
- cool the solution down and filtrate
- check pH and adjust to 7.4 if necessary
- storage at -20 °C until usage

Phosphate buffer (PB) 0.1 M:

- stock 1:
  - dissolve 35.61 g $Na_2HPO_4 \bullet 2H_2O$ in 800 ml aq. dest.
  - aq. dest. ad 1000 ml
- stock 2:
  - dissolve 27.6 g $NaH_2PO_4 \bullet H_2O$ in 800 ml aq. dest.
  - aq. dest. ad 1000 ml
- 500 ml 0.2 M PB: mix 385 ml stock 1 with 115 ml stock 2

- 1000 ml 0.1 M PB: dilute 0.2 M PB 1:1 with aq. dest.

- check pH and adjust to 7.4 if necessary

- store for up to 6 months at 4 °C or add 0.05 % sodium azide

Phosphate buffered saline (PBS) 0.1 M:

- dissolve 40 g paraformaldehyde in 800 ml 0.1 M PB at 60 °C

- add two to three pellets of NaOH until the solution clears

- add up to 1000 ml with 0.1 M PB

- cool the solution down and filtrate

- check pH and adjust to 7.4 if necessary

- storage at -20 °C until usage

Prussian blue:

- mix equal amounts of 5 % HCl and 5 % potassium-hexacyanoferrate

- always prepare fresh before usage

Tris buffer 0.05 M:

- dissolve 121.1 g tris in 800 ml aq. dest.

- adjust pH to 7.6 with 37 % HCl (approximately 50 ml)

- add up to 1000 ml with aq. dest.

- dilute 1:20 to obtain the final concentration of 0.05 M

- store at 4 °C

CHEMICALS AND DISPOSABLES

Substance	Vendor
aluminium sulphate	Carl Roth, Karlsruhe, Germany
Aqua-poly mount	Polysciences Europe, Eppelheim, Germany
bovine serum albumin (BSA)	Sigma-Aldrich, St. Louis, USA
chrome (III) potassium sulphate	Merck, Darmstadt, Germany
cresyl violet	Chroma, Stuttgart, Germany

- 3,3'-diaminobenzidine — Carl Roth, Karlsruhe, Germany
- disodium hydrogen phosphate — Fluka, Buchs, Switzerland
- eosin Y — Chroma, Stuttgart, Germany
- filter paper — Whatman, Kent, UK
- gelatine — Merck, Darmstadt, Germany
- glacial acetic acid — Sigma-Aldrich, St. Louis, USA
- glycerol — Carl Roth, Karlsruhe, Germany
- goat-peroxidase anti-peroxidase — Sigma-Aldrich, St. Louis, USA
- haematoxylin — Merck, Darmstadt, Germany
- hydrochloric acide — Carl Roth, Karlsruhe, Germany
- hydrochloric acide
  (extra pure, for ironhistochemistry) — Fluka, Buchs, Switzerland
- hydrogen peroxide (H_2O_2) — Fluka, Buchs, Switzerland
- monosodium phosphate — Fluka, Buchs, Switzerland
- normal donkey serum — Sigma-Aldrich, St. Louis, USA
- normal goat serum — Sigma-Aldrich, St. Louis, USA
- nuclear fast red — Fluka, Buchs, Switzerland
- paraffin — Carl Roth, Karlsruhe, Germany
- paraformaldehyde — Fluka, Buchs, Switzerland
- potassium alum — Fluka, Buchs, Switzerland
- potassium-hexacyanoferrate — Carl Roth, Karlsruhe, Germany
- Roti Histokit° — Carl Roth, Karlsruhe, Germany
- Roti Mount Aqua — Carl Roth, Karlsruhe, Germany
- Roti Histol° — Carl Roth, Karlsruhe, Germany
- sodium hydroxide — Carl Roth, Karlsruhe, Germany
- sodium iodate — Carl Roth, Karlsruhe, Germany
- toluidine blue — Sigma-Aldrich, St. Louis, USA
- Triton-x 100 — Sigma-Aldrich, St. Louis, USA

Appendix

Table A1: General parameters of the sample specimens and outer ear metrics. In this and the following tables (up to A7), for each specimen, each upper and lower row represent the values obtained from the left ear and right ear, respectively. The mean is given in the next column.

Animal ID	Sex	Condylobasal length CBL (mm)	Zygomatic breadth ZGB (mm)	Age Index AI	Interaural distance IAD (mm)	Skull weight without lower jaw (g)	Pinna length (mm)	Pinna length mean (mm)	Pinna base width (mm)	Pinna base width mean (mm)
Mean		114.7	67.2	7991	40.9	42.3		48.4		30.7
SD		25.5	12.0	3029	3.5	14.1		15.2		3.8
n		52	52	52	29	25	14	7	14	7
VV1	female	77.4	54.3	4202.8						
VV2	male	81.4	56.0	4558.4						
VV3	female	78.8	53.7	4231.6						
VV4	male	78.7	48.8	3840.6						
VV5	female	75.8	51.5	3903.7						
VV6	female	93.5	56.8	5310.8						
VV7	male	93.6	57.7	5400.7			63.0 / 55.0	59.0	30.0 / 30.0	30.0
VV8	male	149.4	80.3	11996.8						
VV9	female	76.1	53.3	4056.1						
VV10	male	92.0	57.6	5299.2						
VV11		100.5	58.1	5839.1						
VV12		92.5	56.0	5180.0			64.0 / 60.0	62.0	36.0 / 35.0	35.5
VV13		94.0	60.0	5640.0						
VV14		99.0	58.9	5831.1						
VV15		86.2	53.1	4577.2						
VV16		83.5	52.8	4408.8						
VV18	female	139.6	80.5	11237.8						
VV26	female	73.0	45.8	3343.4			23.4 / 18.7	21.0	39.6 / 32.1	35.8
VV27	female	76.0	49.4	3754.4			40.5 / 39.6	40.0	27.8 / 25.4	26.6

Table A1 (continued): General parameters of the sample specimens and outer ear metrics.

Animal ID	Sex	Condylobasal length CBL (mm)	Zygomatic breadth ZGB (mm)	Age Index AI	Interaural distance IAD (mm)	Skull weight without lower jaw (g)	Pinna length (mm)	Pinna length mean (mm)	Pinna base width (mm)	Pinna base width mean (mm)
Mean		114.7	67.2	7991	40.9	42.3		48.4		30.7
SD		25.5	12.0	3029	3.5	14.1		15.2		3.8
n		52	52	52	29	25	14	7	14	7
VV28	male	78.6	49.0	3851.4			43.1 / 44.7	43.9	29.1 / 27.0	28.0
VV29	male	98.0	52.8	5174.4			43.8 / 52.7	48.3	27.9 / 26.9	27.4
VV30	female	110.0	59.1	6501.0			65.7 / 63.3	64.5	30.7 / 33.0	31.8
VVT1		134.2	78.6	10548.1	49.7					
VVT2		148.4	84.3	12510.1	48.3					
VVT3		136.3	78.0	10631.4	43.6					
VVT4		132.3	74.5	9856.4	45.8					
VVT5		139.8	77.8	10876.4	45.8					
VVT6		143.4	79.0	11328.6	39.6	57.7				
VVT7		145.8	83.4	12159.7	44.2	60.6				
VVT8		142.6	77.9	11108.5	39.8	54.7				
VVT9		143.3	82.0	11750.6	42.8	62.0				
VVT10		130.0	73.9	9607.0	39.8	40.4				
VVT11		144.0	79.2	11404.8	39.9	52.3				
VVT12		131.4	74.5	9789.3	38.3	40.1				
VVT13		144.7	82.1	11879.9	41.3	52.1				
VVT14		139.7	78.5	10966.5	42.2	48.8				
VVT15		134.4	75.4	10133.8	40.0	44.4				
VVT16		130.4	78.4	10223.4	40.2	38.9				

Table A1 (continued): General parameters of the sample specimens and outer ear metrics.

Animal ID	Sex	Condylobasal length CBL (mm)	Zygomatic breadth ZGB (mm)	Age Index AI	Interaural distance IAD (mm)	Skull weight without lower jaw (g)	Pinna length (mm)	Pinna length mean (mm)	Pinna base width (mm)	Pinna base width mean (mm)
Mean		114.7	67.2	7991	40.9	42.3		48.4		30.7
SD		25.5	12.0	3029	3.5	14.1		15.2		3.8
n		52	52	52	29	25	14	7	14	7
VVT17		138.0	77.9	10750.2	41.0	54.1				
VVT18		133.8	78.4	10489.9	39.9	54.4				
VVT19		142.8	82.8	11823.8	40.2	53.5				
VVT20		143.2	81.4	11656.5	41.2	54.9				
VVT21		142.9	83.7	11960.7	41.6	53.9				
M.5486	male	105.3	66.1	6960.3		20.0				
Z88/22		110.1	64.8	7134.5	37.9	25.4				
Z97/91	male	122.6	66.1	8103.9	40.1	31.8				
M.5626	female	127.9	70.1	8965.8	39.0	38.2				
M.58		116.9	67.6	7902.4	38.5	30.9				
Z88/22.1		103.9	64.5	6701.6	34.8	23.0				
E38/65		105.7	59.0	6236.3	36.4	18.4				
V88/21		108.4	62.3	6753.3	34.5	23.5				
V88/21.1		112.0	64.3	7201.6	38.8	23.8				

Table A2: Middle ear parameters and CBL of the sample specimens.

	Condylobasal length CBL (mm)	Diameter meatus at base (mm)	Diameter meatus mean (mm)	Bulla length (mm)	Bulla length mean (mm)	Bulla width (mm)	Bulla width mean (mm)	Bulla depth (mm)	Bulla depth mean (mm)	Bulla volume (mm³)	Bulla volume mean (mm³)	Area tympanic membrane (mm²)	Area TM mean (mm²)	Effective TM area (mm²)	Area oval window (mm²)
Mean	119.09		5.9		19.8		16.4		11.3		967.3		55.7	35.0	
SD	24.95		0.7		0.9		0.9		1.1		164.2		7.9	10.3	
n	43	50	26	74	38	72	38	74	38	72	38	31	16	17	56
Animal ID															
VV1	77.4			19.4	19.2	15.0	15.2	10.7	10.3	815	783	53.6	54.6	36.4	1.8
				19.0		15.4		9.8		751		55.6			
VV2	81.4	4.5	4.5	19.7	19.7	15.1	15.4	10.4	11.0	810	868	66.8	67.0	44.7	1.8
		4.4		19.6		15.7		11.5		926		67.3			
VV3	78.8	5.5	5.4	19.4	18.9	15.5	15.1	9.9	9.9	779	738	72.5	65.7	43.8	1.8
		5.2		18.4		14.6		9.9		696		58.8			
VV4	78.7	3.8	3.8	18.5	18.2	14.5	14.3	9.4	10.0	660	678	71.8	66.4	44.3	1.9
				17.8		14.1		10.6		696		61.0			
VV5	75.8			19.0	19.0	14.5	14.5	10.0	10.0	721	721	59.6	59.6	39.7	1.6
VV6	93.5			21.2	21.0	17.0	17.0	12.4	12.2	1170	1170	42.3	45.2	30.1	1.4
				20.8				11.9				48.0			
VV7	93.6	4.9	5.0	19.3	19.3	16.5	16.9	11.5	11.8	959	1004	49.6	64.5	43.0	2.0
		5.0		19.3		17.3		12.0		1049		79.3			
VV8	149.4			22.0	21.5	17.0	17.0	10.8	11.6	1054	1054	41.6	47.4	31.6	1.3
				21.0				12.4				53.2			
VV9	76.1	5.6	5.4	19.6	19.3	16.0	15.9	11.4	11.2	936	898	65.4	61.4	40.9	1.5
		5.2		18.9		15.8		11.0		860		57.4			
VV10	92			19.3	19.4	16.0	15.0	9.7	10.1	784	765	47.8	54.2	36.1	1.7
				19.4		14.0		10.5		747		60.6			
VV11	100.5			20.6	20.4	16.9	16.7	10.4	10.6	948	941	56.2	53.1	35.4	1.9
				20.2		16.5		10.7		934		49.9			
VV12	92.5	5.6	5.5	19.8	19.6	16.0	16.2	10.8	11.6	896	958	64.6	58.3	38.9	1.9
		5.4		19.3		16.3		12.4		1021		52.0			
VV13	94			19.4	20.0	17.5	17.5	11.2	11.2	995	1016	44.3	45.6	30.4	1.2
				20.5		17.4		11.1		1037		46.8			
VV14	99			21.0	21.0	17.5	17.7	11.4	11.3	1097	1095	41.6	47.8	31.8	1.2
				21.0		17.9		11.1		1092		54.0			
VV15	86.2			18.5	18.5	16.3	16.2	9.3	9.4	734	735	54.6	55.1	36.7	2.0
				18.4		16.1		9.5		737		55.5			
VV18	139.6			21.0	21.6	17.8	18.2	11.2	11.6	1093	1194	40.3	45.6	30.4	1.4
				22.2		18.6		12.0		1294		50.9			
VV30	110			21.1	21.1	15.7	15.6	12.3	12.1	1063	1041			0.0	2.0
				21.0		15.5		12.0		1019					
VVT1	134.2			20.2	20.4	17.2	17.3	14.4	14.4	1310	1319				1.5
				20.5		17.3		14.3		1328					
VVT2	148.4	7.0	6.6	21.6	21.9	17.4	17.4	14.5	14.2	1427	1412				
		6.2		22.2		17.3		13.9		1398					
VVT3	136.3	6.1	5.7	20.0	20.0	16.7	17.0	10.9	11.0	953	976				
		5.2		20.0		17.2		11.1		1000					
VVT4	132.3	6.6	6.2	19.9	19.9	17.6	17.2	11.3	11.0	1036	986				
		5.8		19.9		16.8		10.7		937					
VVT5	139.8	6.3	6.2	20.5	20.7	16.9	16.7	11.6	11.7	1052	1054				
		6.0		20.9		16.5		11.7		1056					
VVT6	143.4	5.9	6.1	20.0	19.8	17.0	16.5	12.1	11.9	1077	1019				1.8
		6.3		19.6		16.0		11.7		961					

Table A2 (continued): Middle ear parameters and CBL of the sample specimens.

Animal ID	Condylobasal length CBL (mm)	Diameter meatus at base (mm)	Diameter meatus mean (mm)	Bulla length (mm)	Bulla length mean (mm)	Bulla width (mm)	Bulla width mean (mm)	Bulla depth (mm)	Bulla depth mean (mm)	Bulla volume (mm³)	Bulla volume mean (mm³)	Area tympanic membrane (mm²)	Area TM mean (mm²)	Effective TM area (mm²)	Area oval window (mm²)
Mean	119.09		5.9		19.8		16.4		11.3		967.3		55.7	35.0	
SD	24.95		0.7		0.9		0.9		1.1		164.2		7.9	10.3	
n	43	50	26	74	38	72	38	74	38	72	38	31	16	17	56
VVT7	145.8	6.5 / 5.6	6.0	20.6 / 20.7	20.7	17.7 / 17.3	17.5	13.7 / 13.1	13.4	1308 / 1228	1268				
VVT8	142.6	7.2 / 6.3	6.8	19.0 / 20.0	19.5	16.3 / 17.0	16.7	11.6 / 10.6	11.1	941 / 944	942				
VVT9	143.3	6.7 / 6.7	6.7	20.1 / 19.9	20.0	16.0 / 16.5	16.3	12.8 / 11.9	12.4	1078 / 1023	1050				2.0
VVT10	130	6.1	6.1	19.0	19.0	16.0	16.0	12.1	12.1	963	963				2.0
VVT11	144	7.0 / 5.6	6.3	18.5 / 19.8	19.2	16.3 / 16.4	16.4	10.8 / 10.6	10.7	853 / 901	877				
VVT12	131.4	6.5 / 5.9	6.2	18.9 / 18.7	18.8	16.1 / 15.1	15.6	10.7 / 10.9	10.8	852 / 806	829				1.8
VVT13	144.7	6.2 / 5.4	5.8	20.6 / 20.9	20.8	16.8 / 17.2	17.0	12.4 / 12.2	12.3	1123 / 1148	1136				
VVT14	139.7	6.8 / 6.6	6.7	20.1 / 20.6	20.4	15.7 / 15.3	15.5	10.6 / 9.8	10.2	876 / 809	842				2.0
VVT15	134.4	7.0 / 5.8	6.4	19.9 / 18.8	19.4	15.5 / 16.1	15.8	10.9 / 10.8	10.9	880 / 856	868				2.0
VVT16	130.4	6.0 / 5.5	5.8	19.8 / 19.5	19.7	16.5 / 15.6	16.1	11.6 / 11.2	11.4	992 / 892	942				
VVT17	138	5.8 / 5.1	5.5	19.2 / 18.9	19.1	17.1 / 17.0	17.1	11.2 / 11.7	11.5	963 / 984	973				2.1
VVT18	133.8	6.5 / 5.7	6.1	18.8 / 18.9	18.9	16.7 / 15.9	16.3	10.8 / 10.8	10.8	888 / 850	869				1.8
VVT19	142.8	6.2 / 5.6	5.9	19.2 / 19.6	19.4	15.9 / 15.8	15.9	11.1 / 10.8	11.0	887 / 876	881				1.7
VVT20	143.2	5.8 / 5.6	5.7	19.6 / 20.2	19.9	16.5 / 16.4	16.5	10.3 / 11.0	10.7	872 / 954	913				
VVT21	142.9	5.8 / 6.4	6.1	20.0 / 19.8	19.9	16.9 / 17.0	17.0	11.0 / 11.1	11.1	973 / 978	976				
Z88/22	110.1														1.6
Z97/91	122.6														1.7
M.5626	127.9														
V88/21	108.4														1.8
V88/21.1	112														

Table A2 (continued): Middle ear parameters and CBL of the sample specimens.

	Condylobasal length CBL (mm)	Area OW mean (mm²)	Area round window (mm²)	Area RW mean (mm²)
Mean	119.09	1.8		2.3
SD	24.95	0.4		0.6
n	43	36	31	16
Animal ID				
VV1	77.4	1.8	2.1	2.4
VV2	81.4	1.7	2.5	2.2
VV3	78.8	2.0	1.9	1.8
VV4	78.7	2.1	1.6	1.6
VV5	75.8	1.7	2.0	2.2
VV6	93.5	0.0	3.1	3.1
VV7	93.6	2.0	2.4	2.8
VV8	149.4	1.4	2.4	2.2
VV9	76.1	1.7	1.8	1.8
VV10	92	1.7	1.6	1.4
VV11	100.5	2.1	2.3	2.3
VV12	92.5	2.0	2.6	3.4
VV13	94	1.5	2.1	2.4
VV14	99	1.1	3.2	3.2
VV15	86.2	2.1	2.7	2.8
VV18	139.6	1.5	1.7	1.7
VV30	110	2.0		
VVT1	134.2	1.5		
VVT2	148.4			
VVT3	136.3			
VVT4	132.3			
VVT5	139.8			
VVT6	143.4	1.8		

Table A2 (continued): Middle ear parameters and CBL of the sample specimens.

	Condylobasal length CBL (mm)	Area OW mean (mm²)	Area round window (mm²)	Area RW mean (mm²)
Mean	119.09	1.8		2.3
SD	24.95	0.4		0.6
n	43	36	31	16
Animal ID				
VVT7	145.8			
VVT8	142.6	2.0		
VVT9	143.3	2.1		
VVT10	130	2.0		
VVT11	144	2.0		
VVT12	131.4	1.9		
VVT13	144.7	1.8		
VVT14	139.7	2.0		
VVT15	134.4	2.0		
VVT16	130.4	2.0		
VVT17	138	2.1		
VVT18	133.8	1.8		
VVT19	142.8	1.7		
VVT20	143.2			
VVT21	142.9			
Z88/22	110.1	1.6		
Z97/91	122.6	1.7		
M.5626	127.9	1.6		
V88/21	108.4	1.8		
V88/21.1	112	1.9		

Table A3: Middle ear ossicle weight and CBL of the sample specimens.

Animal ID	Condylobasal length CBL (mm)	Malleus (mg)	Malleus mean (mg)	Incus (mg)	Incus mean (mg)	Stapes (mg)	Stapes mean (mg)
Mean	118.14		10.64		5.19		0.63
SD	24.10		1.18		0.63		0.13
n	47	71	41	82	47	31	25
VV1	77.4	8.681 / 8.434	8.557	4.285 / 4.230	4.257		
VV2	81.4	9.281 / 9.137	9.209	4.590 / 4.698	4.644		
VV3	78.8	9.128 / 9.086	9.107	4.220 / 4.253	4.236		
VV4	78.7	8.265 / 8.330	8.297	3.763 / 3.781	3.772		
VV5	75.8			3.732	3.732		
VV6	93.5			4.816	4.816		
VV7	93.6	10.571 / 10.766	10.668	4.905 / 4.846	4.876		
VV8	149.4			5.241	5.241	0.578	0.578
VV9	76.1	8.343 / 8.605	8.474	4.517 / 4.504	4.511	0.520	0.520
VV10	92	9.310 / 10.838	10.074	4.812 / 4.952	4.882		
VV11	100.5	9.944 / 10.007	9.975	5.318 / 5.217	5.267	0.486	0.486
VV12	92.5	8.527 / 8.700	8.613	4.886 / 4.975	4.930		
VV13	94	10.911 / 10.089	10.500	4.692 / 4.593	4.642		
VV14	99	9.713 / 9.684	9.698	4.915 / 4.859	4.887		
VV15	86.2	9.873	9.873	4.840 / 4.838	4.839		
VV18	139.6	12.397 / 12.461	12.429	5.578 / 5.485	5.532		
VV30	110	12.601 / 12.484	12.542	6.101 / 6.210	6.155	0.644	0.644
VVT1	134.2	10.833 / 11.478	11.155	5.553 / 5.631	5.592	0.621 / 0.640	0.630
VVT2	148.4	10.530	10.530	6.616 / 5.667	6.141		
VVT3	136.3	11.649 / 11.539	11.594	6.003 / 6.120	6.062	0.621	0.621
VVT4	132.3	11.742	11.742	5.709 / 5.727	5.718		
VVT5	139.8	11.253	11.253	5.760	5.760		
VVT6	143.4	10.171 / 11.712	10.941	5.226 / 5.139	5.182	0.599	0.599
VVT7	145.8	12.552 / 12.309	12.431	4.940 / 4.924	4.932		
VVT8	142.6	10.741 / 10.734	10.737	5.597 / 5.661	5.629	0.877	0.877
VVT9	143.3	12.615	12.615	6.086 / 6.116	6.101	0.898 / 0.786	0.842
VVT10	130	11.159	11.159	5.842	5.842	0.787	0.787

Table A3 (continued): Middle ear ossicle weight and CBL of the sample specimens.

	Condylobasal length CBL (mm)	Malleus (mg)	Malleus mean (mg)	Incus (mg)	Incus mean (mg)	Stapes (mg)	Stapes mean (mg)
Mean	118.14		10.64		5.19		0.63
SD	24.10		1.18		0.63		0.13
n	47	71	41	82	47	31	25
Animal ID							
VVT11	144			5.341 / 5.116	5.229	0.740	0.740
VVT12	131.4	9.862 / 9.873	9.867	5.409 / 5.462	5.435	0.575 / 0.561	0.568
VVT13	144.7	11.878 / 11.952	11.915	5.548 / 5.667	5.607	0.542	0.542
VVT14	139.7	11.165 / 10.907	11.036	5.453 / 5.134	5.293	0.624 / 0.580	0.602
VVT15	134.4	10.889 / 10.820	10.854	5.173 / 5.486	5.329	0.787	0.787
VVT16	130.4	10.833 / 10.901	10.867	5.590 / 5.604	5.597	0.805	0.805
VVT17	138	11.847 / 11.361	11.604	5.671 / 5.808	5.739	0.773	0.773
VVT18	133.8	11.120 / 10.908	11.014	5.009 / 5.027	5.018	0.548 / 0.675	0.612
VVT19	142.8	10.205 / 10.183	10.194	4.037 / 4.128	4.083	0.484 / 0.467	0.475
VVT20	143.2	12.004	12.004	6.279	6.279		
VVT21	142.9			5.371 / 5.432	5.401		
M.5486	105.3	11.608 / 11.752	11.680	5.642 / 5.689	5.666	0.713	0.713
Z88/22	110.1	10.462	10.462	6.176	6.176	0.531	0.531
Z97/91	122.6	11.896	11.896	5.840	5.840	0.612	0.612
M.5626	127.9	11.023 / 11.100	11.062	4.944 / 4.905	4.925		
M.58	116.9	10.467 / 10.416	10.442	5.062	5.062		
Z88/22.1	103.9	10.476	10.476	5.038	5.038		
E38/65	105.7	8.543 / 8.652	8.598	4.329 / 4.251	4.290	0.536	0.536
V88/21	108.4			4.957	4.957	0.440	0.440
V88/21.1	112	10.082	10.082	5.011	5.011	0.452	0.452

Table A4: Malleus measurements and CBL of the sample specimens.

Animal ID	Condylobasal length CBL (mm)	Manubrium (L1, pivot) (mm)	Manubrium (L1, pivot) mean (mm)	Manubrium (L1, axis) (mm)	Manubrium (L1, axis) mean (mm)	Anterior process (mm)	Anterior process mean (mm)	Lateral process (mm)	Lateral process mean (mm)
Mean	87.11		7.04		3.22		2.25		1.49
SD	8.86		0.31		0.38		0.25		0.11
n	14	58	35	51	34	61	39	63	39
VV1	77.4	6.91 6.77	6.84	2.91 3.02	2.96	2.20 2.24	2.22	1.53 1.56	1.55
VV2	81.4	7.12 7.09	7.11	 3.35	3.35	2.11 2.08	2.10	1.54 1.44	1.49
VV3	78.8	7.20 7.01	7.11	2.94 3.34	3.14	2.24 2.24	2.24	1.48 1.46	1.47
VV4	78.7	6.28 6.85	6.57	3.34 2.79	3.07	2.08 2.43	2.26	1.46 	1.46
VV5	75.8					2.00 	2.00	1.55 	1.55
VV6	93.5					1.92	1.92	1.31	1.31
VV7	93.6	6.84 7.26	7.05	3.48 3.44	3.46	2.18 2.24	2.21	1.43 1.40	1.42
VV9	76.1	6.66 6.50	6.58	 2.99	2.99	 2.06	2.06	1.55 1.47	1.51
VV10	92	6.80 6.63	6.72	3.31 	3.31	2.20 2.24	2.22	1.40 1.47	1.44
VV11	100.5	7.01 7.23	7.12	3.37 3.18	3.28	2.39 2.48	2.44	1.43 1.51	1.47
VV12	92.5	7.11 7.06	7.09	2.75 3.16	2.96	2.15 2.04	2.10	1.41 1.43	1.42
VV13	94	7.32 7.23	7.28	3.77 3.70	3.74	2.03 1.66	1.85	1.48 1.50	1.49
VV14	99	6.93 7.18	7.06	3.70 3.33	3.52	1.92 2.05	1.99	1.35 1.38	1.37
VV15	86.2	 7.26	7.26	 3.23	3.23	2.10 2.07	2.09	1.42 1.58	1.50
VV22		 6.57	6.57	 3.04	3.04	 2.40	2.40	 1.49	1.49
VV30	110	7.61 7.32	7.46	3.33 3.82	3.58	2.68 2.41	2.54	1.62 1.78	1.70
VVT1	134.2	 6.90	6.90	 2.81	2.81	 2.61	2.61	 1.68	1.68
VVT2	148.4	 6.35	6.35	 4.38	4.38	 2.29	2.29	 1.31	1.31
VVT3	136.3	7.25 7.16	7.21	3.24 2.98	3.11	2.22 2.01	2.12	1.34 1.35	1.35

Table A4 (continued): Malleus measurements and CBL of the sample specimens.

	Condylobasal length CBL (mm)	Manubrium (L1, pivot) (mm)	Manubrium (L1, pivot) mean (mm)	Manubrium (L1, axis) (mm)	Manubrium (L1, axis) mean (mm)	Anterior process (mm)	Anterior process mean (mm)	Lateral process (mm)	Lateral process mean (mm)
Mean	87.11		7.04		3.22		2.25		1.49
SD	8.86		0.31		0.38		0.25		0.11
n	14	58	35	51	34	61	39	63	39
Animal ID									
VVT5	139.8	6.65	6.65	2.75	2.75	1.83	1.83	1.54	1.54
VVT6	143.4					2.36	2.36	1.68	1.68
VVT7	145.8	7.67	7.67	3.64	3.64	2.49	2.49	1.63	1.63
VVT8	142.6	7.13 / 6.72	6.92	2.47 / 2.93	2.70	1.97 / 2.02	2.00	1.66 / 1.70	1.68
VVT12	131.4	7.05 / 7.13	7.09	3.07 / 3.15	3.11	2.31 / 2.45	2.38	1.56 / 1.55	1.55
VVT13	144.7	7.92 / 7.85	7.89	3.46 / 3.64	3.55	2.87 / 2.62	2.75	1.53 / 1.51	1.52
VVT14	139.7	7.31 / 7.06	7.19	3.32 / 3.56	3.44	2.34 / 2.36	2.35	1.44 / 1.53	1.49
VVT15	134.4	7.19 / 6.87	7.03	2.84	2.84	2.16	2.16	1.36 / 1.61	1.49
VVT16	130.4	6.97 / 7.06	7.02	3.45 / 3.38	3.41	2.53 / 2.52	2.52	1.60 / 1.46	1.53
VVT17	138	7.29	7.29			2.07	2.07	1.48	1.48
VVT18	133.8	6.69 / 6.71	6.70	2.73	2.73	1.91 / 1.77	1.84	1.37 / 1.25	1.31
VVT19	142.8	7.02 / 7.35	7.19	3.75	3.75	2.50	2.50	1.33 / 1.64	1.48
M.5486	105.3	7.20	7.20	3.10	3.10	2.27 / 2.54	2.41	1.67 / 1.39	1.53
Z88/22	110.1	6.75	6.75	3.12	3.12	2.27	2.27	1.47	1.47
Z97/91	122.6	7.30	7.30	3.28	3.28	2.80	2.80	1.35	1.35
M.5626	127.9	7.16	7.16	2.50	2.50	2.19	2.19	1.29	1.29
M.58	116.9	7.05 / 6.97	7.01	3.36 / 3.61	3.48	2.41 / 2.45	2.43	1.73 / 1.59	1.66
E38/65	105.7	7.05 / 7.22	7.13	3.32 / 3.22	3.27	2.30 / 2.16	2.23	1.37 / 1.60	1.48
V88/21	108.4					2.73	2.73	1.36	1.36
V88/21.1	112	7.09	7.09	2.78	2.78	1.93	1.93	1.64	1.64

Table A5: Incus and stapes measurements and CBL of the sample specimens.

Animal ID	Condylobasal length CBL (mm)	Crus breve (mm)	Crus breve mean (mm)	Crus longum (L2, pivot) (mm)	Crus longum (L2, pivot) mean (mm)	Crus longum (L2, axis) (mm)	Crus longum (L2, axis) mean (mm)	Stapes height (mm)	Stapes height mean (mm)	L1/L2	L1/L2 (Hemilä et al.)	ITR (Dallos 1973) using pivot lever arms	ITR (Dallos 1973) using axis lever arms
Mean	118.14		2.14		2.06		1.54		2.11	2.10	3.26	0.0044	0.0099
SD	24.10		0.19		0.12		0.15		0.15	0.26	0.23	0.0009	0.0023
n	47	79	47	79	47	80	47	36	26	34	29	13	13
VV1	77.4	2.06	2.13	2.08	2.07	1.44	1.49	1.94	1.92	1.989	3.322	0.0046	0.0127
		2.19		2.06		1.54		1.89			3.286		
VV2	81.4	2.00	2.09	2.01	2.03	1.43	1.52			2.211	3.542	0.0031	0.0079
		2.17		2.04		1.60					3.475		
VV3	78.8	2.15	2.16	2.12	2.13	1.41	1.52			2.073	3.396	0.0040	0.0105
		2.16		2.13		1.62					3.291		
VV4	78.7	1.75	1.81	2.08	2.11	1.32	1.33			2.305	3.019	0.0048	0.0087
		1.86		2.14		1.34					3.201		
VV5	75.8	2.12	2.12	2.03	2.03	1.35	1.35						
VV6	93.5	2.05	2.05	2.01	2.01	1.40	1.40						
VV7	93.6	2.17	2.12	2.09	2.16	1.37	1.41	1.87	1.92	2.454	3.273	0.0044	0.0078
		2.06		2.22		1.45		1.96			3.270		
VV8	149.4	1.94	1.94	2.09	2.09	1.36	1.36	2.16	2.16				
VV9	76.1	1.98	2.01	2.24	2.22	1.44	1.44			2.084	2.973	0.0047	0.0095
		2.03		2.20		1.43					2.955		
VV10	92	2.08	2.11	2.12	2.12	1.35	1.30			2.556	3.208	0.0048	0.0074
		2.14		2.12		1.24					3.127		
VV11	100.5	2.13	2.12	2.41	2.37	1.57	1.55	2.11	2.04	2.120	2.909	0.0066	0.0133
		2.11		2.32		1.52		1.96			3.116		
VV12	92.5	2.04	2.09	2.22	2.20	1.40	1.43			2.066	3.203	0.0051	0.0123
		2.14		2.17		1.46					3.253		
VV13	94	2.01	2.08	2.09	2.05	1.51	1.61			2.320	3.502	0.0038	0.0090
		2.15		2.00		1.71					3.615		
VV14	99	1.91	1.98	1.98	1.99	1.40	1.48			2.383	3.500	0.0028	0.0063
		2.05		1.99		1.55					3.608		
VV15	86.2	1.74	1.82	2.11	2.08	1.56	1.56	1.78	1.78	2.077		0.0046	0.0130
		1.89		2.05		1.55					3.541		
VV18	139.6		1.85		1.94	1.35	1.38			2.211		0.0042	0.0100
		1.85		1.94		1.40					3.387		
VV30	110	2.38	2.29	2.10	2.16	1.72	1.69	2.20	2.20	2.115			
		2.20		2.22		1.67							
VVT1	134.2	1.89	1.87	2.31	2.31	1.54	1.50	2.05	2.09	1.880			
		1.85		2.31		1.45		2.13			2.987		
VVT2	148.4	2.18	2.08	2.21	2.29	1.61	1.63			2.687			
		1.97		2.37		1.65					2.679		
VVT3	136.3	2.21	2.15	2.15	2.16	1.57	1.50			2.073	3.372		
		2.09		2.16		1.43					3.315		
VVT4	132.3	2.12	2.09	2.04	2.11	1.66	1.68						
		2.05		2.18		1.69							
VVT5	139.8		2.25		2.16		1.56			1.763			
		2.25		2.16		1.56					3.079		
VVT6	143.4	2.28	2.28	1.97	1.97	1.52	1.52	1.95	1.95				
VVT7	145.8	2.19	2.00	2.01	2.04	1.53	1.59			2.293			
		1.82		2.07		1.65							
VVT8	142.6	2.31	2.34	1.99	2.01	2.05	1.92	2.12	2.21	1.408			
		2.38		2.04		1.78		2.29					
VVT9	143.3	2.39	2.48	2.20	2.22	1.92	1.94	2.30	2.34				
		2.58		2.25		1.96		2.37					
VVT10	130	1.54	1.54	2.21	2.21	1.91	1.91	2.06	2.06				
VVT11	144	2.04	1.87	1.98	1.97	1.65	1.62		2.23				
		1.71		1.97		1.59		2.23					
VVT12	131.4	2.13	2.17	1.95	1.93	1.58	1.64	1.98	2.08	1.894			
		2.21		1.90		1.71		2.17					

Table A5 (continued): Incus and stapes measurements and CBL of the sample specimens.

Animal ID	Condylobasal length CBL (mm)	Crus breve (mm)	Crus breve mean (mm)	Crus longum (L2, pivot) (mm)	Crus longum (L2, pivot) mean (mm)	Crus longum (L2, axis) (mm)	Crus longum (L2, axis) mean (mm)	Stapes height (mm)	Stapes height mean (mm)	L1/L2	L1/L2 (Hemilä et al.)	ITR (Dallos 1973) using pivot lever arms	ITR (Dallos 1973) using axis lever arms
Mean	118.14		2.14		2.06		1.54		2.11	2.10	3.26	0.0044	0.0099
SD	24.10		0.19		0.12		0.15		0.15	0.26	0.23	0.0009	0.0023
n	47	79	47	79	47	80	47	36	26	34	29	13	13
VVT13	144.7	2.40 / 2.45	2.43	2.08 / 2.05	2.06	1.72 / 1.61	1.66	2.10	2.10	2.134			
VVT14	139.7	2.26 / 2.29	2.27	2.04 / 2.02	2.03	1.49 / 1.59	1.54	2.30	2.30	2.239			
VVT15	134.4	2.21 / 2.08	2.14	1.96 / 1.84	1.90	1.66 / 1.65	1.66	2.38 / 2.33	2.35	1.714			
VVT16	130.4	2.36 / 2.35	2.35	1.97 / 1.95	1.96	1.63 / 1.53	1.58	2.13	2.13	2.159			
VVT17	138	2.03 / 2.01	2.02	1.93 / 1.94	1.93	1.48 / 1.61	1.55	2.19	2.19				
VVT18	133.8	2.11 / 2.20	2.15	1.99 / 2.06	2.02	1.62 / 1.58	1.60	2.10 / 2.12	2.11	1.708			
VVT19	142.8	2.10 / 2.20	2.15	2.03 / 2.09	2.06	1.61 / 1.48	1.55	2.02 / 2.02	2.02	2.423			
VVT20	143.2	2.38	2.38	2.03	2.03	1.67	1.67						
VVT21	142.9	2.11 / 2.20	2.16	1.94 / 1.93	1.94	1.27 / 1.48	1.37						
M.5486	105.3	2.08 / 2.18	2.13	2.05 / 2.07	2.06	1.68 / 1.58	1.63	2.31	2.31	1.905			
Z88/22	110.1	2.46	2.46	1.91	1.91	1.49	1.49	2.32	2.32	2.098			
Z97/91	122.6	2.39	2.39	2.08	2.08	1.61	1.61	2.15	2.15	2.033			
M.5626	127.9	2.26	2.26	1.82	1.82	1.46	1.46	1.90	1.90	1.714			
M.58	116.9	2.12	2.12	2.02	2.02	1.54	1.54			2.269			
Z88/22.1	103.9	2.34	2.34	2.00	2.00	1.34	1.34						
E38/65	105.7	2.17 / 2.18	2.17	1.93 / 1.90	1.91	1.52 / 1.44	1.48			2.209			
V88/21	108.4	2.31	2.31	1.96	1.96	1.28	1.28	2.08	2.08				
V88/21.1	112	2.36	2.36	1.94	1.94	1.42	1.42	2.02	2.02	1.955			

Table A6: Cochlear measurements and CBL of the sample specimens.

	Condylobasal length CBL (mm)	Length basilar membrane (mm)	Length basilar membrane mean (mm)	Triad width min (µm)	Triad width min mean (µm)	Triad width max (µm)	Triad width max mean (µm)	IHC	IHC mean	OHC	OHC mean
Mean	95.93		25.8		18.7		36.8		2757.3		10502.1
SD	23.10		1.6		3.3		2.3		218.3		860.1
n	8	11	8	10	8	10	8	10	8	10	8
Animal ID											
VV1	77.4	22.6	22.6	14.7	14.7	36.8	36.8	2437	2437	9261	9261
VV5	75.8	26.6	26.6	15.8	15.8	37.9	37.9	2778	2778	10355	10355
VV7	93.6	26.5	26.5	23.2	23.2	37.9	37.9	2816	2816	11100	11100
VV8	149.4	28.6 / 25.8	27.2	20.0 / 17.9	19.0	36.8 / 41.1	39.0	3519 / 2811	3165	13224 / 10097	11660.5
VV10	92	27.2	27.2	14.7	14.7	37.9	37.9	2908	2908	11213	11213
VV13	94	25.2 / 26.8	26.0	20.0	20.0	36.8	36.8	2683	2683	10488	10488
VV14	99	25.8 / 22.0	23.9	23.2 / 21.1	22.1	30.5 / 32.6	31.6	2910 / 2440	2675	9967 / 8673	9320
VV15	86.2	26.3	26.3	20.0	20.0	36.8	36.8	2596	2596	10619	10619

Table A7: Ocular measurements and CBL of the sample specimens.

Animal ID	Condylobasal length CBL (mm)	Diameter (mm)	Diameter mean (mm)	Corneal diameter (mm)	Corneal diameter mean (mm)	Axial length (mm)	Axial length mean (mm)	Distance Lens-Retina (mm)	Distance Lens-Retina mean (mm)	Lens diameter (mm)	Lens diameter mean (mm)	Lens thickness (mm)	Lens thickness mean (mm)
Mean	92.49		15.7		12.4		16.1		12.0		9.56		5.58
SD	21.67		2.0		1.9		2.0		1.8		1.71		1.06
n	18	37	19	37	19	37	19	11	6	13	8	14	8
VV1	77.4	13.8	14.0	10.9	10.9	13.1	13.6				7.80		4.76
		14.1		10.9		14.1				7.80		4.76	
VV2	81.4	15.0	14.5	11.4	11.7	14.8	15.2						
		14.0		11.9		15.6							
VV3	78.8	14.8	15.2	11.1	11.3	14.7	14.6						
		15.6		11.4		14.4							
VV4	78.7	14.3	14.2	10.9	11.0	14.8	15.3						
		14.1		11.0		15.7							
VV5	75.8	14.8	14.4	10.5	10.6	14.2	14.0			11.11	11.54	6.76	6.83
		14.0		10.7		13.7				11.96		6.89	
VV6	93.5	15.9	15.9	13.5	13.6	17.4	17.4						
		15.9		13.7		17.4							
VV7	93.6	17.0	16.9	12.5	12.9	18.6	18.1			8.72	8.68	5.39	5.29
		16.8		13.3		17.5				8.64		5.19	
VV8	149.4	19.9	19.9	16.6	16.6	20.3	19.9			11.55	11.49	6.93	6.95
		19.9		16.5		19.5				11.43		6.96	
VV9	76.1	16.8	16.8	12.8	12.7	18.0	17.8						
		16.8		12.6		17.6							
VV10	92	16.4	15.7	12.9	12.6	17.4	16.9			9.06	9.06	5.06	5.06
		15.0		12.2		16.4				9.06		5.06	
VV11	100.5									8.30	8.24	4.49	4.57
										8.17		4.64	
VV12	92.5	15.1	15.0	11.8	11.9	16.2	16.1			8.07	8.00	4.46	4.49
		14.8		12.0		15.9				7.92		4.51	
VV17		14.6	14.3	11.5	11.6	15.8	16.3						
		13.9		11.6		16.7							
VV18	139.6		18.5		14.9		19.2		15.4	11..66	11.66	6.50	6.69
		18.5		14.9		19.2		15.4		11.66		6.87	
VV22		19.2	19.9	16.1	16.7	18.1	18.4						
		20.6		17.2		18.7							
VV26	73	13.9	13.6	11.0	11.1	13.3	13.3	10.9	10.5				
		13.3		11.2		13.3		10.1					
VV27	76	14.1	13.8	10.8	10.6	14.0	13.9	11.4	11.2				
		13.6		10.3		13.8		10.9					
VV28	78.6	14.4	14.3	10.5	10.7	14.9	14.6	12.5	11.6				
		14.2		10.9		14.3		10.7					
VV29	98	14.5	14.7	11.4	11.2	14.8	14.6	11.7	11.1				
		14.8		10.9		14.4		10.5					
VV30	110	17.8	17.6	13.8	14.1	16.7	16.8	11.9	12.1				
		17.4		14.3		16.8		12.3					

Table A8: Hair cell densities in ten segments of equal length along the cochlear duct of several red fox specimens. The means of all animals are given at the end of the table.

	Segment	IHCs/mm	SD	OHCs/mm	SD	Triad width (µm)	SD
VV13L length BM: 25.7 mm max width triad: 36.8 µm min width triad: 20.0 µm total no. IHC: 2,683 total no. OHC: 10,488	1-10%	110.5	6.4	441.2	40.0	33.5	2.4
	11-20%	106.7	5.9	449.3	5.7	33.2	0.7
	21-30%	92.7					
	31-40%	103.9	6.7	386.2	15.9	31.9	1.8
	41-50%	107.6	5.4	390.5	27.8	29.5	2.5
	51-60%	107.2	23.6	409.2	18.6	27.8	1.5
	61-70%	107.1	9.8	395.5	29.3	27.1	1.3
	71-80%	104.2	6.6	397.9	26.1	26.9	1.7
	81-90%	101.8		391.3	27.1		
	91-100%			399.5	20.8	20.5	0.6

	Segment	IHCs/mm	SD	OHCs/mm	SD	Triad width (µm)	SD
VV14R length BM: 22.0 mm max width triad: 32.6 µm min width triad: 21.1 µm total no. IHC: 2,440 total no. OHC: 8,673	1-10%	106.7	7.4	424.3	25.2	32.3	0.6
	11-20%	102.8	3.9				
	21-30%	108.1	5.1	395.1	20.0	29.5	1.5
	31-40%	108.1	5.8	371.6	6.2	26.1	1.2
	41-50%	107.5	3.3	382.1	9.6	28.3	1.0
	51-60%	109.6	4.1	383.6	6.9	27.0	1.5
	61-70%	117.9	3.2	396.8	21.9	23.9	1.5
	71-80%	122.8	3.7	395.8	12.1	22.8	1.6
	81-90%	110.3	12.0	395.3	20.4	21.1	
	91-100%	117.4	9.1				

	Segment	IHCs/mm	SD	OHCs/mm	SD	Triad width (µm)	SD
VV14L length BM: 25.9 mm max width triad: 30.5 µm min width triad: 23.2 µm total no. IHC: 2,910 total no. OHC: 9,967	1-10%			386.1	55.0	30.0	1.8
	11-20%						
	21-30%						
	31-40%	115.6	8.7	406.6	27.6	28.4	1.1
	41-50%	107.1	8.5	410.5	29.5	29.1	1.2
	51-60%	103.5	8.7	370.0	9.7	26.3	0.0
	61-70%	107.5	2.8	379.4	17.4	29.5	0.0
	71-80%	107.9	2.1	367.8	11.3	26.1	2.5
	81-90%	118.7		371.7	0.0	23.2	
	91-100%						

	Segment	IHCs/mm	SD	OHCs/mm	SD	Triad width (µm)	SD
VV15L length BM: 26.3 mm max width triad: 36.8 µm min width triad: 20.0 µm total no. IHC: 2,596 total no. OHC: 10,619	1-10%	102.1	2.9	420.2	20.0	30.0	2.0
	11-20%	97.5	4.4	404.5	12.4	32.6	1.7
	21-30%	99.8	3.9	412.3	15.1	34.2	1.5
	31-40%	97.1	2.7	407.4	19.3	32.8	0.6
	41-50%	98.8	4.0	405.4	12.3	32.4	0.6
	51-60%	91.2	5.8	394.5	29.4	29.7	1.4
	61-70%	94.8	4.8	392.2	13.9	28.0	0.7
	71-80%						
	81-90%	101.0	2.4	400.1	8.7	22.9	0.7
	91-100%	105.8	3.5	401.1	11.5	21.1	0.5

Table A8 (continued): Hair cell densities in ten segments of equal length along the cochlear duct of several red fox specimens. The means of all animals are given at the end of the table.

VV8L
length BM: 28.6 mm
max width triad: 36.8 µm
min width triad: 20.0 µm
total no. IHC: 3,519
total no. OHC: 13,224

Segment	IHCs/mm	SD	OHCs/mm	SD	Triad width (µm)	SD
1-10%	114.3	8.4	420.7	15.9	31.6	1.1
11-20%	123.0	8.0	464.4	33.5	33.2	2.1
21-30%	115.9	9.4	447.5	42.5	31.8	2.2
31-40%	110.5	6.0	415.9	16.8	29.7	1.1
41-50%	120.1	9.4	462.2	53.4		
51-60%	138.4	17.3	498.9	66.9	25.4	1.8
61-70%	129.2	9.2	469.2	28.8	24.2	2.6
71-80%	147.4	10.4	490.2	19.4	23.2	1.8
81-90%	105.5				20.0	
91-100%	126.7		475.0		21.1	

VV8R
length BM: 25.8 mm
max width triad: 41.1 µm
min width triad: 17.9 µm
total no. IHC: 2,811
total no. OHC: 10,097

Segment	IHCs/mm	SD	OHCs/mm	SD	Triad width (µm)	SD
1-10%						
11-20%	109.9	8.7				
21-30%	103.9	5.0	388.3	7.6	33.7	1.5
31-40%	102.1	3.4	387.6	15.0	32.3	1.0
41-50%	103.6	4.3	391.2	15.1	31.4	3.2
51-60%	108.4	4.6	389.6	5.2	30.0	0.6
61-70%	112.3	5.1	393.3	9.1	28.2	1.4
71-80%	121.6	3.5	409.2	6.8	25.6	1.3
81-90%	108.6	7.0	380.9	10.7	19.2	1.1
91-100%	110.8		404.2	4.1	21.1	

VV1L
length BM: 22.6 mm
max width triad: 36.8 µm
min width triad: 14.7 µm
total no. IHC: 2,437
total no. OHC: 9,261

Segment	IHCs/mm	SD	OHCs/mm	SD	Triad width (µm)	SD
1-10%						
11-20%	108.9	3.9	429.9	13.7	34.2	3.7
21-30%	98.0	4.3	400.9	8.9	35.3	2.2
31-40%	102.0	0.3	415.2	16.8		
41-50%	106.4	7.6	372.7	10.3		
51-60%	99.2		392.5	3.0	31.6	0.0
61-70%	108.4	6.9	417.1	20.5	28.4	0.0
71-80%	123.6	6.8	431.0	25.3	22.1	1.1
81-90%	116.9	7.5	408.3	17.4	18.9	2.2
91-100%	105.9	5.8	399.1	14.7	15.6	1.0

VV7R
length BM: 26.5 mm
max width triad: 37.9 µm
min width triad: 23.2 µm
total no. IHC: 2,816
total no. OHC: 11,100

Segment	IHCs/mm	SD	OHCs/mm	SD	Triad width (µm)	SD
1-10%	110.1	11.6	416.1	22.4	29.9	3.6
11-20%	106.1	5.1	400.9	23.7	34.9	1.3
21-30%	105.7	4.3	407.3	24.0	36.7	0.8
31-40%	102.1	4.2	444.7	17.8	34.9	2.9
41-50%	103.5	8.1	416.1	27.9	34.5	1.0
51-60%	98.7	10.7	413.8	29.0	32.1	1.2
61-70%	104.9	6.6	426.0	32.5	29.8	2.7
71-80%	112.8	2.3	418.0	27.5	27.4	1.8
81-90%	113.0	3.9	429.3	31.2	27.0	1.4
91-100%	107.4	6.8	423.6	15.7	24.2	1.1

Table A8 (continued): Hair cell densities in ten segments of equal length along the cochlear duct of several red fox specimens. The means of all animals are given at the end of the table.

	Segment	IHCs/mm	SD	OHCs/mm	SD	Triad width (µm)	SD
VV10L length BM: 27.2 mm max width triad: 37.9 µm min width triad: 14.7 µm total no. IHC: 2,908 total no. OHC: 11,212	1-10%	113.9	6.3	430.8	16.0	30.9	4.0
	11-20%	109.4	4.2	419.6	17.9	35.3	1.8
	21-30%	116.6	6.4	434.6	16.4	34.5	1.8
	31-40%	104.0	7.4	408.2	30.3	33.9	1.0
	41-50%	102.2	7.5	413.4	27.7	33.0	1.5
	51-60%	103.2	4.6	422.5	18.7	29.9	1.5
	61-70%	105.6	6.5	423.9	23.8	27.7	0.9
	71-80%	101.6	7.1	397.2	20.0	23.9	1.7
	81-90%	107.9	3.9	395.6	18.2	19.7	1.3
	91-100%	105.5		380.2	10.1	15.8	0.9

	Segment	IHCs/mm	SD	OHCs/mm	SD	Triad width (µm)	SD
VV5L length BM: 26.6 mm max width triad: 37.9 µm min width triad: 15.8 µm total no. IHC: 2,778 total no. OHC: 10,355	1-10%	110.6	6.9	413.1	18.9	28.8	1.6
	11-20%	106.3	5.5	398.9	14.9	33.1	2.4
	21-30%	112.5	5.4	391.1	12.0	35.9	1.2
	31-40%	107.8	3.1	393.8	14.4	32.4	1.9
	41-50%	103.1	4.9	388.4	20.8	30.8	2.2
	51-60%	102.6	7.1	402.3	23.2	28.5	1.3
	61-70%	101.2	4.0	381.6	14.7	25.7	1.4
	71-80%	103.3	9.9	391.8	15.8	21.1	1.5
	81-90%	101.6	3.2	380.5	22.1	19.7	2.2
	91-100%	96.5	7.9	356.2		16.3	0.7

	Segment	IHCs/mm	SD	OHCs/mm	SD	Triad width (µm)	SD
Means length BM: 25.7 ± 1.6 mm max width triad: 36.8 ± 2.3 µm min width triad: 18.7 µm total no. IHC: 2,757 total no. OHC: 10,502	1-10%	109.77	4.25	421.05	11.85	30.82	1.52
	11-20%	106.78	5.45	423.92	25.42	33.80	1.98
	21-30%	105.42	8.04	408.45	14.84	34.10	2.41
	31-40%	104.37	4.41	405.81	18.65	32.04	2.47
	41-50%	105.11	4.02	401.19	17.55	31.48	2.01
	51-60%	104.02	9.35	406.98	20.63	29.25	1.93
	61-70%	106.92	7.68	406.96	19.60	27.45	1.34
	71-80%	113.61	12.11	409.63	24.22	24.31	2.30
	81-90%	107.96	6.29	396.19	16.59	21.43	2.87
	91-100%	108.19	7.64	399.90	27.20	19.22	0.80

Table A9: Basic morphometrics of the auditory system of the red fox together with a collection of published data on other carnivore species.

Trivial name	Latin name	Cochlear turns	Length of basilar membrane (mm)	Area tympanic membrane (mm²)	Area oval window (mm²)	Area round window (mm²)	area ratio	Ossicular lever ratio	BM width basal-apical (mm)	Thickness BM basal-apical (µm)	Total IHC	Total OHC
Red fox	*Vulpes vulpes*	3.2	25.78	55.7	1.78	2.34	31.37	2.1	0.08-0.45	17.7-5.5	2,757	10,502
Domestic dog	*Canis familiaris*	3[10]; 3.25[13,19]; 3.5[11]	23.2[1]; 28.0[2]; 22.1[7]; 24.5[8]; 24[9]; 23.9[11]	30-55.2[4]					0.24-0.39[2]; 0.27-0.4[10]		2,603[2]	10,548[2]
Domestic cat	*Felis catus*	3[13,10]; 3+[19]	21.9[24]; 22-23[13]; 23.5[23]; 23.6[3,5]; 24.25[21]; 25[6]; 22.7[8]; 20[9]; 23[12]; 27.4[16]; 28[20]	41[15]	1.3[15]; 1.12[22]		31.54	2[15]	0.2-0.37[10]; 0.11-0.43[3]; 0.08-0.37[18]; 0.24-0.39[23]	13.5-5[3]; 12-5[20]	2,723[16]	10,105[16]
Jaguar	*Panthera onca*	2.75[17]	33.3[17]	58[17]	2.1[17]		27.62	2.8[17]			3,354[14]	13,076[14]
Tiger	*Panthera leo*	2.75[17]	35.5[17]	61[17]	3.5[17]	10.7[17]	17.43	2.8[17]			3,414[14]	12,936[14]

[1]Mair, 1976; [2]Branis & Burda, 1985; [3]Cabezudo, 1978; [4]Heffner, 1983; [5]Sato et al., 1999; [6]Liberman, 1982; [7]Igarashi et al., 1972; [8]Schuknecht et al., 1965; [9]Keen, 1940; [10]Keen, 1939; [11]Le & Keithley, 2007; [12]West & Harrison, 1973; [13]West, 1985; [14]Ulehlova et al., 1984; [15]Puria & Allen, 1998; [16]Burda, unpublished; [17]Burda et al., 1984; [18]Echteler et al., 1994; [19]Gray, 1907; [20]Ketten, 1997; [21]Liberman & Beil, 1979; [22]Salih et al., 2012; [23]Retzius, 1884; [24]Schuknecht, 1953

Table A10: Directions of wood mice nests built in different magnetic conditions. In the ambient field the Helmholtz coils were operated in antiparallel mode. In the west field, magnetic north was rotated 90° counterclockwise by running the coils in parallel mode. LF = Larmor frequency, FM = frequency-modulated, all directions given in degree (°).

Ambient field	West field	LF	Wideband-FM
0	55	45	135
315	150	330	250
185	155	315	160
90	270	260	345
35	335	25	120
70	105	10	140
90	5	245	20
175	75	205	285
65	120	145	120
40	100	205	115
35	195	160	90
225	75	210	305
185	110	195	205
190	65	125	110
225	305	165	150
245	330	0	85
355	250	175	150
205	75	15	
320	345	20	
195	250	55	
255	310	195	
195		145	
180			
20			

Eidesstattliche Erklärung

Erklärung:

Hiermit erkläre ich, gem. § 7 Abs. (2) d) + f) der Promotionsordnung der Fakultät für Biologie zur Erlangung des Dr. rer. nat., dass ich die vorliegende Dissertation selbständig verfasst und mich keiner anderen als der angegebenen Hilfsmittel bedient habe und alle wörtlich oder inhaltlich übernommenen Stellen als solche gekennzeichnet habe.

Essen, den 25.08.2014   _____

                                                                    (Erich Pascal Malkemper)

Erklärung:

Hiermit erkläre ich, gem. § 7 Abs. (2) e) + g) der Promotionsordnung der Fakultät für Biologie zur Erlangung des Dr. rer. nat., dass ich keine anderen Promotionen bzw. Promotionsversuche in der Vergangenheit durchgeführt habe und dass diese Arbeit von keiner anderen Fakultät/Fachbereich abgelehnt worden ist.

Essen, den 25.08.2014   _____

                                                                    (Erich Pascal Malkemper)

Erklärung:

Hiermit erkläre ich, gem. § 6 Abs. (2) g) der Promotionsordnung der Fakultät für Biologie zur Erlangung der Dr. rer. nat., dass ich das Arbeitsgebiet, dem das Thema „The Sensory Biology of the Red Fox – Hearing, Vision, Magnetoreception" zuzuordnen ist, in Forschung und Lehre vertrete und den Antrag von Erich Pascal Malkemper befürworte und die Betreuung auch im Falle eines Weggangs, wenn nicht wichtige Gründe dem entgegenstehen, weiterführen werde.

Essen, den 25.08.2014   _____

                                                                    (Prof. Dr. Hynek Burda)

List of abbreviations

AL	axial length		mN	magnetic North
ANOVA	analysis of variance		MPM	magnetic-particle based mechanism
aq. dest.	*Aqua destillata*		MW	malleus weight
BM	basilar membrane		N	North
BMl	length of basilar membrane		n.d.	not determined
BSA	bovine serum albumine		n.s.	not significant
CBL	condylobasal length		NDS	normal donkey serum
cf.	confer		NFR	nuclear fast red
Cry	cryptochrome		NGS	normal goat serum
DAB	diaminobenzidin		OHC	outer hair cell
dB	decibel		ONL	outer nuclear layer
dB_{max}	maximum SPL		OPL	outer plexiform layer
dB_{min}	minimum SPL		OW	oval window
dB_{ob}	SPL observing position		OWA	oval window area
dpi	dots per inch		P	position (along cochlea)
dSPL	desired sound pressure level		Pa	Pascal
E	East		PB	phosphate buffer
EDTA	ethylenediaminetetraacetic acid		PBS	phosphate buffered saline
eq.	equation		PE	pigment epithelium
FA	false alarm		PF	pars flaccida
FAD	flavin adenine dinucleotide		PFA	paraformaldehyde
FFT	fast Fourier transformation		PL	pinna height (length)
FM	frequency modulated		PND	posterior nodal point
GCL	ganglion cell layer		PrB	Prussian blue
GMF	geomagnetic field		PT	pars tensa
HE	haematoxylin and eosin		PW	pinna width
HT	half-turn (cochlea)		RF	radiofrequency (magnetic field)
Hz	Hertz		RGC	retinal ganglion cell
IHC	inner hair cell		RMF	retinal magnification factor
ILA	incus lever arm (axis)		RPM	radical pair mechanism
ILD	interaural level difference		RW	round window
ILP	incus lever arm (pivot)		RWA	round window area
INL	inner nuclear layer		S	South
IPL	inner plexiform layer		SD	single domain
IR	infrared		*SD*	standard deviation
ISP	incus short process		SF	single frequency
ITD	interaural time difference		SH	stapes height
IW	incus weight		SPL	sound pressure level
LF	Larmor frequency		SPM	super-paramagnetic
LWS (L)	long wavelength-sensitive		SW	stapes weight
MA	magnetic alignment		SWS (S)	short wavelength-sensitive
MAP	malleus anterior process		T	Tesla
MF	magnetic field		TMA	tympanic membrane area
MLA	malleus lever arm (axis)		tN	topographic North
MLP	malleus lateral process		W	West
MLP	malleus lever arm (pivot)		ZGB	zygomatic breadth
MLS	medium wavelength-sensitive			

Der Lebenslauf ist in der Online-Version aus Gründen des Datenschutzes nicht enthalten.

Der Lebenslauf ist in der Online-Version aus Gründen des Datenschutzes nicht enthalten.

Der Lebenslauf ist in der Online-Version aus Gründen des Datenschutzes nicht enthalten.

Der Lebenslauf ist in der Online-Version aus Gründen des Datenschutzes nicht enthalten.